SIMULTANEOUS FREE AND FORCED CONVECTION AROUND SUBMERGED CYLINDERS AND SPHERES

SIMULTANEOUS FREE AND FORCED CONVECTION AROUND SUBMERGED CYLINDERS AND SPHERES

BY

SUN-WAI WOO

A Thesis

Submitted to The Faculty of Graduate Studies in Partial Fulfilment of the Requirement for the Degree

Doctor of Philosophy

McMaster University

May, 1971

McMASTER UNIVERSITY LIBRARY

DOCTOR OF PHILOSOPHY (1971)
(Chemical Engineering)

McMASTER UNIVERSITY
Hamilton, Ontario.

TITLE : Simultaneous Free and Forced Convection Around Submerged Cylinders and Spheres

AUTHOR : Sun-Wai Woo

B.Sc., (National Taiwan University)
M.A.Sc., (University of Waterloo)

SUPERVISOR : Professor A.E. Hamielec

NUMBER OF PAGES : xi, 224

SCOPE AND CONTENTS:

This dissertation is a theoretical investigation of simultaneous free and forced convection for flow around a sphere or cylinder. This involved a numerical solution of the Navier-Stokes and energy equations by finite difference methods. To this end faster computational techniques were developed. A large number of solutions were computed permitting a significant extension of fluid-mechanical data available in the literature.

TABLE OF CONTENTS

LIST OF TABLES

LIST OF FIGURES

1. INTRODUCTION AND LITERATURE SURVEY

1.1 General

Momentum, heat and mass transfer between blunt objects and surrounding fluids are often experienced in nature and technological processes. Industrial operations involved with a dispersion of essentially spherical particles, include fluidization, sedimentation, crystallization, spray drying, pneumatic transportation, deoxidation of molten steel and many others. An example of a natural phenomenon which is of great interest to meteorologists is the growth of cloud drops and the evaporation of raindrops. Industrial and scientific interest in flows normal to the long axis of a circular cylinder is also significant. Examples include, among others the shell and tube heat exchanger and hot wire anemometry.

Although much experimental and theoretical work has been done in this field of engineering, many gaps in our knowledge still exist. Most experimental studies have involved the measurement of integrated quantities such as the drag coefficient and overall Nusselt number. Detailed temperature, concentration or velocity distributions measured experimentally are almost non-existent. There are also a very limited number of distributions predicted theoretically. Analytical solutions involving limiting dimensionless parameters and solutions obtained by matched asymptotic expansions have provided information which is applicable only over a very small range of parameters. For example, the

Oseen solution for a single sphere in an unbounded fluid is only applicable for Reynolds number less than about 0.1. Boundary layer solutions, although very successful for slender bodies, are of limited applicability for blunt objects. Such solutions are reasonably accurate from the frontal stagnation point to the flow separation point, but do not apply past the separation point. Information obtained from these approaches, does not fulfill all of the requirements for the analysis of processes of technological interest. It is for this reason that this theoretical study of more realistic transfer models was initiated.

This theoretical study of transport phenomena around submerged blunt objects required the solution of the complete Navier-Stokes equations of motion for viscous, incompressible flow and continuity equations of heat and mass transfer subject to various boundary conditions describing different physical situations. Analytical solutions of these equations are not to be expected because of their nonlinearity. However, numerical solutions can be obtained by applying finite-difference techniques. Recent solutions of complex problems in many fields indicate that finite-difference techniques are undoubtedly a powerful tool for obtaining numerical solutions to non-linear partial differential equations. For large complex problems, however, methods of solving the large sets of non-linear algebraic equations are not efficient with respect to computation time with a digital computer. There is a need for the development of faster techniques for the solution of large sets of non-linear algebraic equations.

The following sections will critically review important theoretical works related to convective momentum, heat and mass transfer around blunt objects. Convective flow around a single sphere and infinite long cylinder in an unbounded fluid will be considered.

1.2 Fluid Mechanics

Viscous, incompressible flow of Newtonian fluids around blunt objects is governed by the well-known Navier-Stokes equation. The only exact and useful solution of the Navier-Stokes equations is for creeping axisymmetric flow around a rigid sphere in an unbounded fluid, and is due to Stokes (1851). He neglected inertia terms and thus linearized the Navier-Stokes equations. This is valid for $Re \to 0$. The solution in terms of stream function ψ^* is

$$\psi^* = \frac{1}{4}\left(\frac{1}{r^*} - 3r^* + 2r^{*2}\right)\sin^2\theta \qquad (1.2\text{-}1)$$

and the corresponding total drag coefficient C_{Ds} is

$$C_{Ds} = 24/Re \qquad (1.2\text{-}2)$$

At a distance away from the surface of the sphere the inertia terms dominate the flow field and Stokes' assumption is therefore not valid in this region.

Oseen (1910) linearized the convective velocities in the Navier-Stokes equations by using the undisturbed free stream velocity U_∞ and obtained the following analytical solution

$$\psi^* = \frac{1}{4}\left(2r^{*2} + \frac{1}{r^*}\right)\sin^2\theta - \frac{3}{2Re}\left(1 + \cos\theta\right)\left(1 - e^{\frac{-Re}{2}\left(r^* - \cos\theta\right)}\right) \qquad (1.2\text{-}3)$$

and the total drag coefficient as

$$C_D = \frac{24}{Re}\left(1 + \frac{3}{16} Re\right) \qquad (1.2\text{-}4)$$

This solution is valid for Re << 1, and is not exact in the vicinity of the sphere surface.

For slow uniform streaming motion past a cylinder, there is no Stokes solution; one that remains finite far from the cylinder surface and that satisfies the no-slip condition on the surface. Approximate solutions to this problem have been obtained by Lamb (1911) utilizing Stokes' assumption and by Faxen (1927) and later Tomotika and Aoi (1950) using Oseen's linearization. These solutions were later improved by applying matched asymptotic expansion techniques after Kaplan (1957). This technique matches the flow field to both Stokes' and Oseen's regions by means of a singular perturbation method, which has been used widely to obtain more accurate solutions of the Navier-Stokes equations of flow around spheres and cylinders in the limiting range of Re << 1 (Kaplun 1967, Lagerstrom and Cole 1955). The work of Proudman and Pearson (1957) is a typical example. They matched inner (Stokes') and outer (Oseen's) solutions in the perturbation approach and obtained higher approximations to the solutions for uniform flow disturbed by a single sphere or cylinder in an unbounded fluid.

Recent experimental results of Maxworthy (1965) and Pruppacher and Steinberger (1968) show that for flow around a sphere, the drag approaches Oseen's drag rather than Stokes' drag as Re approaches zero (Pruppacher, LeClair, and Hamielec 1970). Matched asymptotic expansion

solution of Proudman and Pearson (1957) agrees very well with these experimental investigations. However, analytical solutions by the perturbation method are limited by the asymptotic ranges of the parameters and at best provide information over a very narrow range of Reynolds numbers $0 \leq Re \leq 0.1$.

The well developed boundary layer theory for solution of the Navier Stokes equations for high Reynolds number flows has achieved great success in approximating flow behavior for slender bodies. However, geometric factors must be taken into account, for instance, in problems involving flow around blunt objects with the appearance of a trailing vortex ring at moderate Reynolds numbers. Boundary layer assumptions even as $Re \to \infty$ are unapplicable over a good portion of the object. It is because of this loss in generality of the boundary layer approach for the investigation of flows around blunt objects and the limited applicability of matched asymptotic methods that numerical studies of the complete Navier Stokes equations have lately received so much attention.

Approximate solutions of the Navier Stokes equations for viscous, incompressible flow around a single sphere in an unbounded fluid have been obtained with various methods, Kawaguti (1948), using Galerkin's error distribution method, approximated the flow profile around a sphere at $Re > 1$. It was found that a trailing vortex appears at a Reynolds number of 40. Kawaguti's original work was later extended by Hamielec et.al. (1963) up to $Re \leq 5000$. These approximate methods have been shown to give insufficient accuracy when compared with solutions obtained using finite-

difference techniques (Hamielec, Hoffman and Ross 1967).

At present, accurate solutions of the non-linear Navier Stokes equations can only be obtained using numerical techniques. The most powerful methods appear to be finite-difference techniques. There are two main finite-difference methods of obtaining steady state solutions of the Navier Stokes equations, namely, the steady-state methods and the unsteady state methods. The general numerical procedures are similar. They differ in that the derivative with respect to time is dropped in the steady-state method. Steady-state method of solving the Navier Stokes equations was first used by Thom (1933). Flow past a circular cylinder at low Reynolds numbers was considered. Thom split the fourth-order Navier Stokes equation in ψ^* the stream function into two second-order equations by introducing a new variable, ξ^* the vorticity. Allen and Southwell (1955) applied relaxation methods in solving finite-difference equations for flow past a cylinder. Apelt (1958) solved the same problem at Reynolds numbers of 40 and 44. Jenson (1959) used the steady state method and obtained solutions for viscous incompressible flow around a sphere for Re $\leq$ 40. Russell (1962) reviewed the variety of steady-state methods and concluded that modified successive optimum displacement by points seems to be the best method giving fastest rate of convergence with stable solutions. Of these steady-state methods, Jenson's method was computerized by Hamielec et.al. (1967). Prior to computerization, all of the solutions were highly inaccurate because long computation times with desk calculators did not permit the use of sufficiently small mesh sizes

nor proper simulation of an unbounded fluid. Good agreement of predicted quantities (Hamielec et.al. 1967, 1969) with experimental data of Lapple (1954), Tritton (1959), Taneda (1956) and recently Pruppacher and Steinberger (1968) indicated the usefulness of the steady-state method employed. Computation times were sufficiently large so as to indicate a limitation for solution of more complex problems. Unsteady state approach to solutions of Navier-Stokes equations for steady flows can be divided into several groups depending on different difference schemes used. Fromm and Harlow (1963) developed an explicit forward time difference method of solving the Navier Stokes equations. Their method was used by Thoman and Szewczyk (1966) to determine time-dependent two-dimensional cross flow of a viscous incompressible fluid over stationary and rotating cylinders and by Rimon and Cheng (1969) to study uniform flow around a sphere. In this method, the time-dependent, fourth-order equation of motion in ψ^* was split into the vorticity transport equation and the defining equation of vorticity and a relaxation method is used in an iterative scheme for each time step. Fromm and Harlow's method is limited in the choice of a time step size due to the inherent instability of the explicit form and thus requires many time steps to obtain a steady-state solution. Pearson (1965) developed a new time-dependent method for solving viscous flow problem which employs an implicit procedure. Pearson's method is stable and a large time step can therefore be chosen to obtain the steady-state solution. In Pearson's method, the vorticity transport equation is approximated by an implicit Crank-Nicholson form where the non-linear terms, the stream function and its derivatives, are

linearized over the time interval, and an alternating direction implicit method (ADI) devised by Peaceman and Rachford (1955) is used to solve the Crank-Nicholson approximation of the vorticity transport equation. Pearson's method was used by Son and Hanratty (1969), Oosthuizen (1970) for flow around a cylinder and by LeClair (1970) to study the flow around a sphere accelerating under the influence of gravity. This method, usually called ADI is considered to be the fastest method reported in the literature.

Chorin (1967) used the primitive variables (velocity and pressure) and developed a new time dependent-method for solving the Navier Stokes equations, which is equally applicable to problems in two or three dimensions. Pseudo-compressible flow approach is used by introducing an artificial compressibility during the iteration. The method has been used to solve Benard convection problems in three dimensions, a problem which is considered difficult to solve numerically even in two dimensions. The important feature of Chorin's method is its direct applicability to the solution of three dimensional problems which can not be handled by previous methods. However, no comparison has been made of the stability and rate of convergence with other methods.

1.3 Forced Convection

Forced convection heat and mass transfer is governed by the continuity equations of energy or mass if it is assumed that the velocity profile is unaffected by transfer of heat or mass during this process. Therefore, the Navier Stokes equations and the continuity equation of heat or mass are uncoupled and can be solved separately.

Boussinesq (1905) in an early paper showed that this kind of difficulty can be avoided if one assumes potential flow. By transforming the geometric coordinates to flow potential and the stream function as independent coordinates, Boussinesq found that the boundary layer type energy equation applying to heat conduction in a two dimensional flow field can be simplified. In addition, if the longitudinal conduction is neglected, then the equation assumes the same form as that for a flat plate. The one well known solution using this approach is for forced convection from a circular wire due to King (1914). King's solution can be approximated closely by two equations. Written in dimensionless form as

$$\begin{aligned} Nu &= \frac{2}{\log(2e^{\,1-\sigma/Pe})} \quad , \quad Pe < 0.08 \\ Nu &= \frac{1}{\pi} + \left(\frac{2Pe}{\pi}\right)^{\frac{1}{2}} \quad , \quad Pe > 0.08 \end{aligned} \tag{1.3-1}$$

Comparison with experimental data shows that Equ. (1.3-1) overestimates the heat transfer rate by up to 40%. The potential flow solution, of course, does not satisfy the no-slip condition on the cylinder surface.

A useful piece of theory (although of limited scope) is that based on the Oseen approximation. This is, of course, strictly valid only in the limit as $Re \to 0$. Cole and Roshko (1954) found that this approximation yields the solution

$$Nu = \frac{2}{\log \frac{8}{Pe} - \sigma} \tag{1.3-2}$$

Experimental work by the same author failed to substantiate their theoretical result and it was thought that the disagreement is due to disturbance of the two dimensional convection by three dimensional effects.

Grosh and Cess (1958), taking the Boussinesq (1905) approach, solved the forced convection problem numerically for a single cylinder in cross flow and obtained

$$Nu = 1.015\ (Pe)^{\frac{1}{2}} \qquad (1.3\text{-}3)$$

The calculation assumes that the heat transfer connected with vortex motion on the rear portion of the cylinder is negligibly small as compared with heat transfer by conduction. Comparison with experimental measurements indicates that this assumption is justified for values of $Pe < 500$. This kind of solution is probably a good approximation for liquid metal heat transfer because of the thick, thermal boundary layer due to the very low Prandtl numbers for liquid metals, and that is why the neglect of angular diffusion or conduction terms in the energy equation does not change the overall result appreciably.

Matched asymptotic solutions for axisymmetric forced convection around a sphere and cylinder have been studied by various authors. Acrivos and Taylor (1962) and recently Rimmer (1969) have derived forced convection asymptotic solutions for heat transfer around a sphere for the limiting case of $Pe \ll 1$. Acrivos and Taylor used Stokes' velocity profile while Rimmer applied a more accurate velocity profile of Proudman and Pearson (1957). Their solutions are

Acrivos and Taylor

$$Nu = 2+Pe+Pe^2(\log Pe+0.8239) + 0.5Pe^3 \log Re + \ldots \qquad (1.3\text{-}4)$$

Rimmer

$$Nu = 2+Pe+Pe^2\left[\log Pe + \frac{1}{4}\left(2Pr^2-Pr+4\sigma - \frac{231}{40}\right)\right.$$
$$\left. + 2(Pr^3-3Pe-2)\log Pr-2(Pr+1)^2(Pr-2)\log(Pr+1)\right] \qquad (1.3\text{-}5)$$

The Acrivos and Taylor solution will give a lower Nu at Re → 1 than by Rimmer because in Stokes' velocity profile, the term of O(Re) has been ignored. It will be later shown that these solutions have very limited applicability.

A simplification made to the continuity equation of heat or mass is to remove the angular diffusion terms. This leads to an equation parabolic in θ, the angular coordinate. The reduced equation follows

$$V_r \frac{\partial C}{\partial r} + \frac{V_\theta}{r}\frac{\partial C}{\partial \theta} = D\left(\frac{\partial^2 C}{\partial r^2} + \frac{n}{r}\frac{\partial C}{\partial r}\right)$$

where n=1 for a cylinder and n=2 for a sphere. Levich (1962) used Stokes velocity profile for V_r and V_θ and solved the equation analytically for a sphere. The solution which satisfies the boundary conditions

at $r = R$; $C = 1$

$r = \infty$; $C = 0$

$\theta = 0,\ r > R$; $C = 0$

can be expressed as

$$Sh = 0.991\ Pe^{1/3} \qquad (1.3\text{-}6)$$

Baird and Hamielec (1962) solved the same problem using velocity profiles after Kawaguti (Hamielec et.al. 1963) for intermediate Reynolds numbers.

LeClair and Hamielec (1968) solved this problem numerically using velocity profiles calculated by finite-difference techniques. They considered rigid spheres, cylinders and fluid spheres of low viscosity. This approach of solving the continuity equation of mass or energy by neglecting angular diffusion or conduction terms is usually called thin concentration (or thermal) boundary layer theory. This theory is reasonable for systems of high Peclet number. However, local transfer rates so calculated are in appreciable error, especially at the flow separation point and in the trailing vortex. This conclusion is based on a comparison of experimental data with theory by Garner et.al. (1958, 1961), Peltzman and Pfeffer (1967), Rhodes and Peeble (1965). These experimental investigations indicate that a finite transfer rate should occur at the flow separation angle rather than the zero transfer rate predicted by thin thermal boundary layer theory.

Numerical solutions of the elliptic equation which include both angular and radial diffusion terms have been obtained for creeping flow by Johnson and Akehata (1965) and Houghton (1967). The iterative methods used were very slow. Dennis et. al. (1968) using Oseen type linearization of the heat transfer equation, solved for steady laminar forced convection from a circular cylinder from Re = 0.01 to Re = 40. Velocity profiles were calculated by finite-difference methods. Their solutions are in good agreement with those found in the present analysis. Gauss-Seidel iterative scheme was employed in solving the finite-difference equation. They made no mention of the convergence rate of the method they used. Brian and Hales (1969) solved the elliptic continuity equation for a sphere in the

creeping flow regime at various Peclet numbers. Stokes velocity profiles were utilized. Finite-difference techniques were applied to solve smoothed (by variable transformation) continuity equation. A modified numerical procedure of Douglas and Rachford (1956) was employed. Transpiration effect at the surface of the particle was also considered.

In the case of multiparticle systems, particle interaction reduces the size of the vortex ring (LeClair and Hamielec 1968). Thin concentration boundary layer theory gives reasonable average transfer values. However local transfer rates can be appreciably in error. To predict accurate local transfer rates one must solve the complete elliptic equation with accurate velocity distributions.

1.4 Mixed Convection

The effect of free convection associated with a system of non-uniform temperature or concentration is often neglected in studying convection problems. It is well known that a density variation due to non-uniform temperature or concentration can affect the flow profile significantly. The effect is neglected because of the complexity of the flow of interacting free and forced convection.

A large amount of work has been done both theoretically and experimentally on pure free convection phenomena, for example, the nature and stability of Benard convection (Chandrasekhar 1961) and the boundary layer approach to solving free convection problems for curvilinear surfaces (Merk and Prins 1954) . However, the existing literature for simultaneous convection flow is very limited. Acrivos (1958, 1966) analysed combined free and forced convection for a vertical plate and found that the parameter

Gr/Re^2 is of fundamental importance for a flat plate. Numerical results are reported for the heating and cooling with upward flow past a vertical flat plate for three Prandtl numbers, 0.73, 10, 100. It was found that the transition from forced to free convection is gradual and the processes of free and forced convection interact and cannot be superposed. This is especially true at high Prandtl numbers. Shear stress increases in aiding flow and decreases in opposing flow. The boundary layer is stabilized by aiding flow whereas opposing flow hastens the appearance of flow separation. Sparrow, Eichhorn and Gregg (1959) and Kubair and Pei (1968), obtained similar results for laminar boundary layer flows. The same flow characteristics were found. Kubair and Pei considered non-Newtonian fluids as well.

Hieber and Gebhart (1969) solved the convective equations by matched asymptotic expansion techniques for mixed convection for a sphere for the limiting cases of $Re \to 0$ and $Gr \to 0(Re^2)$ for a system of unit Prandtl number. Their results are given in terms of the Nusselt number and drag coefficient as follows

$$Nu = 2 + 1.284\, Re + \frac{Re}{2} \ln\left(\frac{Re}{2}\right) + \frac{Re^3}{16} \ln\left(\frac{Re}{2}\right)$$

$$+ 0.194\, \frac{Gr}{Re} + \frac{Gr}{2} \ln\left(\frac{Re}{2}\right)$$

$$C_D = \frac{24}{Re}\left[1 + \frac{3}{16} Re + \frac{9}{160} Re^2 \ln\left(\frac{Re}{2}\right) + \frac{Gr}{2Re^2}\right.$$

$$\left. + 0.166\, \frac{Gr}{Re} - 0.35\, \frac{Gr^2}{Re^2} + \frac{27}{320} Gr \ln\left(\frac{Re}{2}\right)\right] \quad (1.4\text{-}2)$$

The drag coefficient was found to change with Gr significantly and comparison with the present numerical solutions for the limiting parameters ranges shows excellent agreement. However, these assumptions are valid in the limit of $Re \to 0$ and $Gr \to 0(Re^2)$; this is a very limited range of applicability.

Numerical studies of mixed convection flow around a circular cylinder have been carried out very recently by Öhman (1969) and Oösthuizen (1970). Both authors studied air flow past a cylinder. The vortex ring is shown to be very sensitive to free convection which agrees with the present findings. However, their results are of limited accuracy due to very large step size and wall effect as well as inadequate convergence criteria. They did not make a comprehensive study of the stability and rate of convergence of their numerical method.

2. FORMULATION OF MATHEMATICAL MODELS

2.1 Basic Assumptions and Governing Equations

When a fluid flows over a blunt object at a different temperature or one that causes mass transfer, the density of the fluid near the object surface will change due to heat or mass transfer or both. This density variation will cause a non-uniform body force field which affects the forced flow as well as the transfer rate between the object and the fluid.

In the study of mixed convection flow problems, Boussinesq (1905) approximations are frequently used to simplify the basic flow equations. These assumptions can best be summarized in two statements:

i) The variations in density which appear with the advent of motion results principally from thermal or concentration (as opposed to pressure) effects.

ii) In the equation for the rate of change of momentum and mass, density variations may be neglected except when they are coupled to the gravitational acceleration in the buoyant force.

These approximations have been used extensively (Acrivos 1958, **Aziz and Hellums 1967**, Hieber and Gebhart 1969 etc.). Speigel and Veronis **(1960)** re-examined the applicability of these assumptions for a compressible fluid assuming that the ideal equation of state can be used for the compressible fluid and concluded that Boussinesq approximations are always valid if the flow of compressible fluid is isochoric. In low Reynolds number flows (Mach No. $<<$ 1) of a compressible fluid, the flow

can be considered incompressible. Of course, one can expect that for very high temperature or concentration gradients, these approximations may lead to appreciable error. For small temperature or concentration gradients, the Boussinesq approximations are apparently valid.

The relationship between the density and temperature can be obtained through the Taylor Series expansion of ρ in T about some reference temperature T_R, i.e.,

$$\rho = \rho\Big|_{T_R} + \frac{\partial\rho}{\partial T}\Big|_{T_R} (T-T_R) + \frac{\partial^2\rho}{\partial T^2}\Big|_{T_R} \frac{(T-T_R)^2}{2!} + \text{----}$$

For a reasonably small temperature difference $(T-T_R)$, the bulk viscosity and density μ_{av}. ρ_{av} can be assumed constant and the temperature variation of density in the body force field can be approximated by

$$\rho = \rho_{av} - \rho_{av}\,\beta(T-T_{av}),$$

where the reference temperature T_R is chosen as the bulk temperature T_{av}.

This linear relationship between ρ and T and the Boussinesq approximations will be used to derive the mixed convection transport equations for convective flow around sphere and cylinder. For axisymmetric flow around a sphere and cross flow around an infinite cylinder, only two special coordinates need be considered. In addition, incompressible, Newtonian behavior of the fluid is assumed and viscous dissipation is neglected.

Consider a two dimensional external flow over a curvilinear surface of Figure 2.1-1. The steady state transport equations are:

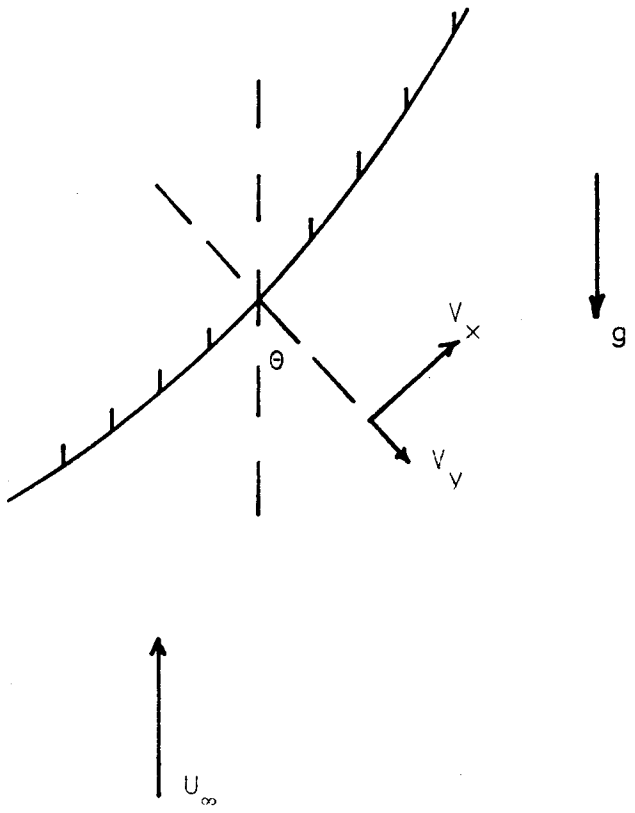

FIGURE 2.1-1 TWO DIMENSIONAL FLOW OVER A CURVILINEAR SURFACE

Navier Stokes momentum equations

x-direction

$$V_x \frac{\partial V_x}{\partial x} + V_y \frac{\partial V_x}{\partial y} = - \frac{\partial P'}{\partial x} + \nu\left(\frac{\partial^2 V_x}{\partial x^2} + \frac{\partial^2 V_y}{\partial y^2}\right)$$

$$- g \sin\theta \, (1-\beta \quad (T-T_{av})) \qquad (2.1\text{-}1)$$

y-direction

$$V_x \frac{\partial V_y}{\partial x} + V_y \frac{\partial V_y}{\partial y} = - \frac{\partial P'}{\partial y} + \nu\left(\frac{\partial^2 V_x}{\partial x^2} + \frac{\partial^2 V_y}{\partial y^2}\right)$$

$$+ g \cos\theta \, (1-\beta \quad (T-T_{av})) \qquad (2.1\text{-}2)$$

equation of continuity

$$\frac{\partial V_x}{\partial x} + \frac{\partial V_y}{\partial y} = 0 \qquad (2.1\text{-}3)$$

Continuity equation of heat or mass

$$V_x \frac{\partial T}{\partial x} + V_y \frac{\partial T}{\partial y} = \frac{k}{\rho \hat{C}_p}\left(\frac{\partial^2 T}{\partial x^2} + \frac{\partial^2 T}{\partial y^2}\right) \qquad (2.1\text{-}4)$$

For a flow problem with two spatial coordinates, a scalar function, ψ, the stream function can be introduced to reduce the number of dependent variables. The relationship between ψ and the velocity components are

$$V_x = \frac{\partial \psi}{\partial y}$$

$$V_y = - \frac{\partial \psi}{\partial x} \qquad (2.1\text{-}5)$$

ψ, thus defined satisfies equation (2.1-3) everywhere.

Substituting equation (2.1-5) into equations (2.1-1)-(2.1-4) and eliminating P' from equations (2.1-1) and (2.1-2), one obtains

$$\nu\nabla^4\psi + \frac{\partial\psi}{\partial x}\frac{\partial}{\partial y}(\nabla^2\psi) - \frac{\partial\psi}{\partial y}\frac{\partial}{\partial x}(\nabla^2\psi)$$

$$+ g\beta \quad (\cos\theta\frac{\partial T}{\partial x} + \sin\theta\frac{\partial T}{\partial y}) = 0 \qquad (2.1\text{-}6)$$

$$\frac{\partial\psi}{\partial y}\frac{\partial T}{\partial x} - \frac{\partial\psi}{\partial x}\frac{\partial T}{\partial y} = \frac{k}{\rho\ \hat{C}_p}(\frac{\partial^2 T}{\partial x^2} + \frac{\partial^2 T}{\partial y^2}) \qquad (2.1\text{-}7)$$

Equations (2.1-6) and (2.1-7) are fourth order and second order non-linear partial differential equations of elliptic type. By introducing another variable, ξ, the vorticity defined as

$$\xi = \nabla^2\psi, \qquad (2.1\text{-}8)$$

equation (2.1-6) can be split into two second-order equations, namely The vorticity transport equation

$$\nu\nabla^2\xi + \frac{\partial\psi}{\partial x}\frac{\partial\xi}{\partial y} - \frac{\partial\psi}{\partial y}\frac{\partial\xi}{\partial x} + g\beta \quad (\cos\theta\frac{\partial T}{\partial x} + \sin\theta\frac{\partial T}{\partial y}) = 0 \qquad (2.1\text{-}9)$$

and the defining equation of vorticity (equation (2.1-8)).

Equations (2.1-7) and (2.1-9) are coupled and must be solved simultaneously for the field functions ψ, ξ and T subject to appropriate boundary conditions. Once the field functions are available, the transport properties, i.e. heat or mass transfer rate, surface pressure distributions, drag coefficient etc. can be calculated.

2.2 Axisymmetric Flow Around a Solid Sphere

2.2.1 Governing Equations for Field Functions

The dimensionless vorticity transport equation, defining equation for vorticity and the continuity equation of energy or mass for axisymmetric flow around a sphere written in spherical polar coordinates (see Figure 3.1-1) with the following dimensionless groups and variables

$$Re = \frac{d\,U_\infty}{\nu}\,, \quad Pe = \frac{d\,U_\infty \rho\ \hat{C}_p}{k}\,, \quad Gr = d^3\beta\ \ g(T_s-T_\infty)/\nu^2$$

$$r^* = r/R\ \ , \quad \psi^* = \psi/U_\infty R^2\ \ , \quad \xi^* = \xi R/U_\infty\ , \quad \eta^* = \frac{T-T_\infty}{T_s-T_\infty}$$

are

Vorticity transport equation

$$\left[\frac{\partial\psi^*}{\partial r^*}\frac{\partial}{\partial\theta}\left(\frac{\xi^*}{r^*\sin\theta}\right) - \frac{\partial\psi^*}{\partial\theta}\frac{\partial}{\partial r^*}\left(\frac{\xi^*}{r^*\sin\theta}\right)\right]\sin\theta$$

$$= \frac{2}{Re}E_s^{*2}(\xi^* r^*\sin\theta) + \frac{Gr}{2Re^2}\left(\cos\theta\sin\theta\frac{\partial\eta^*}{\partial\theta} + r^*\sin^2\theta\frac{\partial\eta^*}{\partial r^*}\right) \qquad (2.2\text{-}1)$$

Defining equation for vorticity

$$\xi^* = E_s^{*2}\psi^*/r^*\sin\theta \qquad (2.2\text{-}2)$$

Continuity equation of heat or mass

$$\left[\frac{\partial\psi^*}{\partial r^*}\frac{\partial\eta^*}{\partial\theta} - \frac{\partial\psi^*}{\partial\theta}\frac{\partial\eta^*}{\partial r^*}\right] = \frac{2r^{*2}\sin\theta}{Pe}\left(\frac{\partial^2\eta^*}{\partial r^{*2}} + \frac{2}{r^*}\frac{\partial\eta^*}{\partial r^*} + \frac{1}{r^{*2}}\frac{\partial^2\eta^*}{\partial\theta^2}\right.$$

$$\left. + \frac{\cot\theta}{r^{*2}}\frac{\partial\eta^*}{\partial\theta}\right) \qquad (2.2\text{-}3)$$

2.2.1 Pertinent Equations for Drag Coefficients and Nusselt (Sherwood) Numbers

Surface Pressure Distribution:

Integration of the θ-component of the equation of motion from the frontal stagnation point over the surface along the parametric line $r^* = 1$ gives the surface pressure distribution

$$P^*_{(\theta)} = P^*_o + \frac{4}{Re}\int_o^\theta \left(\frac{\partial\xi^*}{\partial r^*} + \xi^*\right)\Big|_{r^*=1} d\theta \qquad (2.2\text{-}4)$$

where P^*_o, is the frontal stagnation pressure, is obtained by integrating

the r-component of the equation of motion along the line $\theta=0°$, and can be expressed as

$$P^*_o = 1 + \frac{8}{Re}\int_1^\infty \left(\frac{\partial \xi^*}{\partial \theta}\right)_{|\theta=o} \frac{dr^*}{r^*} \qquad (2.2\text{-}5)$$

Form Drag Coefficient:

Integration of surface pressure distribution over the sphere surface gives the form (or pressure) drag coefficient as

$$C_{DP} = \int_o^\pi P^*_{(\theta)}{}_{|r^*=1} \sin 2\theta d\theta \qquad (2.2\text{-}6)$$

Friction Drag Coefficient:

Integration of surface vorticity distribution over the sphere surface gives the friction drag coefficient as

$$C_{DF} = \frac{8}{Re}\int_o^\pi \xi^*{}_{|r^*=1} \sin^2\theta d\theta \qquad (2.2\text{-}7)$$

and the total drag coefficient is

$$C_D = C_{DF} + C_{DP} \qquad (2.2\text{-}8)$$

Local Nusselt or Sherwood Number:

The local Nusselt or Sherwood number can be written as

$$Nu(\theta) \text{ or } Sh(\theta) = -2\frac{\partial \eta^*}{\partial r^*}{}_{|r^*=1} \qquad (2.2\text{-}9)$$

Average Nusselt or Sherwood Number:

Integration of $Nu(\theta)$ or $Sh(\theta)$ over the sphere surface gives the average Nusselt or Sherwood number

$$Nu \text{ or } Sh = \int_o^\pi \left(-\frac{\partial \eta^*}{\partial r^*}\right)_{|r^*=1} \sin\theta d\theta \qquad (2.2\text{-}10)$$

2.3 Cross Flow to an Infinite Circular Cylinder

2.3.1 Governing Equations for Field Functions

The dimensionless vorticity transport equations, defining equation of vorticity, and the continuity equation of energy or mass for cross flow over an infinite circular cylinder written in cylindrical polar coordinates (see Figure 2.2-1) with the following dimensionless groups and variables

$$Re = \frac{d\,U_\infty}{\nu} \quad , \quad Pe = \frac{d\,U_\infty \rho\, C_p}{k} \quad , \quad Gr = d^3 \beta\, g\,(T_s - T_\infty)/\nu^2$$

$$r^* = r/R \quad , \quad \psi^* = \psi/U_\infty R \quad , \quad \xi^* = \xi R/U_\infty \quad , \quad \eta^* = \frac{T - T_\infty}{T_s - T_\infty}$$

are

Vorticity Transport Equation

$$\left[\frac{\partial \psi^*}{\partial r^*}\frac{\partial \xi^*}{\partial \theta} - \frac{\partial \psi^*}{\partial \theta}\frac{\partial \xi^*}{\partial r^*}\right] = \frac{2r^*}{Re} E_c^{*2}\xi^* + \frac{Gr}{2Re^2}\left(\cos\theta \frac{\partial \eta^*}{\partial \theta} + r^* \sin\theta \frac{\partial \eta^*}{\partial r^*}\right) \qquad (2.3\text{-}1)$$

Defining Equation for Vorticity

$$\xi^* = E_c^{*2}\psi^* \qquad (2.3\text{-}2)$$

Continuity Equation of Heat or Mass

$$\left[\frac{\partial \psi^*}{\partial r^*}\frac{\partial \eta^*}{\partial \theta} - \frac{\partial \psi^*}{\partial \theta}\frac{\partial \eta^*}{\partial r^*}\right] = \frac{2r^*}{Pe}\left(\frac{\partial^2 \eta^*}{\partial r^{*2}} + \frac{1}{r^*}\frac{\partial \eta^*}{\partial r^*} + \frac{1}{r^{*2}}\frac{\partial^2 \eta^*}{\partial \theta^2}\right) \qquad (2.3\text{-}3)$$

2.3.2 Pertinent Equations for Drag Coefficients and Nusselt (Sherwood) Numbers

Surface Pressure Distribution:

Integration of the θ-component of the equation of motion from the frontal stagnation point over the surface along the parametric line $r^*=1$ gives the surface pressure distribution

$$P^*_{(\theta)} = P^*_o + \frac{4}{Re}\int_o^{\theta} \frac{\partial \xi^*}{\partial r^*}\Big|_{r^*=1} d\theta \qquad (2.3\text{-}4)$$

where P^*_o is the frontal stagnation pressure, is obtained by integrating the r-component of the equation of motion along the line $\theta=0°$ and can be expressed as

$$P^*_o = 1 + \frac{4}{Re}\int_1^{\infty} \frac{\partial \xi^*}{\partial \theta}\Big|_{\theta=o} \frac{dr^*}{r^*} \qquad (2.3\text{-}5)$$

Form Drag Coefficient:

Integration of surface pressure distribution over the cylinder surface gives the form (or pressure) drag coefficient as

$$C_{DP} = \int_o^{\pi} P^*(\theta)\Big|_{r^*=1} \cos\theta d\theta \qquad (2.3\text{-}6)$$

Friction Drag Coefficient:

Integration of surface vorticity distribution over the cylinder surface gives the friction drag coefficient as

$$C_{DF} = \frac{4}{Re}\int_o^{\pi} \xi^*\Big|_{r^*=1} \sin\theta d\theta \qquad (2.3\text{-}7)$$

and the total drag coefficient is

$$C_D = C_{DF} + C_{DP} \qquad (2.3\text{-}8)$$

Local Nusselt or Sherwood Number:

The local Nusselt or Sherwood number can be written as

$$Nu(\theta) \text{ or } Sh(\theta) = -2\frac{\partial \eta^*}{\partial r^*}\Big|_{r^*=1} \qquad (2.3\text{-}9)$$

Average Nusselt or Sherwood Number:

Integration of Nu(θ) or Sh(θ) over the cylinder surface gives the average Nusselt or Sherwood number

$$\text{Nu or Sh} = \frac{2}{\pi} \int_0^{\pi} \left(-\frac{\partial \eta^*}{\partial r^*}\right)\Big|_{r^*=1} d\theta \qquad (2.3\text{-}10)$$

Mixed convection problems can be classified as two types, namely aiding flow and opposing flow. If the free convection current is in the same direction as the forced convection stream, the flow is aiding otherwise the flow is opposing. Aiding and opposing flow can be classified from the sign of the Grashof number in the vorticity transport equation, positive Grashof number refers to aiding flow whereas negative Grashof number indicates opposing flow.

3. MATHEMATICAL ANALYSIS AND METHODS OF SOLUTION

3.1 Coordinate Transformation

The solution of the transport equations derived in the previous section can be obtained only through numerical means because of their non-linearity (asymptotic solutions which are available in the limiting ranges of the parameters are not taken into account). Finite difference techniques are the most powerful available for problems of this complexity and these will be used here.

In the study of convective flows around a blunt object, the changes in the field functions ψ^*, ξ^* and η^* through the whole domain of interest must be investigated. Generally, the gradients in the normal direction of ψ^*, ξ^* and η^* near the surface of the object are large (especially for high Re, Pr and Gr systems). Far from the surface, these gradients are small. As a result, in carrying out finite difference calculations, a non-uniform mesh system - small near the surface, large away from the surface - should be used in the domain of the solution. For the sake of simplifying the mathematical formulation and numerical calculation, the transformation

$$r^* = e^z$$

is used such that a constant step change in the transformed coordinate z will give an exponential step change in the real physical coordinate r^*. A constant step size in θ is adopted in this study. Figure 3.1-1 illustrates the transformed rectangular domain and the real physical domain.

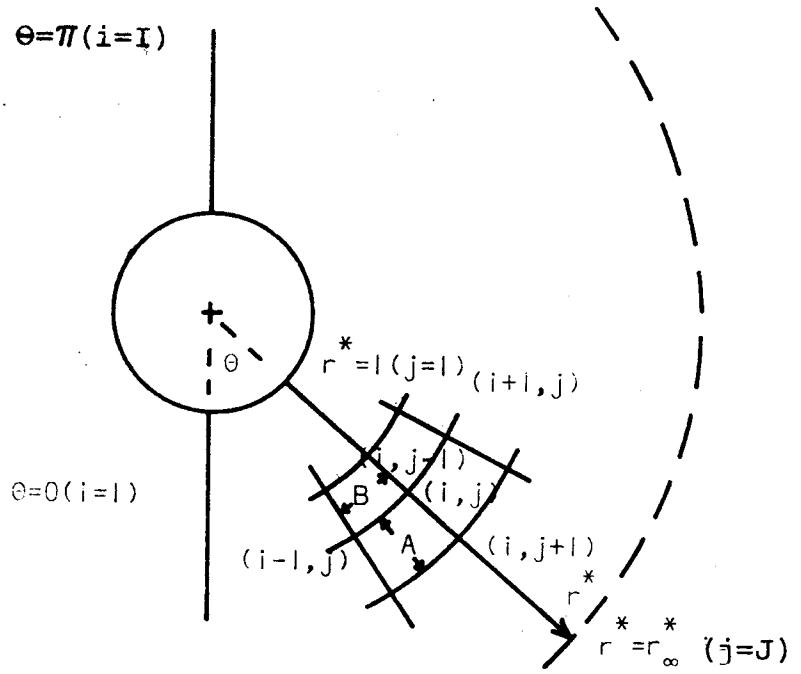

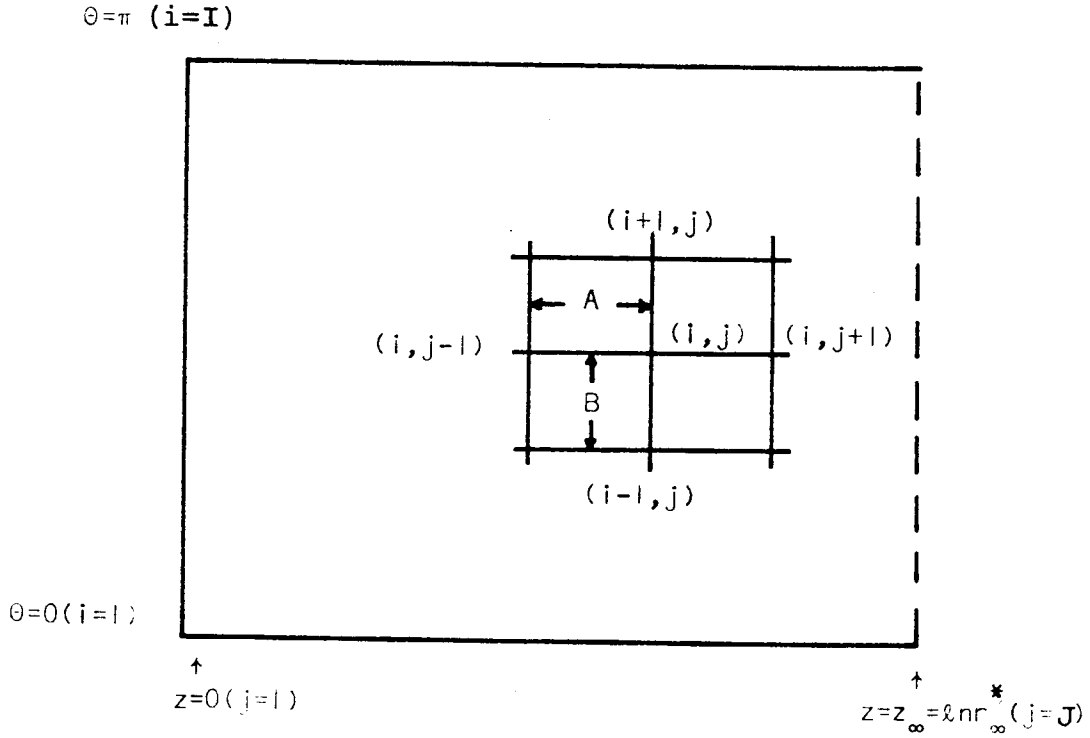

FIGURE 3.1-1 REAL AND TRANSFORMED MESH SYSTEMS USED IN THE PRESENT FINITE DIFFERENCE METHOD

The governing transport equations for ψ^*, ξ^* and η^* and the pertinent equations for calculating fluid mechanical and heat or mass transfer properties in the transformed coordinate (θ,z) are listed in Table (3.1-1) and (3.1-2).

3.2 Finite Difference Approximations

Finite differential representations for partial derivatives can be found in any standard texts. In accordance with the recommendations of Russell (1962) and Lapidus (1962), small molecule formulae are preferred to large molecule formula as being more suitable for digital computer calculations. In this study, central differences of a five point molecule were used for the approximations of the partial derivatives which is accurate to second order. These finite difference approximations of the partial derivatives, according to mesh point system in Figure 3.1-1 for a general field function F are

in z direction

$$\frac{\partial F}{\partial z} = \frac{F_{(i,j+1)} - F_{(i,j-1)}}{2A}, \quad \frac{\partial^2 F}{\partial z^2} = \frac{F_{(i,j+1)} - 2F_{(i,j)} + F_{(i,j-1)}}{A^2}$$

in θ direction

$$\frac{\partial F}{\partial \theta} = \frac{F_{(i+1,j)} - F_{(i-1,j)}}{2B}, \quad \frac{\partial^2 F}{\partial \theta^2} = \frac{F_{(i+1,j)} - 2F_{(i,j)} + F_{(i-1,j)}}{B^2}$$

These finite difference representations of partial derivatives are then substituted into equations in Tables (3.1-1) and (3.1-2) and the resulting difference equations are listed in Tables (3.2-1) and (3.2-2).

Table 3.1-1 Transport and Other Pertinent Equations for Sphere in Coordinates (θ, z)

Vorticity transport equation:

$$\left[\frac{\partial\psi^*}{\partial z}\frac{\partial}{\partial\theta}\left(\frac{\xi^*}{e^z\sin\theta}\right) - \frac{\partial\psi^*}{\partial\theta}\frac{\partial}{\partial z}\left(\frac{\xi^*}{e^z\sin\theta}\right)\right] e^z\sin\theta$$

$$= \frac{2}{Re} E_{sz}^{*2} (\xi^* e^z \sin\theta) + \frac{e^{2z} Gr}{2Re^2} \left(\cos\theta\sin\theta \frac{\partial\eta^*}{\partial\theta} + \sin^2\theta \frac{\partial\eta^*}{\partial z}\right)$$

Defining equation for vorticity:

$$\xi^* = E_{sz}^{*2}\psi^*/e^{3z}\sin\theta$$

Continuity equation of heat or mass:

$$\left[\frac{\partial\psi^*}{\partial z}\frac{\partial\eta^*}{\partial\theta} - \frac{\partial\psi^*}{\partial\theta}\frac{\partial\eta^*}{\partial z}\right] = \frac{2e^z\sin\theta}{Pe}\left(\frac{\partial^2\eta^*}{\partial z^2} + \frac{\partial^2\eta^*}{\partial\theta^2} + \frac{\partial\eta^*}{\partial z} + \cot\theta\frac{\partial\eta^*}{\partial\theta}\right)$$

Frontal Stagnation pressure:

$$P_o^* = 1 + \frac{8}{Re}\int_o^\infty \left(\frac{\partial\xi^*}{\partial\theta}\right)\Big|_{\theta=o} dz$$

Surface pressure distribution:

$$P_{(\theta)}^* = P_o^* + \frac{4}{Re}\int_o^\theta \frac{\partial\xi^*}{\partial z} + \xi^*)\Big|_{z=o} d\theta$$

Form drag coefficient:

$$C_{DP} = \int_o^\pi P_{(\theta)}^* \sin^2\theta d\theta$$

Friction drag coefficient:

$$C_{DF} = \frac{8}{Re}\int_o^\pi \xi^*\Big|_{z=o} \sin^2\theta d\theta$$

Table 3.1-1 (Cont'ed)

Local Nusselt or Sherwood Number:

$$Nu(\theta) \text{ or } Sh(\theta) = -2 \frac{\partial \eta^*}{\partial z} \Big|_{z=o}$$

Average Nusselt or Sherwood Number:

$$Nu \text{ or } Sh = \int_o^{\pi} \left(-\frac{\partial \eta^*}{\partial z}\right)_{z=o} \sin\theta d\theta$$

Table 3.1-2 Transport and Other Pertinent Equations for Cylinder in Coordinates (θ, z)

Vorticity transport equation:

$$\left(\frac{\partial \psi^*}{\partial z}\frac{\partial \xi^*}{\partial \theta} - \frac{\partial \psi^*}{\partial \theta}\frac{\partial \xi^*}{\partial z}\right) = \frac{2}{Re} E^{*2}_{cz}\xi^* + \frac{e^z Gr}{\partial Re^2}\left(\cos\theta \frac{\partial \eta^*}{\partial \theta} + \sin\theta \frac{\partial \eta^*}{\partial z}\right)$$

Defining equation for vorticity:

$$E^{*2}_{cz}\psi^* = e^{2z}\xi^*$$

Continuity equation of heat or mass:

$$\left(\frac{\partial \psi^*}{\partial z}\frac{\partial \eta^*}{\partial \theta} - \frac{\partial \psi}{\partial \theta}\frac{\partial \eta^*}{\partial z}\right) = \frac{2}{Pe}\left(\frac{\partial^2 \eta^*}{\partial z^2} + \frac{\partial^2 \eta^*}{\partial \theta^2}\right)$$

Frontal stagnation pressure:

$$P^*_o = 1 + \frac{4}{Re}\int_0^\infty \left(\frac{\partial \xi^*}{\partial \theta}\right)\Big|_{\theta=o} dz$$

Surface pressure distribution:

$$P^*_{(\theta)} = P^*_o + \frac{4}{Re}\int_o^\theta \frac{\partial \xi^*}{\partial z}\Big|_{z=o} d\theta$$

Form drag coefficient:

$$C_{DP} = \int_o^\pi P^*_{(\theta)}\Big|_{z=o} \cos\theta d\theta$$

Friction drag coefficient:

$$C_{DF} = \frac{4}{Re}\int_o^\pi \xi^*\Big|_{z=o} \sin\theta d\theta$$

Table 3.1-2 (Cont'ed)

Local Nusselt or Sherwood Number:

$$Nu(\theta) \text{ or } Sh(\theta) = -2 \left.\frac{\partial \eta^*}{\partial z}\right|_{z=o}$$

Average Nusselt of Sherwood Number:

$$Nu \text{ or } Sh = -\frac{2}{\pi} \int_o^{\pi} \left.\frac{\partial \eta^*}{\partial z}\right|_{z=o} d\theta$$

Table 3.2-1 Finite Difference Equations for Sphere

Vorticity transport equation:

$$G_{(i,j)}\left(\frac{A^2+B^2}{A^2B^2}\right) = \{G_{(i,j+1)}\left(\frac{2-A}{4A^2}\right) + G_{(i,j-1)}\left(\frac{2+A}{4A^2}\right) + G_{(i+1,j)}\left(\frac{2-B\cot\theta(i)}{4B^2}\right)$$

$$+ G_{(i-1,j)}\left(\frac{2+B\cot\theta(i)}{4B^2}\right) + \frac{Gr}{Re}\frac{e^{2z(j)}}{16AB}[\cos\theta(i)\sin\theta(i)A$$

$$(\eta^*_{(i+1,j)} - \eta^*_{(i-1,j)}) + \sin^2\theta(i)B(\eta^*_{(i,j+1)} - \eta^*_{(i,j-1)}]$$

$$- \frac{Re}{16AB}e^{z(j)}\sin\theta(i)[\psi^*_{(i,j+1)} - \psi^*_{(i,j-1)})(H_{(i+1,j)} - H_{(i-1,j)})$$

$$- (\psi^*_{(i+1,j)} - \psi^*_{(i-1,j)})(H_{(i,j+1)} - H_{(i,j-1)})]\}$$

where $G_{(i,j)} = \xi^*_{(i,j)}\, e^{z(j)}\, \sin\theta(i)$

$H_{(i,j)} = \xi^*_{(i,j)}/e^{z(j)}\, \sin\theta(i)$

Defining equation for vorticity:

$$\psi^*_{(i,j)}\left(\frac{A^2+B^2}{A^2B^2}\right) = \{\psi^*_{(i,j+1)}\left(\frac{2-A}{4A^2}\right) + \psi^*_{(i,j-1)}\left(\frac{2+A}{4A^2}\right) - G_{(i,j)}\, e^{2z(j)}$$

$$+ \psi^*_{(i+1,j)}\left(\frac{2-B\cot\theta(i)}{4B^2}\right) + \psi^*_{(i-1,j)}\left(\frac{2+B\cot\theta(i)}{4B^2}\right)\}$$

Continuity equation of heat or mass:

$$\eta^*_{(i,j)}\left(\frac{A^2+B^2}{A^2B^2}\right) = \{\eta^*_{(i+1,j)}\left[\frac{2+B\cot\theta(i)}{4B^2} - \frac{Pe(\psi^*_{(i,j+1)} - \psi^*_{(i,j-1)})}{16ABe^{z(j)}\sin\theta(i)}\right]$$

$$+ \eta^*_{(i-1,j)}\left[\frac{2-B\cot\theta(i)}{4B^2} + \frac{Pe(\psi^*_{(i,j+1)} - \psi^*_{(i,j-1)})}{16ABe^{z(j)}\sin\theta(i)}\right]$$

Table 3.2-1 (Cont'ed)

$$+ \eta^*_{(i,j+1)}\left[\frac{2+A}{4A^2} + \frac{Pe(\psi^*_{(i+1,j)} - \psi^*_{(i-1,j)})}{16ABe^{z(j)}\sin\theta(i)}\right]$$

$$+ \eta^*_{(i,j-1)}\left[\frac{2-A}{4A^2} - \frac{Pe(\psi^*_{(i+1,j)} - \psi^*_{(i-1,j)})}{16ABe^{z(j)}\sin\theta(i)}\right]\}$$

Frontal stagnation pressure

$$P^*_o = 1 + \frac{8}{Re}\sum_{j=1}^{j=J}\frac{(4\xi^*_{(2,j)} - \xi^*_{(3,j)} - 3\xi^*_{(1,j)})A}{2B}$$

Surface pressure distribution

$$P^*_{(i)} = P^*_o + \frac{4}{Re}\sum_{i=1}^{i}\left(\frac{4\xi^*_{(i,2)} - \xi^*_{(i,3)} - 3\xi^*_{(i,1)}}{2A} + \xi^*_{(i,1)}\right) B$$

Form drag coefficient

$$C_{DP} = \sum_{i=1}^{i=I} P^*_{(i)} \sin 2\theta(i)\, B$$

Friction drag coefficient

$$C_{DF} = \frac{8}{Re}\sum_{i=1}^{i=I} \xi^*_{(i,1)} \sin^2\theta(i)\, B$$

Local Nusselt or Sherwood Number:

$$Nu(i) \text{ or } Sh(i) = \frac{3\eta^*_{(i,1)} + \eta^*_{(1,3)} - 4\eta^*_{(i,2)}}{A}$$

Average Nusselt or Sherwood Number:

$$Nu \text{ or } Sh = \sum_{i=1}^{i=I}\frac{3\eta^*_{(i,1)} + \eta^*_{(i,3)} - 4\eta^*_{(i,2)}}{2A}\sin\theta(i)\, B$$

Table 3.2-2 Finite Difference Equations for Cylinder

Vorticity transport equation

$$\xi^*_{(i,j)}\left(\frac{A^2+B^2}{A^2B^2}\right) = \left\{\frac{\xi^*_{(i,j+1)} + \xi^*_{(i,j-1)}}{2A^2} + \frac{\xi^*_{(i+1,j)} + \xi^*_{(i-1,j)}}{2B^2} + \right.$$

$$+ \frac{Gr}{Re^2}\frac{e^z}{16AB}\left(\cos\theta(i)\left(\eta^*_{(i+1,j)} - \eta^*_{(i-1,j)}\right)A\right.$$

$$+ \sin\theta(i)\left(\eta^*_{(i,j+1)} - \eta^*_{(i,j-1)}\right)B$$

$$- \frac{Re}{16AB}\left[\left(\psi^*_{(i,j+1)} - \psi^*_{(i,j-1)}\right)\left(\xi^*_{(i+1,j)} - \xi^*_{(i-1,j)}\right)\right.$$

$$\left.\left. - \left(\psi^*_{(i+1,j)} - \psi^*_{(i-1,j)}\right)\left(\xi^*_{(i,j+1)} - \xi^*_{(i,j-1)}\right)\right]\right\}$$

Defining equation for vorticity:

$$\psi^*_{(i,j)}\left(\frac{A^2+B^2}{A^2B^2}\right) = \left[\frac{\psi^*_{(i,j+1)} + \psi^*_{(i,j-1)}}{2A^2} + \frac{\psi^*_{(i+1,j)} + \psi^*_{(i-1,j)}}{2B^2}\right.$$

$$\left. - \xi^*_{(i,j)}\, e^{2z(j)}/2\right]$$

Continuity equation of heat or mass

$$\eta^*_{(i,j)}\left(\frac{A^2+B^2}{A^2B^2}\right) = \left\{\frac{\eta^*_{(i,j+1)} - \eta^*_{(i,j-1)}}{2A^2} + \frac{\eta^*_{(i+1,j)} - \eta^*_{(i-1,j)}}{2B^2}\right.$$

$$- \frac{Pe}{16AB}\left[\left(\psi^*_{(i,j+1)} - \psi^*_{(i,j-1)}\right)\left(\eta^*_{(i+1,j)} - \eta^*_{(i-1,j)}\right)\right.$$

$$\left.\left. - \left(\psi^*_{(i+1,j)} - \psi^*_{(i-1,j)}\right)\left(\eta^*_{(i,j+1)} - \eta^*_{(i,j-1)}\right)\right]\right\}$$

Table 3.2-2 (Cont'ed)

Frontal stagnation pressure

$$P^*_o = 1 + \frac{4}{Re} \sum_{j=1}^{j=J} \frac{(4\xi^*(2,j) - \xi^*(3,j) - 3\xi^*(1,j)) A}{2B}$$

Surface pressure distribution

$$P^*(i) = P^*_o + \frac{4}{Re} \sum_{i=1}^{i} \frac{(4\xi^*(i,2) - \xi^*(i,3) - 3\xi^*(i,1)) B}{2A}$$

Form drag coefficient

$$C_{DP} = \sum_{i=1}^{i=I} P^*(i) \cos\theta(i) B$$

Friction drag coefficient

$$C_{DF} = \frac{4}{Re} \sum_{i=1}^{i=I} \xi^*(i,1) \sin\theta(i) B$$

Local Nusselt or Sherwood Number:

$$Nu(i) \text{ or } Sh(i) = \frac{3\eta^*(i,1) + \eta^*(i,3) - 4\eta^*(i,2)}{A}$$

Average Nasselt or Sherwood Number:

$$Nu \text{ or } Sh = \frac{2}{\pi} \sum_{i=1}^{i=I} \left(\frac{3\eta^*(i,1) + \eta^*(i,3) - 4\eta^*(i,2)}{2A} \right) B$$

3.3 Methods of Solution and Convergence Acceleration Techniques

3.3.1 Iterative Solution of a Large Set of Algebraic Equations

The solution of field functions ψ^*, ξ^* and η^* at every mesh point in the domain of interest can be obtained by solving sets of difference equations taken from Tables 3.2-1 and 3.2-2. This solution can be obtained either by a direct method or by an indirect method. The direct method of solution is to invert the coefficient matrix by elimination and the indirect method is by iteration. The direct method is the most efficient approach available for small sets of equations; it is not for large sets. The procedure requires $2N^2$ arithmetic operations to solve N equations of the type being considered. When N becomes relatively large, it is more efficient to use an iterative procedure for solving the equations. In addition to computational efficiency, iterative procedures possess other advantages over the elimination method. In computer applications they require much smaller memory capacity for storage of intermediate data, and they are easier to program. Furthermore, they are applicable to nonlinear sets of equations, whereas solution by elimination is not. As a result of these several advantages, iterative procedures are generally preferred for solutions of the moderate to large sets of equations encountered in problems of this study.

The most elementary iterative method available is the relaxation method. Among these relaxation methods, the most successfull and frequently used is successive overrelaxation (SOR) (Young 1954) and alternating direction implicit iteration (ADI) (Peaceman and Rachford 1955).

Many other relaxation methods are described in the text by Varga (1962).

SOR, also known as extrapolated Liebman method (Frankel 1950), involves the use of a single iterative parameter (other terms for iterative parameter, often used are forcing parameter, marching or movement factor). This iterative parameter is usually called relaxation factor. In most cases, the choice of this relaxation factor can only be made by trial and error. If the optimum choice is made, SOR is quite fast and the amount of computing required is proportional to $N^{3/2}$, where N is the number of equations in the set. Unfortunately, this optimum value of the relaxation factor is unknown for most problems.

ADI, in some simple cases, is a great deal more efficient than SOR. The best treatment of ADI is that the computing work required is proportional to N&nN. But again this efficiency extends only in part to more complex problems. In extreme cases, solutions obtained by ADI converge very slowly or not at all. One reason for this slow convergence is that ADI requires the selection of a set of iteration parameters to be applied cyclically during the iteration. For a very simple problem there exists a theoretical basis for selection of this set of iteration parameter that will give rapid convergence (Varga 1962), but for the general case no practical basis exists, thus, ADI frequently is applied with non-optimal sets of iteration parameters.

A qualitative explanation of the higher convergence rates achieved by ADI is that this method is more implicit than SOR. Stated another way, each step of ADI is more closely related to direct solution by elimination than is the step of SOR.

3.3.2 The Iterative Parameter (Relaxation Factor)

The relaxation factor W in iterative processes plays an important role in determining the rate of convergence of the solution. An optimum value of this factor usually exists and results in the fastest convergence rate, however for most cases, there exists no theoretical basis for calculating this relaxation factor, except for the particular case of a square grid system (Lapidus 1962). In general the optimum relaxation factor can only be obtained by trial and error. Moreover, this optimum may vary from point to point in the grid system. In this study, W varies from point to point except for the Poisson equation (defining equation for vorticity), which is linear and known to have excellent convergence properties. This is in contrast to the studies of Hamielec et.al. (1967, 1969, 1970) where uniform relaxation factors over the entire grid field were used. The use of a uniform relaxation factor in iteration procedures must be questioned, because at some locations of the domain of interest, the residual from iteration to iteration of the field function is extremely large and requires a very small relaxation factor for stabilization, whereas, at other locations, this residual is small and a relatively large relaxation factor should be employed. The use of a small relaxation factor slows down the convergence rate and the use of a large relaxation factor can cause the solution to diverge. In the case of the solution of non-linear difference equations, the relaxation factor can vary from iteration to iteration as well, a point to be discussed later. In this study, several cases have been investigated to examine the effect of varying relaxation factors, and in general it was found

that a varying relaxation factor gave significantly faster convergence rates.

Russell (1962) in studying solutions of the Navier Stokes equation for flow over flat plates, used a square grid system and suggested that the relaxation factor for the Poisson's equation can be selected as uniform over the entire field and the relaxation factor for the vorticity transport equation should vary from point to point and from iteration to iteration. The equation used to calculate the relaxation factor employed by Russell is an approximate one obtained by analysing the linearized vorticity transport equation. It cannot be applied directly to problems of this study, because of the rectangular grid system employed here. Russell's formulas for relaxation factor which do not include the effect of step size are rather oversimplified The step size is known to have a significant effect on stability as well as relaxation factor (Hamielec, Johnson and Houghton 1967).

A general second-order elliptic partial differential equation can be expressed in the form

$$\nabla^2_{xy} F = P \frac{\partial F}{\partial x} + Q \frac{\partial F}{\partial y} \qquad (3.3\text{-}1)$$

where P, Q are functions of x,y and F. The modification of Russell's formula for the relaxation factors in the rectangular grid system taking into account both the physical parameters and step sizes is of the form

$$W_{F(i,j)} = 2/\{1 + [0.5(P^2 + Q^2)]^{\frac{1}{2}}\} \qquad (3.3\text{-}2)$$

According to this equation, the formulae for relaxation factors for sphere and cylinder are as follows

Sphere

$$W^*_{\xi(i,j)} = 2/\{1 + \frac{Re\, e^{z(i)} \sin\theta(i)}{8}\left[\left(\frac{\psi^*_{(i,j+1)} - \psi^*_{(i,j-1)}}{2A}\right)^2 + \left(\frac{\psi^*_{(i+1,j)} - \psi^*_{(i-1,j)}}{2B}\right)^2\right]^{1/2}\} \qquad (3.3\text{-}3)$$

$$W^*_{\eta(i,j)} = 2/\{1 + \frac{Pe}{8e^{z(i)}\sin\theta(i)}\left[\left(\frac{\psi^*_{(i,j+1)} - \psi^*_{(i,j-1)}}{2A}\right)^2 + \left(\frac{\psi^*_{(i+1,j)} - \psi^*_{(i-1,j)}}{2B}\right)^2\right]^{1/2}\} \qquad (3.3\text{-}4)$$

Cylinder

$$W^*_{\xi(i,j)} = 2/\{1 + \frac{Re}{8}\left[\left(\frac{\psi^*_{(i,j+1)} - \psi^*_{(i,j-1)}}{2A}\right)^2 + \left(\frac{\psi^*_{(i+1,j)} - \psi^*_{(i-1,j)}}{2B}\right)^2\right]^{1/2}\} \qquad (3.3\text{-}5)$$

$$W^*_{\eta(i,j)} = 2/\{1 + \frac{Pe}{8}\left[\left(\frac{\psi^*_{(i,j+1)} - \psi^*_{(i,j-1)}}{2A}\right)^2 + \left(\frac{\psi^*_{(i+1,j)} - \psi^*_{(i-1,j)}}{2B}\right)^2\right]^{1/2}\} \qquad (3.3\text{-}6)$$

These relaxation factors when applied to problems of viscous flow around a sphere or a cylinder, forced convection around a sphere and a cylinder and mixed convection around a sphere generally gave faster convergence rates, although they are by no means optimum. They are, however, easy to use in a computer program and give reasonably rapid solution. The relaxation factor for the Poisson's equation according to Russell (1962) is

$$W^*_{\psi} = \frac{2}{1 + \pi^2 \sqrt{(I^{-2} + J^{-2})^{1/2}}} \qquad (3.3\text{-}7)$$

The application of these varying relaxation factors to iterative solutions of elliptic partial differential equations gave the greatest saving in computation time for the case of the linear elliptic partial differential equation (e.g. forced convection around a sphere and a cylinder) where (P, Q) are already known and $W_{\eta^*(i,j)}$ in equations (3.3-4) and (3.3-6) can be calculated and stored for permanent use and no additional computer time is required. For the case of non-linear elliptic equations, the calculation of $W_{\eta^*(i,j)}$ and $W_{\xi^*(i,j)}$ during every iteration is time consuming. However, one can avoid this difficiency by calculating $W_{\eta^*(i,j)}$ and $W_{\xi^*(i,j)}$ every M iterations ($M \geq 20$), since the Poisson equation for calculating ψ^* is linear and is known to have excellent convergence properties. From computer experience with the solution of problems of this nature ψ^* does converge faster than ξ^* or η^*, and investigations of $W_{\eta^*(i,j)}$ and $W_{\xi^*(i,j)}$ every M fold iterations indicate that they do not vary too much. In reality this procedure is just an approximate method for reducing computer time. One can ensure a better approximation by employing a small M.

Several studies were made to investigate the effect of varying the relaxation factor in the grid system. For low Prandtl numbers and small r_∞^*, a considerably larger relaxation factor can be used and a selection of uniform relaxation factor over the whole field is quite adequate and the solution converges very rapidly. The situations become worse when the Prandtl number and r_∞^* increase, very small W_{η^*}must be used in order to stabilize the iterative process. Table 3.3-I indicates the variation of W_{η^*}in the grid field for forced convection around a

sphere at Re = 57, Pr = 5 and r^*_∞ = 3.32 according to equation (3.3-4). W_{η^*} decreases monotonically with increasing r*. It is understandable that near the surface the grid dimension in the physical coordinates (r, θ) is small whereas near the outer boundary it is large because of the transformation $r^* = e^z$. It is known that the smaller the grid size the larger the relaxation factor that can be accepted. Near the separation point, the relaxation factor is quite large; this is because of the small gradients existing around this point. The extremely small W_{η^*} near the outer boundary is the main reason why the use of a uniform relaxation factor must be chosen as low as 0.006 in order to get the iterative process going. The rate of convergence is extremely slow and it is estimated that 20 times more computation time is required with a uniform relaxation factor of 0.006 than with the varying relaxation factor of Table 3.3-1.

For the case of non-linear elliptic partial differential equations (viscous flow around a sphere and a cylinder and mixed convection around a sphere), the same conclusions apply. Table 3.3-2 shows the variation of $W_{\xi^*(i,j)}$ with r* and θ at the final stage of iterative solution of viscous flow around a cylinder at Re = 40. Small W_{ξ^*} is found near the outer boundary and large W_{ξ^*} near the surface especially at the flow separation point. With the calculations for mixed convection around a sphere, the varying relaxation factor method provides faster convergence; however not as pronounced as the other cases because of the low Prandtl and Reynolds numbers involved. Solutions take about half the time using the variable relaxation factors.

Table 3.3-1 $W_{\eta^*(i,j)}$ Sphere

Re=57, Pr=5, r^*_∞=3.32

θ°	r*	1.05	1.22	1.49	1.82	2.23	2.72	3.32
12		0.163	0.045	0.022	0.014	0.010	0.008	0.007
24		0.092	0.031	0.019	0.013	0.010	0.008	0.007
36		0.068	0.023	0.016	0.013	0.010	0.008	0.007
48		0.059	0.020	0.014	0.012	0.010	0.008	0.006
60		0.057	0.018	0.013	0.011	0.009	0.007	0.006
72		0.061	0.018	0.012	0.010	0.009	0.007	0.006
84		0.072	0.020	0.012	0.010	0.008	0.007	0.006
96		0.095	0.023	0.013	0.010	0.008	0.007	0.006
108		0.145	0.024	0.014	0.010	0.008	0.007	0.006
120		0.261	0.037	0.019	0.011	0.008	0.007	0.006
132		0.606	0.069	0.030	0.014	0.009	0.007	0.006
144		1.505	0.171	0.059	0.023	0.012	0.008	0.006
156		0.864	0.826	0.173	0.051	0.023	0.012	0.009
168		0.943	0.456	0.661	0.202	0.059	0.026	0.016

Table 3.3-2 $W_{\xi(i,j)}$ Cylinder

Re = 40, r^*_∞ = 59.4

θ°	r*	1.082	2.028	4.111	8.336	16.90	34.27
12		0.326	0.054	0.020	0.009	0.004	0.002
24		0.207	0.047	0.019	0.009	0.004	0.002
36		0.162	0.041	0.019	0.009	0.004	0.002
48		0.146	0.036	0.018	0.009	0.004	0.002
60		0.145	0.033	0.017	0.008	0.004	0.002
72		0.160	0.031	0.016	0.008	0.004	0.002
84		0.195	0.029	0.016	0.008	0.004	0.002
96		0.263	0.029	0.016	0.008	0.004	0.002
108		0.392	0.031	0.015	0.008	0.004	0.002
120		0.622	0.037	0.015	0.008	0.004	0.002
132		0.901	0.055	0.015	0.008	0.004	0.002
144		0.761	0.107	0.016	0.008	0.004	0.002
156		0.726	0.310	0.028	0.008	0.004	0.002
168		0.792	0.434	0.114	0.015	0.004	0.002

One concludes that the relaxation factors given by equations (3.3-2) to (3.3-7) provide rapid convergence rates and can be taken as a guide for choosing W's for other problems. This is preferable to choosing W's by trial and error, of course they are by no means optimum and there is no theoretical expression available to calculate optimum values. In the calculation a damping factor α whose value lies between 0 and 1 can be introduced into equations (3.3-2) to (3.3-7) in case the system diverges. The proper value of α can be chosen based on the history of the initial several iterations.

3.3.3 Convergence Acceleration Technique

The dominant eigenvalue method of convergence promotion of iterative processes developed by Orbach and Crowe (1971) was used to accelerate the iterative solution of problems of this study. The method itself is essentially a generalization of the linear extrapolation method of Aitken (1925, 1936) and Wegstein (1958). The application of this method of accelerating iterative solutions of non-linear as well as linear algebraic equations for the present study has been very successful when new sequences of calculation are employed to the iterative processes. Moreover, the dominant eigenvalue method is very simple to apply in computer calculations.

If $\bar{f} = (f_1, f_2, f_3 \text{ --- } f_m)$ is the input vector, or initial guess vector, and $\bar{f}_o = (f_{o1}, f_{o2}, f_{o3} \text{ --- } f_{om})$ is the output vector which is related by

$$\bar{f}_o = \bar{\Phi}(\bar{f}) \qquad (3.3\text{-}8)$$

Any iterative process will lead to $\bar{f}_s$ such that

$$| \bar{f}_o - \bar{f}_s | \leq | \bar{\varepsilon} | \tag{3.3-9}$$

where $\bar{\varepsilon}$ is a tolerance vector which depends on the specified accuracy of the solution.

The general form of the iteration can be written as

$$\bar{f}_o^{\,n} = \bar{\Phi} (\bar{f}^n)$$

and
$$\bar{f}^{n+1} = \bar{f}^n + \bar{\bar{W}} (\bar{f}_o^{\,n} - \bar{f}^n) \equiv \bar{\Phi} (\bar{f}^n) \tag{3.3-10}$$

where n represents iteration number and $\bar{\bar{W}}$ is the matrix of relaxation factors and depends on n. Equation (3.3-10) is SOR with variable relaxation factor.

If equation (3.3-10) can be approximated sufficiently closely by a Taylor series accurate to first-order about an arbitrary point $\bar{f}_a$ in the neighbourhood of $\bar{f}^n$, i.e.

$$\bar{f}^{n+1} = \bar{\bar{C}} \bar{f}^n + \bar{b} \tag{3.3-11}$$

where
$$\bar{\bar{C}} = [\partial \bar{\Phi} / \partial \bar{f}]_{\bar{f}=\bar{f}_a}$$

$$\bar{b} = (\bar{\bar{I}} - \bar{\bar{C}}) \bar{f}_a \tag{3.3-12}$$

then the matrix $\bar{\bar{C}}$ can be evaluated using equation (3.3-12). This, however, required too much computation time and therefore an alternative approach was developed.

The necessary and sufficient condition that the iterative process represented by equation (3.3-11) to converge is

$$\lambda_1 \equiv \underset{k}{\text{Max}} \, | \lambda_k | < 1 \tag{3.3-13}$$

(Fadeeva 1959). λ_1 is the dominant eigenvalue. The solution of equation (3.3-11) can be written as

$$\bar{f}^n - \bar{f}_s = \bar{\bar{C}}^n(\bar{f}_o - \bar{f}_s) \tag{3.3-14}$$

If all λ_k are distinct,

$$\bar{f}^n - \bar{f}_s = \sum_{k=1}^{m} \frac{\bar{\Omega}_k^T(\bar{f}_o-\bar{f}_s)}{\bar{\Omega}_k^T \bar{\gamma}_k} \bar{\gamma}_k \lambda_k^n \tag{3.3-15}$$

where $\bar{f}_s = (\bar{\bar{I}}-\bar{\bar{C}})^{-1}\bar{b}$, the steady state solution and $\bar{\gamma}_k$ and $\bar{\Omega}_k$ are the eigenvectors and eigenrows of λ_k.

If λ_1 is the dominant eigenvalue, equation (3.3-15) can be approximated by

$$\bar{f}^n - \bar{f}_s = \frac{\Omega_1^T (\bar{f}_o-\bar{f}_s)}{\Omega_1^T \bar{\gamma}_1} \bar{\gamma}_1 \lambda_1^n \tag{3.3-16}$$

If the dominant eigenvalue λ_1 is not distinct, equation (3.3-16) is still valid, although the convergence rate is much slower (Orbach and Crowe 1971). However, it is unlikely that two or more eigenvalues would be numerically identical for problems of this nature.

The apparent value of λ_1 can be obtained from

$$\Delta\bar{f}^{n-1} \equiv \bar{f}^n - \bar{f}^{n-1} = \frac{\Omega_1^T (\bar{f}_o-\bar{f}_s)}{\Omega_1^T \bar{\gamma}_1} \bar{\gamma}_1 (\lambda_1-1)\lambda_n^{n-1} \tag{3.3-17}$$

The ratio of the norm of successive $\Delta\bar{f}$ gives the absolute value of λ_1 as

$$||\Delta\bar{f}^n|| / ||\Delta\bar{f}^{n-1}|| = |\lambda_1| \tag{3.3-18}$$

where the vector norm can be defined in various ways

$$||\Delta\bar{f}||_{\infty} \equiv \max_{k} |\Delta f_k|$$

$$||\Delta\bar{f}||_{1} \equiv \sum_{k=1}^{m} |\Delta f_k| \qquad (3.3\text{-}19)$$

$$||\Delta\bar{f}||_{2} \equiv \{ \sum_{k=1}^{m} \Delta f_k^2 \}^{\frac{1}{2}}$$

If the successive apparent values of λ_1 calculated from equation (3.3-18) are sufficiently close, equation (3.3-16) can be said to hold and it can therefore be used to estimate the apparent solution $\bar{f}'_s$

$$\bar{f}'_s = \bar{f}^{n-1} + \alpha \frac{\bar{f}^{n} - \bar{f}^{n-1}}{1-|\lambda_1|} \qquad (3.3\text{-}20)$$

where $0 < \alpha \leq 1$ is introduced as a damping factor to depress oscillation.

Comparison of equations (3.3-16) and (3.3-20) indicates that if $|\lambda_1|$ is close to unity, the application of equation (3.3-20) improves the rate of convergence significantly. For most of the problems studied in this work, $|\lambda_1|$ is very close to 1, and therefore a faster rate of convergence was achieved by applying dominant eigenvalue method in the iterative process.

In solving the linear elliptic difference equation of forced convection around a sphere and a cylinder, there is involved only one dependent variable, η. Convergence promotion equation (3.3-20) is applied as soon as $|\lambda_1|'_s$ for successive iterations satisfy

$$||\lambda_1|^{n} - |\lambda_1|^{n-1}| \leq \varepsilon_{\lambda_1} \qquad (3.3\text{-}21)$$

where ε_{λ_1} was chosen as 10^{-3} in this study. However, in case of mixed convection around a sphere and viscous flow around a sphere and a cylinder,

there are involved more than one dependent variable, e.g., ψ^*, ξ^*, and two dominant eigenvalues $|\lambda_1|_{\psi^*}$, $|\lambda_1|_{\xi^*}$ are estimated every iteration. There is very small chance that equation (3.3-21) for both ψ^* and ξ^* will be satisfied. This situation is even more pronounced in case of mixed convection around a sphere since three variables ψ^*, ξ^* and η^* are encountered. An alternate process must therefore be adopted, which is to apply equation (3.3-20) after an arbitrary number of iterations M and choose an arbitrary λ_1. M and λ_1 can only be obtained by trial and error with the aid of the history of λ_1 during the iteration. A big M slows down the rate of convergence and a small M causes it to oscillate. The computer experience from the present investigation indicated that M=20 is a good choice.

In most calculations, $|\lambda_1|$ is very close to unity, e.g., 0.99. The damping factor α in equation 13.3-20) is set equal to 0.7 and $1-|\lambda_1|$ is bounded by a certain maximum depends on the problem being solved.

3.3.4 Sequence of Calculation

Application of the convergence promotion technique (dominant eigenvalue method) to iterative solution of sets of algebraic equations can be made more successful if the physical characteristics of the problem are taken into account. The convergence acceleration technique is essentially used to give a pulse change to the relaxation factor after a certain number of iterations. One then reverts to the original relaxation factor in the next several iterations. This process was repeated many times during the entire iterative process. The sudden

increase of the relaxation factor causes oscillation of the system and thus leads to instability. For example, when the dominant eigenvalue convergence promotion method is applied to SOR iteration, the system oscillates and even diverges because of error propagation. In order to overcome this problem, new sequences of calculation were developed, which stabilized the solution by reducing error propagation.

Linear Elliptic Equation:

Linear elliptic difference equations appear in solving forced convection problems around a sphere and a cylinder where only one dependent variable η needs to be determined. The matrix representation of all difference equations in every mesh point is

$$\bar{\bar{C}}\,\bar{\eta} = \bar{b} \tag{3.3-22}$$

First of all $\bar{\bar{C}}$ is split into two matrices

$$\bar{\bar{C}}_1\,\bar{\eta} + \bar{\bar{C}}_2\,\bar{\eta} = \bar{b} \tag{3.3-23}$$

where $\bar{\bar{C}}_1$ is a tridiagonal matrix and $\bar{\bar{C}}_2$ is a bidiagonal matrix of order (IxJ) and $\bar{\eta}$ is the vector of all η in every mesh point and $\bar{b}$ is a vector including boundary conditions.

An iterative scheme can be designed so that

$$\bar{\bar{C}}_1\bar{\eta}^{n} = \bar{b} - \bar{\bar{C}}_2\bar{\eta}^{n-1} = \bar{b}_1{}^{n-1} \tag{3.3-24}$$

Equation (3.3-24) can be solved efficiently by the method of Thomas (Lapidus, 1962) provided that $\bar{\eta}^{n-1}$ is known. This process is repeated from the starting solution $\bar{\eta}^{o}$ (or initial guess of η) until $\bar{\eta}^{n}$ satisfies a given criteria.

A more detailed description of this iterative scheme can be illustrated by looking at a particular grid point (i,j). The elliptic difference equation can be written as

$$- \eta_{(i-1,j)}\, a_{(i-1)} + \eta_{(i,j)} - \eta_{(i+1,j)}\, a_{(i+1)} - \eta_{(i,j-1)}\, b_{(j-1)} - \eta_{(i,j+1)}\, b_{(j+1)} = 0 \qquad (3.3\text{-}25)$$

where $a_{(i-1)}$, $a_{(i+1)}$ and $b_{(j+1)}$ are related to ψ and are constants. By assigning the values of $\eta_{(i,j-1)}$ and $\eta_{(i,j+1)}$ equal to those of the previous iteration, the value of $\eta_{(i-1,j)}$, $\eta_{(i,j)}$ and $\eta_{(i+1,j)}$ can be obtained from

$$- \eta^{n}_{(i-1,j)}\, a_{(i-1)} + \eta_{(i,j)}^{\,n} - \eta_{(i+1,j)}^{\,n}\, a_{(i+1)} = \eta^{n-1}_{(i,j-1)}\, b_{(j-1)} + \eta^{n-1}_{(i,j+1)}\, b_{(j+1)} \qquad (3.3\text{-}26)$$

The same treatment has been applied to all grid points along the constant j line. The matrix representation of this tridiagonalization procedure is essentially equation (3.3-24). Therefore by solving equation (3.3-24), all i values of $\eta_{(i,j)}$ along the constant j line are calculated at iteration level n. This procedure is then repeated for all j lines. This method of iteration has proved that the convergence rate is about twice as fast as SOR iteration.

A more rapid convergence rate can be obtained by applying the convergence acceleration technique. However, the stability problem related to error propagation must be considered. This can limit the applicability of the convergence acceleration technique.

Consider the mesh system in Figure 3.3-1. Iteration by equation (3.3-24) revises the values of η for all i's starting from j = 2, 3, 4 --- j-1 (j=1 and j=J are boundaries where η's are known). Divide the iteration into two half iterations as follows:

i) Calculate new values of η^n along the lines

j = 2, 4, 6, 8 --- using values of η^{n-1} at lines

j = 1, 3, 5, 7 ---

ii) Calculate new values of η^n along the lines

j = 1, 3, 5, 7, 9 --- using values of η^n at line

j = 2, 4, 6, 8 calculated from the first half iteration.

This sequence of calculation reduces error propagation.

In the first half of the iteration, successive substitution is applied, i.e.

$$\bar{\eta}^n = \bar{\eta}^{n**} \tag{3.3-27}$$

where $\bar{\eta}^{n**}$ is calculated from equation (3.3-24). For the second half of the iteration relaxation with convergence promotion is used.

$$\bar{\eta}^n = \bar{\eta}^{n-1} + \delta \bar{\bar{W}}_\eta (\bar{\eta}^{n**} - \bar{\eta}^{n-1}) \tag{3.3-28}$$

where δ is the promotion factor and

$$\delta = \alpha \; / \; (1 - |\lambda_1|) \tag{3.3-29}$$

Of course δ in equation (3.3-28) is set equal to unity except at the iteration level when convergence promotion applies and has the value given by equation (3.3-29). In some extreme cases, $|\lambda_1|$ is very close to unity and δ can reach a large value, which leads to divergence. To avoid this, δ is bounded by δ max, a value which depends on $|\lambda_1|$.

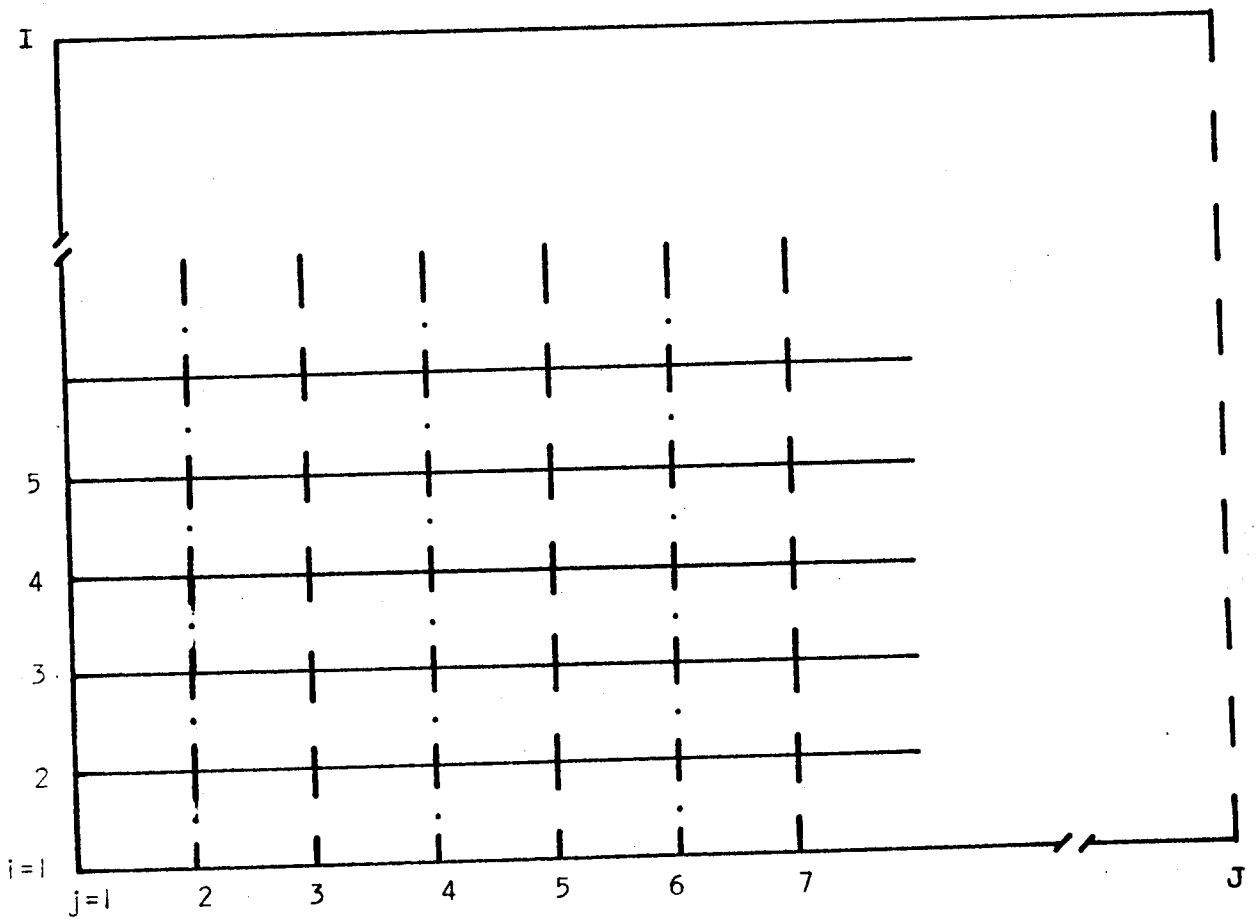

FIGURE 3.3-1 **GRAPHICAL ILLUSTRATION OF SEQUENCE OF CALCULATION-LINEAR ELLIPTIC EQUATION**

This sequence of calculation was found to be 3-4 times faster than SOR iteration with varying relaxation factor and is much faster then SOR with uniform relaxation factor. Comparison of computational work between SOR and the new sequence tridiagonalization with convergence promotion are shown in Figure 3.3-2. It can be seen that δ can vary over quite a wide range with very small effect on convergence.

Nonlinear Coupled Elliptic Equations

Nonlinear coupled elliptic equations appear in problems of viscous flow around a sphere and a cylinder and mixed convection flow around a sphere and a cylinder. These equations are vorticity transport equation and the continuity equation of heat or mass. Direct application of the convergence promotion technique gives rise to error propagation even worse than encountered with the linear elliptic difference equation. A new sequence with convergence promotion was developed to overcome this problem.

The new sequence of calculation is a modification of the sequence for linear equations. One complete iteration was divided into two half iterations, one by direct substitution and one by relaxation with convergence promotion. Consider the mesh system in Figure 3.3-3. The sequence of calculation of the field function F is such that, as iteration sweep from i = 2, 3, 4, 5 --- for all j at each i line the X points are calculated in the first half iteration and direct substitution (equation 3.3-27) of the calculated F value is used as the new F value; in the second half iteration 0 points are calculated. Relaxation with convergence promotion is used for calculating new F value (equation 3.3-28).

Figure 3.3-2 Comparison of Computation Time; Linear Elliptic Equation

Sphere Re = 57, Pr = 5, A = 0.05, B = $\pi/30$, r^*_∞ = 3.32

SOR with uniform W_{η^*} = 0.1 ■

SOR with varying $W_{\eta^*(i,j)}$ ●

New sequence convergence promotion with varying $W_{\eta^*(i,j)}$

δ = 30 ✱

60 ○

100 □

CDC6400 cpu time per iteration

SOR 0.097 sec

New sequence convergence promotion 0.095 sec.

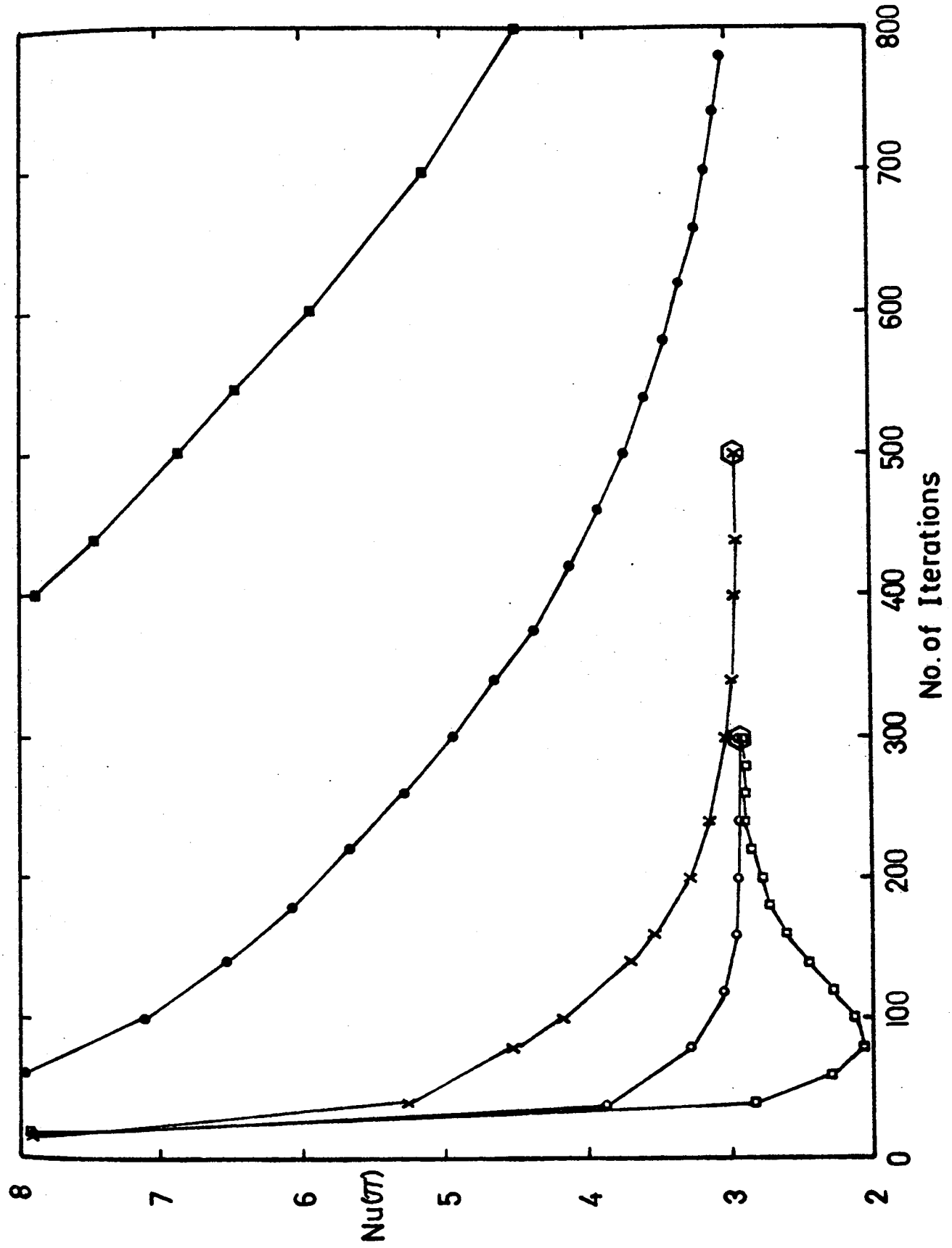
Nu(m)
8
7
6
5
4
3
2
0
100
200
300
400
500
600
700
800
No. of Iterations

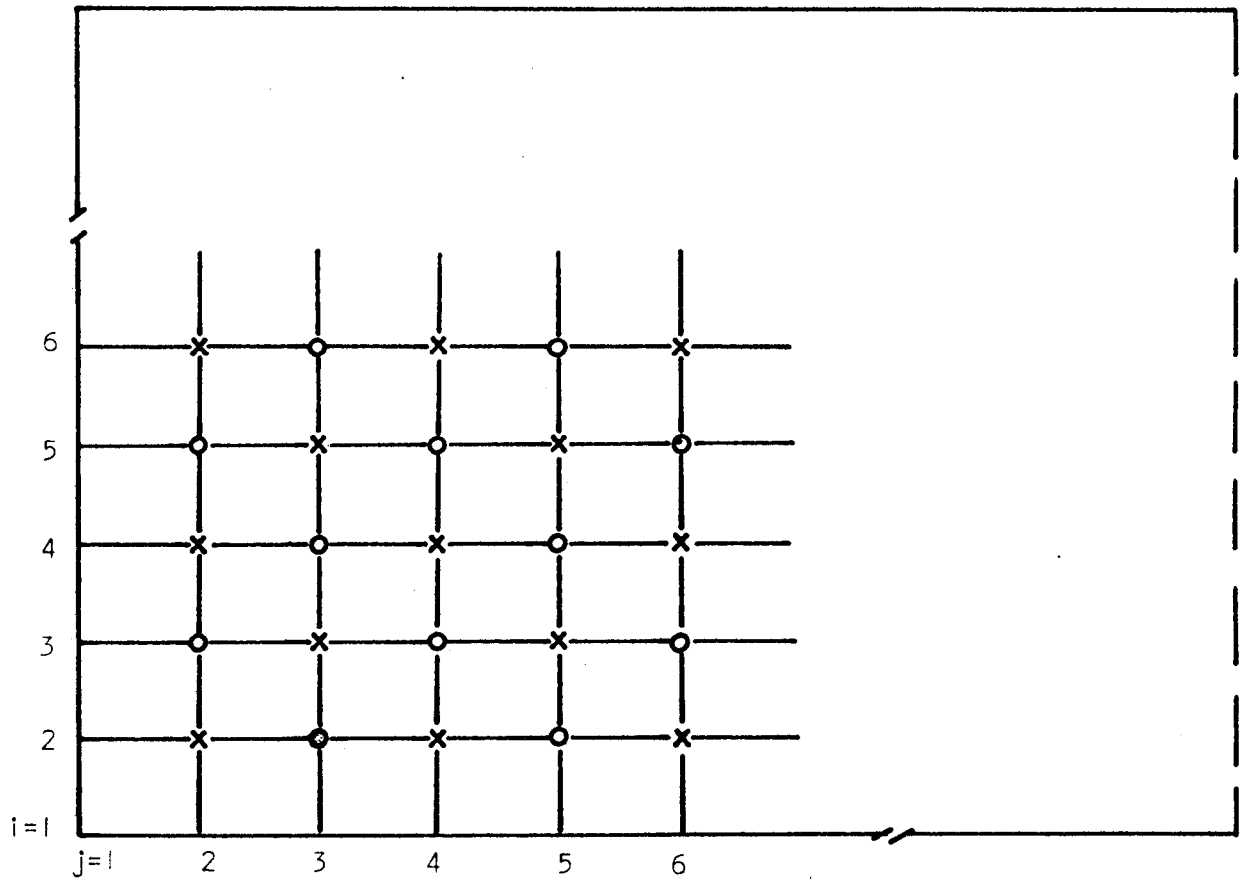

FIGURE 3.3-3 GRAPHICAL ILLUSTRATION OF SEQUENCE OF CALCULATION-NON-LINEAR COUPLED ELLIPTIC EQUATION

This completes one iteration. This new sequence of calculation was found to be more stable and converged 2-3 times faster than SOR iteration. A comparison of computation work for SOR and new sequence iteration are shown in Figure 3.3-4. The rational of this new sequence of calculation is the same as that for the linear elliptic equation, in other words to reduce the error propagation in the system.

A comparison between ADI and the present method has not been made, however computer time of Son and Hanratty (1969), using ADI for cylinder at Re=40 takes 40 minutes using an IBM 360/75. The study of exactly the same problem (same number of mesh points, same step sizes and same r_∞^*) by the present method takes 15 minutes using the CDC6400 computer which is comparable to the IBM 360/75 in speed.

In conclusion, the new sequence with convergence promotion methods developed here are generally faster than SOR, ADI iterations. Other advantages of this method may be summarized as follows

i) The effects of step sizes, physical parameters on stability are mild and therefore these methods can be applied to a variety of problems.

ii) The stability is not sensitive to the convergence promotion factor δ so that a wide range of δ can be chosen.

iii) For the case of non-linear, coupled elliptic equations, the choices of relaxation factors given in Section 3.3-2 vary slightly from iteration to iteration, since these relaxation factors depend only on stream function ψ^* which converges much faster than ξ^* and η^* Therefore W_ξ^*'s and W_η^*s can be revised every M iterations. This leads

Figure 3.3-4 Comparison of Computer Time; Coupled Non linear Elliptic Equations

Sphere Pr = 0.71, Gr = -300, Re = 30

A = 0.05, B = $\pi/30$, r^*_∞ = 14.88

SOR with uniform W's ■

W_{ψ^*} = 0.4, W_{ξ^*} = 0.2, W_{η^*} = 0.4

SOR with varying W's ●

New sequence convergence promotion with varying $W's_{(i,j)}$ [revising every 20 iteration]

δ = 10 ✖

= 15 ○

CDC6400 C_p time per iteration

SOR = 0.79 sec.

New sequence convergence promotion with varying $W's_{(i,j)}$ 0.8 sec.

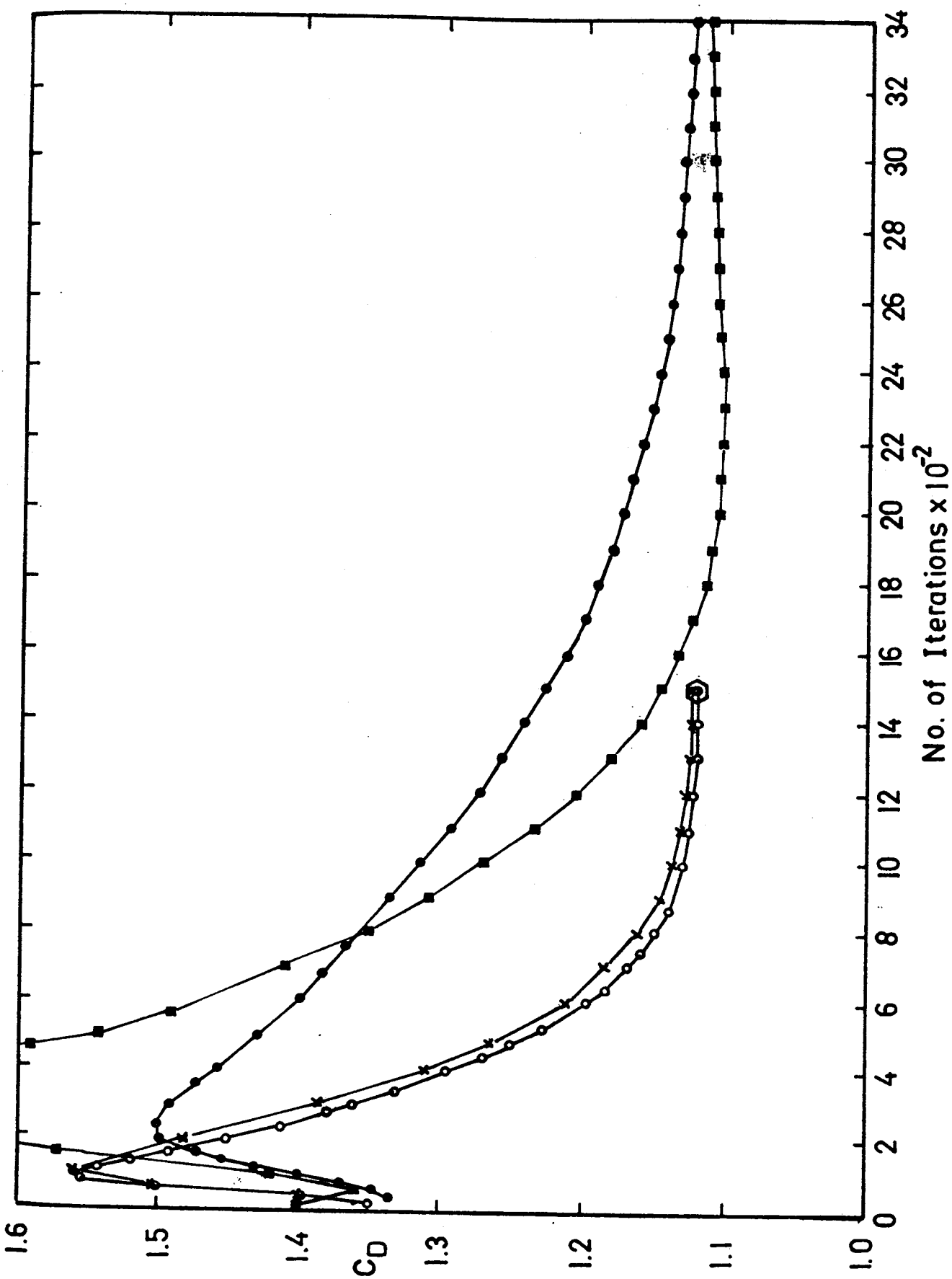
1.6
1.5
1.4
1.3
1.2
1.1
1.0
C_D
0
2
4
6
8
10
12
14
16
18
20
22
24
26
28
30
32
34
No. of Iterations x 10^{-2}

to a significant reduction of computation time.

iv) The sequence and convergence promotion techniques are easy to program for a digital computer.

3.4 Convergence Tests of Numerical Solutions

In general, the iteration procedure of the field function $F(\psi^*, \xi^* \text{ or } \eta^*)$ is said to converge if the following condition is satisfied

$$\max_{i,j} \frac{|F^{n}_{(i,j)} - F^{n-1}_{(i,j)}|}{|F_{(i,j)}{}^{n-1}|} \leq \varepsilon \qquad (3.3\text{-}30)$$

where ε is an arbitrary tolerance and depends on the degree of accuracy required. More accurate results can be achieved if ε is set smaller. However, the value of ε depends on $|F_{(i,j)}{}^{n-1}|$, the denominator of equation (3.3-30). In some cases the value of $|F_{(i,j)}{}^{n-1}|$ is extremely small, e.g., in solving forced convection problems $\max_{i,j} \frac{|F_{(i,j)}{}^{n} - F_{(i,j)}{}^{n-1}|}{|F_{(i,j)}{}^{n-1}|}$ usually appears at the rear end and near the outer boundary where $|F_{(i,j)}{}^{n-1}|$ is small and the change $|F_{(i,j)}{}^{n} - F_{(i,j)}{}^{n-1}|$ is relatively large. As a result a proper ε must be chosen based on the error of the local or integrated values such as $Nu(\theta)$, Nu or C_D per iteration. In this work the change in these properties were less than 0.1%. The convergence can also be tested by varying the step sizes A and B. Large values of A and B increase truncation error, however smaller values of A and B lead to a great number of mesh points and larger computation time. The selection of A and B is a matter of trial and error. The various A and B used in this study are the same as those used by Hamielec,

Hoffman and Ross (1967), Hamielec and Raal (1969) and LeClair (1970).

The integrated values (e.g., Nu, C_D etc.) are less sensitive than the local values (e.g., Nu(θ), ξ^* etc.) per iteration. In this study all local changes in field functions per iteration must be less than 0.1% at convergence. This convergence criterion is used throughout.

4. SPECIFIC PROBLEMS SOLVED

4.1 Viscous Flow Around a Single Sphere and a Circular Cylinder in an Unbounded Fluid

4.1.1 Governing Equations, Boundary Conditions and Method of Solution.

The governing equations for viscous flow around a sphere and a cylinder is the Navier Stokes equation described by Hamielec et. al. (1967, 1969). In coordinates (θ, z) they are

Sphere

$$\left[\frac{\partial\psi^*}{\partial z}\frac{\partial}{\partial\theta}\left(\frac{\xi^*}{e^z\sin\theta}\right) - \frac{\partial\psi^*}{\partial\theta}\frac{\partial}{\partial z}\left(\frac{\xi^*}{e^z\sin\theta}\right)\right]\sin\theta$$

$$= \frac{2}{Re}\, E_{sz}^{*2}\,(\xi^*\, e^z\sin\theta) \qquad (4.1\text{-}1)$$

$$\xi^* = E_{sz}^{*2}\,\psi^* \,/\, e^{3z}\sin\theta$$

Cylinder

$$\left[\frac{\partial\psi^*}{\partial z}\frac{\partial\xi^*}{\partial\theta} - \frac{\partial\psi^*}{\partial\theta}\frac{\partial\xi^*}{\partial z}\right] = \frac{2}{Re}\, E_{cz}^{*2}\,\xi^* \qquad (4.1\text{-}2)$$

$$\xi^* = E_{cz}^{*2}\,\psi^*$$

Undisturbed parallel flow boundary conditions are used to simulate flow in an unbounded fluid. These boundary conditions are

Sphere

$$\text{at } z = 0;\quad \psi^* = 0,\quad \xi^* = E_{sz}^{*2}\,\psi^*/\sin\theta$$
$$\text{at } z = z_\infty;\quad \psi^* = \frac{e^{2z}}{2}\sin^2\theta,\quad \xi^* = 0 \qquad (4.1\text{-}3)$$
$$\text{at } \theta = o,\pi;\quad \psi^* = \xi^* = 0$$

Cylinder

$$\text{at } z = o\ ; \quad \psi^* = o, \quad \xi^* = E_{cz}^{*2}\,\psi^*$$

$$\text{at } z = z_\infty; \quad \psi^* = e^z \sin\theta, \quad \xi^* = o \qquad (4.1\text{-}4)$$

$$\text{at } \theta = o,\pi; \quad \psi^* = \xi^* = o$$

The method used to solve these non-linear equations was the new sequence convergence promotion method described in Section 3.3-2. FORTRAN IV computer program for sphere is listed in Appendix A.1. For the case of cylinder, the logic of programming is the same as that for sphere except the finite difference equations, and the computer program of cylinder is therefore not shown in detail. Initial guesses of ψ^* and ξ^* for sphere are Stokes creeping flow solution for $Re<10$ and Kawaguti's approximate solution for $Re\geq 10$. Potential flow theory was used for the cylinder.

4.1.2 An Extrapolation Technique to Obtain Flow Behavior for an Unbounded Fluid

Solutions of vorticity and stream function obtained by solving the Navier Stokes equation subject to finite boundary r_∞^* which simulates $r^* = \infty$ (as finite difference solution for $r^* = \infty$ is impossible) usually include wall effects unless r_∞^* is chosen large enough. The proper r_∞^* is obtained by trial and error. The choice of too large r_∞^* leads to excessive computation time and poor stability of the iterative scheme.

An efficient method was developed to estimate flow behavior for $r^* = \infty$. This involved extrapolation of two sets of solutions for finite r_∞^*. By examining ψ^* and ξ^* distributions of the Navier Stokes equation solutions obtained at different r_∞^*, it was found that both ψ^* and ξ^*

change monotonically with r^*_∞, which indicates that ψ^* and ξ^* can be expressed as an infinite series expansion of $1/r^*$, i.e.,

$$F = F_o + \frac{C_1}{r^*_\infty} + \frac{C_2}{r^{*2}_\infty} + \frac{C_3}{r^{*3}_\infty} + \text{---} \qquad (4.1\text{-}5)$$

where F represents ψ^* or ξ^* and F_o is the value of F at $r^* = \infty$ and C_1, C_2, C_3 --- are constants.

Assume r^*_∞ is chosen large enough such that terms $\leq 1/r^{*3}_\infty$ can be neglected from equation (4.1-5). Therefore

$$F \doteq F_o + \frac{C_1}{r^*_\infty} + \frac{C_2}{r^{*2}_\infty} \qquad (4.1\text{-}6)$$

At $r^*_\infty \to \infty$, $F \to F_o$ and the 1st derivative of F with respect to $1/r^*_\infty$ is assumed zero, that is

$$\left.\frac{dF}{d(1/r^*_\infty)}\right|_{1/r^*_\infty \to o} = 0 \qquad (4.1\text{-}7)$$

condition (4.1-7) implies $C_1 = 0$, therefore

$$F \doteq F_o + \frac{C_2}{r^{*2}_\infty} \qquad (4.1\text{-}8)$$

F_o can be obtained from two sets of solutions of $r^*_{\infty 1}$ and $r^*_{\infty 2}$ by eliminating C_2 as follows

$$F_o = \frac{r^{*2}_{\infty 1} F_1 - r^{*2}_{\infty 2} F_2}{r^{*2}_{\infty 1} - r^{*2}_{\infty 2}} \qquad (4.1\text{-}9)$$

This equation is used to calculate all local values of ψ^* and ξ^*, these values are then used to calculate drag coefficient etc.

This extrapolation method has been tested by considering three sets of solutions of different r^*_∞ for the case of viscous flow around a circular cylinder at Re = 85 (cylinder is known to have a very large wall

effect, Hamielec and Raal (1969)) and the results are tabulated in Table 4.1-1. Excellent extrapolated values are indicated. Comparison of drag coefficients so obtained with experimental measurements is also excellent as will be shown later in tabular form.

Table 4.1-1 Extrapolated C_D Values

Cylinder Re = 85
A = 0.05, B = 6°

	$C_{DP}(\infty)$	$C_{DF}(\infty)$	$C_D(\infty)$
$r_\infty^* = 7.03$ and 9.03	0.90	0.35	1.25
$r_\infty^* = 9.03$ and 11.59	0.87	0.34	1.21
$r_\infty^* = 7.03$ and 11.59	0.88	0.35	1.23

4.1.3 Mesh Dimensions and Accuracy of Solutions

The step size selected for A and B in the numerical calculations were selected based on the work of Hamielec, Hoffman and Ross (1967), Hamielec and Raal (1970) and LeClair (1970). A and B used for different Reynolds number ranges for both sphere and cylinder are as follows

$$0.01 \leq Re \leq 1 \quad ; A = 0.1, B = \pi/30 \quad (6°)$$

$$1 < Re < 100; A = 0.05, B = \pi/30 \quad (6°)$$

$$100 \leq Re \leq 400; A = 0.025, B = \pi/60 \quad (3°)$$

A must be chosen considerably smaller at high Reynolds numbers because the gradient near the surface is steep.

The effects of angular and radial step size have been investigated thoroughly for the case of Re = 85 for cylinder. The results are shown in Table 4.1-2. This table indicates that the choices of A = 0.05 and B = $\pi/30$ is small enough to provide accurate C_D at Re = 85.

Table 4.1-2 Effects of A and B for Cylinder at Re = 85

r_∞^*	A	B	C_{DP}	C_{DF}	C_D
7.03	0.05	$\pi/30$	1.20	0.44	1.64
	0.05	$\pi/60$	1.20	0.44	1.64
9.03	0.05	$\pi/30$	1.09	0.40	1.49
	0.05	$\pi/60$	1.08	0.40	1.48
9.01	0.0314	$\pi/60$	1.09	0.40	1.49

The size of the outer boundary r^*_∞ must be obtained by trial and error, too small r^*_∞ increases the wall effect and too large an r^*_∞ increases the number of mesh points and therefore increases computation time. At low Reynolds numbers the wall effect is very important and at moderately high Reynolds numbers the wall effect becomes less significant. In the case of the high Reynolds number range ($100 \leq Re \leq 400$) the quite long vortex at the rear must be taken into account. Too small a choice of r^*_∞ will decrease the dimension of this vortex. In this study $r^*_\infty = 11.88$ is chosen for $100 \leq Re \leq 400$, and is considered to be large enough since the calculated drag coefficients are in excellent agreement with experimental measurements. In the case of the cylinder, the wall effect is larger than for the sphere. The extrapolation technique described in Section 4.1-2 was used to obtain ψ^* and ξ^* at unbounded fluid flow from two sets of ψ^* and ξ^* of different r^*_∞.

The accuracy of an iterative solution depends on the tolerance ε in equation (3.3-30). In this study ε is set equal to 10^{-4} which will give less than 0.1% change in the field functions ψ^*, ξ^*.

4.1.4 Discussion of Results and Comparison with Existing Data

Sphere in an Unbounded Fluid

A. Flow Field Phenomena

The surface pressure and surface vorticity distributions for $0.01 \leq Re \leq 400$ are listed in Appendix B.1. Figure 4.1-1 shows constant ψ^* and ξ^* lines around a sphere at Re = 400. A secondary vortex motion immediately beyond the flow separation angle is observed.

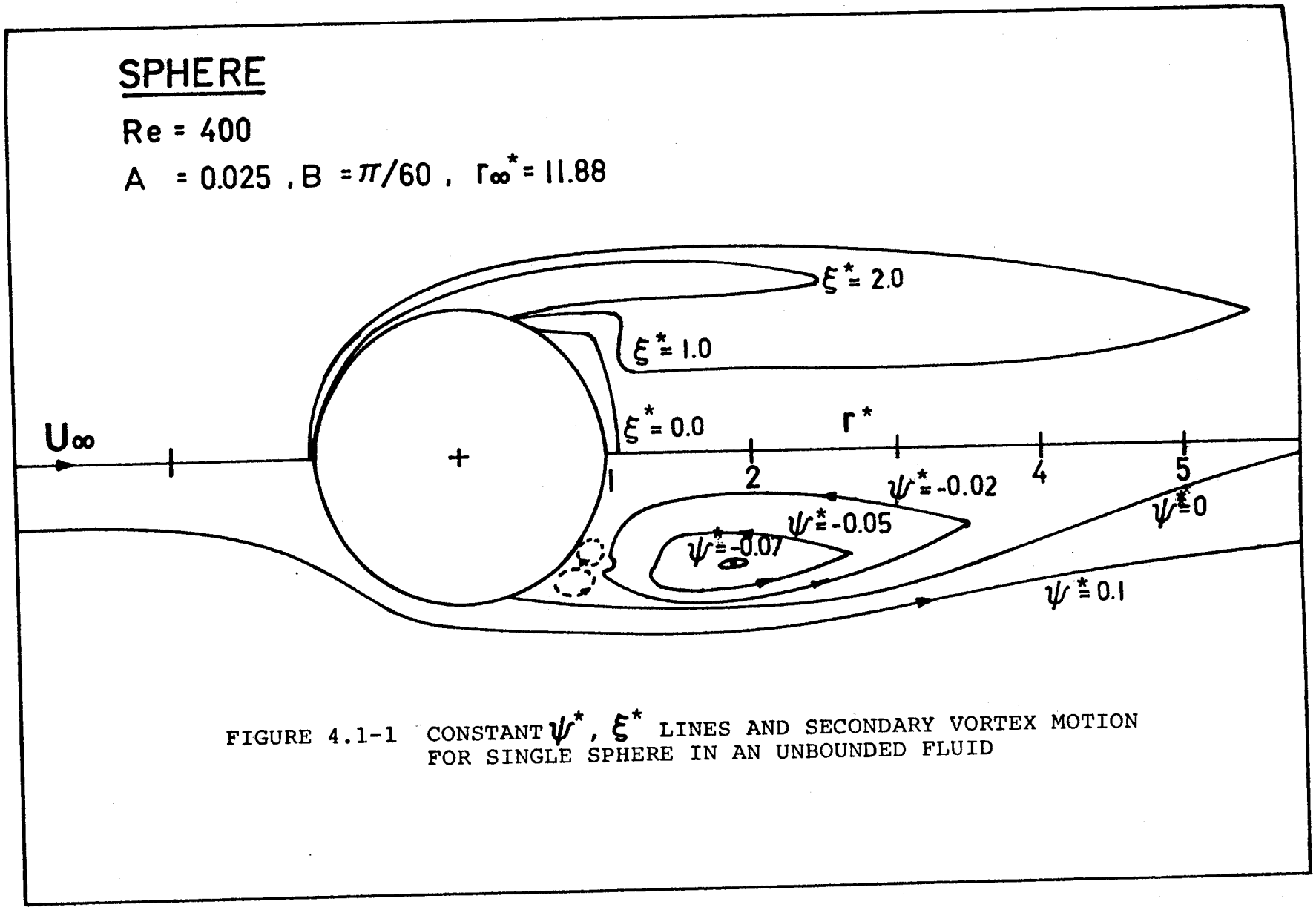

FIGURE 4.1-1 CONSTANT ψ^*, ξ^* LINES AND SECONDARY VORTEX MOTION FOR SINGLE SPHERE IN AN UNBOUNDED FLUID

Son and Hanratty (1969) in their numerical study of viscous flow around a cylinder also observed this secondary vortex at Re = 500. At Reynolds numbers of 300 and 200, it is small and a finer mesh system is required for a more comprehensive investigation. At Re = 100 it vanishes. The presence of this secondary vortex motion can also be observed by investigating the surface vorticity distribution shown in Figure 4.1-2. The wavy curves beyond the separation angle appear to be a result of this secondary vortex.

The surface vorticity distributions are used to determine the flow separation angles θ_s where $\xi^*_s = 0$. The vortex length is the distance from the rear stagnation point to the point where $V_r = 0$ along the parametric line $\theta = \pi$ and the wake volume is obtained simply by integration of the revolution of zero stream function line (which is the boundary of the vortex ring) around the axis $\theta = \pi$. These calculated results are listed in Table 4.1-1.

Figures 4.1-3 and 4.1-4 show the variation of θ_s and L/d with Reynolds number, respectively. Numerical solutions of Jenson (1959), Rimon and Cheng (1969), Rhodes (1967) and the recent results are shown. Predictions by the matched asymptotic expansion technique of Proudman and Pearson (1957) are also shown. Comparison with experimental measurements of Taneda (1956), Garner and Grafton (1954) and Nisi and Porter (1923) is good except at low Reynolds numbers where Taneda somewhat underestimates the vortex length. This may be the effect of extreme difficulties in visualizing the flow with tracer particles of finite size and finite fall velocities. The experimental results of Nisi and

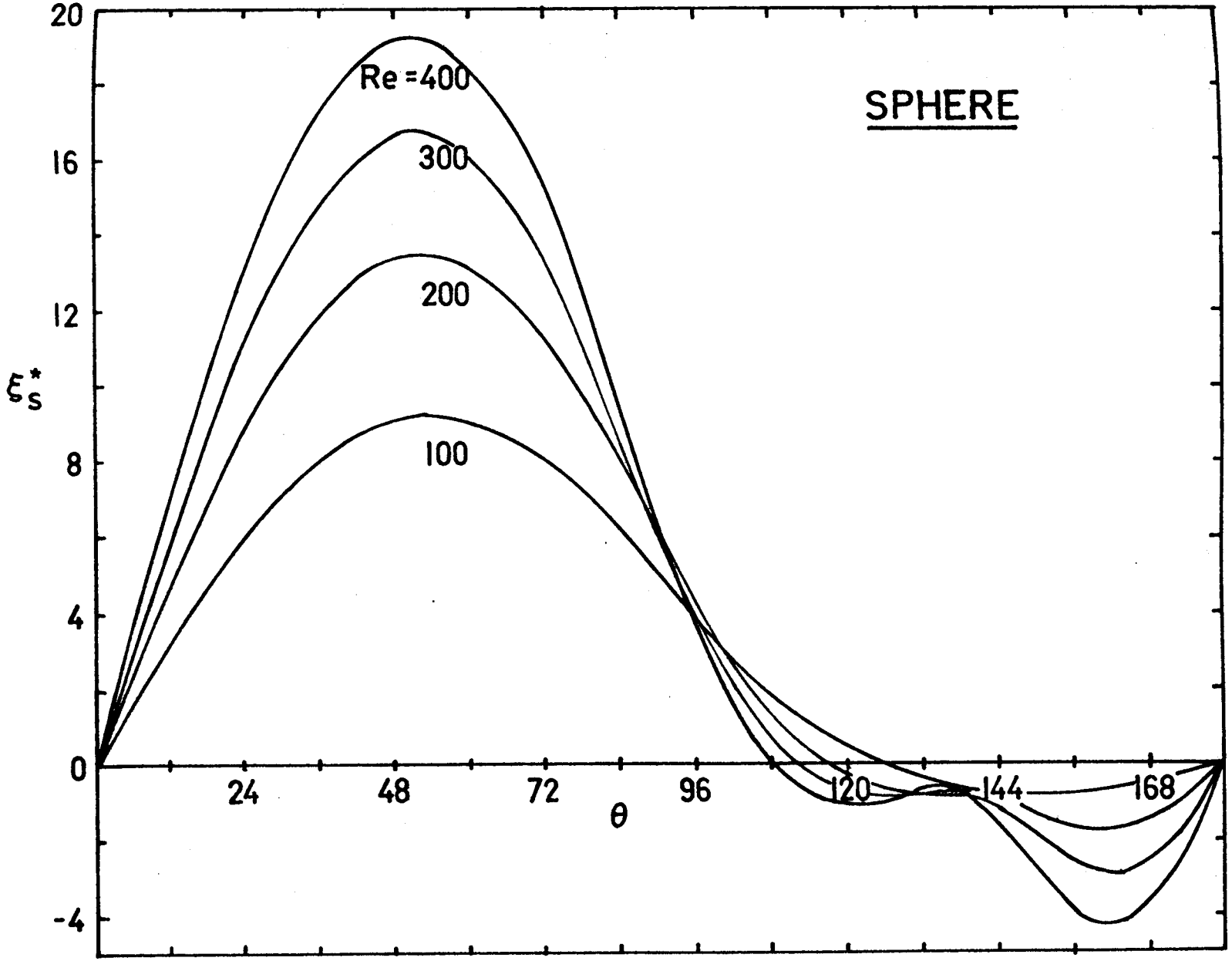

FIGURE 4.1-2 ξ_s^* DISTRIBUTIONS FOR SINGLE SPHERE IN AN UNBOUNDED FLUID

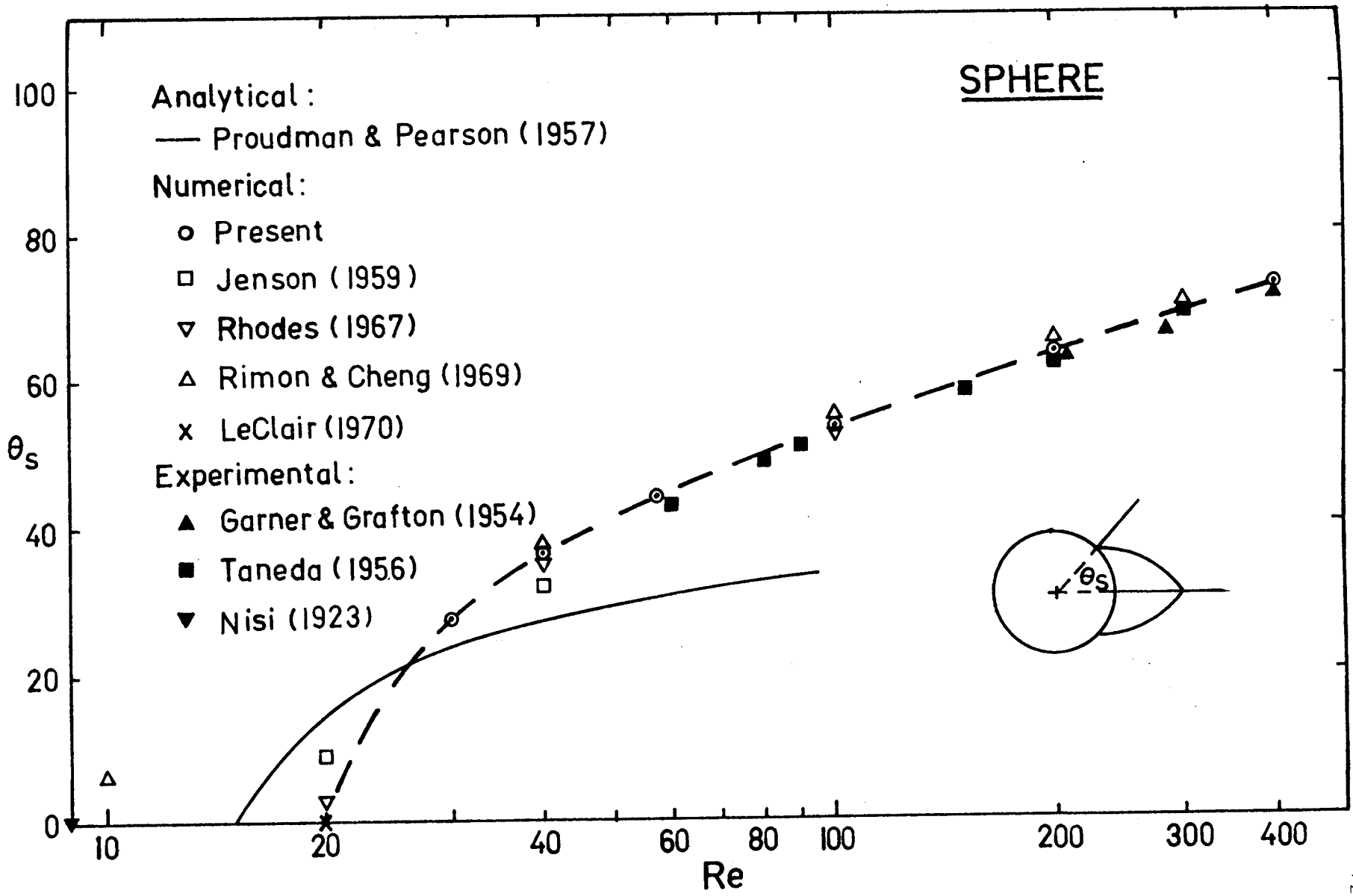

FIGURE 4.1-3 SEPARATION ANGLE θs vs Re FOR SINGLE SPHERE IN AN UNBOUNDED FLUID

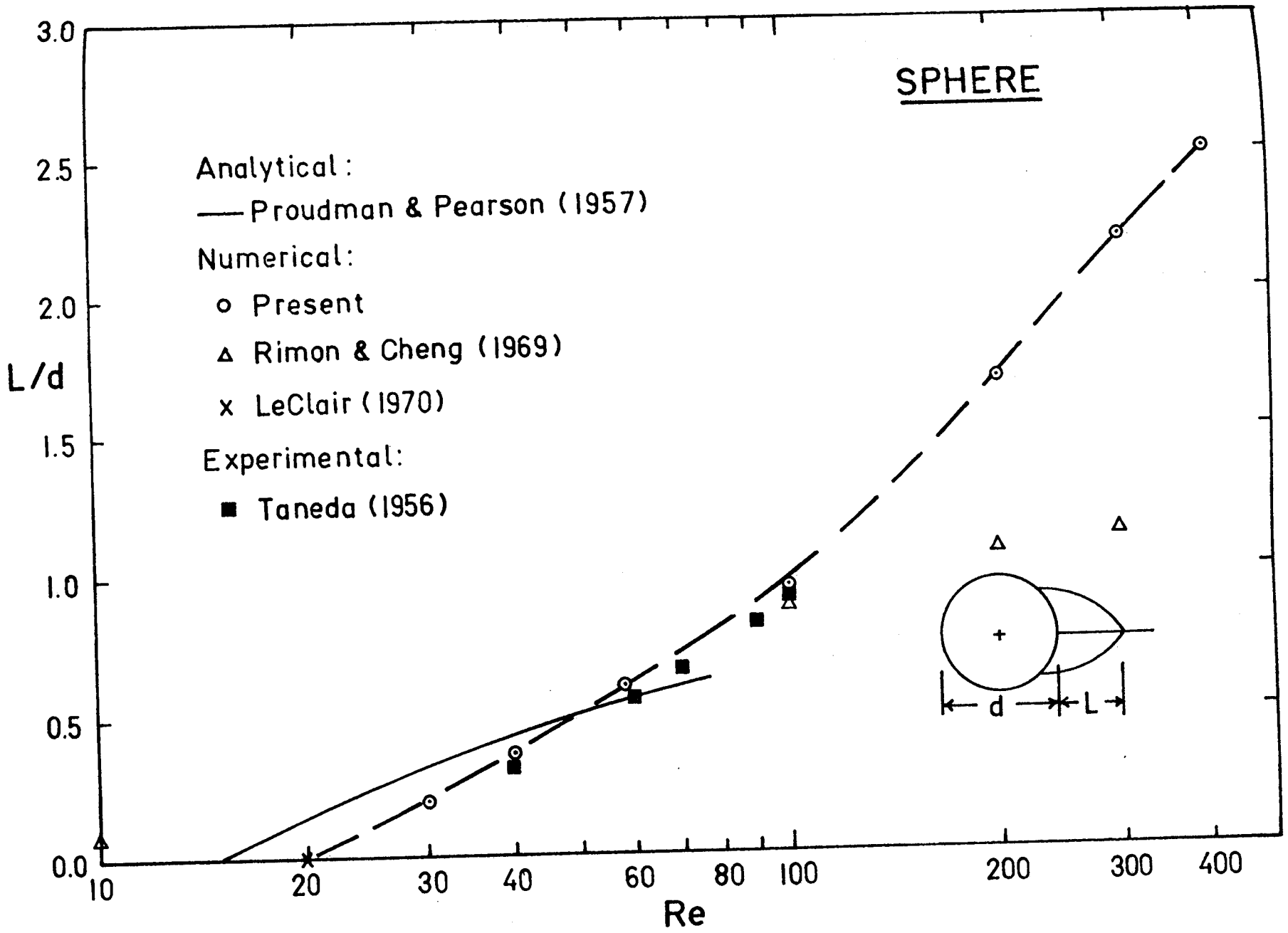

FIGURE 4.1-4 L/d vs Re FOR SINGLE SPHERE IN AN UNBOUNDED FLUID

Table 4.1-1 Present Calculations of θ_s, L/d and V_w/V_s for Sphere

Re	θ_s	L/d	V_w/V_s
30	27.6°	0.20	0.0287
40	36.0°	0.34	0.0891
57	43.5°	0.60	0.246
100	52.8°	0.95	0.698
200	63.3°	1.66	1.59
300	68.4°	2.16	2.29
400	72.3°	2.50	-

Porter were probably biased by their method of suspending the sphere. The value of L/d obtained numerically by Rimon and Cheng for low and high Reynolds numbers is biased by the boundary conditions they used which do not simulate unbounded fluid flow; in addition, the step sizes they used are considered to be too large. The critical Reynolds number for the initiation of vortex motion has been shown to be 20 by LeClair (1970), by varying the step sizes and distance to the outer boundary which ensured that the computed values for L/d and θ_s were not biased by these parameters. Another indication of this critical Reynolds number can be more or less drawn from the plot of $C_D/C_{Ds}-1$ vs Re as suggested by Maxworthy (1965), Pruppacher and Steinberger (1968) and Pruppacher, LeClair and Hamielec (1970). This drag curve indicates that there are two pronounced breaks, one at Re = 20 and one at Re = 400. These breaks may be explained by the formation of a wake at Reynolds number around 20 and the vortex shedding phenomenon at Reynolds number of around 400.

The calculated volumes of the vortex at the rear of the sphere at Re = 30, 57, 100, 200 and 300 are plotted in Figure 4.1-5 together with experimental data after Hendrix et.al. (1967) for liquid drops. The present numerical solutions give higher wake volumes than those measured. This is undoubtedly the result of circulation within the drop which tends to decrease the flow separation angle and wake length. Recent measurements of Karla (1971) at Monash University in Australia for rigid spheres indicates good agreement.

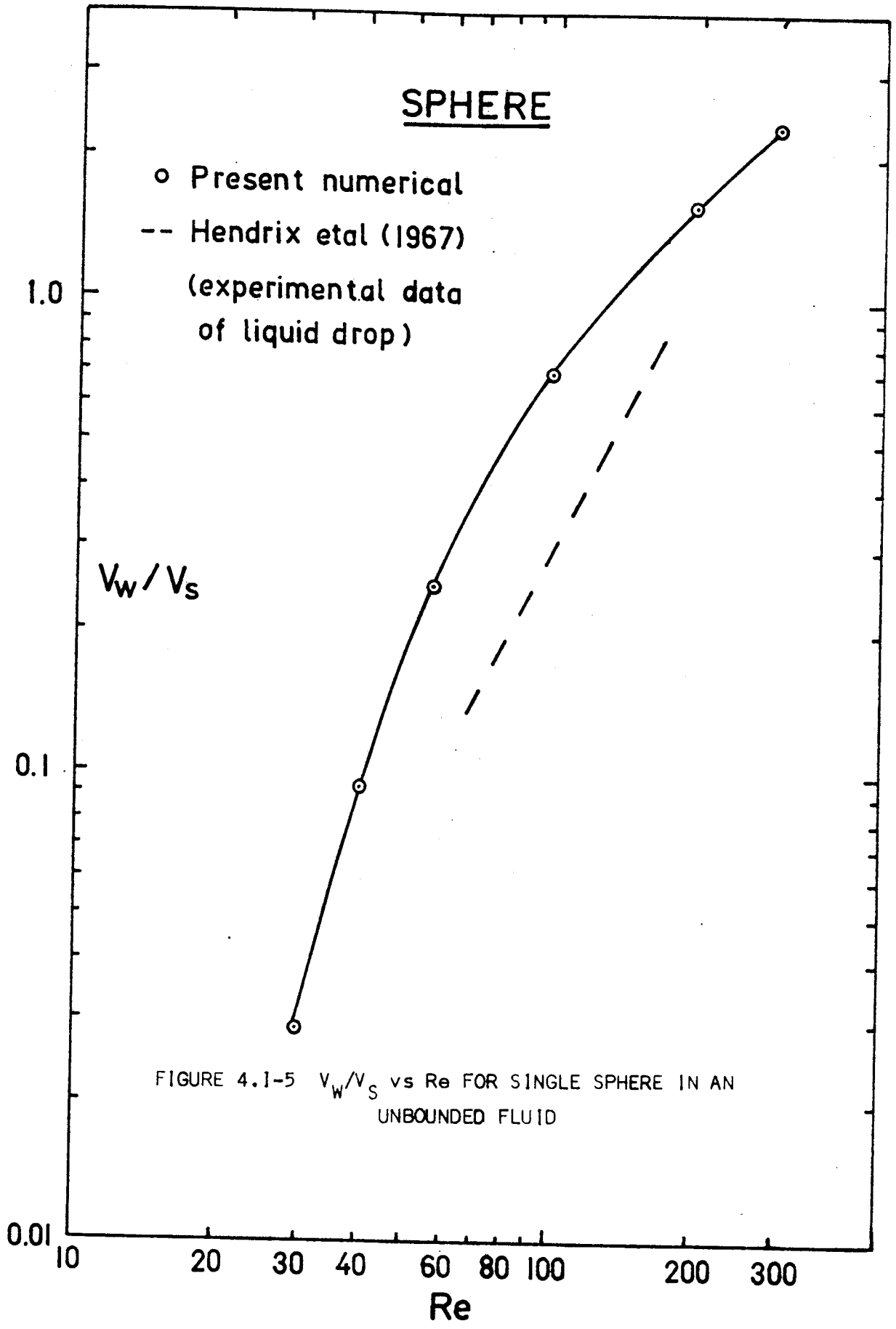

FIGURE 4.1-5 V_W/V_S vs Re FOR SINGLE SPHERE IN AN UNBOUNDED FLUID

B. Drag Coefficient

The predicted form and friction drag coefficients are tabulated in Table 4.1-2. Computational parameters, extrapolated values of drag coefficient using the extrapolation technique described in Section 4.1.2 and experimental measurements are also shown. Excellent agreement with experimental data is apparent. This is especially true for recent measurements of Pruppacher and Steinberger (1968). Figure 4.1-6 shows the variation of C_D with Reynolds number, analytical solutions of Stokes (1851), Oseen (1910). The analytical solutions deviate significantly from the experimental data for Reynolds number greater than about unity. Recent experimental results of Maxworthy (1965) and Pruppacher and Steinberger (1968) suggest that the drag approaches the Oseen drag rather than Stokes drag as $Re \to 0$. Numerical solutions at low Reynolds numbers did verify this fact (LeClair, Hamielec and Pruppacher 1970). Stokes solution is therefore only valid for $Re = 0$ whereas solutions by Oseen, Proudman and Pearson are applicable at Reynolds number below 0.1. At larger Reynolds numbers, these theories fail to give results of sufficient accuracy.

Single Cylinder in an Unbounded Fluid

A. Flow Field Phenomena

The surface pressure and surface vorticity distributions are tabulated in Appendix B.1. for Reynolds numbers 23, 40, 85 and 175. Hamielec and Raal (1969) studied the variation of separation angle θ_s and vortex length for the Reynolds number range, 1 to 500, and for this reason these quantities will not be discussed in detail in this thesis.

Table 4.1-2 Drag Coefficients for a Single Sphere in an Unbounded Fluid-Experimental and Present Theoretical

Re	r^*_∞	A	B	θ_s	L_w	$C_{DP}(r^*_\infty)$	$C_{DF}(r^*_\infty)$	$C_D(r^*_\infty)$	$C_{DP}(\infty)$	$C_{DF}(\infty)$	$C_D(\infty)$	C_D experimental (1)*	C_D experimental (2)**
5	31.5	0.05	6°	0	1	2.45	4.77	7.22				6.81	6.9
10	11.59	"	"	0	1	1.55	2.87	4.42				4.15	4.1
20	7.03	"	"			1.07	1.81	2.88	1.00	1.72	2.72	2.73	2.55
	11.59	"	"	0	1	1.03	1.75	2.78					
	90.	0.05	3°			1.02	1.72	2.73					
30	11.59	0.05	6°	27.6°	1.4	0.83	1.33	2.16				2.13	2.0
40	7.03	"	"			0.76	1.13	1.89	0.71	1.09	1.80		
	11.59	"	"	36°	1.68	0.73	1.10	1.83					
57	11.59	"	"	43.5°	2.2	**0.63**	**0.88**	**1.51**					
100	4.37	0.025	3°			0.60	0.65	1.25	0.48	0.58	1.06	1.07	1.07
	7.21	"	"			0.52	0.61	1.13					
	11.88	"	"	52.8°	2.9	0.51	0.59	1.09					
200	7.21	"	"			0.42	0.38	0.80					
	11.88	"	"	63.3°	4.32	0.40	0.37	0.77				0.766	0.77
300	7.21	"	"			0.37	0.29	0.66					0.65
	11.88	"	"	68.4°	5.33	0.35	0.28	0.63					
400	7.21	"	"			0.34	0.24	0.58					0.58
	11.88	"	"	72.3°	6.0	0.32	0.23	0.55					

(1)* Pruppacher & Steinberger (1968)

(2)** Lapple (1951)

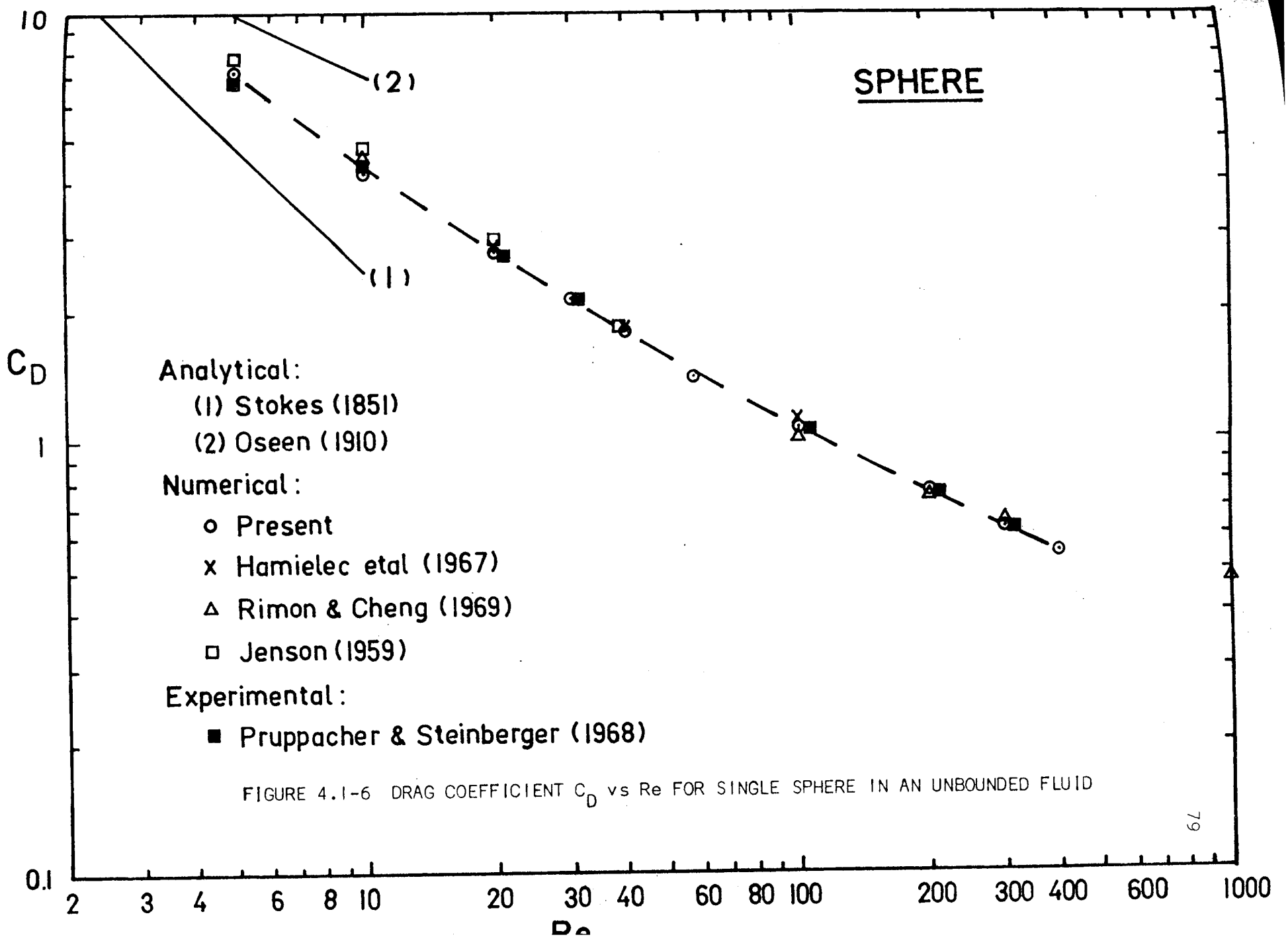

FIGURE 4.1-6 DRAG COEFFICIENT C_D vs Re FOR SINGLE SPHERE IN AN UNBOUNDED FLUID

Table 4.1-3 C_D for Cylinder

Re	r_∞^*	A	B	$C_{DP}(r_\infty^*)$	$C_{DF}(r_\infty^*)$	$C_D(r_\infty^*)$	$C_{DP}(\infty)$	$C_{DF}(\infty)$	$C_D(\infty)$	$C_D(\infty)^*$
23	11.59	0.05	6°	1.41	0.86	2.27	1.21	0.76	1.97	
	19.10	0.05	6°	1.28	0.80	2.08				
40	11.59	0.05	6°	1.19	0.61	1.80	0.99	0.53	1.52	1.58
	19.10	0.05	6°	1.07	0.56	1.63	(0.99)**	(0.52)**	(1.51)**	
	59.39	0.07854	6°	0.98	0.53	1.51				
85	7.03	0.05	6°	1.20	0.44		0.90	0.35	1.25	
	9.03	0.05	6°	1.09	0.40	1.49				
	11.59	0.05	6°	1.00	0.38	1.38				1.29
	7.03	0.05	3°	1.20	0.44	1.64	0.90	0.35	1.25	
	9.03	0.05	3°	1.08	0.40	1.48				
	9.01	0.314	3°	1.09	0.40	1.49				
175	5.34	0.025	3°	1.26	0.31	1.57	0.86	0.23	1.09	
	7.21	0.025	3°	1.08	0.28	1.36				
200							(0.73)**	(0.19)**	(0.92)**	
500							(0.51)**	(0.09)**	(0.60)**	

* Tritton (1959) {experimental}

** Son & Hanratty (1969) {theoretical}

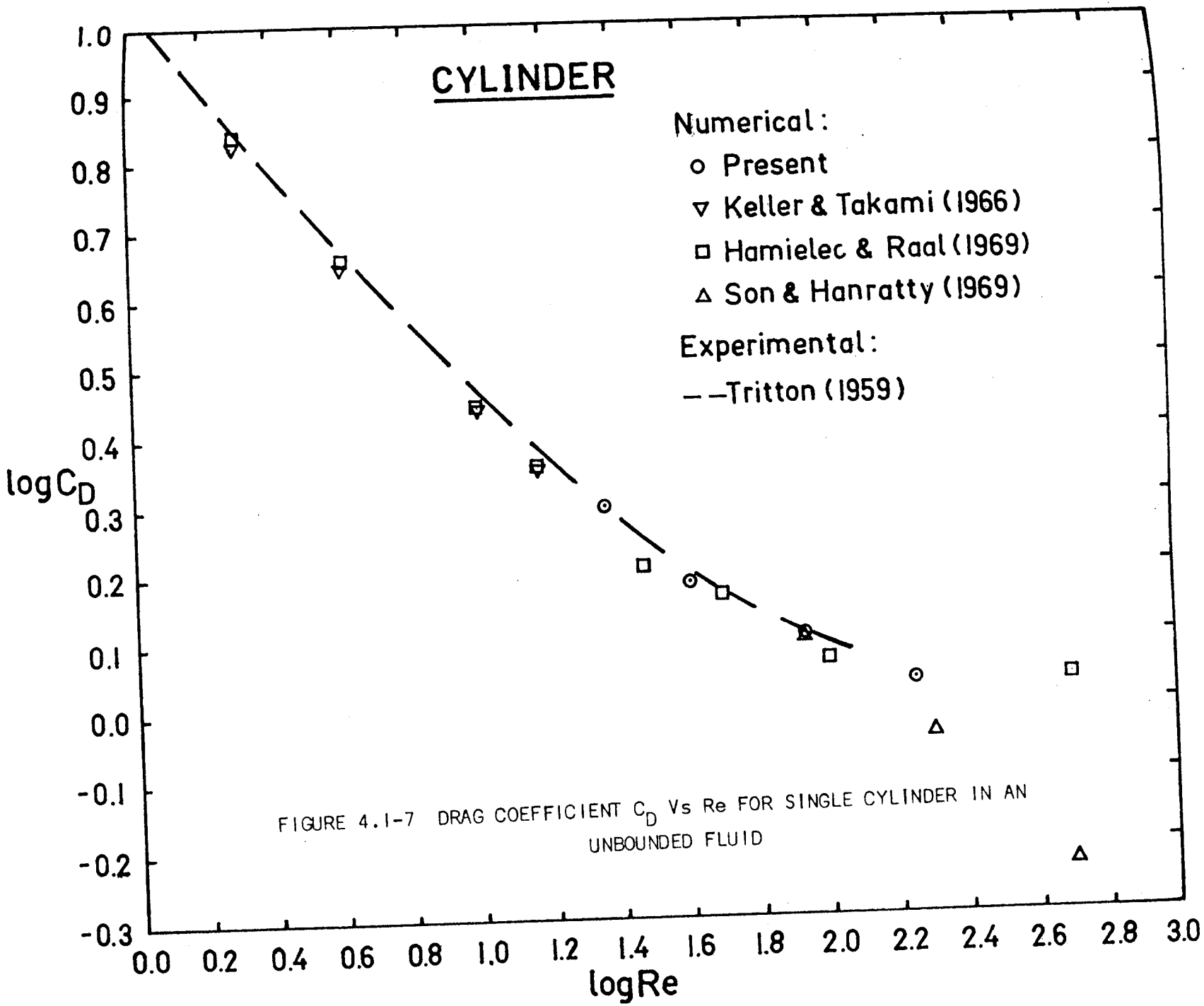

FIGURE 4.1-7 DRAG COEFFICIENT C_D Vs Re FOR SINGLE CYLINDER IN AN UNBOUNDED FLUID

B. Drag Coefficient

The predicted form and friction drag coefficients are tabulated in Table 4.1-3. Computational parameters, extrapolated values of drag coefficient and experimental measurements of Tritton (1959) are also shown. Agreement between predicted and measured data is good. Figure 4.1-7 shows a graphical comparison.

4.2 Forced Convection Around a Single Sphere in an Unbounded Fluid and in an Assemblage

4.2.1 Governing Equation, Boundary Conditions and Method of Solution

The governing equation for forced convection around a sphere and sphere assemblage is the elliptic continuity equation of heat or mass,

$$\frac{\partial \psi^*}{\partial z}\frac{\partial \eta^*}{\partial \theta} - \frac{\partial \psi^*}{\partial \theta}\frac{\partial \eta^*}{\partial z} = \frac{2e^z \sin\theta}{Pe}\left(\frac{\partial^2 \eta^*}{\partial z^2} + \frac{\partial^2 \eta^*}{\partial \theta^2} + \frac{\partial \eta^*}{\partial z} + \cot\theta \frac{\partial \eta^*}{\partial \theta}\right)$$

and the boundary conditions with constant surface temperature or concentration are

$$\text{at } z = 0 \quad ; \quad \eta^* = 1$$

$$\text{at } z = z_\infty \quad ; \quad \eta^* = 0$$

$$\text{at } \theta = 0, \pi \; ; \quad \frac{\partial \eta^*}{\partial \theta} = 0$$

The stream function ψ^*, which is already known, is that calculated in Section 4.1. However, for a sphere in an assemblage, ψ^* calculated by LeClair (1970) is used.

This linear elliptic partial differential equation was solved using the new sequence tridiagonalization with convergence promotion described in Section 3.3.4. The initial guess of η^* field is $\eta^* = 0$

everywhere. FORTRAN IV computer program listing may be found in Appendix A.2.

4.2.2 Mesh Dimensions and Accuracy of Solutions

The step sizes A and B for the η^* field are selected identical to those listed in Section 4.1.3 for the flow field such that the calculated stream function ψ^* in Section 4.1 can be used directly because the mesh system of η^* field is exactly the same as ψ^* field. For larger Prandtl numbers, reduction of the mesh size is required to account for the thin thermal boundary layer near the frontal stagnation point. In the low Prandtl number range studied here ($Pr \leq 5$), the chosen step sizes should provide solutions of sufficient accuracy.

The η^* field is not as sensitive to the outer boundary r^*_∞ as the ψ^* and ξ^* fields especially at high Prandtl numbers where the thermal boundary layer is considerably thinner and the boundary condition $\eta^* = 0$ at moderate r^*_∞ is most likely satisfied. Of course at very low Prandtl number, where the thermal boundary layer is relatively thick, r^*_∞ must be chosen sufficiently large to closely approximate an unbounded fluid.

The accuracy of the numerical solution also depends on the tolerance ε of equation (3.3-30). In this case ε was set equal to 10^{-3} to give a maximum change in the local or average Nusselt or Sherwood number of less than 0.1% per iteration.

4.2.3 Discussion of Results and Comparison with Existing Data

Single Sphere in an Unbounded Fluid

Calculations were made for Re = 0.05, 0.1, 0.2, 0.5, 0.75, 1, 2, 3, 5, 10, 30, 57, 100, 200 and 300 and for Pr = 0.25, 0.35, 0.5, 0.71, 1, 2, 3.5 and 5. This covers the possible Prandtl number range for gases between 25°C and 2500°C.

Local Nusselt (or Sherwood) numbers are tabulated in Appendix B.2. Figure 4.2-1 shows the plot of local Nusselt (or Sherwood) number at Pr = 0.71 for Re = 57, 100, 200 and 300. The transfer rate at the point of minimum transfer is finite rather than zero as predicted by thin thermal boundary layer theory (Baird and Hamielec 1962, LeClair and Hamielec 1968). This is in agreement with experimental observations of Peltzman and Pfeffer (1967), Rhodes and Peeble (1965) and Garner et.al. (1958, 1958, 1961). No quantitative comparison can be made because of the difference in Prandtl numbers. Comparison between local transfer rates obtained by thin thermal boundary layer theory and present numerical results are shown in Figure 4.2-2, which indicates that calculation by thin approximate theory is significantly in error especially in the circulating wake regime where the thermal boundary is thick due to internal circulation and the assumption involving the neglect of angular diffusion is obviously invalid.

Figure 4.2-3 shows the variation of local Nusselt (or Sherwood) number with Prandtl number at Re = 300. Local transfer rate increases with increasing Prandtl number. This is a result of the thinner thermal

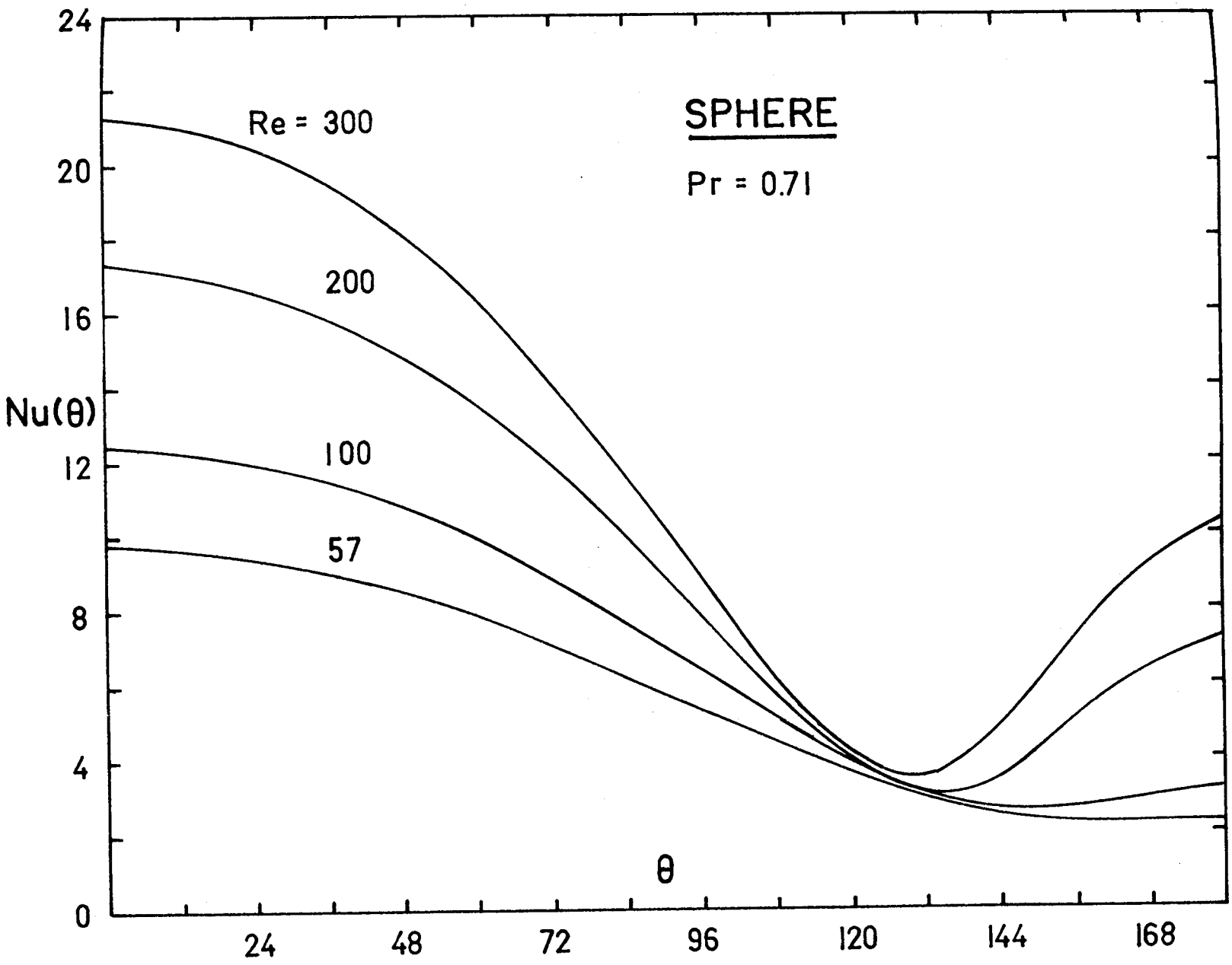

FIGURE 4.2-1 LOCAL NUSSELT NUMBER FOR SINGLE SPHERE IN AN UNBOUNDED FLUID

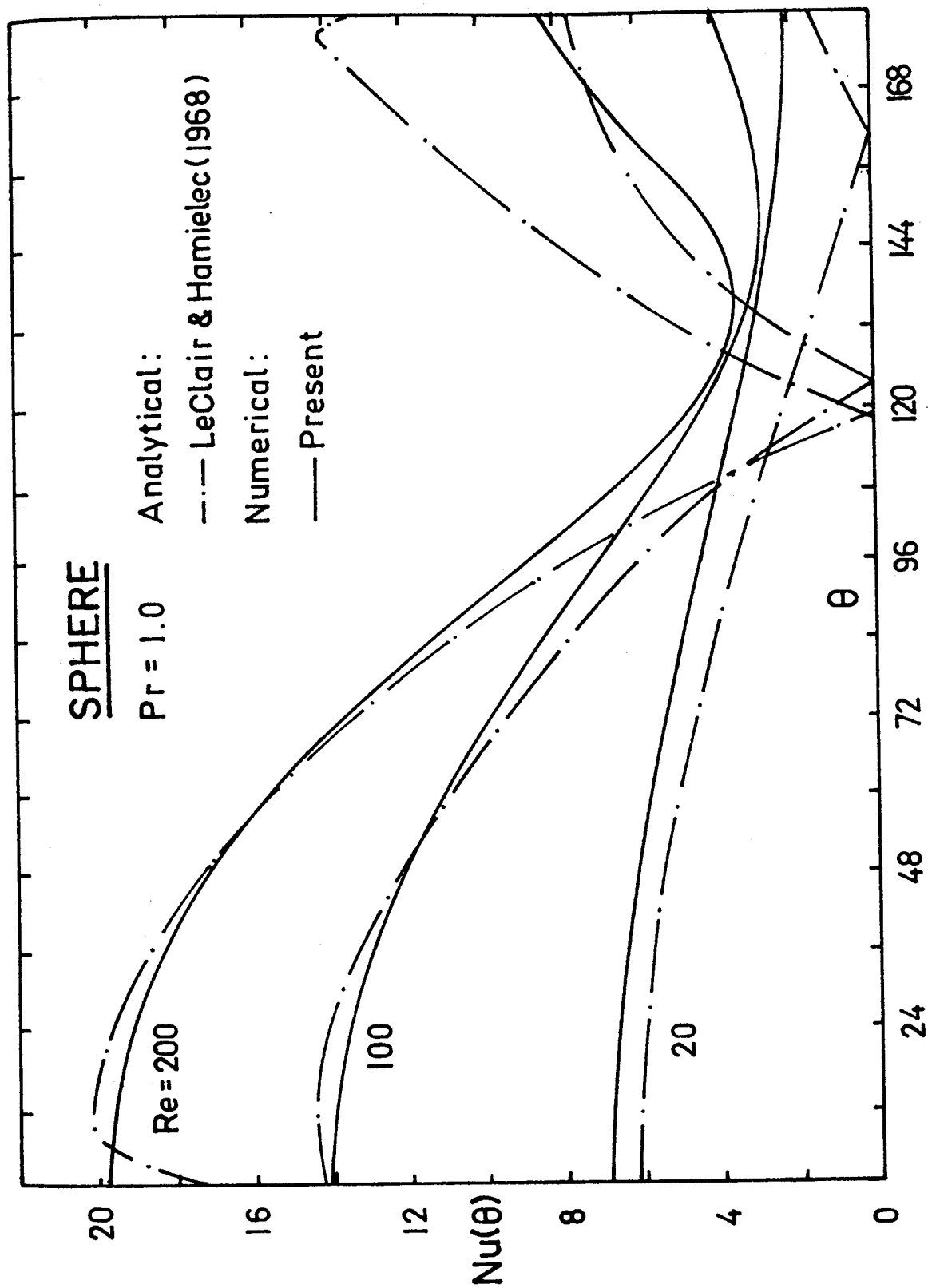

FIGURE 4.2-2 COMPARISON OF THIN THERMAL BOUNDARY LAYER THEORY WITH PRESENT NUMERICAL SOLUTIONS FOR SINGLE SPHERE IN AN UNBOUNDED FLUID

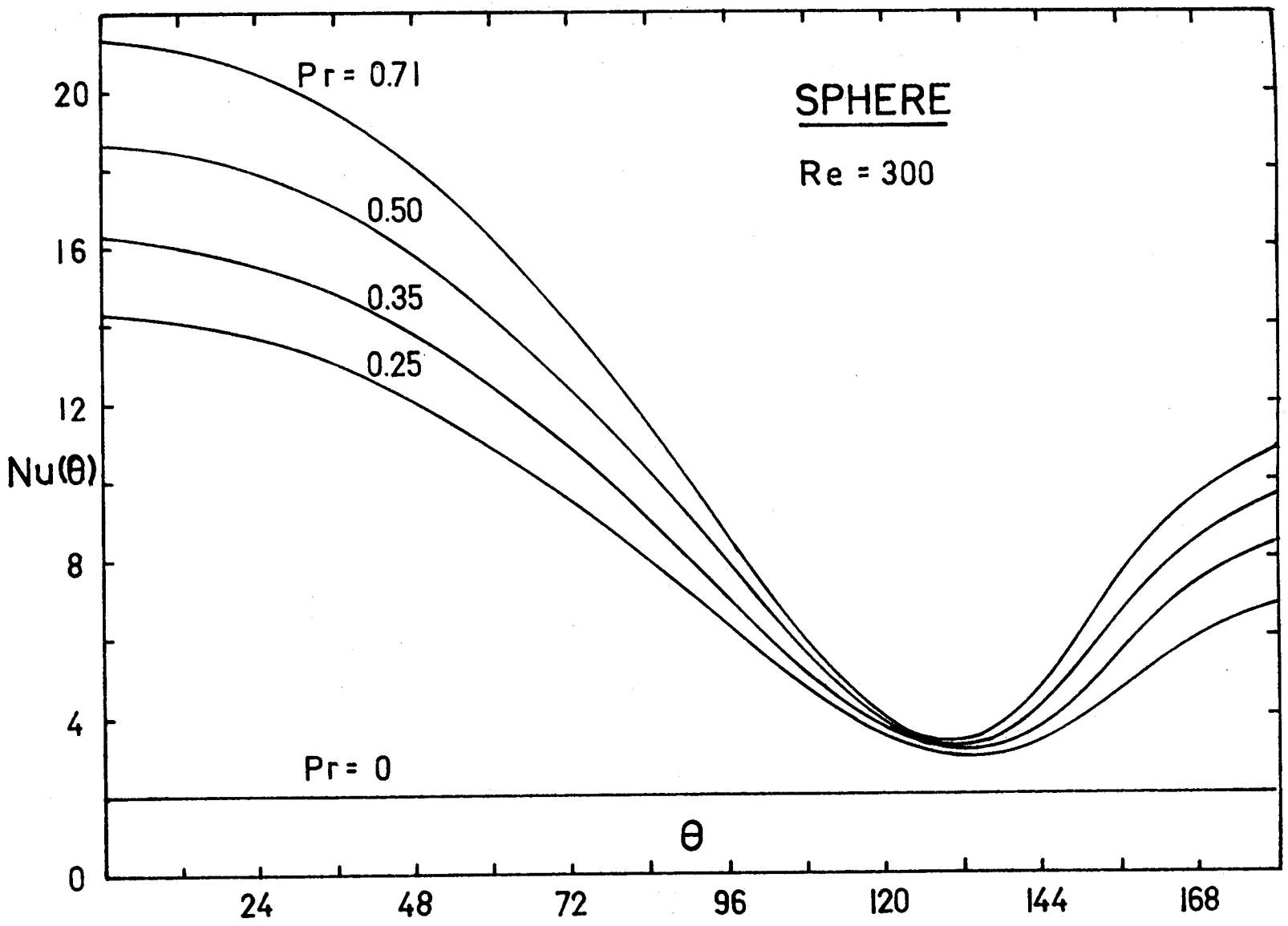

FIGURE 4.2-3 Nu(θ) AT VARIOUS Pr, FOR SINGLE SPHERE IN AN UNBOUNDED FLUID

boundary layers at higher Prandtl numbers. The angle of minimum transfer, as observed in this figure moves away from the rear stagnation point as the Prandtl number increases. For Pr = 0, the transfer rate is uniform over the surface. Within the low Prandtl number range investigated in this study, the minimum transfer angle Θ_M is significantly smaller than the flow separation angle Θ_s. This is undoubtedly the result of angular diffusion which tends to move the minimum transfer angle Θ_M towards the rear stagnation point. The difference between Θ_s and Θ_M is less pronounced at higher Prandtl numbers because of the thinner thermal boundary layer and the reduction in importance of angular diffusion. It can be predicted that as $Pr \to \infty$, $\Theta_M \to \Theta_s$ asymptotically. This observation indicates that flow separation angles measured by estimation of the point of minimum heat or mass transfer at low Pr or Sc systems can be significantly in error. The variation of Θ_M with Pr at various Re are tabulated in Table 4.2-1 and shown graphically in Figure 4.2-2.

Average Nusselt (or Sherwood) numbers are tabulated in Table 4.2-2. Nu **vs** Pr are plotted for various Re in Figure 4.2-5. The linear relationship between log Nu and log Pr for Re = 10 to 300 suggests a correlation of the form

$$Nu = a\ Pr^b \qquad (4.2\text{-}1)$$

where a, b are functions of Re. Linear regressions were made on a, b at various Re and the results are shown in Figure 4.2-6. This figure suggests that a and b can be expressed as

Table 4.2-1 θ_M for Sphere

Re	Pr 0.25	0.5	0.71	1.0
20	0°	0°	0°	0°
30	0°	0°	0°	0°
57	0°	6°	12°	18°
100	27°	30°	33°	36°
200	39°	42°	45°	47.4°
300	45°	48°	51°	53.4°

FIGURE 4.2-4 SEPARATION ANGLE Θs, MINIMUM TRANSFER ANGLE Θ_M, vs Re FOR SINGLE SPHERE IN AN UNBOUNDED FLUID

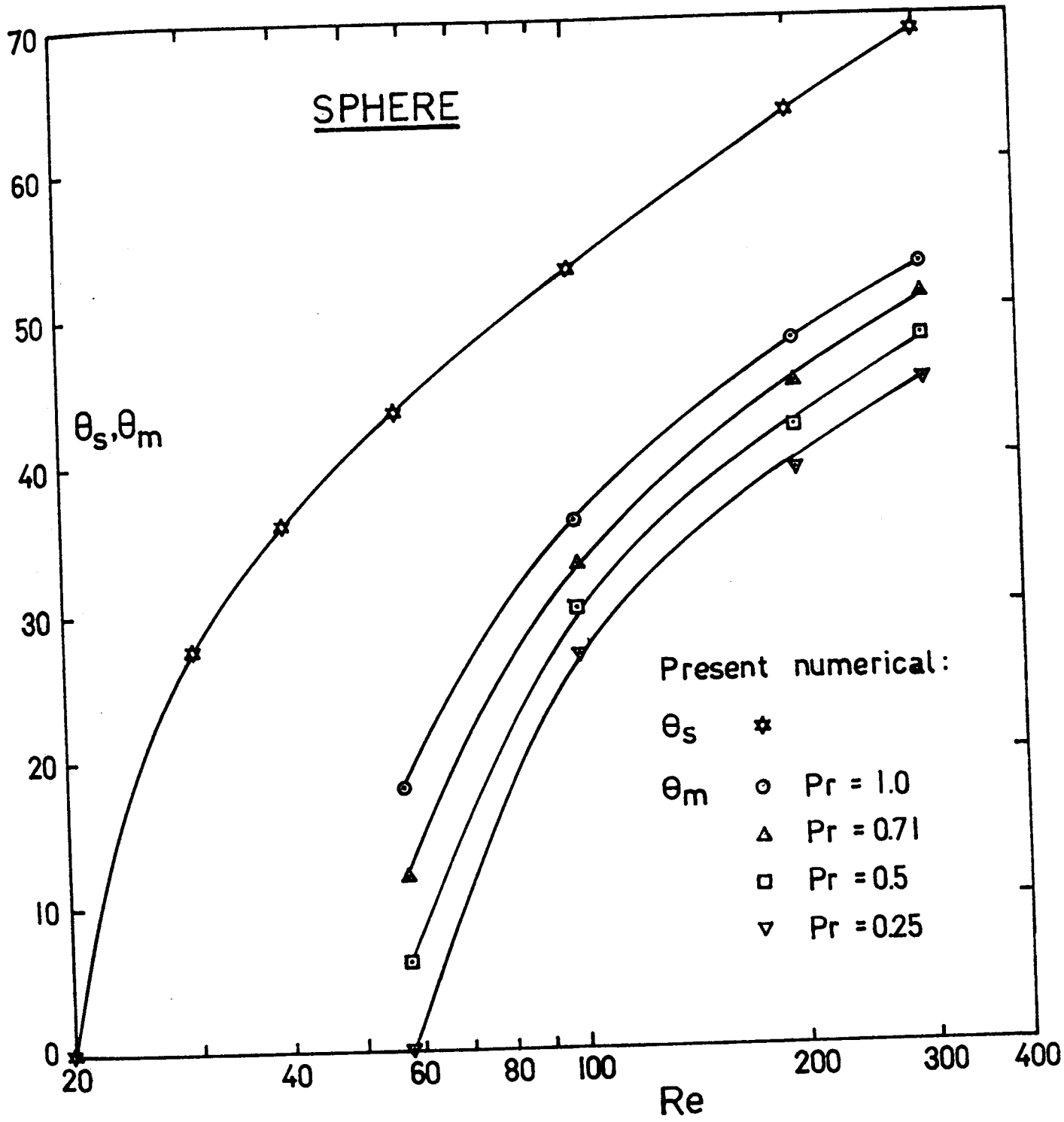

Table 4.2-2 Nu for a Single Sphere in an Unbounded Fluid

	Re						
Sc	1	10	30	57	100	200	300
0.25				4.28	5.13	6.59	7.77
0.35					5.66	7.34	8.70
0.50	2.187	3.10	4.20	5.20	6.29	8.25	9.83
0.71	2.246	3.34	4.61	5.75	6.99	9.26	10.95
1.0	2.321	3.61	5.06	6.36	7.80	10.44	12.51
2.0	2.521	4.26	6.14	7.85			
3.5	2.743	4.91	7.23	9.38			
5.0	2.916	5.41	8.06	10.56			

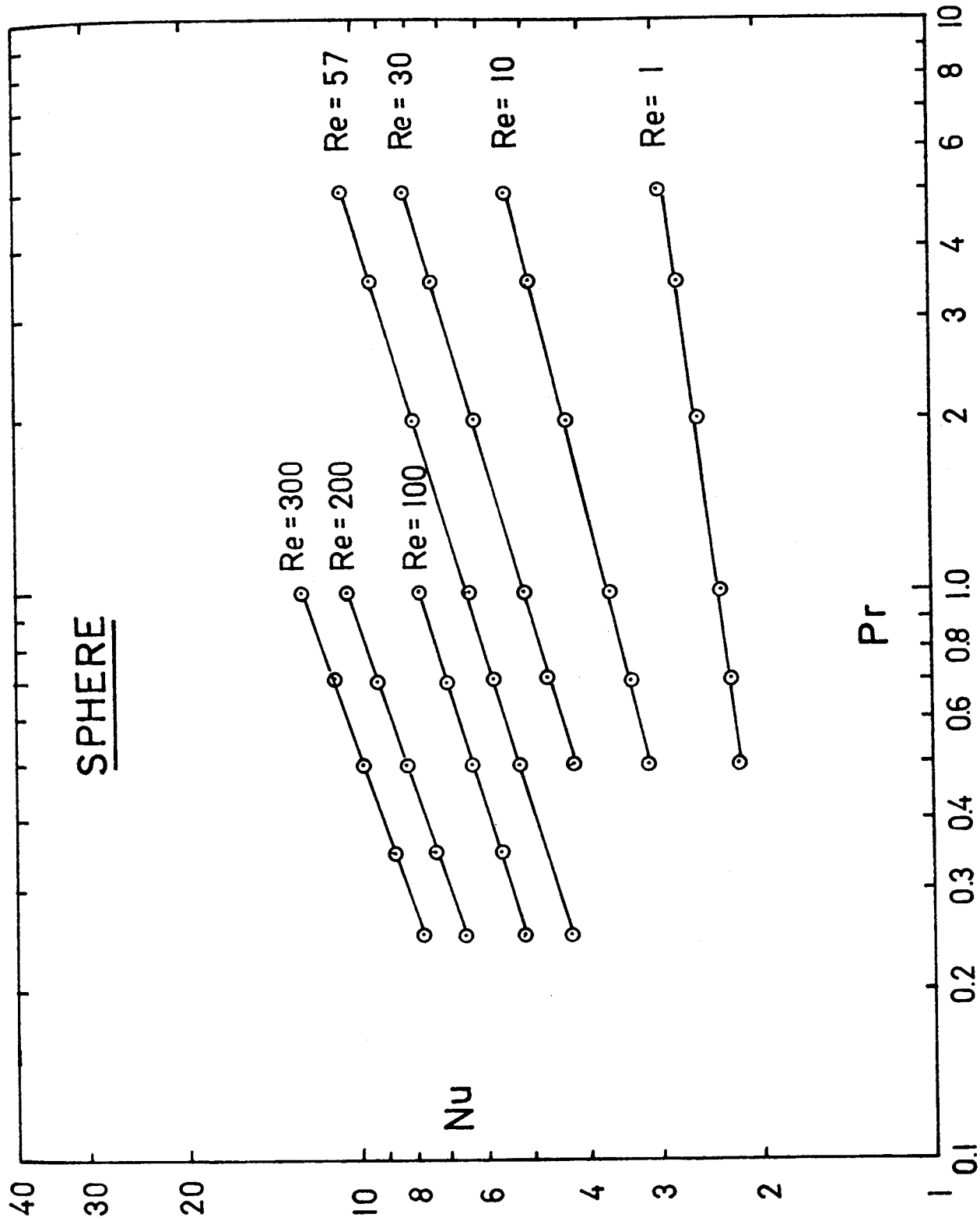

FIGURE 4.2-5 Nu vs Pr AT VARIOUS Re FOR SINGLE SPHERE IN AN UNBOUNDED FLUID

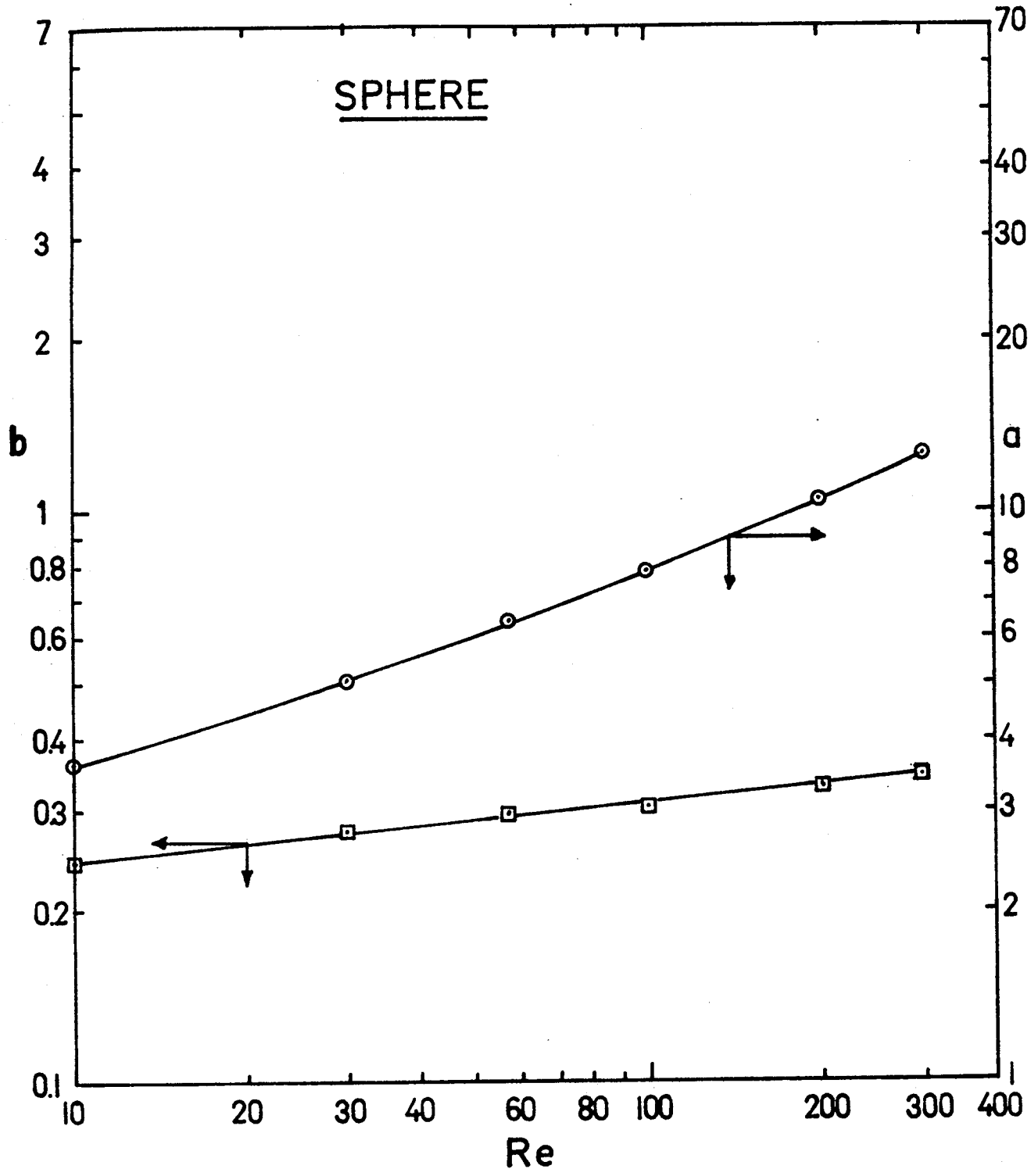

FIGURE 4.2-6 a, b vs Re

$$a = d_o + d_1 Re + d_2 Re^2 + d_3 Re^3 + ---$$

$$b = C_1 \, Re^{C_2}$$

Least square fitting of these curves gave

$$a = 3.103 + 0.681 \times 10^{-1} Re - 0.233 \times 10^{-3} Re^2 + 0.365 \times 10^{-6} Re^3$$

$$b = 0.198 \, Re^{0.096} \qquad (4.2\text{-}2)$$

The final correlation for forced convection heat or mass transfer takes the form of equation (4.2-1) with a, b functions of Re given by equation (4.2-2). This correlation is valid for $10 < Re < 300$ and $0.25 < Pr < 5$.

For the case of Pr = 0.71, calculations have also been made for Re = 0.05, 0.1, 0.2, 0.5, 0.75, 0.2, 3, and 5 in addition to those Reynolds numbers mentioned earlier and results are listed in Table 4.2-3. These calculated values are in excellent agreement with recently measured values of Beardand Pruppacher (1971). Figures 4.2-7 and 4.2-8 show the variation of Nu/2 or Sh/2 with $Re^{\frac{1}{2}} Pr^{1/3}$ or $Re^{\frac{1}{2}} Sc^{1/3}$ at low and high $Re^{\frac{1}{2}} Pr^{1/3}$ respectively. Analytical solutions of Acrivos and Taylor (1962), Rimmer(1969) and numerical solutions of Brian and Hales (1969) and experimental measurements of Ranz and Marshall (1952) and Beard and Pruppacher (1971) are also shown with present predictions. It is seen that analytical solutions by perturbation analysis are valid only at very low $Re^{\frac{1}{2}} Pr^{1/3}$ range (≤ 0.6) where they agree satisfactorily with numerical solutions of present study and Brian and Hales who employed Stokes velocity profiles. Measurements of Ranz and Marshall probably over estimated the transfer rates due to suspension technique used, and low values of Beard and Pruppacher may be caused by the difficulty of

Table 4.2-3 Nu or Sh Single Sphere in an Unbounded Fluid

$Sc = Pr = 0.71$

$Sc^{1/3} = 0.892$

$Re = 0.05 \sim 300$

Re	Sh	$Re^{\frac{1}{2}}$	$Sc^{1/3} Re^{\frac{1}{2}}$
0.05	2.016	0.2235	0.199
0.1	2.028	0.316	0.282
0.2	2.058	0.4475	0.399
0.5	2.136	0.707	0.631
0.75	2.194	0.866	0.772
1.0	2.246	1.000	0.892
2.0	2.430	1.414	1.262
3.0	2.588	1.732	1.544
5.0	2.844	2.236	1.992
10	3.34	3.16	2.820
30	4.61	5.48	4.88
57	5.75	7.55	6.73
100	6.98	10.0	8.92
200	9.26	14.14	12.60
300	10.95	17.32	15.43

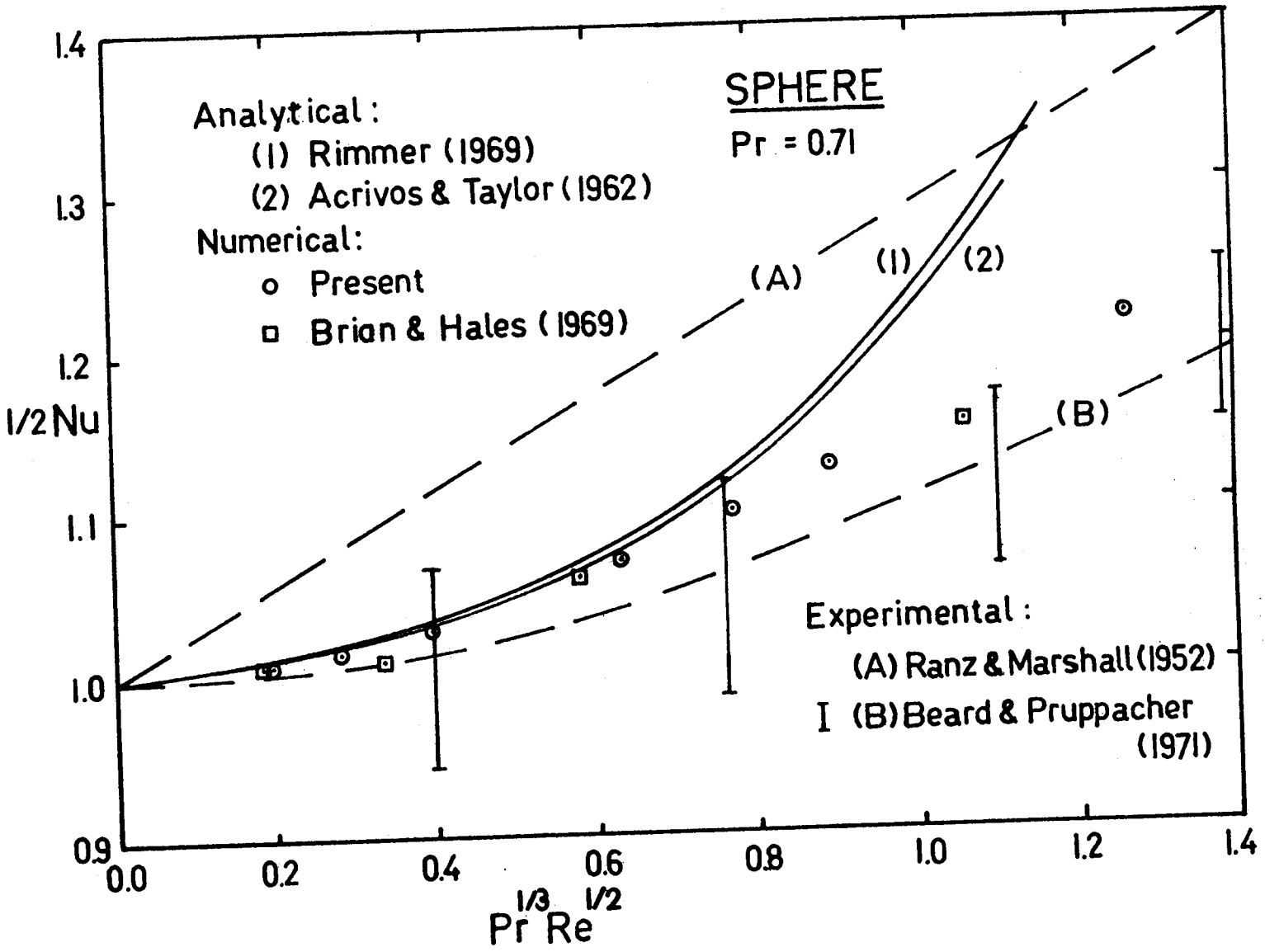

FIGURE 4.2-7 Nu/2 vs $Pr^{1/3} Re^{1/2}$ FOR $Pr^{1/3}Re^{1/2} \leq 1.4$ FOR SINGLE SPHERE IN AN UNBOUNDED FLUID

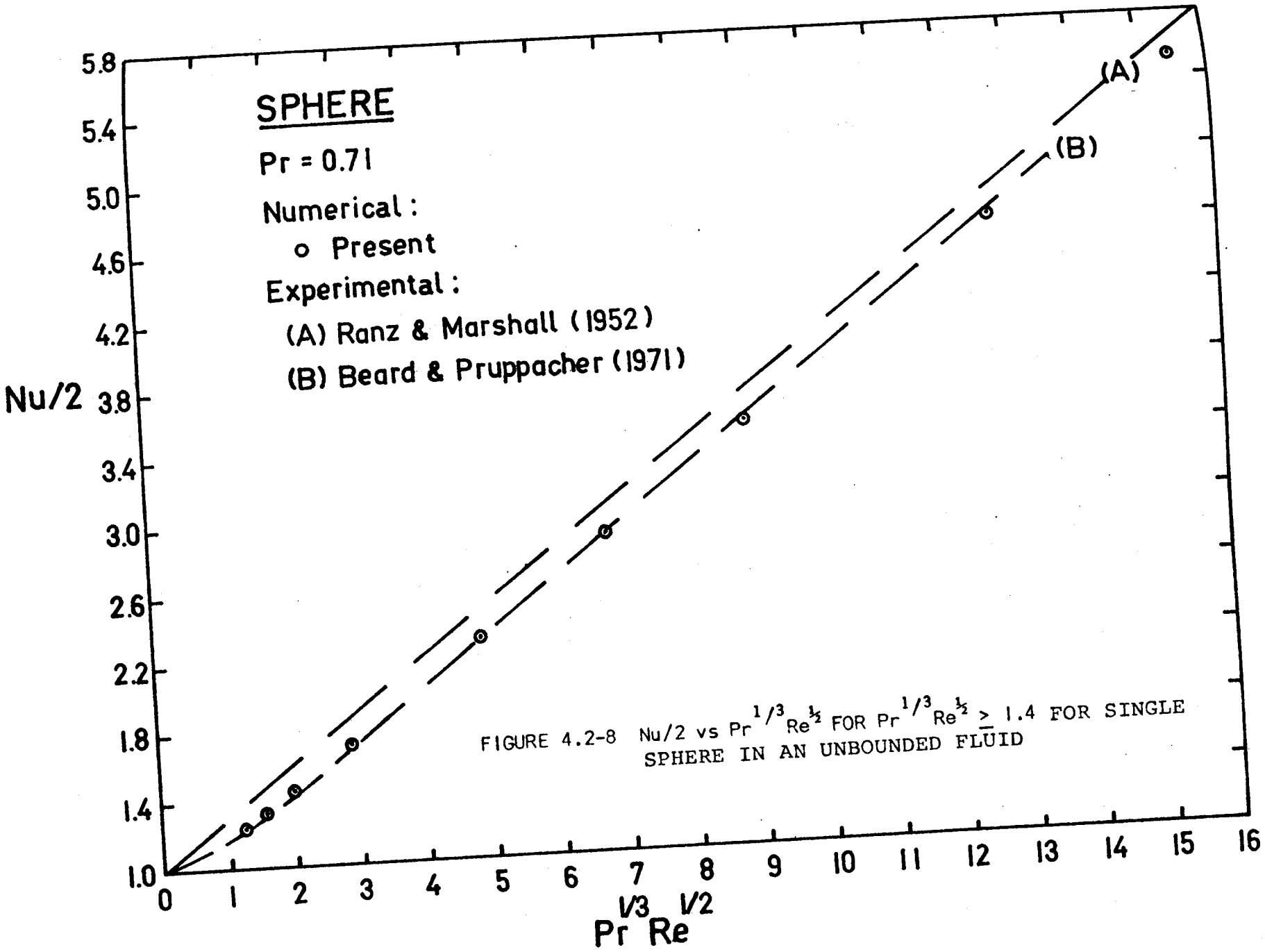

FIGURE 4.2-8 Nu/2 vs $Pr^{1/3}Re^{1/2}$ FOR $Pr^{1/3}Re^{1/2} \geq 1.4$ FOR SINGLE SPHERE IN AN UNBOUNDED FLUID

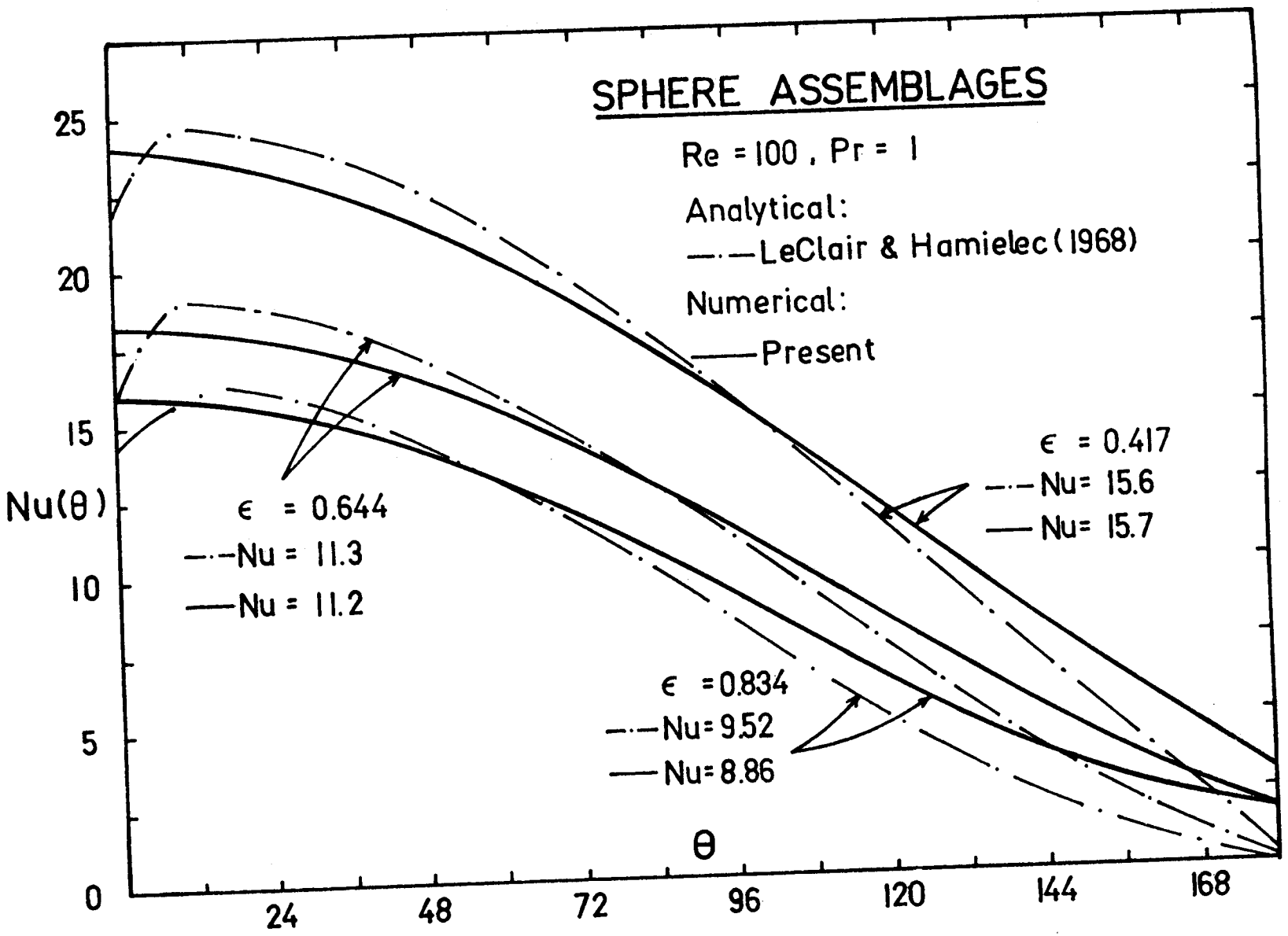

FIGURE 4.2-9 COMPARISON OF THIN THERMAL BOUNDARY LAYER THEORY WITH PRESENT NUMERICAL SOLUTIONS FOR SINGLE SPHERE IN AN ASSEMBLAGE AT VARIOUS POROSITIES

low Reynolds number measurements. At moderately high $Re^{\frac{1}{2}} Pr^{1/3}$ (> 1.4), the present predictions agree very well with Beard and Pruppacher, who used freely suspended drops. The maximum error is about 4%.

Sphere Assemblages

Calculations were made for Re = 100, Pr = 1.0 and three porosities ε = 0.417, 0.644 and 0.834. Velocity profiles used in these calculations were originally calculated by LeClair and Hamielec (1968). Local Nusselt or Sherwood numbers which are difficult to measure experimentally are also calculated and these are tabulated in **AppendixB.2** Comparison between local transfer rates predicted in present numerical analysis and analytical solutions using thin thermal boundary layer theory (LeClair and Hamielec 1968) are shown in Figure 4.2-9. It is observed that in concentrated particle systems, the average Nusselt(or Sherwood) numbers calculated analytically agree quite well with numerical solutions. Best agreement is observed at low porosities where particle interaction is strongest. Particle interaction suppresses the formation of a vortex ring making the approximations of the thin thermal boundary layer theory more reasonable. The local transfer rates differ somewhat.

4.3 Forced Convection Around a Single Cylinder in an Unbounded Fluid and in a Bundle

4.3.1 Governing Equations, Boundary Conditions and Method of Solution

The governing equation for forced convection around a cylinder is the elliptic continuity equation of heat or mass,

$$\frac{\partial \psi^*}{\partial z}\frac{\partial \eta^*}{\partial \theta} - \frac{\partial \psi^*}{\partial \theta}\frac{\partial \eta^*}{\partial z} = \frac{2}{Pe}\left(\frac{\partial^2 \eta^*}{\partial z^2} + \frac{\partial^2 \eta^*}{\partial \theta^2}\right)$$

and the boundary conditions of constant surface temperature or concentration are

$$\text{at } z = 0 \quad ; \quad \eta^* = 1$$

$$\text{at } z = z_\infty \quad ; \quad \eta^* = 0$$

$$\text{at } \theta = 0, \pi; \quad \frac{\partial \eta}{\partial \theta} = 0$$

The stream function ψ^* has already been calculated in Section 4.1 for a single cylinder in an unbounded fluid. For a cylinder in a bundle, ψ^* values calculated by LeClair **and Hamielec (1970) are used.**

The linear elliptic partial differential equation was solved using the new sequence tridiagonalization with convergence acceleration described in Section 3.3.4. Initial guess of η^* field is $\eta^* = 0$ everywhere. FORTRAN IV computer program is similar to that for sphere except the energy equation.

4.3.2 Mesh Dimensions and Accuracy of Solutions

The step sizes A and B for η^* field used are identical to those listed in Section 4.1.3 for the flow field of a cylinder. Calculations were made for A = 0.0314 and 0.05 at Re = 85, Pr = 0.74, B = $\pi/30$ and r^* = 9.03. Local Nusselt numbers are listed in Table 4.3-1. Maximum difference (< 2%) appears at the frontal stagnation point where thermal boundary is thinnest. Average Nusselt numbers however differed by less than 1%. From this test, the A and B used are believed to give average Nusselt numbers with errors less than those of experimental investigations.

The η^* field is not as sensitive to the outer boundary r^*_∞ as the ψ^* and ξ^* fields which is similar to the case of the sphere however more pronounced effect may be observed since the wake behind a cylinder

Table 4.3-1 Nu(θ) for Cylinder

Re = 85, Pr = 0.74

$r^* = 9.03$, $B = 30/\pi$

ANGLE	A	
	0.0314	0.05
0	9.02	9.17
12	8.93	9.08
24	8.70	8.82
36	8.30	8.40
48	7.73	7.80
60	7.01	7.04
72	6.13	6.14
84	5.13	5.13
96	4.07	4.08
108	3.07	3.08
120	2.22	2.23
132	1.69	1.69
144	1.58	1.56
156	1.79	1.74
168	2.06	1.99
180	2.17	2.10
Average Nusselt Number	4.76	4.78

at intermediate Reynolds number has much larger dimensions than that of the sphere, and therefore considerably larger r^*_∞ must be used to closely simulate $\eta^* = 0$ at r^*_∞. Table 4.3-2 indicates the local Nusselt and average Nusselt numbers for cylinder at Re = 85, Pr = 0.74 at r^*_∞ = 9.03 and 7.03. The average Nusselt number differed by less than 4%. However the local Nusselt numbers are appreciably in error. This is because the choice of r^*_∞ = 7.03 which is less than the length of the vortex (L ≐ 8.5, Hamielec and Raal 1969) and the boundary condition $\eta^* = 0$ near the rear end is not satisfied since the trailing vortex is known to have high concentration due to internal circulation. A choice of r^* = 9.03 which is comparable to the length of the vortex is believed to give better result. It is therefore recommended that r^*_∞ be chosen considerably larger than the length of the vortex ring.

The accuracy of the numerical solutions also depends on the tolerance ε of equation 13.3-30). ε was set equal to 10^{-3} to give a maximum change of less than 0.1% per iteration of the local or average Nusselt number.

4.3.3 Discussion of Results and Comparison with Existing Data

Calculations were made for Re = 2, 10, 23, 40, 85 and 175 for Pr = 0.74. Local Nusselt or Sherwood numbers are tabulated in Appendix B.3. Comparison of present predictions with the experimental data of Eckert and Soehngen (1952) obtained using a Mach Zender interferometer are shown in Figure 4.3-1. The agreement is good. Finite transfer rates at minimum transfer angle are indicated in contrast to zero transfer predicted by thin thermal boundary layer theory (LeClair and Hamielec 1968).

Table 4.3-2 Nu(θ) for Cylinder

Re = 85, Pr = 0.74

A = 0.05, B = π/30

ANGLE	r_∞^*	
	9.03	7.03
0	9.17	8.94
12	9.08	8.85
24	8.83	8.59
36	8.40	8.15
48	7.80	7.55
60	7.04	6.78
72	6.14	5.87
84	5.13	4.86
96	4.08	3.82
108	3.08	2.85
120	2.23	2.10
132	1.69	1.77
144	1.56	1.96
156	1.74	2.44
168	1.99	2.87
180	2.10	3.04
Average Nusselt Number	4.78	4.67

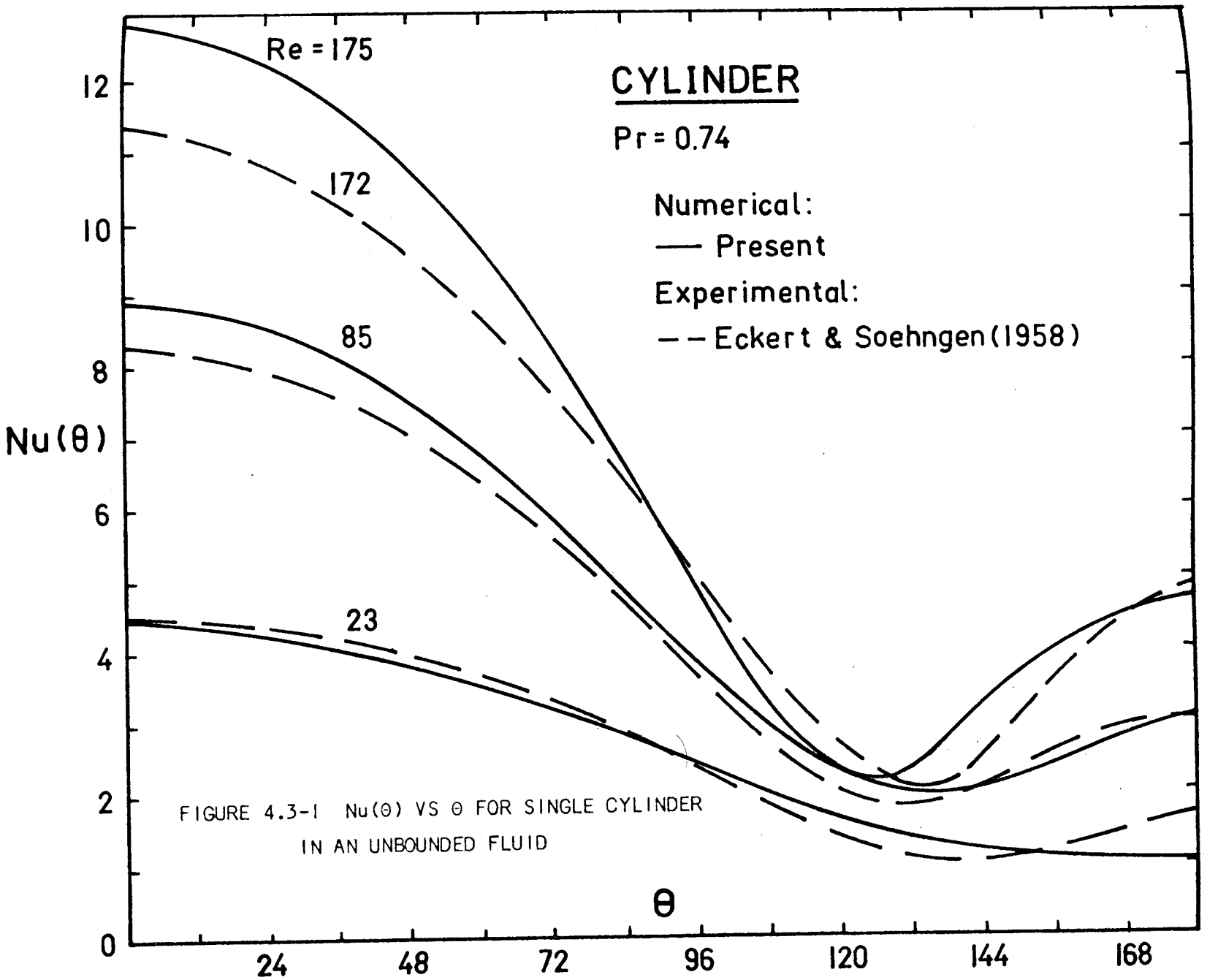

FIGURE 4.3-1 Nu(θ) VS θ FOR SINGLE CYLINDER IN AN UNBOUNDED FLUID

Comparisons have also been made with numerical calculations of Dennis et.al. (1968) for Re = 2, 10 and 40 at Pr = 0.73 in Figure 4.3-2 and the agreement is excellent.

The average Nusselt numbers are tabulated in Table 4.3-1 and comparison with Dennis et.al. (1968) and experimental measurements of Collis and Williams (1959) shows excellent agreement. These are shown in Figure 4.3-3.

Single Cylinder in a Bundle

Calculations were made for Re = 100, Pr = 0.74 and three porosities ε = 0.399, 0.605, 0.798. Velocity profiles used in these calculations were originally calculated by LeClair and Hamielec (1970). Local Nusselt or Sherwood numbers calculated here are tabulated in Appendix B.3. Comparison of predicted local transfer rates of present study and those obtained through use of the thin thermal boundary layer theory are presented in Figure 4.3-4. It can be seen that local transfer rates are not in good agreement even at the lowest porosity ε = 0.399 (highest density). The average Nusselt (or Sherwood) numbers deviate more than 10%. This is because the particle interaction in cylinder bundles does not suppress wake formation as much as for the case of a sphere assemblage. Therefore application of thin thermal boundary layer theory for the calculation of heat or mass transfer in cylinder bundles is not recommended.

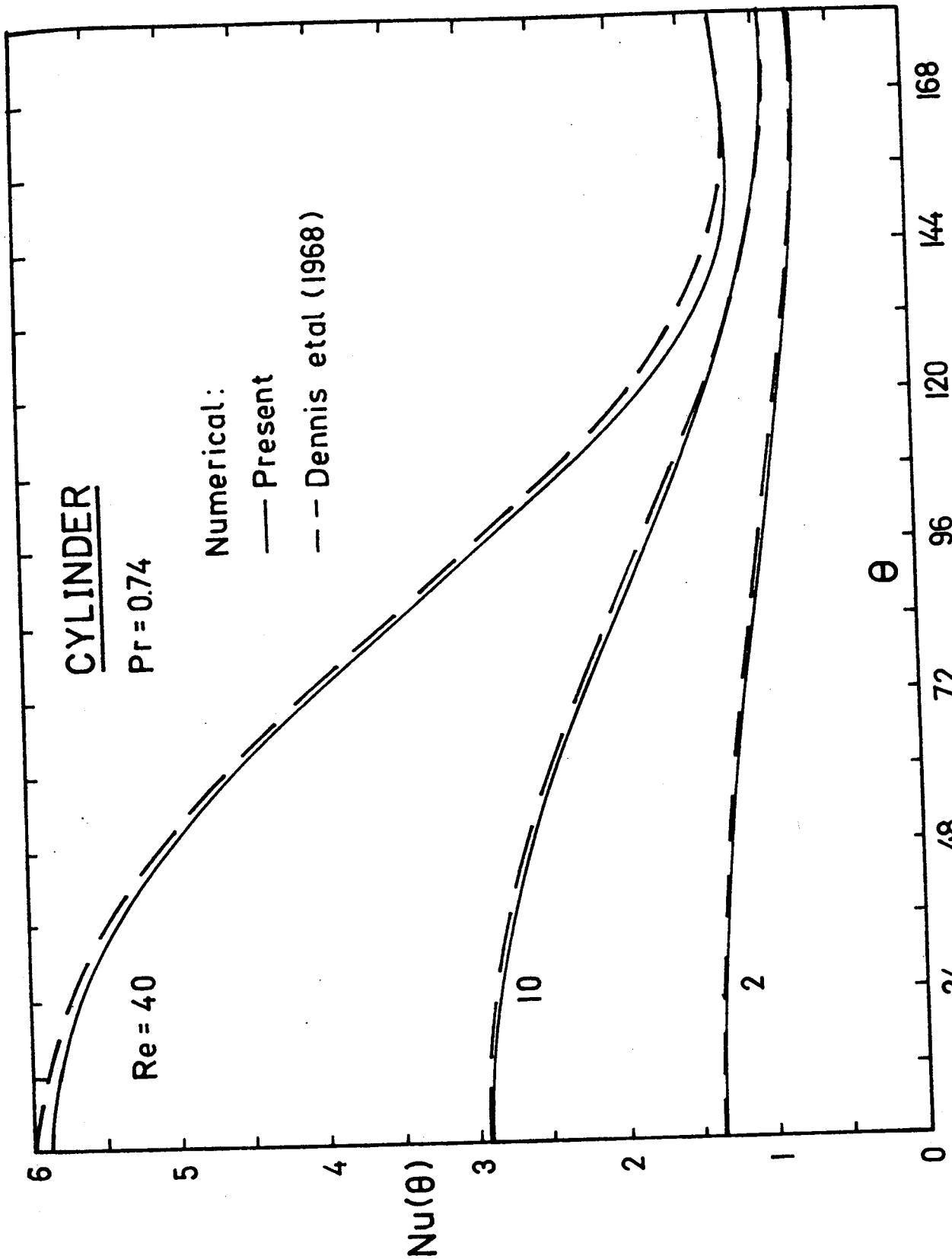

FIGURE 4.3-2 Nu(θ) AT VARIOUS Re FOR SINGLE CYLINDER IN AN UNBOUNDED FLUID

Table 4.3-1 Nu for Cylinder

Re	Nu*	Nu**
1		0.812
2	1.043	1.023
4		1.318
7		1.633
10	1.884	1.897
20		2.557
23	2.638	
40	3.263	3.480
85	4.670	
175	6.466	

* Present, Pr = 0.74

** Dennis et.al. (1968), Pr = 0.73

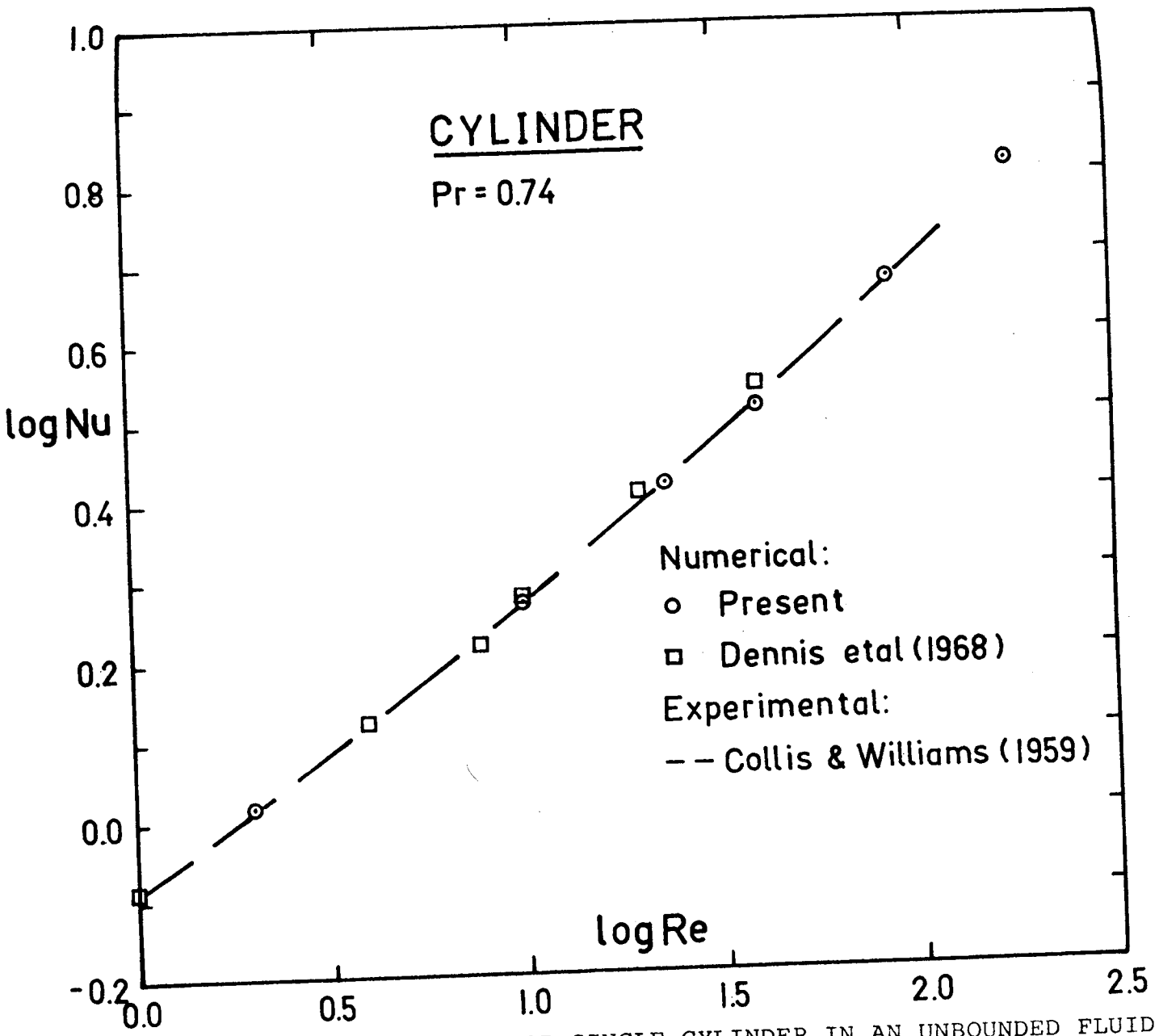

FIGURE 4.3-3 Nu vs Re FOR SINGLE CYLINDER IN AN UNBOUNDED FLUID

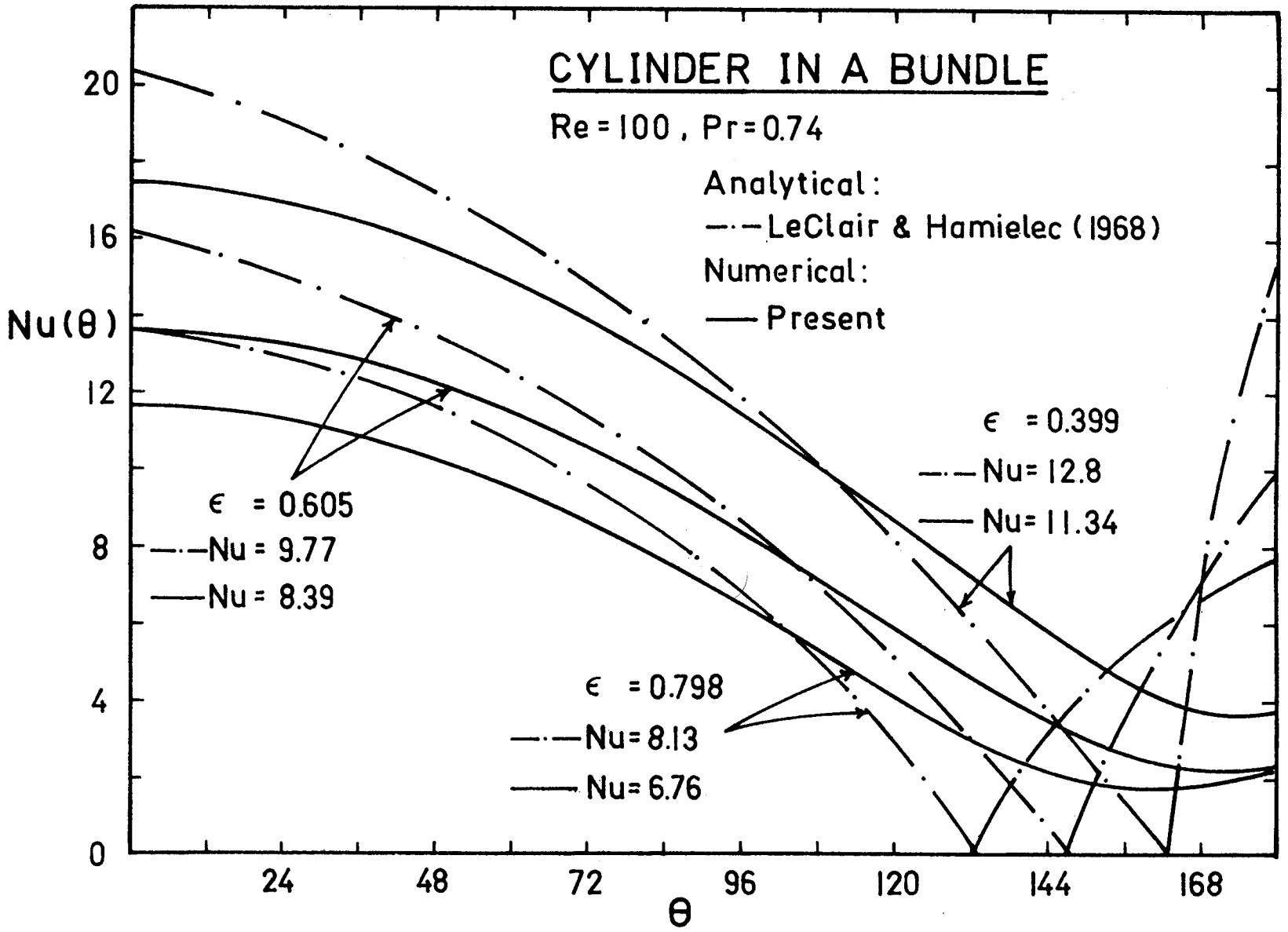

FIGURE 4.3-4 Nu(θ) VS θ, PRESENT NUMERICAL, THIN THERMAL BOUNDARY LAYER SOLUTION FOR SINGLE CYLINDER IN A BUNDLE

4.4 Mixed Convection Around a Single Sphere in an Unbounded Fluid at Pr = 1.0 and 0.71

4.4.1 Governing Equations, Boundary Conditions and Method of Solution

The governing equations for mixed convection around a sphere are the coupled Navier Stokes equations and the continuity equation of heat or mass described in Table 3.1-1. The boundary conditions satisfied follow

$$\text{at } z = 0 \;;\; \psi^* = 0 \qquad , \; \xi^* = \frac{E^*_{sz}\psi^*}{\sin^2\theta} \;, \; \eta^* = 1$$

$$\text{at } z = z_\infty \;;\; \psi^* = \frac{e^{2z}}{2}\sin^2\theta, \; \xi^* = 0 \;, \quad \eta^* = 0$$

$$\text{at } \theta = 0,\pi; \; \psi^* = \xi^* = 0, \qquad \frac{\partial \eta^*}{\partial \theta} = 0$$

The coupled Navier Stokes and energy equations were solved using the new sequence convergence acceleration iteration described in Section 3.3-4. Initial guesses of ψ^*, ξ^* and η^* are Stokes creeping flow solution for Re < 10 and Kawaguti's approximate solution for Re $\geq$ 10 and $\eta^* = 0$ everywhere. FORTRAN IV computer program listing may be found in Appendix A.3.

4.4.2 Mesh Dimensions and Accuracy of Solutions

The step sizes A and B used were

$$0.01 \leq \text{Re} \leq 1.0; \quad A = 0.1 \;, \quad B = \pi/30$$

$$5 \leq \text{Re} \leq 30 \;; \quad A = 0.05 \;, \quad B = \pi/30$$

The size of the outer boundary was selected by trial and error. The values tried will be shown later. At low Reynolds numbers, the wall effect is significant and r^*_∞ of up to several thousands was used. At

moderate Reynolds numbers, smaller r_∞^* were used. The extrapolation technique described in Section 4.1-2 was not used as r_∞^* values used were sufficiently large to closely simulate an unbounded fluid.

A convergence tolerance of $\varepsilon = 10^{-3}$ in equation (3.3-30) was used.

4.4.3 Discussion of Results and Comparison with Existing Data

Heat and Mass Transfer

At Pr = 1.0, calculations were made for Re = 0.01, 0.1 and 1 and Gr from 10^{-2} to 0 for both aiding and opposing flows. To study the effect of Prandtl number on this low Reynolds number system, two illustrative cases were calculated at Pr = 10 for Re = 0.1 and Gr = 0.1, -0.05. Local Nusselt (or Sherwood) numbers are tabulated in Appendix B.4.

Figure 4.4-1 shows the variation of Nu(θ) or Sh(θ) with Gr at Re = 0.1. It can be seen that aiding flow (Gr > 0) increases the rate of transfer at the frontal stagnation point and descreases it at the rear stagnation point. This is a consequence of the aiding natural convection current steepening the thermal boundary layer at the front and thickening it at the rear. For the case of opposing flow (Gr < 0), the opposing natural convection current thickens the thermal boundary layer at the front and steepens it at the rear and at a certain negative Grashof number the natural convection current dominates the flow and the minimum transfer point moves to the frontal stagnation point. It can be concluded that there exist certain Grashof numbers where the minimum transfer point θ_M lies between $\theta = 0, \pi$. The flow separation

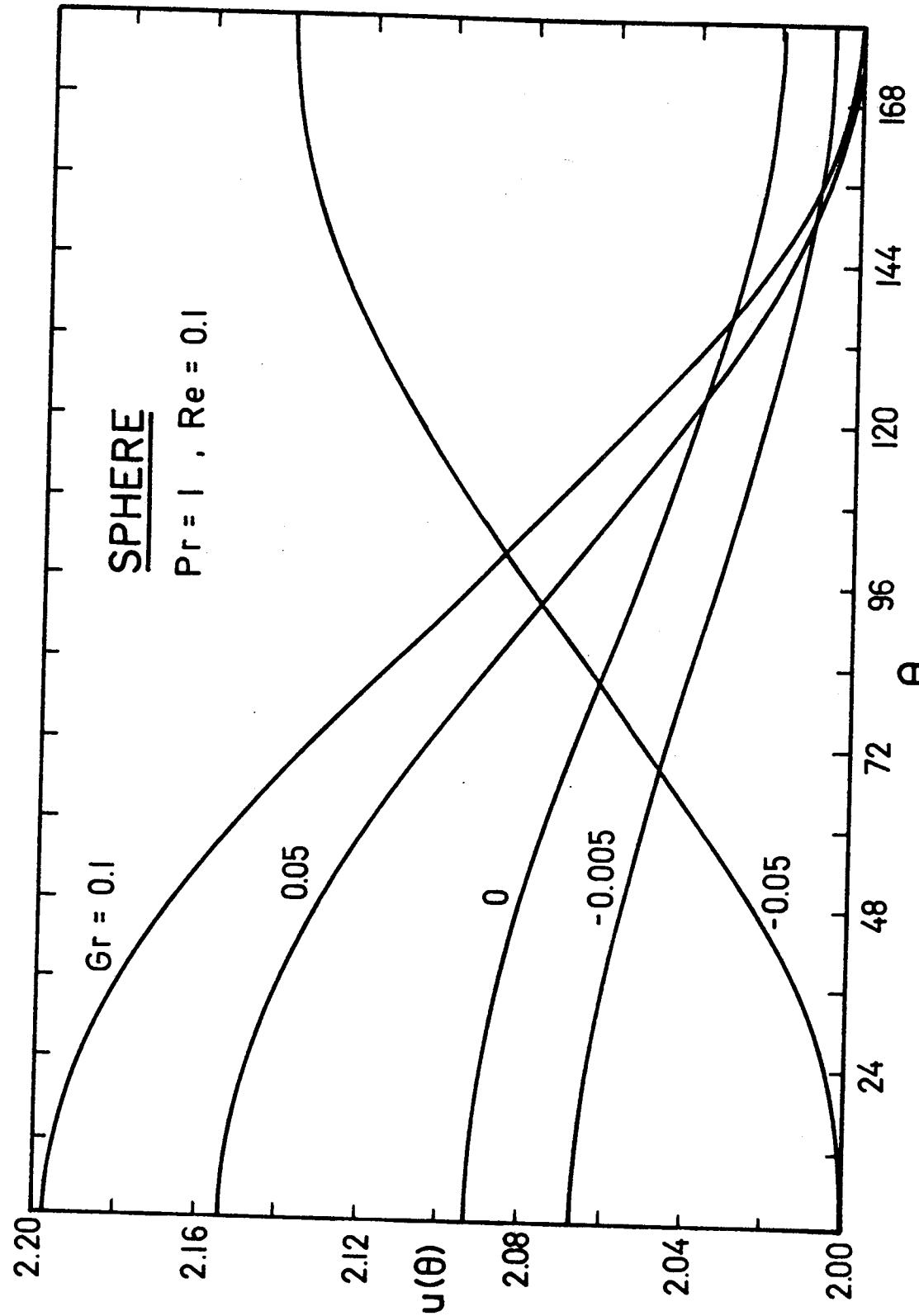

FIGURE 4.4-1 Nu(θ) AT VARIOUS Gr FOR SINGLE SPHERE IN AN UNBOUNDED FLUID

angles θ_s also lie between 0, π and θ_M and θ_s are different in magnitude. It is important to note that even though the Reynolds numbers are in the so called creeping flow regime, flow separation may occur due to opposing free convection flow.

Figure 4.4-2 shows the effect of Prandtl number on Nu(θ) at Re = 0.1 and Gr = -0.05. At Pr = 1.0 and Gr = -0.05 an opposing natural convection current alters the flow significantly with the minimum transfer rate appearing at the frontal stagnation point. When Pr increases to 10, the minimum transfer point moves to the rear stagnation point which indicates that the natural convection field is now not as strong and does not dominate the flow field.

In Table 4.4-1, is tabulated the variation of average Nusselt (or Sherwood) number with Grashof number for both aiding and opposing flows. It can be seen that for Re = 0.01 and 0.1, Nu and Sh is close to 2 (the pure conduction or diffusion asymptotic limit) with a maximum deviation of about 5%. There exists a certain Gr which will give a minimum average transfer rate for both aiding and opposing flows. However as the mechanism of mixed convection flow is very complicated and non-additive (Acrivos 1958, 1966), this small variation may be the result of step size and or wall effect errors. For the case of Re = 1, Nu is seen to increase and decrease monotonically with Gr for aiding and opposing flow, respectively in the Gr range under consideration.

At Pr = 0.71, calculations have been made for Re = 5, 10, 20 and 30 and Gr from 0 - 300 for both aiding and opposing flows. Local Nusselt (or Sherwood) numbers are tabulated in Appendix B.4.

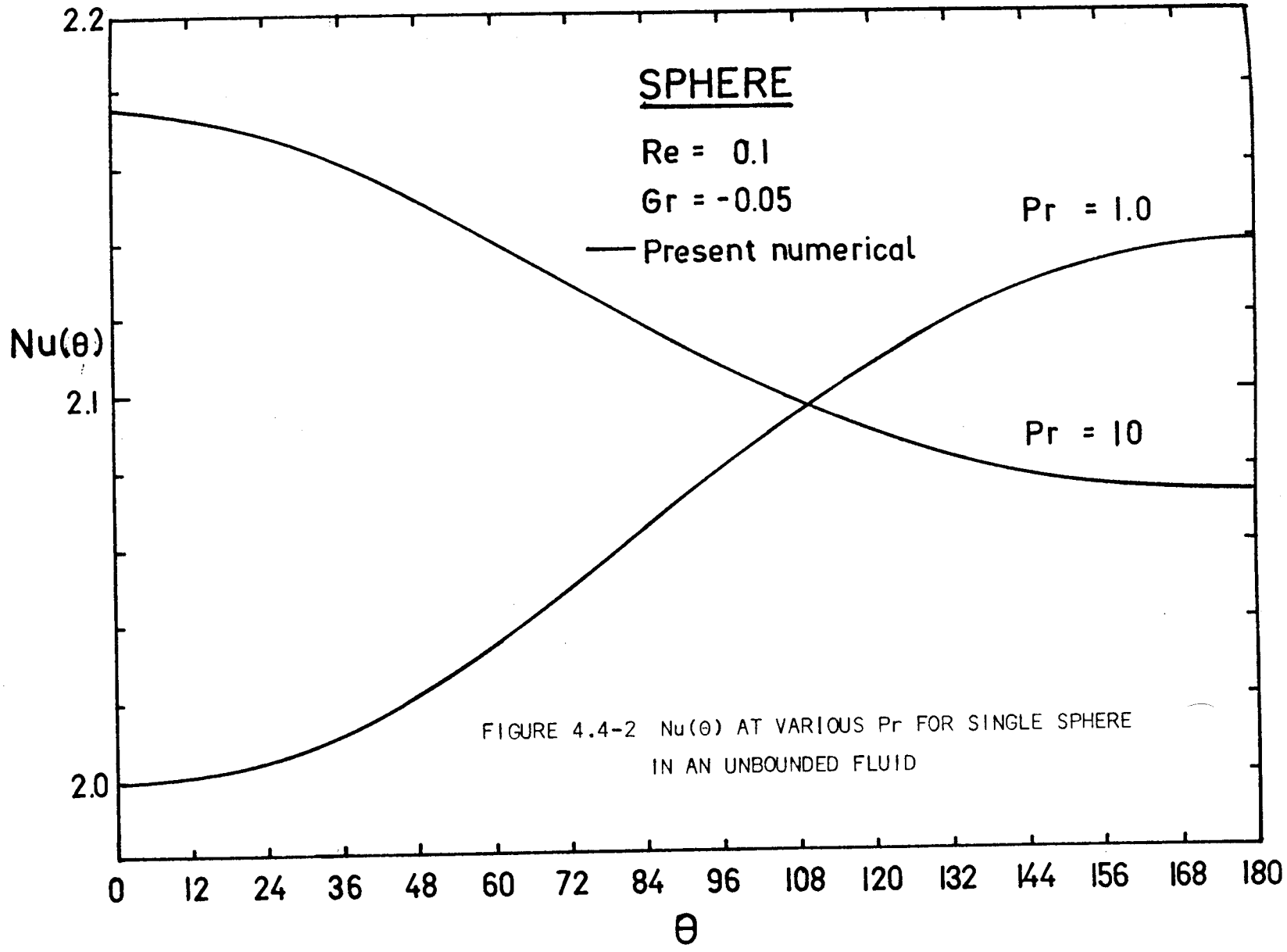

FIGURE 4.4-2 Nu(θ) AT VARIOUS Pr FOR SINGLE SPHERE IN AN UNBOUNDED FLUID

Table 4.4-1 Nu or Sh at Pr = 1.0

Single Sphere in an Unbounded Fluid

Aiding Flow

Re/Gr	0	5×10^{-4}	10^{-3}	5×10^{-3}	10^{-2}	5×10^{-2}	10^{-1}	5×10^{-1}	1.0
10^{-2}	2.021	2.004	2.005	2.018	2.028				
				2.046	2.048	2.078	2.100		
10^{-1}	2.060					2.323	2.327	2.354	2.383
1.0	2.321								

Opposing Flow

Re/Gr	0	5×10^{-4}	10^{-3}	5×10^{-3}	10^{-2}	5×10^{-2}	10^{-1}	5×10^{-1}	1.0
10^{-2}	2.021	2.000	2.000	2.018	2.028				
				2.035	2.027	2.069	2.104		
10^{-1}	2.060					2.318	2.312	2.275	2.197
1.0	2.321								

Figure 4.4-3 shows the variation of Nu(θ) or Sh(θ) with Gr at Re = 30. It can be seen that aiding flow increases the transfer rate at the frontal stagnation point and decreases it at the rear whereas opposite results are obtained for opposing flow. Also minimum transfer points do exist at Gr = -300 and -200 and for other Grashof numbers, the minimum transfer points all appears at the rear stagnation point. This is because opposing flow moves the flow separation angle to the front and aiding flow moves it to the rear, a point to be discussed later.

The average Nu or Sh are tabulated in Table 4.4-2. Nu or Sh increases for aiding flow and decreases for opposing flow, however the changes are small in the Gr range considered. Comparisons of present predictions with experimental measurements of Yuge (1960) indicate good agreement. Experimental measurements of Narasimham and Gauvin (1966) are for very high Grashof numbers outside our range. Unfortunately there exists no data in the literature in the low Grashof number range under consideration here.

Flow Phenomena and Drag Coefficient

The properties of mixed convection flow around a sphere are extremely complex, particularly for opposing flows. Surface pressure and vorticity distributions for various Gr and Re are tabulated in Appendix B.4.

Figures 4.4-4 and 4.4-5 show surface pressure and vorticity distributions respectively at Re = 0.1 and Pr = 1.0 for various Gr.

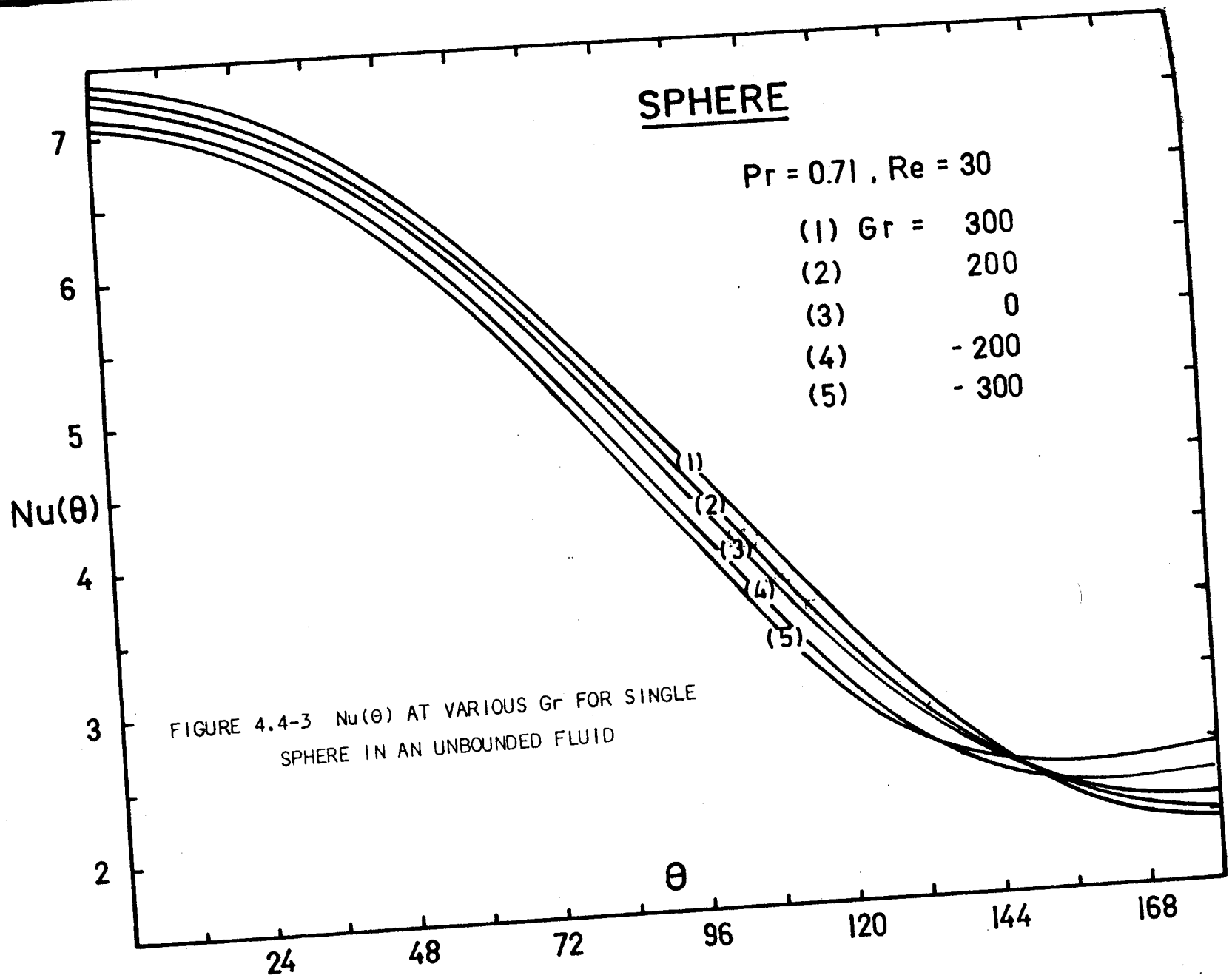

FIGURE 4.4-3 Nu(θ) AT VARIOUS Gr FOR SINGLE SPHERE IN AN UNBOUNDED FLUID

Table 4.4-2 Nu or Sh at Pr = 0.71

for Single Sphere in an Unbounded Fluid

Aiding flow

Re/Gr	1	5	10	15	25	50	100	200	300
5	2.850	2.876	2.908	2.937					
10		3.35	3.36		3.40	3.46	3.55		
20			4.07		4.08	4.11	4.15 *	4.21 **	4.30 ***
30					4.63	4.64	4.67	4.73	4.77

Opposing flow

Re/Gr	1	5	10	15	25	50	100	200	300
5	2.836	2.802	2.754	2.695					
10		3.32	3.31		3.26	3.16			
20			4.04		4.02	3.99	3.93	3.76	
30					4.59	4.58	4.54	4.47	4.39

* Gr = 99

** Gr = 179

*** Gr = 293

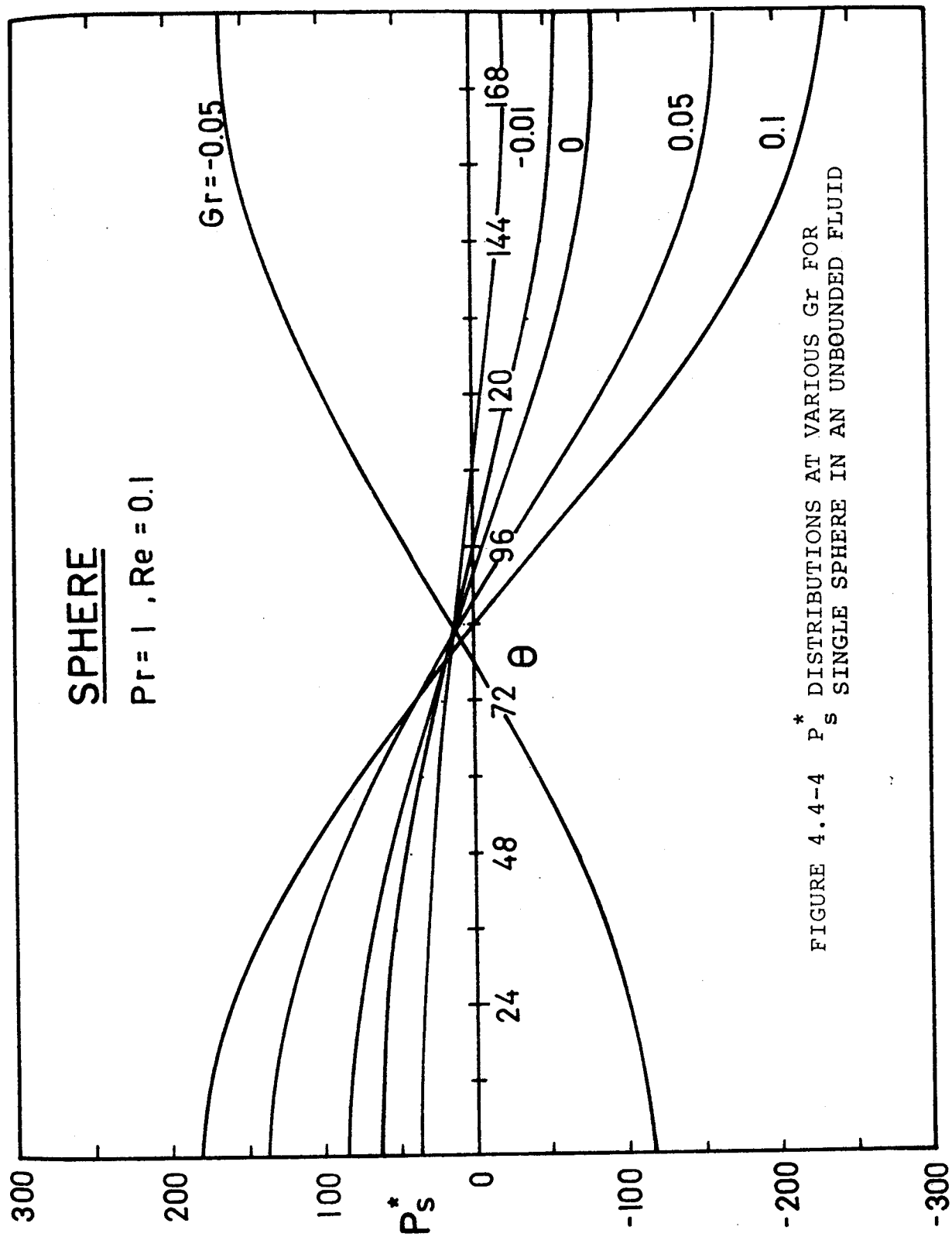

FIGURE 4.4-4 P_s^* DISTRIBUTIONS AT VARIOUS Gr FOR SINGLE SPHERE IN AN UNBOUNDED FLUID

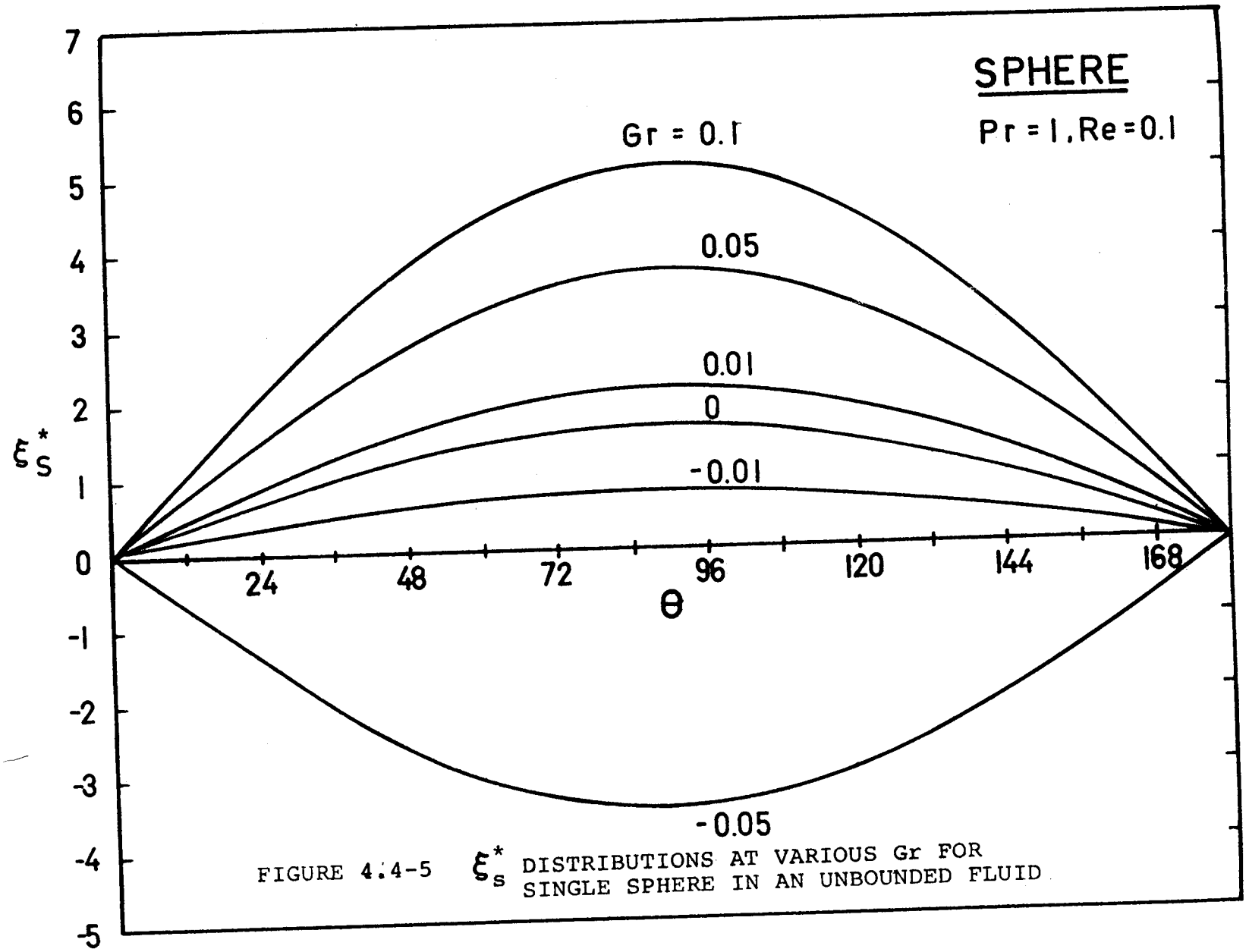

FIGURE 4.4-5 ξ_s^* DISTRIBUTIONS AT VARIOUS Gr FOR SINGLE SPHERE IN AN UNBOUNDED FLUID

The frontal stagnation pressure increases with increasing Gr in aiding flow and decreases in the case of opposing flow. Negative frontal stagnation pressure is experienced at a certain negative Gr. The rear stagnation pressure behaves exactly opposite to the frontal stagnation pressure as can be seen in Figure 4.4-4. The surface vorticity as shown in Figure 4.4-5 increases for aiding flow and decreases for opposing flow. Negative surface vorticity is experienced at a certain negative Gr. These phenomena including the surface pressure indicate that the natural convection current for this Gr completely dominates the flow, and negative drag is experienced by the particle.

The form and friction drag coefficients are tabulated in Tables 4.4-3, 4.4-4 and 4.4-5 at Pr = 1.0. The outer boundary r_∞^* is also shown. Analytical solutions of Hieber and Gebhart (1969) obtained by matched asymptotic expansion technique compares well with the present numerical results (see Tables 4.4-3, 4 and 5) for the limiting values of $Re \to 0$ and $Gr \to Re^2$. The error in the analytical solution increases with increasing Re. It can be seen that the effect of natural convection on drag coefficient is significant. Figures 4.4-6, 7 show the variation of C_D/C_{Do} with Gr where C_{Do} is the drag coefficient at Gr = 0. It is seen that aiding flow increases the drag coefficient whereas opposing flow decreases it. Negative drag can appear at a certain negative Gr. This will never be experienced for a freely suspended sphere because at $C_D \leq 0$ the sphere would accelerate. Steady state can be maintained by suspending the sphere with an external support. In Table 4.4-3 it can be

Table 4.4-3 C_D for Single Sphere in an Unbounded Fluid

Pr=1.0

Re=0.01

Gr	C_{DP}	C_{DF}	C_D	C_D/C_{DO}	r^*_∞
0	789	1630	2420	1.000	992
0.5×10^{-3}	1680	3450	5130	2.124	"
1.0×10^{-3}	2350	4820	7170	2.968	"
5.0×10^{-3}	5340	10900	16200	6.705	"
1.0×10^{-2}	7610	15400	23000	9.532	"
-0.5×10^{-3}	-564	-1150	-1710	-0.710	"
-1.0×10^{-3}	-1880	-3850	-5720	-2.368	"
-5.0×10^{-3}	-5320	-10800	-16200	-6.685	"
-1.0×10^{-2}	-7640	-15500	-23100	-9.579	"

Table 4.4-4 C_D for Single Sphere in an Unbounded Fluid

Pr = 1.0
Re = 0.1

Gr	C_{DP}	C_{DF}	C_D			C_D/C_{DO}	r^*_∞
0	79.9	165	244			1.000	365
0.5×10^{-3}	81.4	168	249	(250	)**	1.017	"
1.0×10^{-3}	83.3	172	255	(256	)**	1.042	"
5.0×10^{-3}	96.2	197	293	(298	)**	1.198	"
1.0×10^{-2}	111	226	337	(334	)**	1.499	"
5.0×10^{-2}	196	391	587			2.398	"
	198	394	592			3.419	601
1.0×10^{-1}	270	534	804			3.285	365
	273	536	809			3.308	601
-0.5×10^{-2}	61.1	128	189			0.772	365
-1.0×10^{-2}	38.0	81.4	119			0.488	"
-5.0×10^{-2}	-187	-372	-559			-2.284	"
*-5.0×10^{-2}	-3.22	6.95	3.73			0.015	134
* 1.0×10^{-1}	163	308	471			1.925	134

* Pr = 10

** Hieber & Gebhart (1969)

Table 4.4-5 C_D for Single Sphere in an Unbounded Fluid

Pr = 1.0
Re = 1.0

Gr	C_{DP}	C_{DF}	C_D		C_D/C_{DO}	r^*_∞
0	8.96	18.4	27.4		1	134
10^{-3}	8.96	18.4	27.4	(28.5)**	1.000	"
5×10^{-3}	8.98	18.4	27.4	(28.7)**	1.001	"
5×10^{-2}	9.23	18.9	28.1		1.026	"
10^{-1}	9.53	19.5	28.9		1.054	"
5×10^{-1}	11.7	22.7	34.4		1.257	"
1.	14.2	26.4	40.7		1.484	"
-5×10^{-2}	8.66	17.9	26.6		0.971	"
-10^{-1}	8.35	17.4	25.8		0.942	"
-5×10^{-1}	5.72	13.1	18.8		0.687	"
-1	1.18	5.08	6.25		0.228	"

** Hieber & Gebhart (1969)

MCMASTER UNIVERSITY LIBRARY

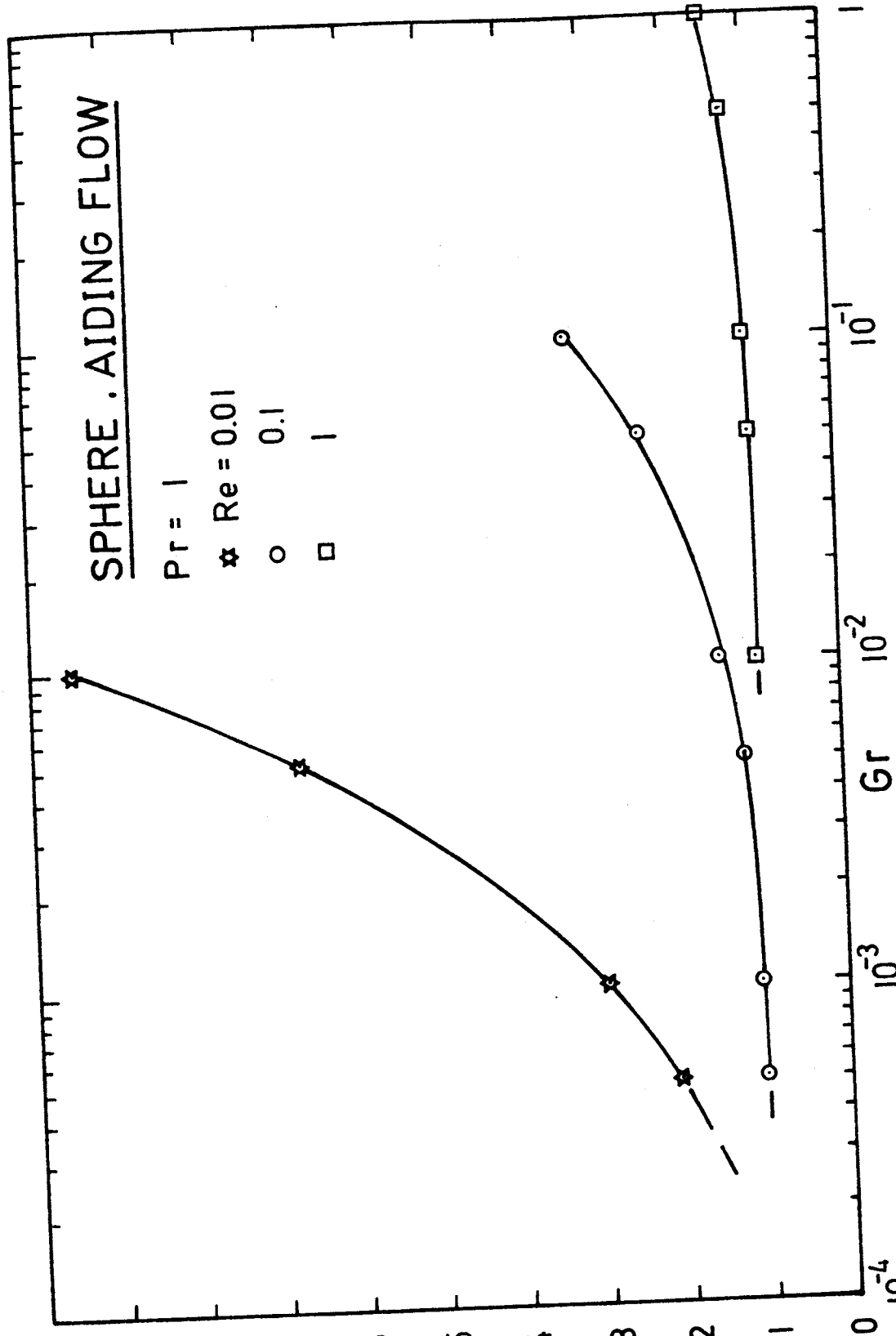

FIGURE 4.4-6 C_D/C_{DO} vs Gr FOR SINGLE SPHERE IN AN UNBOUNDED FLUID (AIDING FLOW)

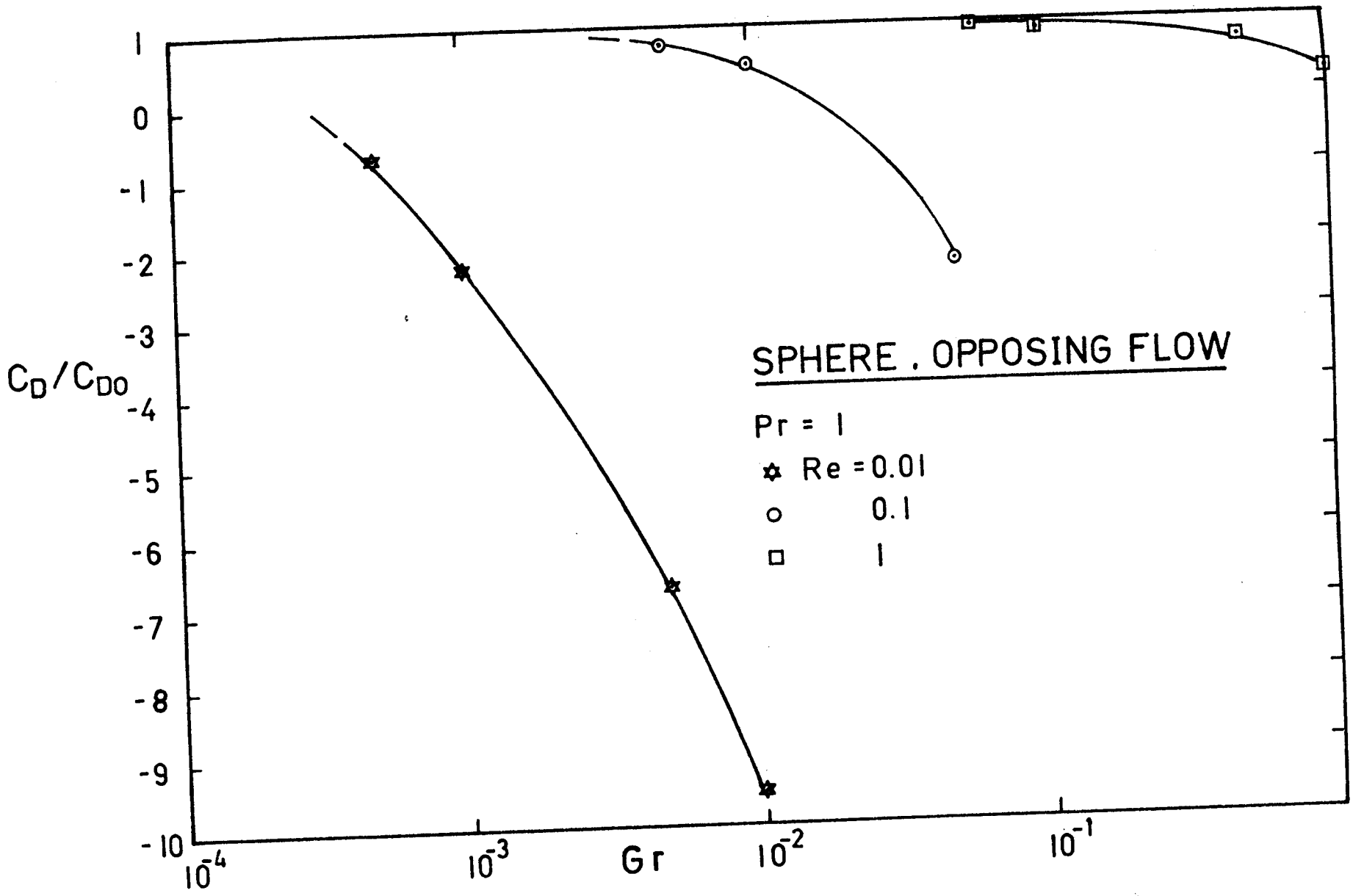

FIGURE 4.4-7 C_D/C_{DO} **vs** Gr FOR SINGLE SPHERE IN AN UNBOUNDED FLUID (OPPOSING FLOW)

seen that Re = 0.01 and Gr = $5 \times 10^{-3}(-5 \times 10^{-3})$ and $10^{-2}(-10^{-2})$ that the drag coefficients are equal, but of opposite sign (for both aiding and opposing flows). For this small Reynolds number free convection dominates forced convection giving rise to the symmetry noted. Consider the case of a cold sphere suspended with a wire in a hot fluid moving vertically upward. The sphere is fixed in space and the fluid velocity and temperature are constant giving rise to steady state. A temperature difference can be found at which the Grashof number (opposing flow) is sufficiently negative to give zero fluid drag. Further increases in the temperature difference will give negative drag. The apparent weight of the sphere would now be greater than its true weight. If the sphere were now suddenly released it would accelerate until the drag become positive and equal to the true weight of the sphere. One concludes, that for a freely suspended sphere, steady state can only be achieved when the drag is positive.

The increasing and decreasing of sphere drag with Gr shown in these figures indicates that when the sphere is falling or rising, aiding flow (natural convection in the same direction as the forced flow) reduces the sphere velocity and opposing flow (natural convection in opposite direction to the forced flow) increases it.

Calculations also were made for the case of Re = 0.1, Gr = -0.05, -0.1 and 0.1 at Pr = 10 to study the effect of Pr. The results are tabulated in Table 4.4-4. It is observed that the effect of Gr on drag is smaller. This is a result of the thinner thermal boundary layer at higher Pr. The natural convection currents are concentrated in a confined

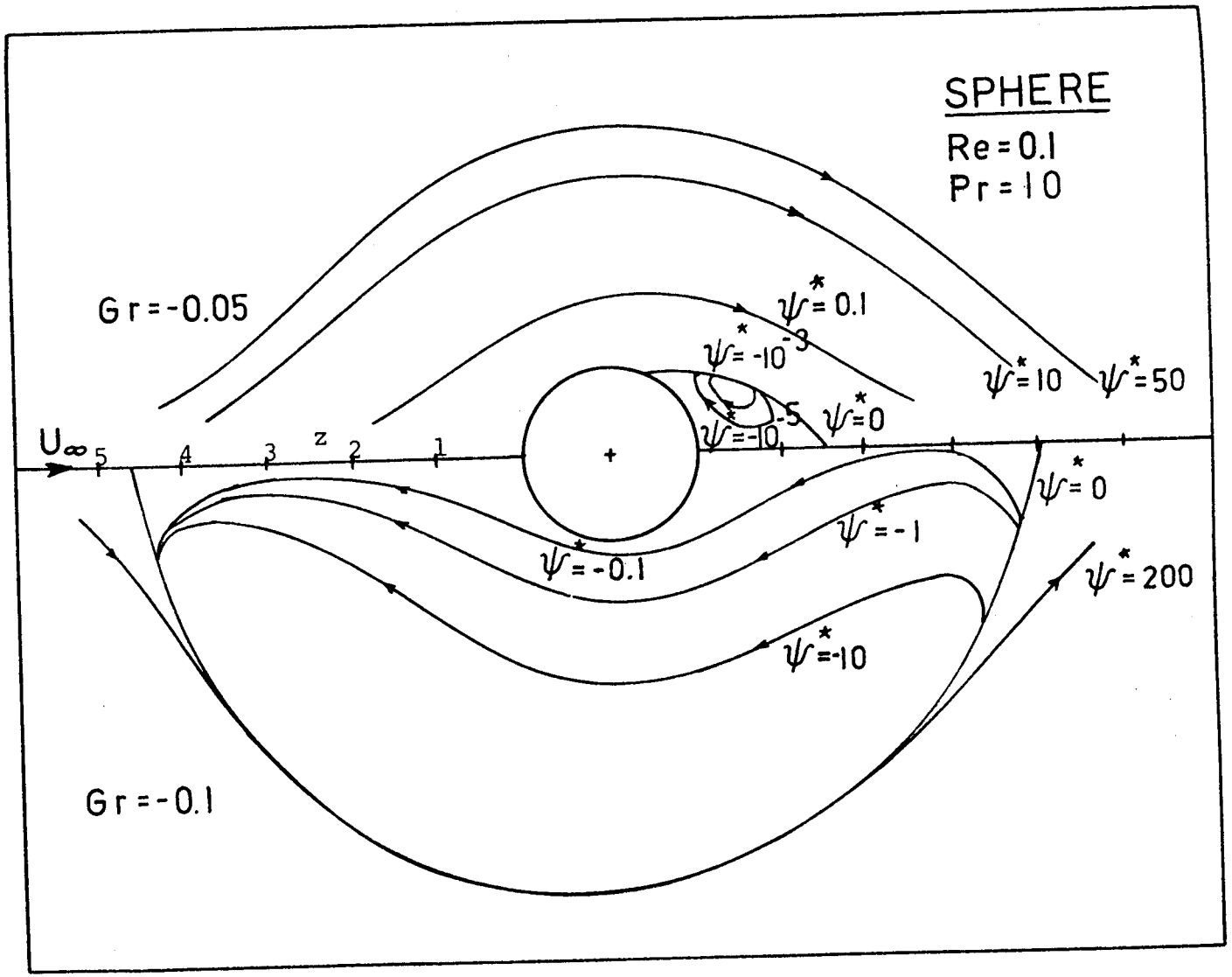

FIGURE 4.4-8 STREAMLINES FOR SINGLE SPHERE IN AN UNBOUNDED FLUID AT OPPOSING FLOW

region and lose intensity. Figure 4.4-8 shows stream lines around the sphere for Gr=-0.05 and -0.1 for the case of Re=0.1 and Pr=10. At Gr=-0.1 natural convection completely dominates the flow whereas at Gr=-0.05 the forced convection field is only partially overcome as can be seen from the vortex ring formed at the rear. It can be concluded that the effect of natural convection on drag is less significant for higher Pr and at Pr → ∞, the effect vanishes.

At Pr = 0.71, calculations have been made for Re = 5, 10, 20, 30 and Gr from 300 to 0 for both aiding and opposing flows in order to study the effects of natural convection on drag coefficient, separation angle, wake length and wake volume. Surface pressure and vorticity distributions are tabulated in Appendix B.4.

Figure 4.4-9 shows surface pressure distributions for Re = 30. The frontal stagnation pressure is invariant over the Gr range studied for this Reynolds number. For lower Reynolds numbers, however, aiding flow increases the frontal stagnation pressure and opposing flow decreases it. (see Appendix B.5). The rear stagnation pressure is affected significantly by natural convection. Aiding flow decreases it and opposing flow increases it. The behavior of the frontal stagnation pressure for this moderately high Reynolds number range under the influence of natural convection is quite different from that at low Reynolds numbers (see Figure 4.4-4). The opposing natural convection current is not large enough to affect the flow at the frontal stagnation point where forced convection dominates. With significantly high Gr free convection would

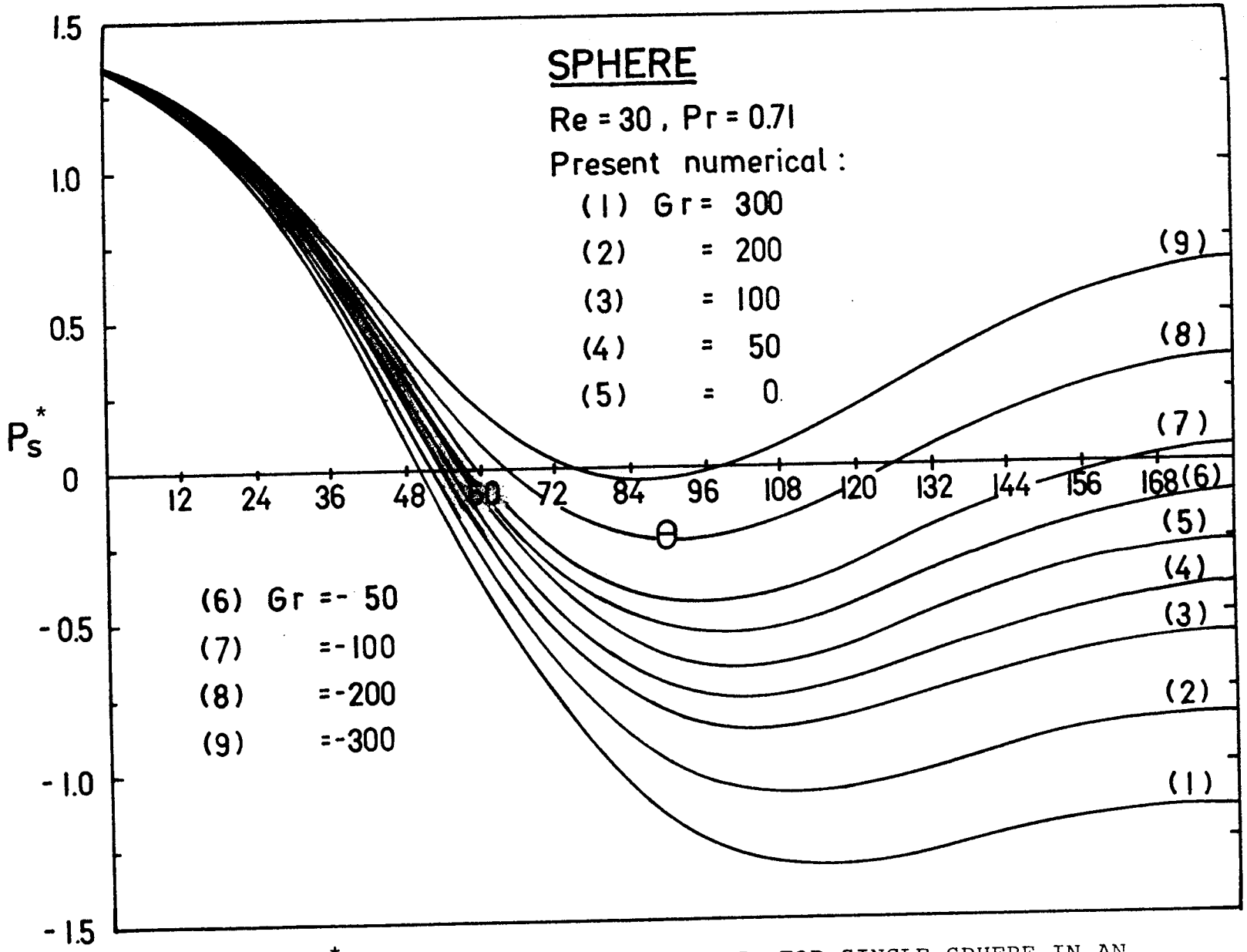

FIGURE 4.4-9 P_s^* DISTRIBUTIONS AT VARIOUS Gr FOR SINGLE SPHERE IN AN UNBOUNDED FLUID

dominate the whole flow field and the behavior of frontal stagnation pressure would be the same for both cases. The present study is concerned mainly with positive drag ($C_D \geq 0$) and freely suspended particles. These are of greater technological interest. Grashof numbers were selected to give positive drag. The surface vorticity distributions are shown in Figure 4.4-10 for Re = 30. Aiding flow increases the surface vorticity and moves the flow separation angle to the rear, however opposing flow decreases the surface vorticity and moves the flow separation angle to the front.

Table 4.4-6 displays the separation angle θ_s, normalized wake length L/d and normalized wake volume V_w/V_s for Re = 30 and 20. At Re = 30 there exists a wake at Gr = 0. Aiding flow suppresses it whereas opposing flow causes it to increase. At Re = 20 there is no wake at Gr = 0. Opposing flow generates a wake. The corresponding graphical representations are shown in Figures 4.4-11 and 4.4-12. The flow separation angle and wake length are affected similarly by free convection they increase with opposing flow and decrease with aiding flow. The variation of θ_s, L/d and V_w/V_s are shown in Figures 4.4-13, 4.4-14 and 4.4-15, and corresponding numerical values are reported in Table 4.4-6.

The drag coefficients are listed in Tables 4.4-7, 4.4-8, and 4.4-9. The drag coefficient is found to decrease with opposing flow and to increase with aiding flow. The same arguments as used earlier can be used to explain the effects of free convection on particle velocity. The corresponding values are displayed in Figures 4.4-16 and 4.4-17. The present results agree qualitatively with experimental observations

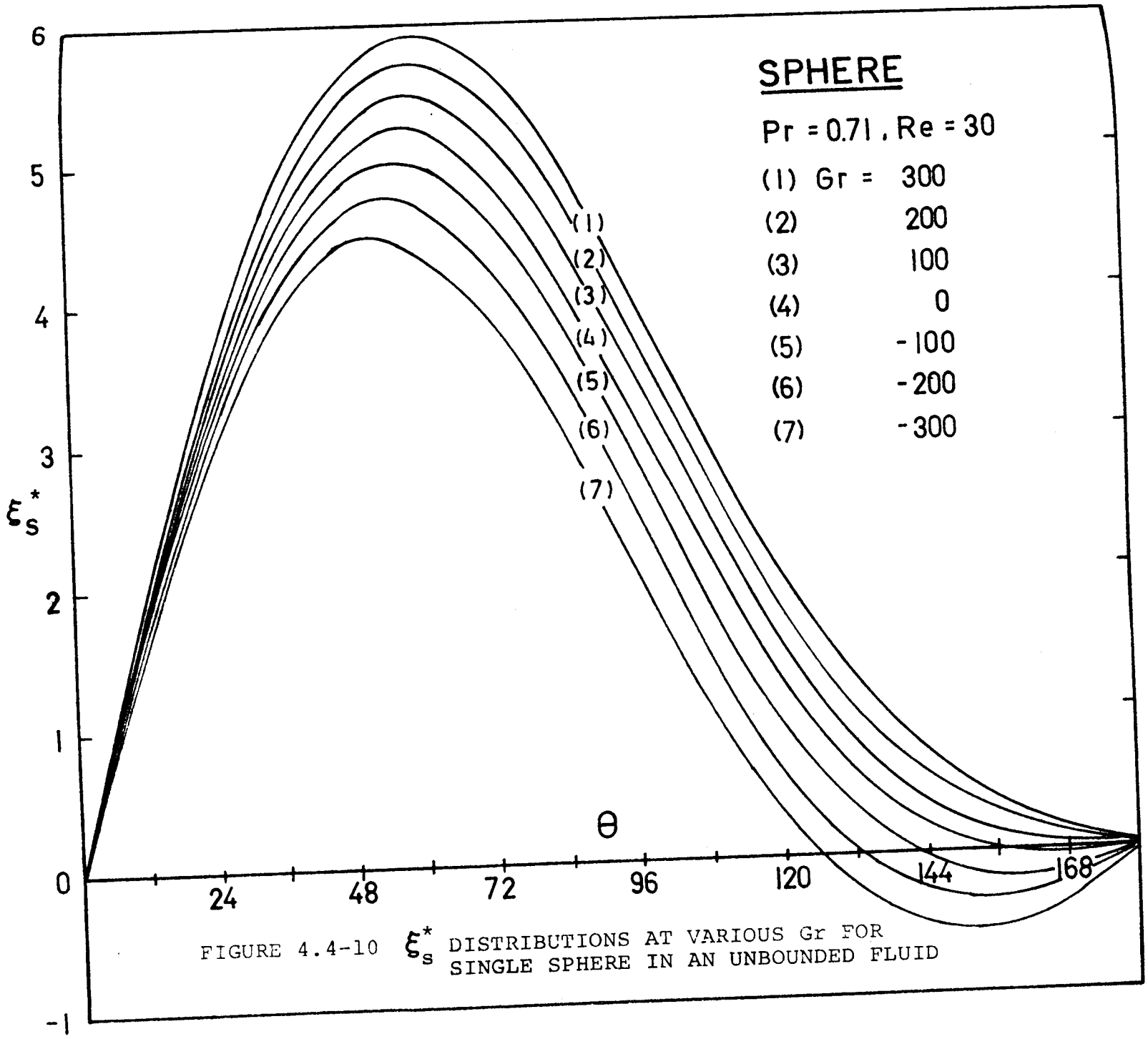

FIGURE 4.4-10 ξ_s^* DISTRIBUTIONS AT VARIOUS Gr FOR SINGLE SPHERE IN AN UNBOUNDED FLUID

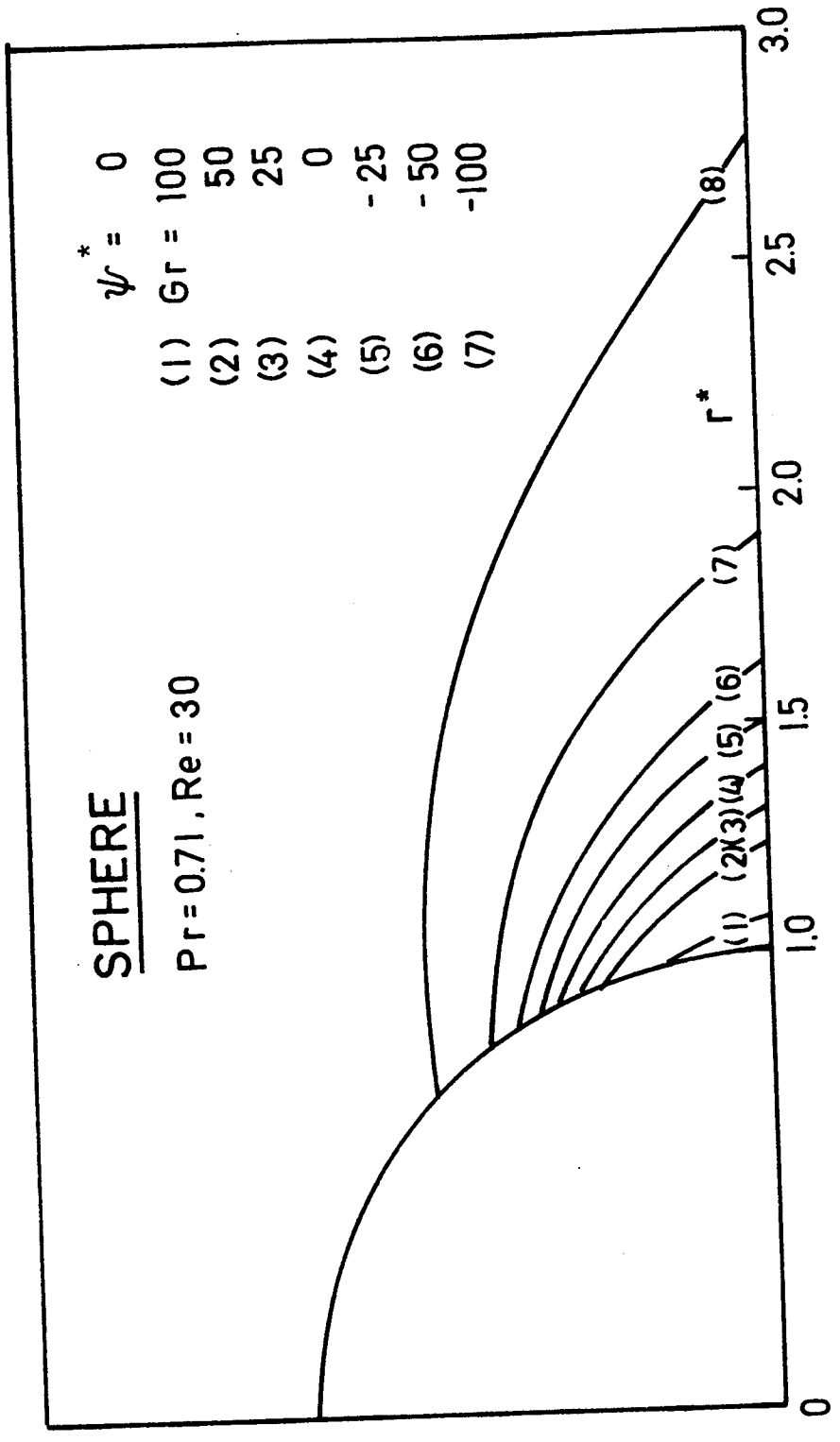

FIGURE 4.4-11 VORTEX RING, AIDING AND OPPOSING FLOW, FOR SINGLE SPHERE IN AN UNBOUNDED FLUID

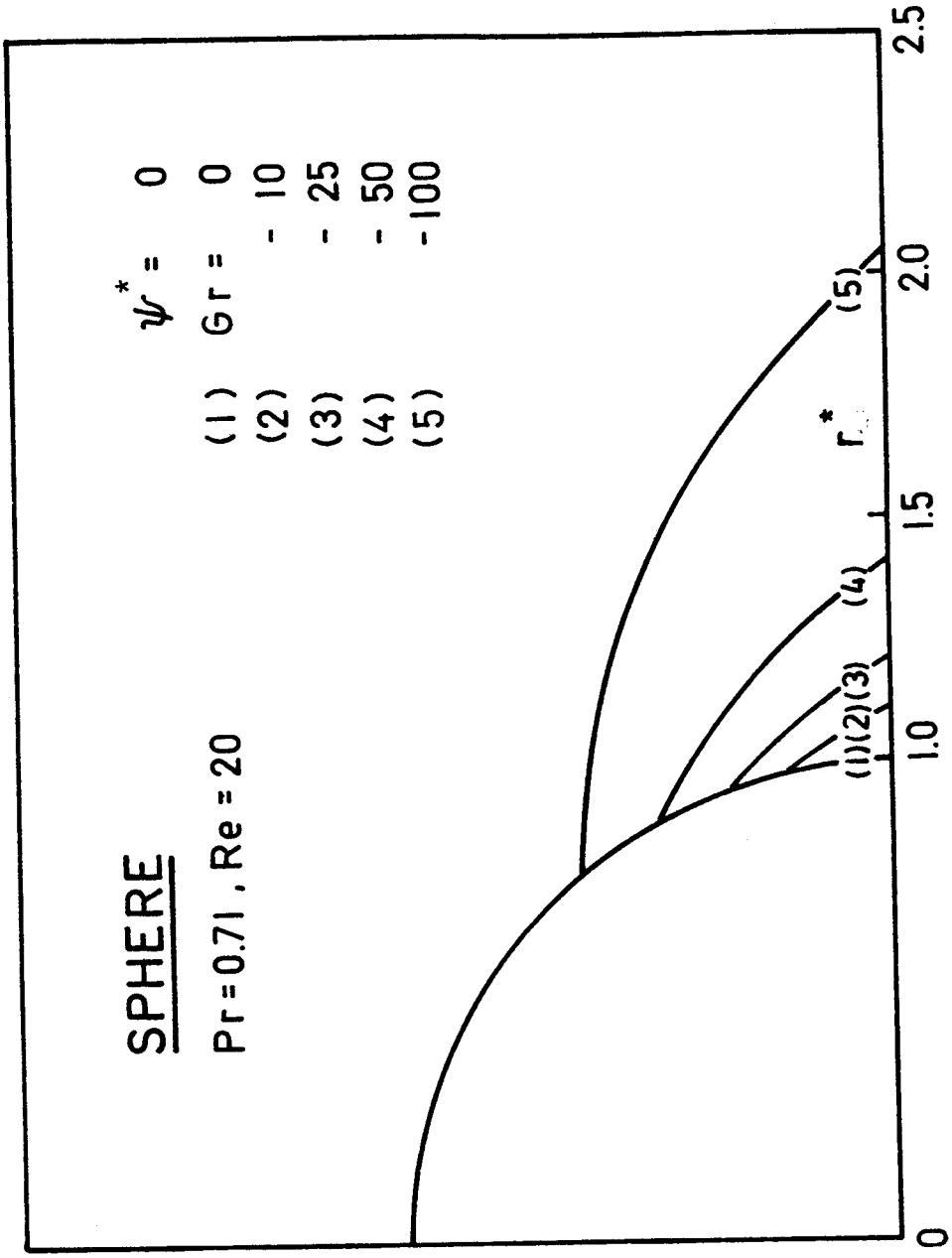

FIGURE 4.4-12 VORTEX RING FORMATION DUE TO OPPOSING FLOW FOR SINGLE SPHERE IN AN UNBOUNDED FLUID

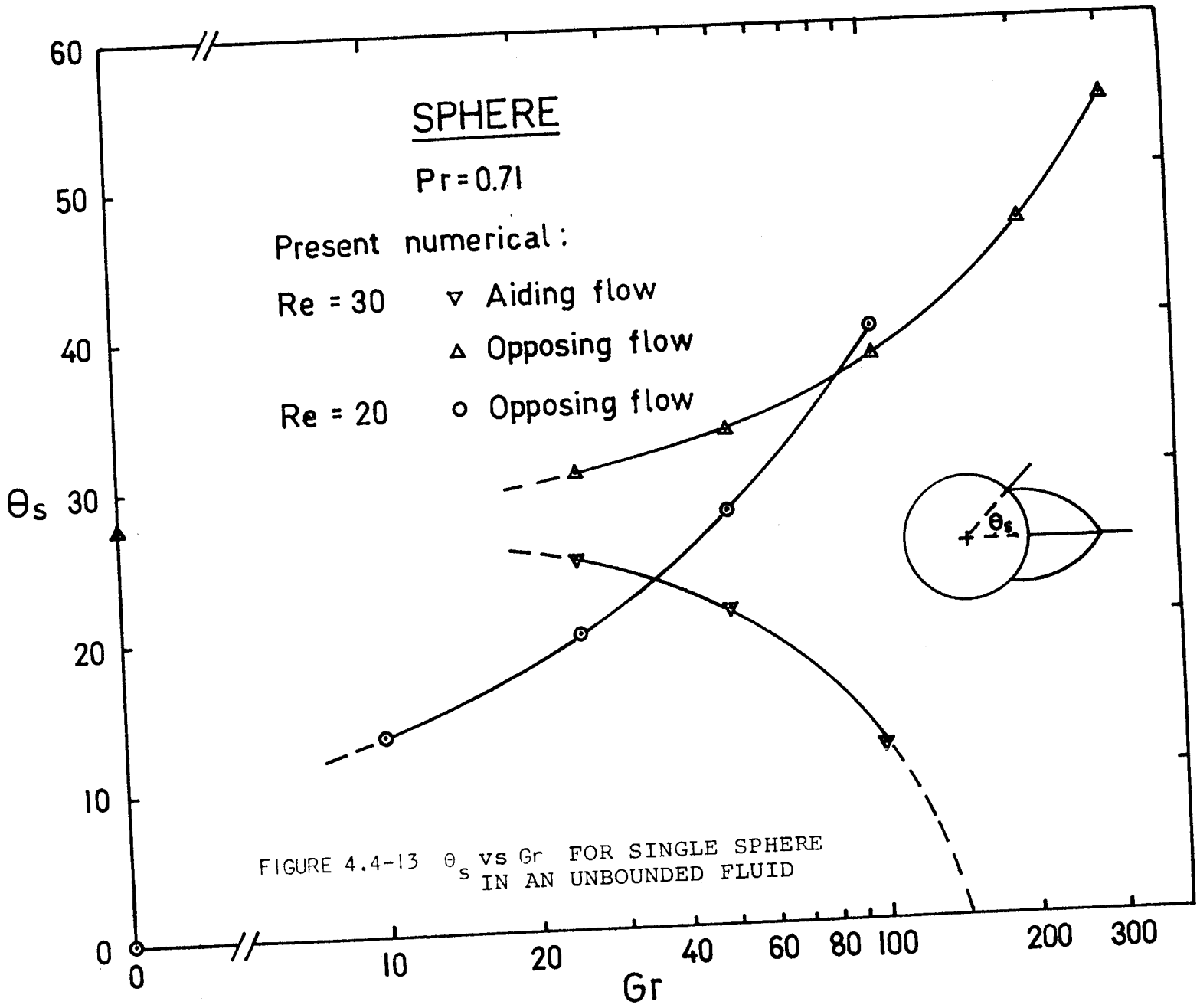

FIGURE 4.4-13 θ_s vs Gr FOR SINGLE SPHERE IN AN UNBOUNDED FLUID

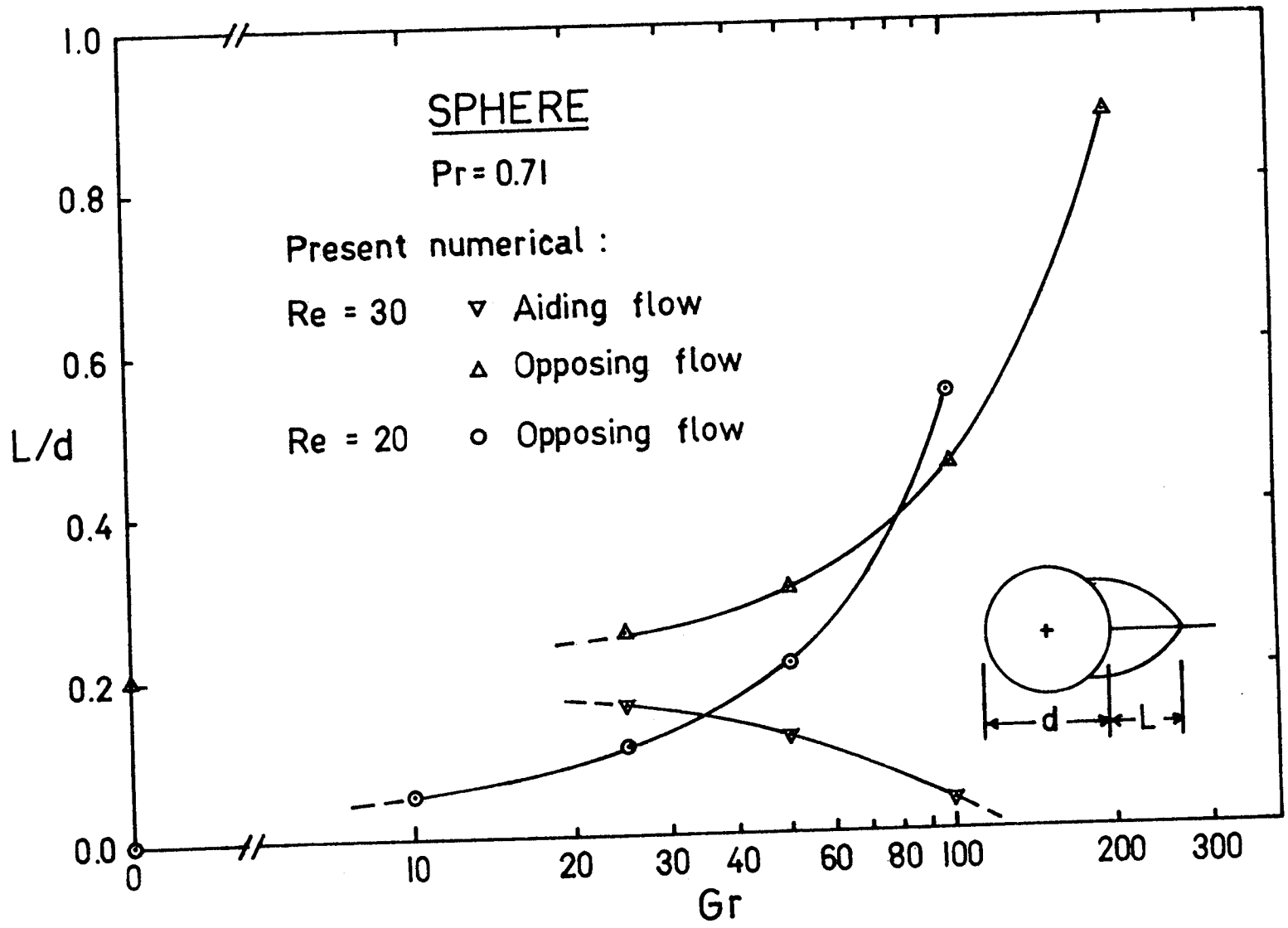

FIGURE 4.4-14 L/d vs Gr FOR SINGLE SPHERE IN AN UNBOUNDED FLUID

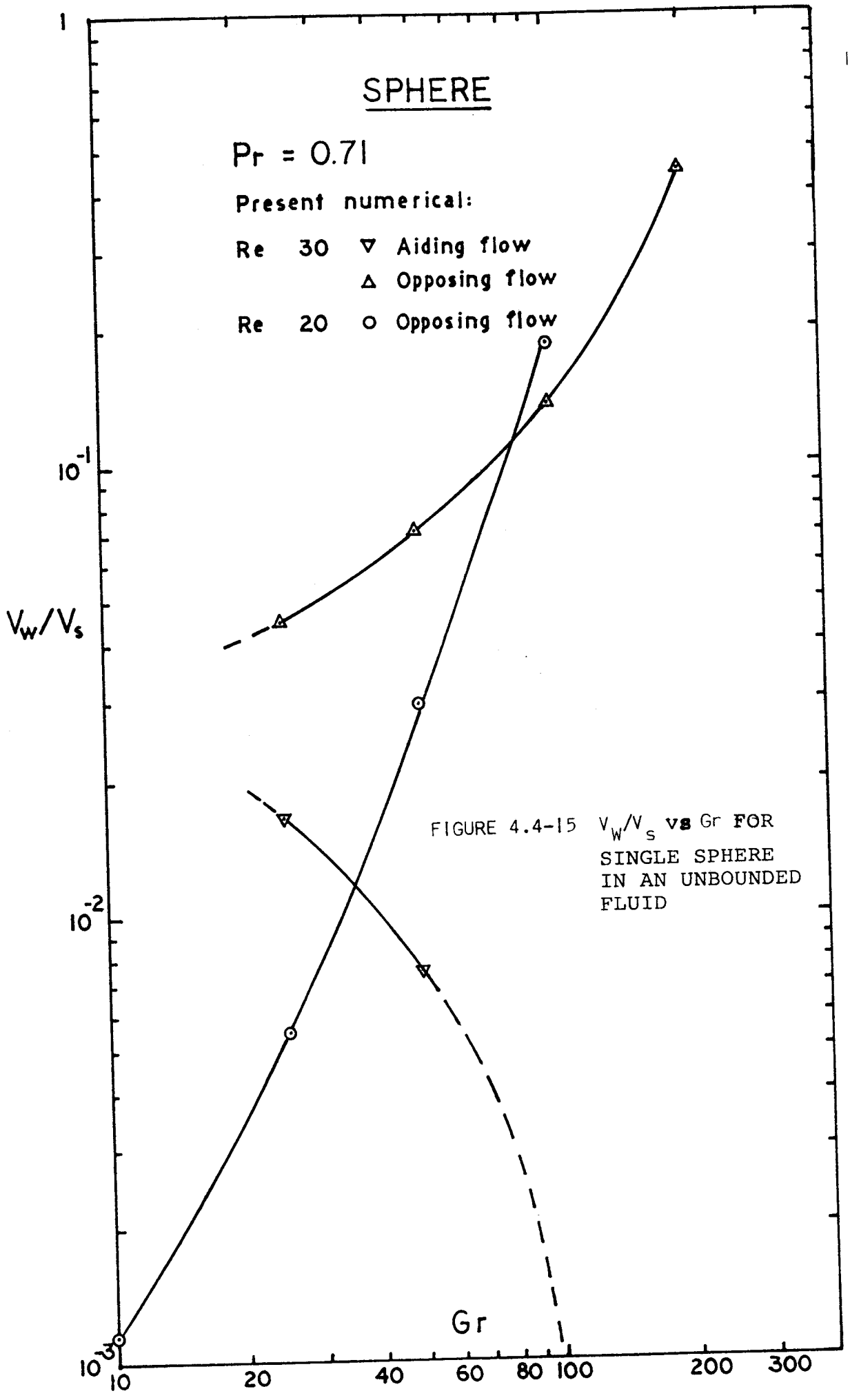

FIGURE 4.4-15 V_w/V_s vs Gr FOR SINGLE SPHERE IN AN UNBOUNDED FLUID

Table 4.4-6 θ_s, L/d and V_w/V_s for Single Sphere in an Unbounded Fluid at Re = 30 and 20

Gr	θ_s	L/d	V_w/V_s
Re = 30			
25	24.6°	0.155	0.0165
50	21°	0.128	0.00746
100	11.4°	0.04	0
200	0	0	0
300	0	0	0
-25	30.6°	0.25	0.0459
-50	33°	0.31	0.0703
-100	37.8°	0.45	0.137
-200	46.2°	0.885	0.441
-300	54.6°	(*)	(*)
Re = 20			
-10	13.2°	0.06	0.00114
-25	19.80	0.11	0.00544
-50	27.6°	0.21	0.0293
-100	39.6°	0.535	0.182

(*) Not accurate due to wall effect.

Table 4.4-7 C_D for Single Sphere in an Unbounded Fluid

Pr = 0.71, Re = 5

Gr	C_{DP}	C_{DF}	C_D	C_D/C_{DO}	r^*_∞
0			7.22		31.5
1	2.57	4.87	7.43	1.030	"
5	3.01	5.35	8.36	1.158	"
10	3.55	5.89	9.44	1.310	"
15	4.08	6.40	10.48	1.453	"
	4.10	6.43	10.53	1.460	51.9
-1	2.33	4.64	6.97	0.965	31.5
-5	1.86	4.12	5.98	0.830	"
-10	1.24	3.41	4.66	0.645	"
-15	0.58	2.60	3.18	0.440	"

Table 4.4-8 C_D for Single Sphere in an Unbounded Fluid

Pr = 0.71, Re = 10

Gr	C_{DP}	C_{DF}	C_D	C_D/C_{DO}	r^*_∞
0	1.54	2.84	4.38	1	19.11
5	1.64	2.93	4.57	1.043	"
10	1.76	3.02	4.77	1.090	"
25	2.10	3.29	5.39	1.230	"
50	2.65	3.70	6.34	1.450	"
100	3.71	4.44	8.15	1.860	19.11
-5	1.42	2.71	4.16	0.950	19.11
-10	1.30	2.64	3.94	0.900	"
-25	0.945	2.33	3.28	0.748	"
-50	0.328	1.74	2.07	0.472	"
-100		(negative drag occurs)			
-179	-2.41	-1.43	-3.84		11.59

Table 4.4-9 C_D for Single Sphere at Re = 20 in an Unbounded Fluid

Pr = 0.71, Re = 20

Gr	C_{DP}	C_{DF}	C_D	C_D/C_{DO}	r^*_∞
0	1.02	1.72	2.74		11.59
10	1.08	1.78	2.86	1.043	
25	1.16	1.83	2.99	1.092	11.59
50	1.28	1.90	3.18	1.162	"
99	1.52	2.04	3.55	1.299	"
179	1.89	2.24	4.13	1.510	"
293	2.42	2.53	4.95	1.809	"
	2.43	2.55	4.98		19.11
-10	0.975	1.72	2.69	0.983	14.88
-25	0.900	1.67	2.57	0.938	"
-50	0.775	1.58	2.36	0.862	"
-100	0.520	1.40	1.92	0.703	"
	0.509	1.39	1.90	0.694	19.11
-200	0.035	1.05	1.08		11.59
	-0.009	0.982	0.973		14.88
	-0.042	0.931	0.889		19.11
-179	0.144	1.19	1.33	wall effect	

Table 4.4-10 C_D for Single Sphere at Re = 30 in an Unbounded Fluid

Pr = 0.71, Re = 30

Gr	C_{DP}	C_{DF}	C_D	C_D/C_{DO}	r^*_∞
0	0.835	1.33	2.17		11.59
25	0.888	1.36	2.25	1.037	
50	0.939	1.39	2.33	1.073	"
100	1.04	1.44	2.48	1.144	"
200	1.24	1.54	2.78	1.284	"
300	1.44	1.64	3.08	1.421	"
-25	0.786	1.30	2.09	0.964	"
-50	0.734	1.28	2.01	0.926	"
-100	0.630	1.22	1.85	0.852	"
-200	0.422	1.09	1.51	0.700	"
-300	0.210	0.955	1.16	0.537	11.59
	0.190	0.929	1.12	0.516	14.88

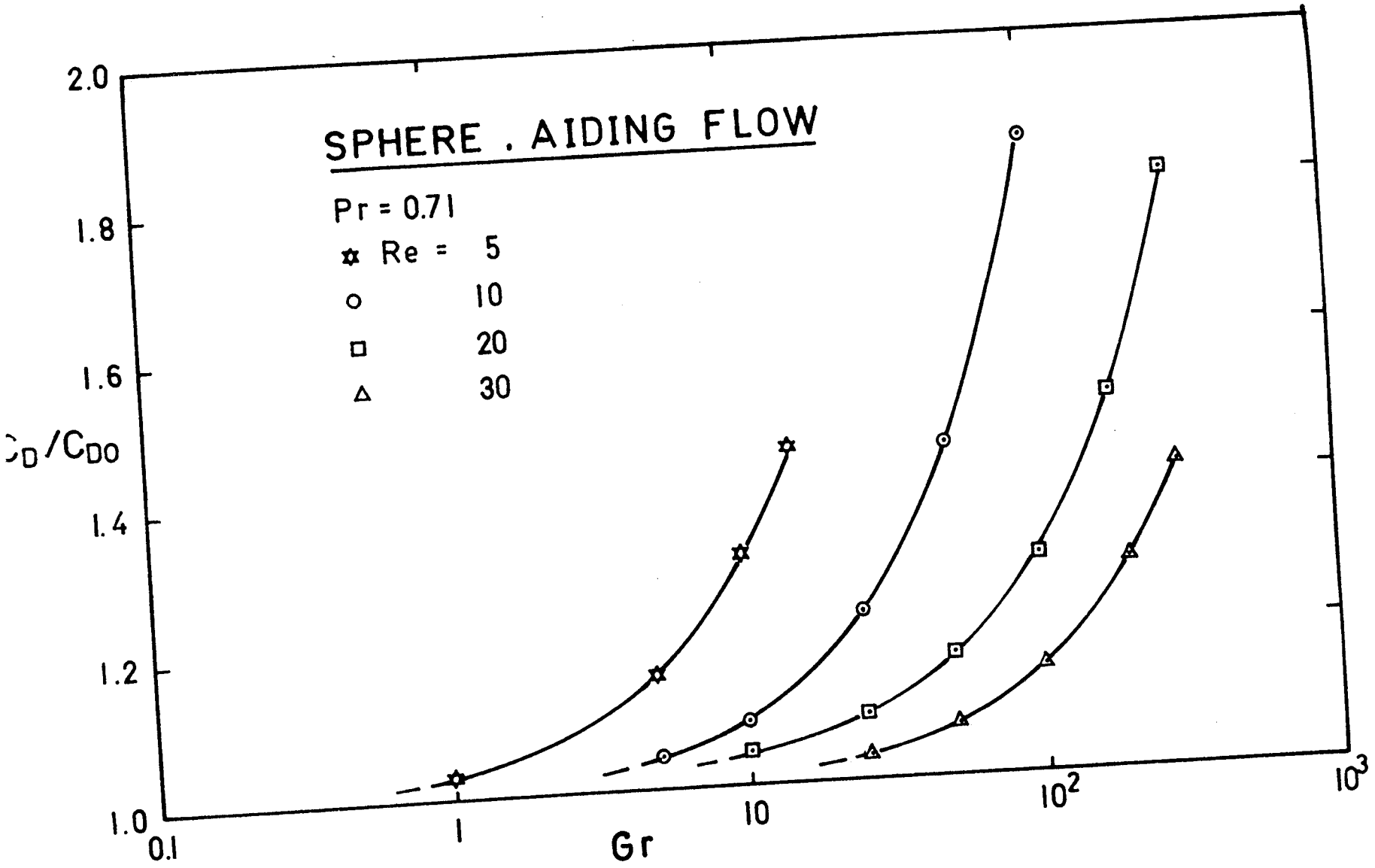

FIGURE 4.4-16 C_D/C_{DO} vs Gr FOR SINGLE SPHERE IN AN UNBOUNDED FLUID (AIDING FLOW)

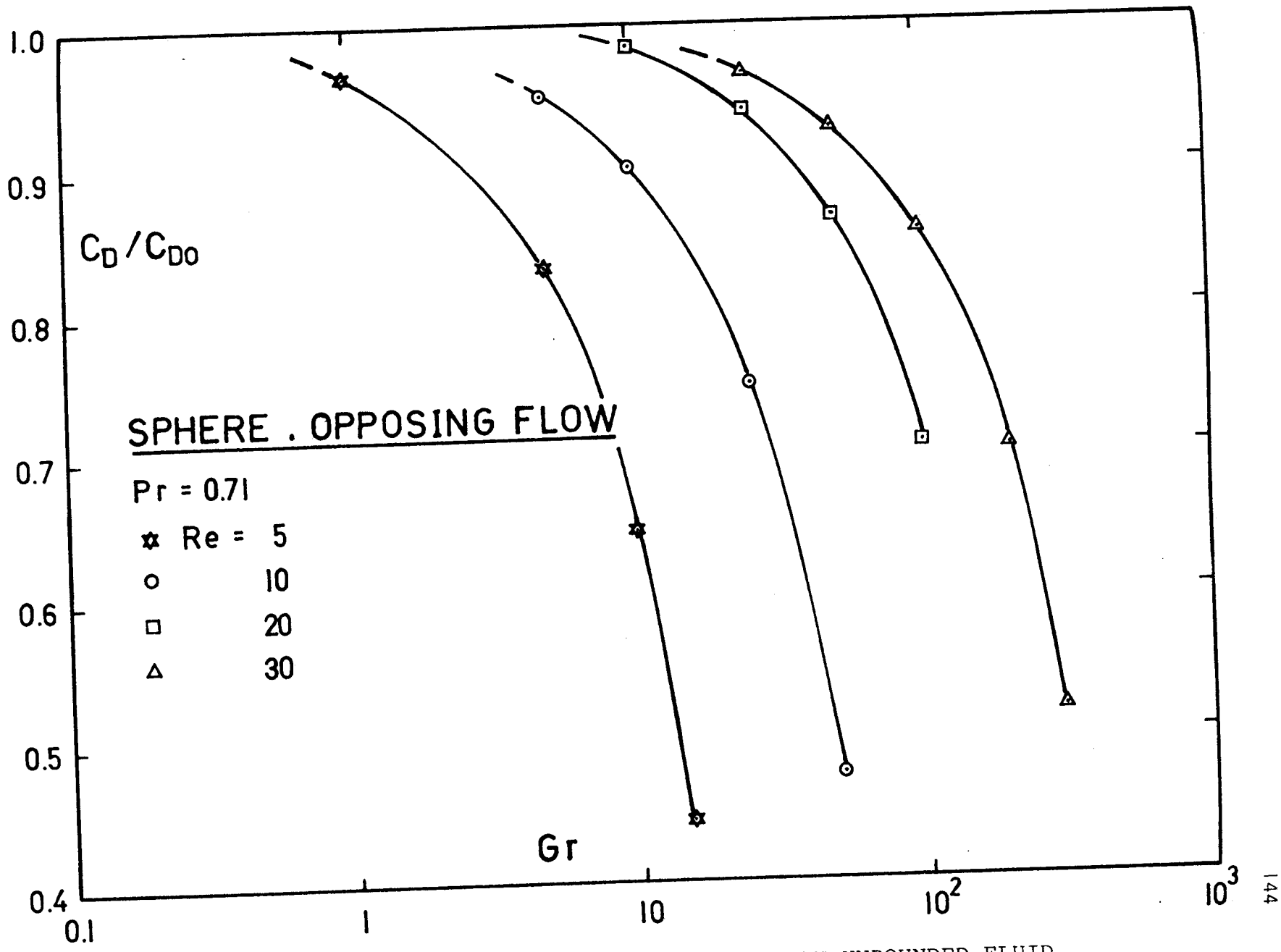

FIGURE 4.4-17 C_D/C_{DO} vs Gr FOR SINGLE SPHERE IN AN UNBOUNDED FLUID (OPPOSING FLOW)

of Narasimhan and Gauvin (1966), theoretical observations of Acrivos (1958, 1966) and Sparrow et.al. (1959) on a flat plate and a wedge.

In conclusion, the effects of natural convection on heat or mass transfer, surface pressure, vorticity distributions, flow separation angle, wake length and volume and drag coefficient discussed previously can be explained phenomenologically by considering the mechanism of fluid flow with aiding or opposing flow current over the freely suspended spherical particle. Aiding flow natural convection current enhances the forced flow whereas opposing flow natural convection current suppresses the forced flow.

4.5 Mixed Convection Around a Sphere in an Unbounded Fluid - zero Prandtl Number

4.5.1 Governing Equations, Boundary Conditions and Method of Solution

At zero Prandtl number, the thermal boundary layer is of infinite thickness and the temperature field can be considered radially symmetric with $\eta^* = 1/r^*$ as the distribution. Substituting this relation into the vorticity transport equation of Table 3.1-1 one obtains

$$\left[\frac{\partial\psi^*}{\partial z}\frac{\partial}{\partial\theta}\left(\frac{\xi^*}{e^z\sin\theta}\right) - \frac{\partial\psi^*}{\partial\theta}\frac{\partial}{\partial z}\left(\frac{\xi^*}{e^z\sin\theta}\right)\right] e^z\sin\theta$$

$$= \frac{2}{Re}\, E_{sz}^{*2}\,(\xi^* e^z\sin\theta) - \frac{e^z}{2}\,\frac{Gr}{Re^2}\,\sin^2\theta$$

This equation, together with the defining equation for vorticity

$$\xi^* = E_{sz}^{*2}\,\psi^* \,/\, e^{3z}\sin\theta$$

are the governing equations of flow of zero Prandtl number fluid around

a sphere. The momentum and energy equations are uncoupled.

Undisturbed parallel flow boundary conditions are used. They are

$$\text{at } z = 0 \quad ; \quad \psi^* = 0 \ , \ \xi^* = E_{sz}^{*2} \ \psi^*/\sin\theta$$

$$\text{at } z = z_\infty \quad ; \quad \psi^* = \frac{e^{2z}}{2} \ \sin^2\theta, \quad \xi^* = 0$$

$$\text{at } \theta = 0,\pi \ ; \quad \psi^* = \xi^* = 0$$

The method of solving these equations was the new sequence iteration with convergence promotion described in Section 3.3.4. Initial guesses of ψ^* and ξ^* were Stokes' velocity profiles. FORTRAN IV computer program is the same as in Appendix A.1 except the finite difference equation for vorticity transport equation.

4.5.2 Mesh Dimensions and Accuracy of Solutions

The step sizes used were A = 0.1 and B = $\pi/30$ for the low Reynolds numbers (0.01 , 0.05, 0.1) studied. The size of the outer boundary r_∞^* was chosen extremely large to avoid wall effect. The wall effect for this problem is great because of the very thick thermal boundary layer. Suitable values for r_∞^* were found by trial and error.

The convergence tolerance used was $\varepsilon = 10^{-4}$ in equation (3.3-30).

4.5.3 Discussion of Results

Calculations were made for Re = 0.01, 0.05 and 0.1 at Gr from 0.5×10^{-5} to 3.0×10^{-3}. Surface pressure and vorticity distributions are tabulated in Appendix B.5. Figures 4.5-1 and 4.5-2 show the variation of P_s^* and ξ_s^* with Gr at Re = 0.05. Similar results for low

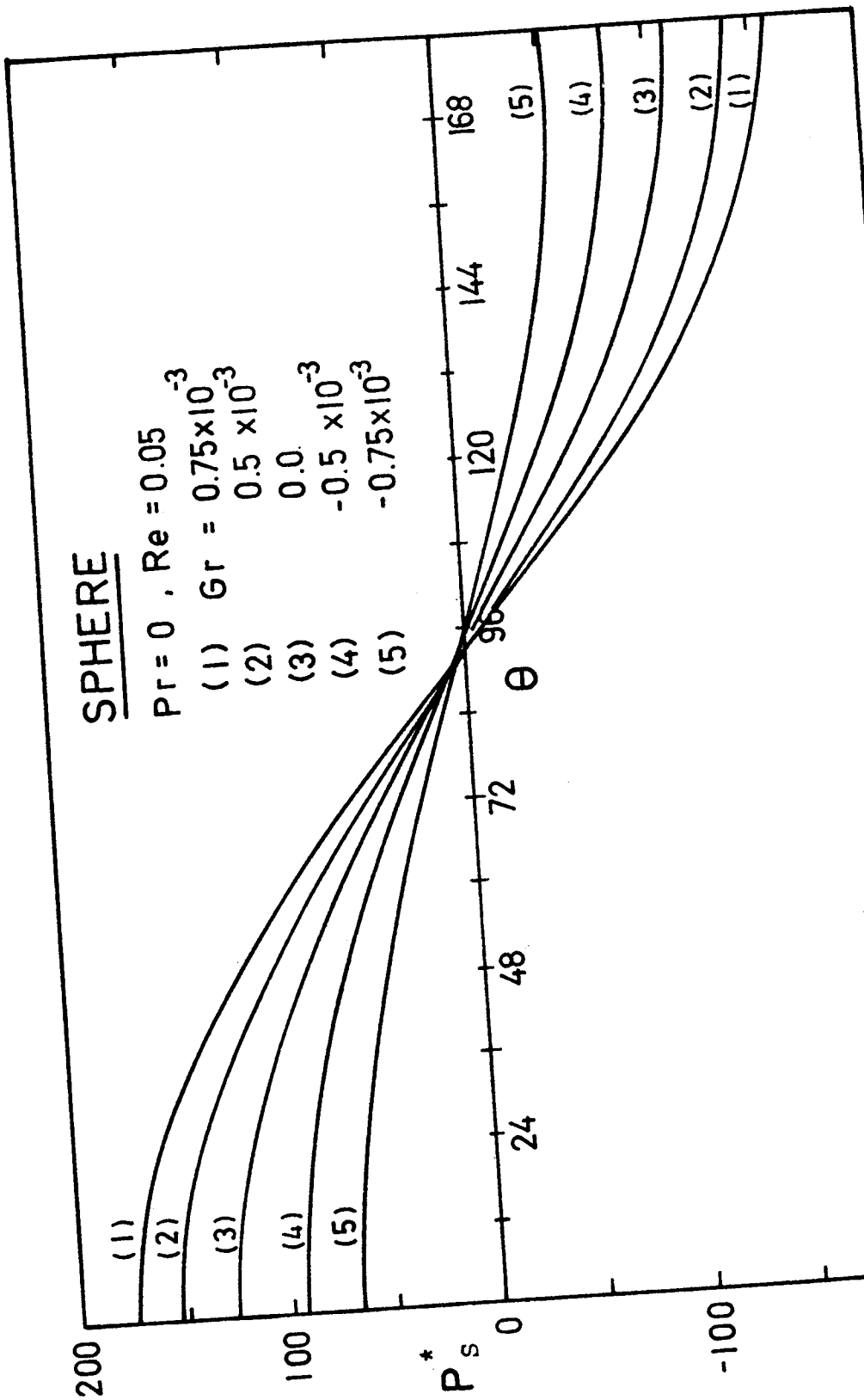

FIGURE 4.5-1 P_s^* DISTRIBUTIONS AT VARIOUS Gr FOR SINGLE SPHERE IN AN UNBOUNDED FLUID OF Pr=0

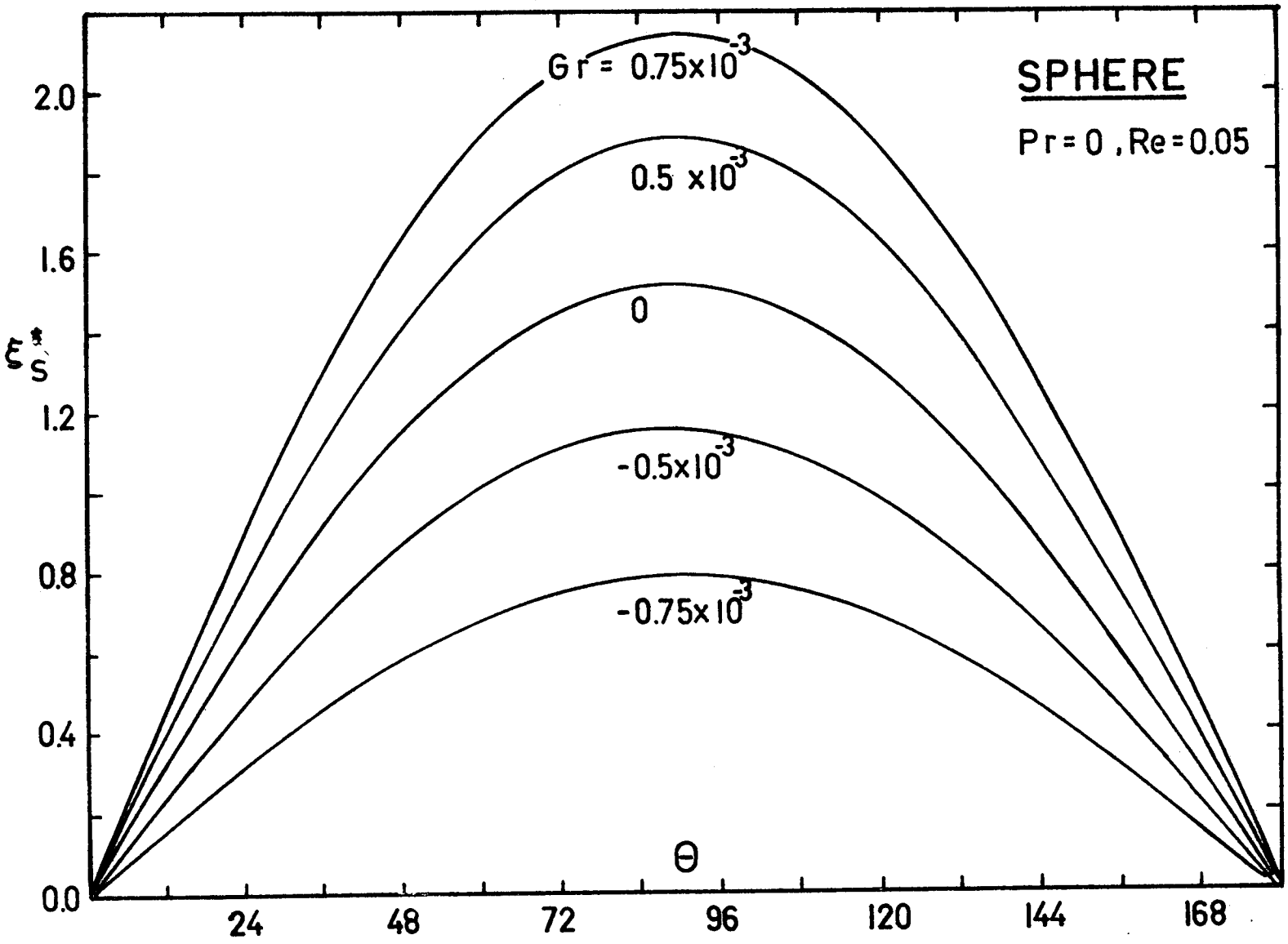

FIGURE 4.5-2 ξ_s^* DISTRIBUTIONS AT VARIOUS Gr FOR SINGLE SPHERE IN AN UNBOUNDED FLUID OF Pr=0

Reynolds numbers at Pr = 1.0 were observed, however the effect is greater. Tables 4.5-1, 4.5-2 and 4.5-3 show the variation of drag coefficient with Grashof number. Similar but larger effects are observed. These results are displayed graphically in Figure 4.5-3 and 4.5-4. Unfortunately no data exists in the literature for comparison with the present calculations.

For the case of the cylinder, the zero Prandtl number limit gives a uniform η^* distribution and a zero buoyant force (uniform body force field). This limit has therefore already been covered in Section 4.1 for viscous flow around a single cylinder in an unbounded fluid.

This specific study simulates liquid metal flow around a sphere. Liquid metals have very low Prandtl number ($0.005 \sim 0.03$) because of their high conductivity. Deoxidation of molten steel is a process where the effect of simultaneous forced and natural convection on particle drag may play a significant role.

Table 4.5-1 C_D for Single Sphere at Pr = 0 in an Unbounded Fluid

Re = 0.01

Gr	C_{DP}	C_{DF}	C_D	C_D/C_{DO}	r^*_∞
0					
0.5×10^{-5}	819	169	251	1.046	2697
1.0×10^{-5}	850	175	260	1.083	"
2.0×10^{-5}	913	186	277	1.153	"
3.0×10^{-5}	999	207	307	1.280	4447
-0.5×10^{-5}	761	158	234	0.975	2697
-1.0×10^{-5}	735	151	225	0.937	"
-2.0×10^{-5}	678	1400	207	0.865	"
-3.0×10^{-5}	563	1160	172	0.718	4447

Table 4.5-2 C_D for Single Sphere at Pr = 0.0 in an Unbounded Fluid

Re = 0.05

Gr	C_{DP}	C_{DF}	C_D	C_D/C_{DO}	r^*_∞
0	157	323	481	1	1636
0.125×10^{-3}	168	348	517	1.075	"
0.25×10^{-3}	178	367	545	1.134	"
0.5×10^{-3}	195	403	599	1.246	"
0.75×10^{-3}	221	457	678	1.410	2697
-0.125×10^{-3}	149	308	458	0.952	1636
-0.25×10^{-3}	139	287	426	0.887	"
-0.5×10^{-3}	118	244	363	0.756	"
-0.75×10^{-3}	80.8	167	248	0.516	2697

Table 4.5-3 C_D for Single Sphere Pr = 0.0 in an Unbounded Fluid

Re = 0.1

Gr	C_{DP}	C_{DF}	C_D	C_D/C_{DO}	r^*_∞
0	80.2	166	246	1	992
0.5×10^{-3}	85.3	176	261	1.063	"
1.0×10^{-3}	90.2	186	276	1.125	"
2.0×10^{-3}	99.7	206	305	1.243	"
3.0×10^{-3}	109	224	333	1.356	992
	113	234	348	1.414	1636
-0.5×10^{-4}	79.8	164	244	0.994	992
-0.5×10^{-3}	74.7	154	229	0.932	992
	75.6	156	232	0.942	601
-1.0×10^{-3}	69.3	143	212	0.864	992
-2.0×10^{-3}	57.8	119	177	0.721	"
-3.0×10^{-3}	37.0	77.1	114	0.464	1636

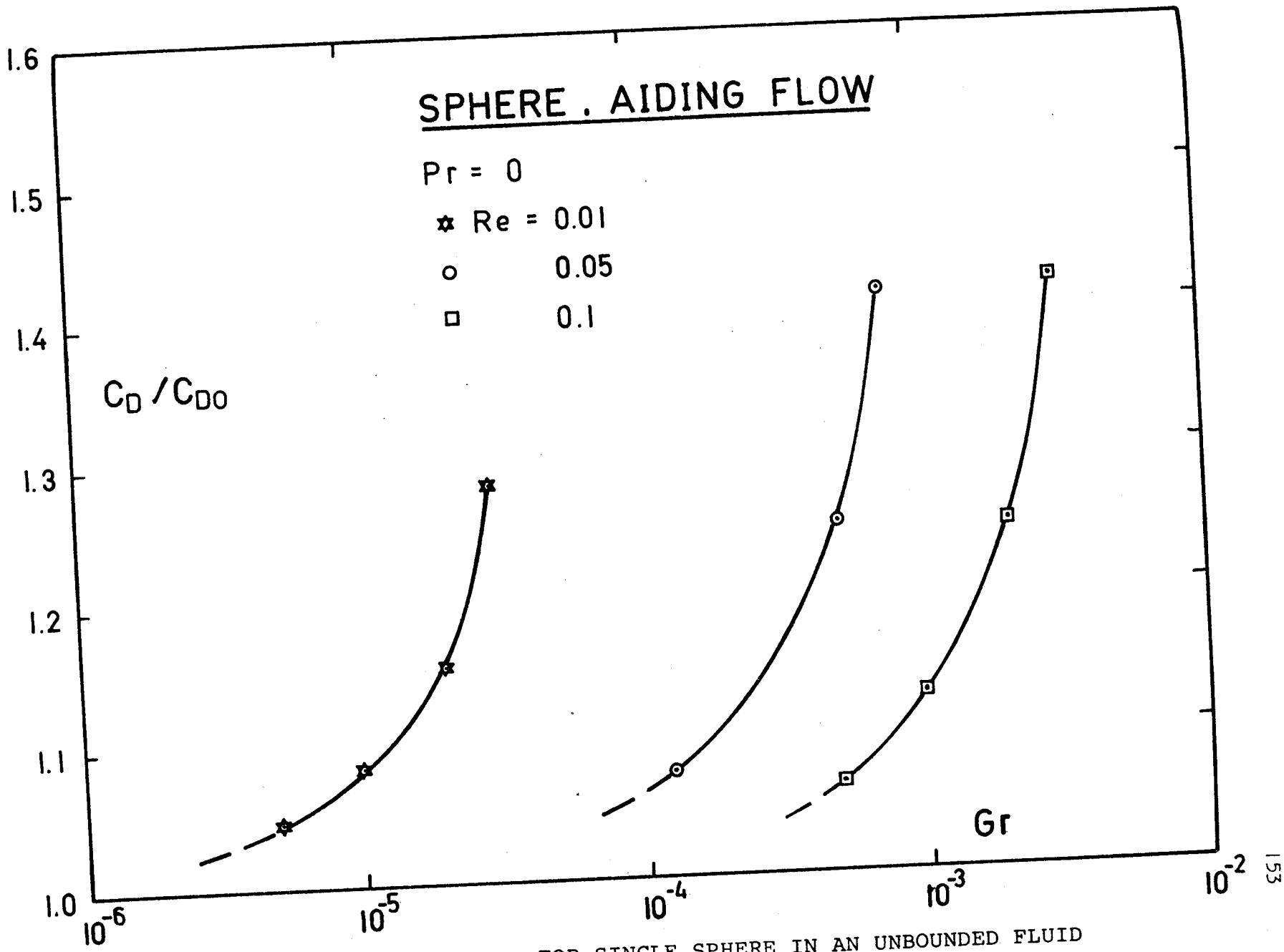

FIGURE 4.5-3 C_D/C_{DO} vs Gr FOR SINGLE SPHERE IN AN UNBOUNDED FLUID OF Pr=0 (AIDING FLOW)

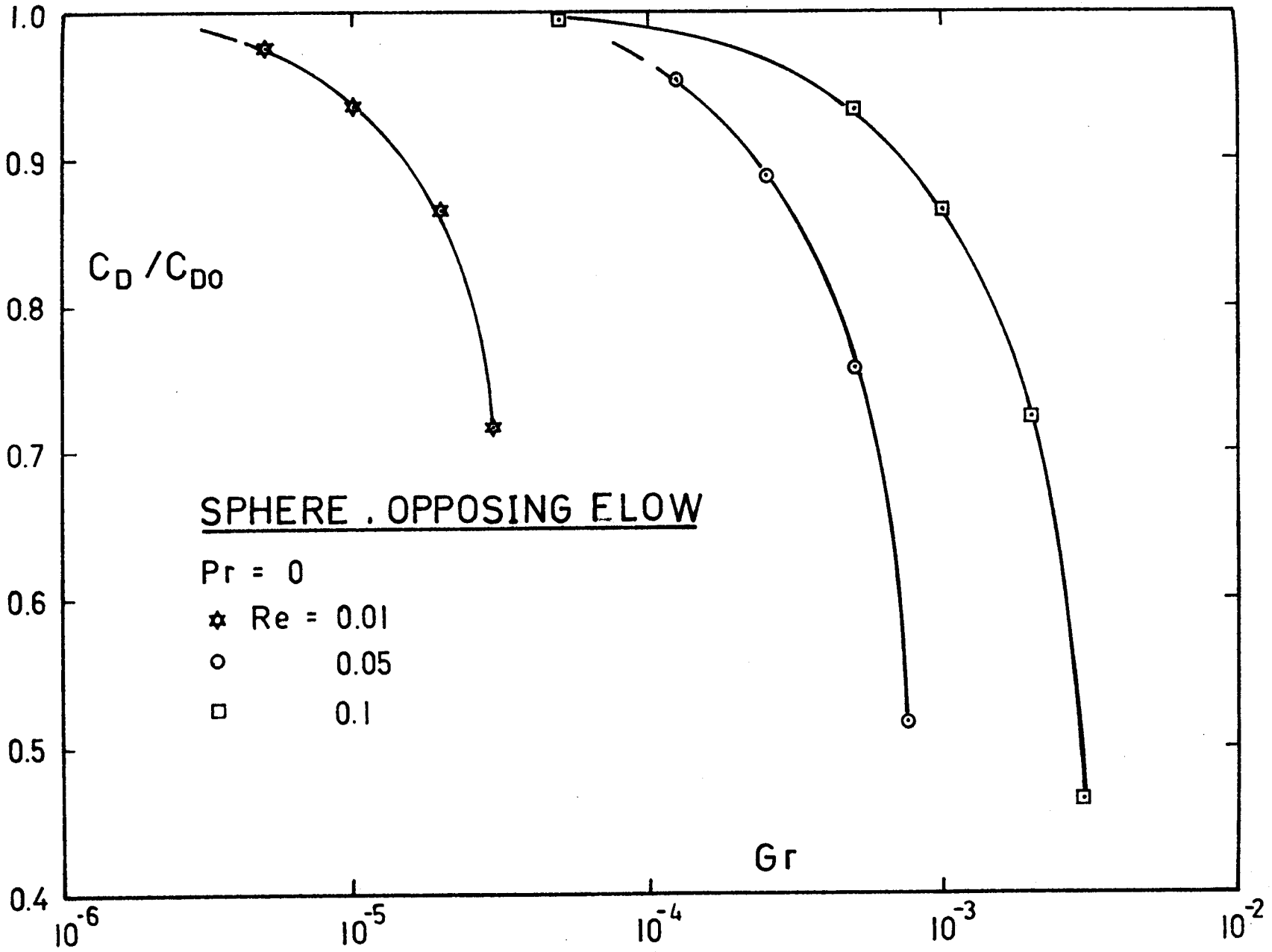

FIGURE 4.5-4 C_D/C_{DO} vs Gr FOR SINGLE SPHERE IN AN UNBOUNDED FLUID OF Pr=0 (OPPOSING FLOW)

5. CONCLUSIONS, LIMITATIONS OF SOLUTION AND CALCULATION METHOD AND RECOMMENDATIONS.

5.1 Conclusions

Numerical methods with a new sequence of calculation and convergence acceleration have been developed to solve linear elliptic difference equations and non-linear coupled difference equations. These methods were found to be much faster than the ADI and SOR methods; these methods are generally used in numerical studies of this kind.

Fluid mechanical data for a single sphere and for a single cylinder in an unbounded fluid have been calculated theoretically. Ranges of dimensionless parameters, Reynolds, Prandtl and Grashof numbers covered extend significantly those which have been considered in previous numerical studies. Present solutions are generally more accurate than those published in the literature.

5.2 Limitation of Solution and Calculation Method

The limitations of solutions and calculation method involved in this study are caused by two main sources, namely, the flow instability and computational instability. They are described in the following sections.

The numerical solutions obtained in this study were for steady state conditions. The flow phenomena in question may become transient under certain conditions and for certain values of the dimensionless parameters. For example vortex shedding from a sphere is observed experimentally at a Reynolds number of about 400, the critical value depending on main stream turbulent intensity. Beyond this critical Reynolds number the flow is transient and the steady state solution can only hope to approximate the actual behaviour.

For certain values of the dimensionless parameters, the flow becomes unstable, and the growth in intensity of this instability can eventually result in turbulent flow. An example of this is opposing flow at high Grashof numbers where the large natureal convection current extensively disturbs the forced convection current. Without considering the transient term in the Navier Stokes and energy

studies at high Pr and intermediate Re thin thermal boundary layer theory and integral method should be considered for solving the energy equation. The application of the finite element method for the solution of Navier Stokes equations of motion should be considered.

equations, one cannot be sure that the steady-state solution which has been reported here actually exists. It is well known that opposing natural and forced convection leads to instabilities. This is suspected in this case where the calculated flow field shows a zero streamline separating the natural and forced flow field at a position away from the sphere surface. The steady-state solution itself became highly unstable in this region.

In case of high Prandtl and intermediate Reynolds number, the thermal boundary layer up to the separation point is extremely thin although the vortexring regime can still be considerably thick due to circulating motion. The temperature gradient over the upstream region is very steep near the surface and this necessitates a fine mesh in the radial direction in the energy equation to make the second order finite-difference equations stable. This will lead to a large increase in mesh points and therefore computation time. In this study, situations in which large differences in velocity and temperature gradients were not investigated.

In the mixed convection problems solved in this study, the Prandtl numbers considered are of order 1 and 0 where the natural convection is important. Under these conditions, the thermal boundary layer is thick and a relatively large outside boundary must be chosen to ensure undisturbed parallel flow. At a Grashof number where the radio Gr/Re^2 is greater than unity, it was found that the computation for opposing flow becomes unstable, and the outside boundary must be chosen extremely large to bound the large reversing natural convection contour. The instability problem can be reduced by employing a smaller mesh system; however, very large computation times are required.

All solutions obtained in this work assume constant property flow and this can be a serious limitation in many practical applications.

5.3 Recommendations

A faster numerical method should be developed. The Galerkin method looks attractive for future study in this area of computation. In forced convection

NOMENCLATURE

A - Lattice spacing in z direction, dimensionless

a - Constant in the correlation $Nu=aPr^b$, dimensionless

B - Lattice spacing in Θ direction, dimensionless

b - Constant in the correlation $Nu=aPr^b$, dimensionless

$\bar{b}$ - Column vector

C - Concentration, dimensional

C_D - Total drag coefficient, dimensionless

C_{DF}, C_{DP} - Friction and form drag coefficients, dimensionless

C_{DO} - Total drag coefficient at Gr=0, dimensionless

C_{DS} - Stokes drag coefficient, dimensionless

$\bar{\bar{C}}, \bar{\bar{C}}_1, \bar{\bar{C}}_2$ - Coefficient matrices

$\hat{C}_p$ - Heat capacity, dimensional

D - Molecular diffusivity, dimensional

d - Diameter of sphere, dimensional

E_c^{*2}, E_{cz}^{*2} - Differential operators for cylindrical coordinates

$$E_c^{*2} = \frac{\partial^2}{\partial r^{*2}} + \frac{1}{r^*} \frac{\partial}{\partial r^*} + \frac{1}{r^{*2}} \frac{\partial^2}{\partial \Theta^2}$$

$$E_{cz}^{*2} = \frac{\partial^2}{\partial z^2} + \frac{\partial^2}{\partial \Theta^2}$$

E_s^{*2}, E_{sz}^{*2} - Differential operators for spherical coordinates

$$E_s^{*2} = \frac{\partial^2}{\partial r^{*2}} + \frac{\sin\theta}{r^{*2}} \frac{\partial}{\partial \theta} \left(\frac{1}{\sin\theta} \frac{\partial}{\partial \theta}\right)$$

$$E_{sz}^{*2} = \frac{\partial^2}{\partial z^2} - \frac{\partial}{\partial z} + \sin\theta \frac{\partial}{\partial \theta}\left(\frac{1}{\sin\theta} \frac{\partial}{\partial \theta}\right)$$

F - Field function (stream function, vorticity, temperature or concentration)

$\bar{f}, \bar{f}_o, \bar{f}_s$ - Dummy vectors

Gr - Grashof number, $d^3 \beta g (T_s - T_\infty)/\nu^2$

g - Gravitational constant, dimensional

$\bar{g}$ - Gravitational acceleration vector

H, G - Dummy functions of vorticity ξ^*, dimensionless

h - Average heat transfer coefficient, dimensional

$h(\theta)$ - Local heat transfer coefficient, dimensional

I - Total number of mesh points in θ direction

$\bar{\bar{I}}$ - Identity matrix

i - Subscript determining mesh point in θ direction

J - Total number of mesh points in z direction

j - Subscript determining mesh point in z direction

K - Average mass transfer coefficient, dimensional

$K(\theta)$ - Local mass transfer coefficient, dimensional

L - Length of vortex, dimensional

M - Dummy integer

m - Subscript for mass transfer

N - Total number of mesh points

Nu - Nusselt number, dh/k

$Nu(\theta)$ - Local Nusselt number, $dh(\theta)/k$

n - Iteration level

P,Q - Dummy coefficients in the generalized second order elliptic partial differential equation

P' - Dummy variable of pressure, pressure/ρ

P^* - Dimensionless pressure, pressure/$\frac{1}{2}\rho U_\infty^2$

$P^*(\theta), P_s^*$ - Surface pressure distribution

P_o^* - Frontal stagnation pressure, $P^*(\theta=0)$

Pe - Peclet number, $dU_\infty \rho \hat{c}_p/k$

Pr - Prandtl number, $\mu \hat{c}_p/k$

R - Radius of sphere or cylinder, dimensional

r - Radial distance from center of sphere or cylinder

r^* - Dimensionless radial distance, r/R

r_∞^* - Dimensionless radius of outer spherical boundary or cylindrical shell

Sc - Schmidt number, ν/D

Sh - Sherwood number, dK/D

$Sh(\theta)$ - Local Sherwood number, $dK(\theta)/D$

T - Temperature, dimensional

T_s, T_∞ - Temperature at $r^*=1$ and $r^*=\infty$

U_∞ - Main stream velocity or terminal velocity of sphere or cylinder, dimensional

V_r, V_θ - Velocity components in r, θ directions

V_s, V_w - Volumes of sphere and trailing vortex

V_x, V_y - Velocity components in x, y directions

W - Relaxation factor

$\bar{\bar{W}}$ - Matrix of relaxation factors

W_{η^*} - Relaxation factor for η^*

W_{ξ^*} - Relaxation factor for ξ^*

W_{ψ^*} - Relaxation factor for ψ^*

x, y - Coordinates

z - Modified radial spherical or cylindrical coordinate

Greek Letters

α - Damping factor

β - Volumetric expansion coefficient, dimensional

$\bar{\gamma}$ - Eigenvector

δ - Convergence acceleration factor

ϵ - Tolerance or porosity $\left(\frac{\text{vol.of fluid}}{\text{vol.of fluid+vol.of solid}}\right)$

η^* - Dimensionless temperature or concentration

θ - Angular coordinate

θ_m - Minimum surface transfer angle, dimensional

θ_s - Flow separation angle where $\xi^*_s=0$

λ - Eigenvalue of a matrix

μ - Viscosity, dimensional

ν - Kinematic viscosity, μ/ρ , dimensional

ξ - Vorticity, dimensional

ξ^* - Dimensionless vorticity

ξ_s^* - Surface vorticity distribution

ρ - Density of fluid, dimensional

σ - Euler's constant, 0.577

ψ - Stream function

ψ^* - Dimensionless stream function

BIBLIOGRAPHY

Acrivos, A.,
AIChEJ.,4, 285 (1958).

Acrivos, A.,
Chem. Engng. Sci., 21, 343 (1966).

Acrivos, A., and Taylor, T.D.,
Phys. Fluids, 5, 387 (1962).

Aitken, A.C.,
Proc. R. Soc., Edinburgh (1925).

Aitken, A.C.,
Proc. R. Soc., Edinburgh (1936).

Allen, D.N., and Southwell, R,V.,
Quart. J. Mech. App. Math. VIII. Part 2, June (1955).

Apelt, C.J.,
ARC R & M No 3175, London (1958).

Aziz, K., and Hellums, J.D.,
Phys. Fluids, 10, 314 (1967).

Baird, M.H.I., and Hamielec, A.E.,
Can. J. Chem. Eng., 40, 119 (1962).

Beard, K.V.K., and Pruppacher, H.R.,
To be published in J. Atmos. Sci. (1971).

Boussinesq, J.,
Theorie Analytique de la Chaleur, 2, (1903).

Boussinesq, J.,
J. Math., 1, 285 (1905).

Brian, P.L.T., and Hales, H.B.,
AIChEJ., 15, 419 (1969).

Chandrasekhar, S.,
"Hydrodynamic and Hydromagnetic Stability",
Clarendon Press, Oxford, England (1961).

Chorin, A.J.,
J. Comp. Phys., 2, 12 (1967).

Cole, J., and Roshko, A.,
Proc. Heat Transfer and Fluid Mechanics Inst.,
Univ. of Calif., Berkeley (1954).

Collis, D.C., and Williams, M.J.,
J. Fluid Mech., 6, 357 (1959).

Dennis, S.C.R., Hudson, J.D., and Smith, N.,
Phys. Fluids, 5, 933 (1968).

Douglas, J. Jr., and Rachford, H.H.,
J. Trans. Am. Math. Soc., 82, 421 (1956).

Eckert, E.R.G., and Soehngen, E.,
Trans. Am. Soc. Mech. Engrs., 74, 343 (1952).

Fadeeva, V.N.,
"Computational Methods of Linear Albebra",
Dover Publications, Inc., New York (1959).

Faxen, H.,
Nova Acta Societatis Scientianum Upsaliensis.
Volumen Extra Ordinem (1927).

Frankel, S.P.,
Math. Tables Aids. Comput., 4, 65 (1950).

Fromm, J.E., and Harlow, F.H.,
Phys. Fluids, 6, 975 (1963).

Garner, F.H., and Grafton, R.W.,
Proc. R. Soc., A224, 70 (1954).

Garner, F.H., and Keey, R.B.,
Chem. Engng. Sci., 9, 119 (1958).

Garner, F.H., and Suckling, R.D.,
AIChEJ., 4, 114 (1958).

Garner, F.H., and Hoffman, A.E.,
I & EC Fundamentals, 7, 347 (1961).

Grosh, R.J., and Cess, R.D.,
Trans. ASME, 80, 667 (1958).

Hamielec, A.E., Storey, S.H., and Whitehead, J.M.,
Can. J. Chem. Eng., 41, 246 (1963).

Hamielec, A.E., Hoffman, T.W., and Ross, L.L.,
AIChEJ., 13, 222 (1967).

Hamielec, A.E., Johnson, A.I., and Houghton, W.T.,
AIChEJ., 13 379 (1967).

Hamielec, A.E., and Raal, J.D.,
Phys. Fluids, 12, 11 (1969).

Hendrix, C.D., Dare, S.B., and Johnson, H.F.,
AIChEJ., 13, 1072 (1967).

Hieber, C.A., and Gebhart, B.,
J. Fluid Mech., 38, 137 (1969).

Houghton, W.T.,
Ph.D. Thesis, McMaster Univ., Hamilton, Ontario (1967).

Jenson, V.G.,
Proc. R. Soc., A249, 346 (1959).

Johnson, A.I., and Akehata, T.,
Can. J. Chem. Eng., 43, 10 (1965).

Kaplun, S.,
"Singular Perturbations and Fluid Mechanics",
Academic Press (1967).

Karla, T.R.,
"Private Communication, Dept. of Chemical Engineering,
Monash Univ., Australia".

Kawaguti, M.,
Rept. Inst. Sci., Tokyo, 2, 66 (1948).

Keller, H.B., and Takami, H.,
"Numerical Solutions of Nonlinear Differential Equations",
John Wiley & Sons, Inc., New York (1966).

King, L.V.,
Phil. Trans. A214, 373 (1914).

Kubair, V.G., and Pei, D.C.T.,
Int. J. Heat and Mass Transfer, 11, 855 (1968).

Lamb, H.,
Phil. Mag., (6), 21, 112 (1911).

Lagerstrom, P.A., and Cole, J.D.,
F. Rational Mech. Analysis, 4, 817 (1955).

Lapidus, L.,
"Digital Computation for Chemical Engineers",
McGraw-Hill, New York (1962).

Lapple, C.E.,
"Fluid and Particle Mechanics",
Univ. of Delaware Press., Newark (1954).

LeClair, B.P.,
Ph.D. Thesis, McMaster Univ., Hamilton, Ontario (1970).

LeClair, B.P., and Hamielec, A.E.,
I. Chem. E. Symposium Series, No. 30 (1968).

LeClair, B.P., and Hamielec, A.E.,
I&EC Fundamentals, 7, 542 (1968).

LeClair, B.P., and Hamielec, A.E.,
I&EC Fundamentals, 9, 608 (1970).

Levich, V.G.,
"Physicochemical Hydrodynamics",
Prentice-Hall, New York (1962).

Maxworthy, T.,
J. Fluid Mech., 23, 369 (1965).

Merk, H.J., and Prins, J.A.,
Appl. Sci. Res., 44, 11, 195, 207 (1954).

Narasimhan, C.,
Ph.D. Thesis, McGill Univ., Montreal, Quebec (1966).

Narasimhan, C., and Gauvin, W.H.,
Can. J. Chem. Eng., 45, 181 (1967).

Nisi, H., and Porter, A.W.,
Phil. Mag., (B), 754 (1923).

Ohman, G.A.,
ACTA, Physics including Nucleonics Series No. 68,
Helsinki (1969).

Oosthuisen, P.H.,
Rept. 2-70, Dept. of Mech. Eng., Queens Univ.,
Kingston (1970).

Orbach, O., and Crowe, C.M.,
To be published in Can. J. Chem. Eng. (1971).

Oseen, C.W.,
Ark. Mat. Astr. Rys., 6,No.29 (1910).

Peaceman, D.W., and Rachford, H.H.,
J. SIAM., 3, 28 (1955).

Pearson, C.E.,
J. Fluid Mech., 21, 611 (1965).

Peltzman, A., and Pfeffer, R.,
Chem. Eng. Symposium Series, 77, 63 (1967).

Proudman, I., and Pearson, J.R.A.,
J. Fluid Mech., 2, 237 (1957).

Pruppacher, H.R., LeClair, B.P., and Hamielec, A.E.,
J. Fluid Mech., 44, 781 (1970).

Pruppacher, H.R., and Steinberger, E.H.,
J. Appl. Phys., 39, 4129 (1968).

Ranz, W.E., and Marshall, W.R. Jr.,
Chem. Eng. Progr., 48, 141, 173 (1952).

Rhodes, J.M.,
Ph.D. Thesis, Univ. of Tennessee, Tennessee (1967).

Rhodes, J.M, and Peebles, F.N.,
AIChEJ., 11, 481 (1965).

Rimmer, P.L.,
J. Fluid Mech., 32, 1 (1969).

Rimon, Y., and Cheng, S.I.,
Phys. Fluids, 12, 949 (1969).

Russell, D.B.,
ARC R & M No. 3331, London (1962).

Son, J.S., and Hanratty, T.J.,
J. Fluid Mech., 35, 369 (1969).

Sparrow, E.M., Eichhorn, R., and Gregg, J.L.,
Phys. Fluids, 2, 319 (1959).

Speigel, A.E., and Veronis, G.,
Astrophys. J., 131, 441 (1960).

Stokes, G.G.,
Trans. Cambridge Phil. Soc., 9, 8 (1851).

Taneda, S.,
Rept. Res. Inst. Appl. Mech., Japan, 4, 99 (1956).

Thom, A.,
Proc. R. Soc., A141, 651 (1933).

Thoman, D.C., and Szewczyk, A.A.,
Rept. 66-14, Dept. of Mech. Eng., Univ. of Notre Dame (1966).

Tomotika, S., and Aoi, T.,
Quart. J. Mech. Appl. Math., 3, 140 (1950).

Tritton, D.J.,
J. Fluid Mech., 6, 547 (1959).

Varga, R.S.,
"Matrix Iterative Analysis",
Prentice-Hall, Inc., N.J. (1962).

Wegstein, J.H.,
Comm. ACM, 1, No. 6, 9 (1958).

Young, D.,
Trans. Am. Math. Soc., 75, 92 (1954).

Yuge, T.,
Trans. Am. Soc. Mech. Engrs., C82, 214 (1960).

Appendix A. Computer Programs

APPENDIX A.1
****

```
     END OF RECORD
    NAVIER STOKES EQUATIONS FOR SPHERE
  SEQUENCING WITH CONVERGENCE PROMOYION
C RE              =REYNOLDS NUMBER
C M,N             =TOTAL NO. OF STEPS IN ANGULAR AND RADIAL DIRECTIONS
C A,B             =STEP SIZES IN Z AND ANGULAR DIRECTIONS
C NLOOPS          = MAX. NO. OF ITERATIONS ALLOWED IN ONE RUN
C KKC             =COUNTER FOR APPLYING CONVERGENCE PROMOTION AND REVISING W
C NSTART          =CONTROL STATEMENT FOR READING IN INTERMEDIATE
C                  DATA OR CALCULATING INITIAL GUESSES
C                  0-- INITIAL GUESSES
C                  1-- READ IN INTERMEDIATE DATA
C I1,I2,J1        =SEQUENCEING CONTROL CARDS
C FIELD FUNCTIONS
C PSI             =STREAM FUNCTION
C G               =DUMMY FUNCTION OF VORTICITY
C RELAXATION FACTORS
C WV              =FOR G
C WS              =FOR PSI
      PROGRAM TST (INPUT,OUTPUT,PUNCHB,TAPE5=INPUT,TAPE6=OUTPUT,
     1TAPE7=PUNCHB,TAPE8,TAPE1)
      DIMENSION Z(102),EZ1(102),EZ2(102),EZ3(102),EZ4(102),EZ5(102)
     1,EZ6(102)
      DIMENSION THETA(62),ANGLE(62),SI(62),CO(62),COT(62),DUMSI(62)
      DIMENSION PSI(61,101),G(61,101),REZS(61,101),VR(101)
      DIMENSION DUM3(61),DUM4(61),P(61,1),SVORT(61,1)
      DIMENSION WV(61,101)

      READ (5,10) RE,C1,D1
      READ (5,11) EPSS,EPSV
      READ (5,12) M,N,A
      READ (5,13) KKC,EXRC
      READ (5,15) NLOOPS
      READ (5,15) NSTART

   51 FORMAT (1H0,10X,*AXISYMMETRIC FLOW AROUND A SOLID SPHERE*/)
      WRITE (6,51)
      WRITE (6,52)
   52 FORMAT (1H0,10X,*WITH CONVERGENCE PROMOTION*/)
      WRITE (6,20) RE
      WRITE (6,22) M,N,A
      WRITE (6,23) KKC,EXRC

      MP1=M+1
      NM1=N-1
      FMP1=FLOAT(MP1)
      FN=FLOAT(N)
      DMN=3.1416*3.1416*(1./FMP1/FMP1+1./FN/FN)
      WS=1./(1.+SQRT(DMN)/1.4142)
      A2=A*A
      B=3.1416/(FLOAT(M))
      B2=B*B
      DUM1=(1.-A*0.5)/A2
```

```
      DUM2=(1.+A*0.5)/A2
      DUM6=0.5*A2*B2/(A2+B2)
      DREAB=RE/32./A/B
      THETA(1)=0.0
      THETA(2)=B
      DO 100 I=2,M
      THETA(I+1)=THETA(I)+B
      ANGLE(I)=THETA(I)*180.0/3.1416
      CO(I)=COS(THETA(I))
      SI(I)=SIN(THETA(I))
      DUMSI(I)=SI(I)*SI(I)
      COT(I)=CO(I)/SI(I)
      DUM3(I)=(1.-0.5*B*COT(I))/B2
      DUM4(I)=(1.+0.5*B*COT(I))/B2
  100 CONTINUE
      Z(1)=0.0
      DO 110 J=1,N
      Z(J+1)=Z(J)+A
      EZ1(J)=EXP(Z(J))
      EZ2(J)=EZ1(J)*EZ1(J)
      EZ3(J)=EZ2(J)*EZ1(J)
      EZ4(J)=EZ3(J)*EZ1(J)
      EZ5(J)=EZ1(J)*EZ4(J)
      FZ6(J)=EZ5(J)*EZ1(J)
  110 CONTINUE
      SI(1)=0.0
      SI(MP1)=0.0
      CO(1)=1.0
      CO(MP1)=-1.0
      DUMSI(1)=0.0
      DUMSI(MP1)=0.0
      ANGLE(1)=0.0
      ANGLE(MP1)=180.
      DO 120 I=1,MP1
      DO 120 J=1,N
      REZS(I,J)=RE*EZ1(J)*SI(I)/A/B/8.0
  120 CONTINUE

      IF(NSTART.EQ.1) GO TO 1000

C     INITIAL GUESS OF STREAM FUNCTION AND VORTICITY (KAWAGUTI)
      C2=-(120.+75.*C1)/29.
      C3=(153.+63.*C1)/29.
      C4=-(47.5+17.*C1)/29.
      D2=-69.*D1/27.
      D3=57.*D1/27.
      D4=-15.*D1/27.
      DO 300 I=2,M
      DO 300 J=1,NM1
      PSI(I,J)=SI(I)*SI(I)*(0.5*FZ2(J)+C1/EZ1(J)+C2/EZ2(J)+C3/EZ3(J)+C4
     1/EZ4(J)-CO(I)*(D1/EZ1(J)+D2/EZ2(J)+D3/EZ3(J)+D4/EZ4(J)))
      G(I,J)=SI(I)*SI(I)*((4.*C2/EZ4(J)+10.*C3/EZ5(J)+18.*C4/EZ6(J))
     1+CO(I)*(4.*D1/EZ3(J)-6.*D3/EZ5(J)-14.*D4/EZ6(J)))
  300 CONTINUE

C     SETTING UP OF BOUNDARY CONDITIONS
```

```
      DO 400 I=1,MP1
      PSI(I,1)=0.0
      G(I,N)=0.0
  400 PSI(I,N)=0.5*EZ2(N)*DUMSI(I)
      DO 410 J=1,N
      PSI(1,J)=0.0
      PSI(MP1,J)=0.0
      G(1,J)=0.0
  410 G(MP1,J)=0.0
      DO 720    I=2,M
      DO 720 J=2,NM1
      AP=2.*A*(PSI(I+1,J)-PSI(I-1,J))
      BP=2.*B*(PSI(I,J+1)-PSI(I,J-1))
      XI=DREAB*BP/EZ1(J)/SI(I)
      XJ=DREAB*AP/EZ1(J)/SI(I)
      XIJ=SQRT(0.5*(XI*XI+XJ*XJ))
      WV(I,J)=0.7/(1.+XIJ)
  720 CONTINUE

      GO TO 1010

 1000 REWIND 8
      READ (8)  ((PSI(I,J),I=1,MP1),J=1,N)
      READ (8)  (( G (I,J),I=1,MP1),J=1,N)

 1010 JJ=0

      I2=I1=0
      KK=0
      FAS1=FAV1=1.0
      BIGS1=BIGV1=1.0
      EXRA=1.0

 1100 II=0

      JJ=JJ+1
      KK=KK+1
      NPS=NPV=0
      IF(KK.NE.KKC) GO TO 309
      KK=0
      EXRA=EXRC
  309 CONTINUE
      BIGSA=BIGVA=0.0
      FAS=FAV=0.0
      IBS=IBV=2
      JBS=JBV=2
      DO 700 I=2,M
      G(I,1)=(4.0*PSI(I,2)-0.5*PSI(I,3))/A2
  700 CONTINUE
  310 CONTINUE
      DO 500 I=2,M

      IF(I1.EQ.1) GO TO 312
      I1=J1=1
      GO TO 311
```

```
312 CONTINUE
    I1=J1=0
311 CONTINUE

    DO 500 J=2,NM1

    IF(J1.EQ.0) GO TO 322
    J1=0
    GO TO 321
322 J1=1
    GO TO 500
321 CONTINUE

    DMPSII= PSI(I+1,J)-PSI(I-1,J)
    DMPSIJ= PSI(I,J+1)-PSI(I,J-1)
    DUMA=G(I,J+1)/(EZ2(J+1)*DUMSI(I))
    DUMC=G(I,J-1)/(EZ2(J-1)*DUMSI(I))
    IF(I.EQ.2) GO TO 501
    DUMD=G(I-1,J)/(EZ2(J)*DUMSI(I-1))
    GO TO 502
501 DUMD=G(2,J)/(EZ2(J)*SI(2)*B)
502 IF(I.EQ.M) GO TO 503
    DUMB=G(I+1,J)/(EZ2(J)*DUMSI(I+1))
    GO TO 504
503 DUMB=G(M,J)/(EZ2(J)*SI(M)*B)

504 STRMF=DUM6*(PSI(I,J+1)*DUM1+PSI(I,J-1)*DUM2+PSI(I+1,J)*DUM3(I)
   1+PSI(I-1,J)*DUM4(I)-G(I,J)*EZ2(J))
    AS=STRMF-PSI(I,J)

    DPSI=DMPSIJ*(DUMB-DUMD)-DMPSII*(DUMA-DUMC)
    VORT=DUM6*(G(I,J+1)*DUM1+G(I,J-1)*DUM2+G(I+1,J)*DUM3(I)+G(I-1,J)*
   1DUM4(I)-REZS(I,J)*DPSI)
    AV=VORT-G(I,J)

    IF(I2.EQ.1) GO TO 341
    IF(ABS(STRMF).LT.0.001) GO TO 510
    NPS=NPS+1
    ASF=AS/STRMF
    FAS=FAS+ASF*ASF
    ASA=ABS(ASF)
    IF(ASA.GT.EPSS) II=1
    IF(ASA.LT.BIGSA) GO TO 510
    BIGSA=ASA
    BIGS=ASF
    IBS=I
    JBS=J
510 CONTINUE
    IF(ABS(VORT).LT.0.05) GO TO 520
    NPV=NPV+1
    AVF=AV/VORT
    FAV=FAV+AVF*AVF
    AVA=ABS(AVF)
    IF(AVA.GT.EPSV) II=1
    IF(AVA.LT.BIGVA) GO TO 520
    BIGVA=AVA
```

```
      BIGV=AVF
      IBV=I
      JBV=J
  520 CONTINUE
      PSI(I,J)=PSI(I,J)+EXRA*WS*AS
      G(I,J)=G(I,J)+EXRA*WV(I,J)*AV
      GO TO 500
  341 CONTINUE
      PSI(I,J)=PSI(I,J)+AS
      G(I,J)=G(I,J)+AV
  500 CONTINUE
      IF(I2.EQ.0) GO TO 332
      I1=I2=0
      GO TO 331
  332 I1=I2=1
      GO TO 310
  331 CONTINUE
      FAS=SQRT(FAS)/FLOAT(NPS)
      FAV=SQRT(FAV)/FLOAT(NPV)
      RFAS=FAS/FAS1
      RFAV=FAV/FAV1
      RBIGS=BIGS/BIGS1
      RBIGV=BIGV/BIGV1
      WRITE (6,50) JJ,IBS,JBS,BIGS,RBIGS,FAS,RFAS,IBV,JBV,BIGV,RBIGV
     1,FAV,RFAV
   50 FORMAT (1H ,I10,3X,2(2I5,4E12.3,2X))
      BIGV1=BIGV
      BIGS1=BIGS
      FAS1=FAS
      FAV1=FAV
      EXRA=1.0
      IF((KK+1).EQ.KKC) GO TO 3000
 3333 CONTINUE

      IF(JJ.EQ.NLOOPS) GO TO 2000
      IF(II.EQ.1) GO TO 1100

 3000 CONTINUE

      DO 721 I=2,M
      DO 721 J=2,NM1
      AP=2.*A*(PSI(I+1,J)-PSI(I-1,J))
      BP=2.*B*(PSI(I,J+1)-PSI(I,J-1))
      XI=DREAB*BP/EZ1(J)/SI(I)
      XJ=DREAB*AP/EZ1(J)/SI(I)
      XIJ=SQRT(0.5*(XI*XI+XJ*XJ))
      WV(I,J)=0.7/(1.+XIJ)
  721 CONTINUE
      WRITE (6,2010) (EZ1(J),(WV(I,J),I=1,MP1,4),J=1,N,10)
C     CALN. FOR SURFACE VORTICITY
      SVORT(1,1)=0.0
      SVORT(MP1,1)=0.0
      DO 660 I=2,M
  660 SVORT(I,1)=G(I,1)/SI(I)
      WRITE (6,39)
      WRITE (6,2050) (SVORT(I,1),I=1,MP1,2)
```

```
C     CALN. FOR FRONTAL STAGNATION PRESS.
      DMGF=0.0
      DO 620 J=2,NM1
  620 DMGF=DMGF+(4.0*G(2,J)/SI(2)-G(3,J)/SI(3))/EZ1(J)
      FSPRES=1.0+(DMGF+0.5*((4.0*G(2,1)/SI(2)-G(3,1)/SI(3))/EZ1(1)
     1+(4.0*G(2,N)/SI(2)-G(3,N)/SI(3))/EZ1(N)))*4.0*A/(RE*B)
C     CALN. FOR SURFACE PRESS. DISTRIBUTION
      P(1,1)=FSPRES
      DO 630 K=2,M
      DUMG=0.0
      DO 631 I=2,K
  631 DUMG=DUMG+(4.0*G(I,2)/EZ1(2)-G(I,3)/EZ1(3)-3.0*G(I,1))
     1/(2.0*A*SI(I))+G(I,1)/SI(I)
  630 P(K,1)=P(1,1)+4.0/RE*B*(DUMG-0.5*((4.0*G(K,2)/EZ1(2)-G(K,3)/EZ1(3)
     1-3.0*G(K,1))/(2.0*A*SI(K))+G(K,1)/SI(K)))
      P(MP1,1)=P(M,1)+4.0/RE*B*(0.5*((4.0*G(M,2)/EZ1(2)-G(M,3)/EZ1(3)
     1-3.0*G(M,1))/(2.0*A*SI(M))+G(M,1)/SI(M)))
      WRITE (6,36)
      WRITE (6,2030) (P(I,1),I=1,MP1)
C     CALN. FOR FORM DRAG COEFF.
      DUMP=0.0
      DO 640 I=2,M
  640 DUMP=DUMP+P(I,1)*SI(I)*CO(I)*2.0
      CDP=DUMP*B
      WRITE (6,37)
      WRITE (6,2020) CDP
C     CALN. FOR FRICTION DRAG COEFF.
      DUMPSI=0.0
      DO 650 I=2,M
  650 DUMPSI=DUMPSI+G(I,1)*SI(I)
      CDF=8.0*DUMPSI*B/RE
      WRITE (6,35)
      WRITE (6,2020) CDF
C     CALN. FOR TOTAL DRAG COEFF.
      CTOTAL=CDF+CDP
      WRITE (6,38)
      WRITE (6,2020) CTOTAL

      IF(II.NE.1) GO TO 2000
      GO TO 3333

 2000 CONTINUE

      WRITE (7) ((PSI(I,J),I=1,MP1),J=1,N)
      WRITE (7) ((G(I,J),I=1,MP1),J=1,N)

      WRITE (6,24) JJ
      WRITE (6,30)
      WRITE (6,2040) (ANGLE(I),I=1,16)
      WRITE (6,2010) (EZ1(J),(PSI(I,J),I=1,16),J=1,N)
      WRITE  (6,2040) (ANGLE(I),I=17,32)
      WRITE (6,2010) (EZ1(J),(PSI(I,J),I=17,32),J=1,N)
      WRITE  (6,2040) (ANGLE(I),I=33,48)
      WRITE (6,2010) (EZ1(J),(PSI(I,J),I=33,48),J=1,N)
      WRITE  (6,2040) (ANGLE(I),I=49,61)
      WRITE (6,2011) (EZ1(J),(PSI(I,J),I=49,61),J=1,N)
```

```
      WRITE (6,31)
      WRITE (6,2040) (ANGLE(I),I=1,16)
      WRITE (6,2010) (EZ1(J),( G (I,J),I=1,16),J=1,N)
      WRITE  (6,2040) (ANGLE(I),I=17,32)
      WRITE (6,2010) (EZ1(J),( G (I,J),I=17,32),J=1,N)
      WRITE  (6,2040) (ANGLE(I),I=33,48)
      WRITE (6,2010) (EZ1(J),( G (I,J),I=33,48),J=1,N)
      WRITE  (6,2040) (ANGLE(I),I=49,61)
      WRITE (6,2011) (EZ1(J),( G (I,J),I=49,61),J=1,N)

C     CALN. FOR RADIAL VELOCITY AT THE REAR STAGNATION POINT
      DO 555 J=1,N
      VR(J)=(8.*PSI(M,J)-PSI(M-1,J))/(2.*B*B*EZ2(J))
  555 CONTINUE
      WRITE (6,55)
      WRITE (6, 2070) (EZ1(J),VR(J),J=1,N)
   55 FORMAT (1H0,15HRADIAL VELOCITY/)
 2070 FORMAT (1H ,20X,F10.4,F20.6)

      REWIND 8
      WRITE (8) ((PSI(I,J),I=1,MP1),J=1,N)
      WRITE (8) ((G(I,J),I=1,MP1),J=1,N)
      END FILE 8


   10 FORMAT (3F10.6)
   11 FORMAT (2F10.6)
   12 FORMAT (2I5,F10.6)
   13 FORMAT(I10,F10.6)
   15 FORMAT (I5)
   20 FORMAT (1H0,10X,*RE=*,F20.6/)
   21 FORMAT (1H0,10X,*WS=*,F20.6,5X,*WV=*,F20.6/)
   22 FORMAT (1H0,10X,*M=*,I10,5X,*N=*,I10,5X,*A=*,F10.5/)
   23 FORMAT (1H0,10X,*KKC=*,I10,5X,*EXRC=*,F20.6/)
   24 FORMAT (1H0,10X,*JJ=*,I10/)
   30 FORMAT (1H0,15HSTREAM FUNCTION/)
   31 FORMAT (1H0,9HVORTICITY/)
   35 FORMAT (1H0,20HFRICTION DRAG COEFF./)
   36 FORMAT (1H0,27HSURFACE PRESS. DISTRIBUTION/)
   37 FORMAT (1H0,16HFORM DRAG COEFF./)
   38 FORMAT (1H0,17HTOTAL DRAG COEFF./)
   39 FORMAT (1H0,30HSURFACE VORTICITY DISTRIBUTION/)
 2010 FORMAT (1H ,F6.3,16F8.4)
 2020 FORMAT (1H ,10X,F20.6)
 2030 FORMAT (1H ,6X,8F16.6)
 2040 FORMAT (1H0,6X,16F8.2/)
 2050 FORMAT (1H ,6X,16F8.4)
 2011 FORMAT (1H ,F6.3,13F8.4)
      STOP
      END
         END OF RECORD
```

CD TOT 0389

APPENDIX A.2
****

```
      6400 END OF RECORD
C     FORCED CONVECTION AROUND A SPHERE
C     SEQUENCING WITH CONVERGENCE PROMOTION
C     PE,RE          =PECLET AND REYNOLDS NUMBER
C     M,N            =TOTAL NUMBER OF STEPS IN ANGULAR AND RADIAL DIRECTION
C     A,B            =STEP SIZES INZ AND ANGULAR DIRECTION
C     EPST           =TOLERANCE FOR CONVERGENCE
C     NLOOPS         =MAX. NO. OF ITERATIONS ALLOWED IN ONE RUN
C     NSTART         =CONTROL STATEMENT FOR READING IN INTERMEDIATE DATA
C                     OR STARTING INITIAL CALCULATIONS OR GUESSES
C                     0--CALCULATING INITIAL GUESSES
C                     1--READ IN OF INTERMEDIATE DATA
C     J1,J2          =CONTROL STATEMENTS FOR SEQUENCING CALCULATIONS
      PROGRAM TST (INPUT,OUTPUT,PUNCHB,TAPE5=INPUT,TAPE6=OUTPUT,TAPE7
     1=PUNCHB,TAPE1,TAPE2)
      COMMON T(31,50),DUMA(31,50),DUMB(31,50),DUM34(31)
      DIMENSION X(31)
      DIMENSION THETA(31),SI(31),CO(31),COT(31),ANGLE(31)
      DIMENSION Z(81),EZ1(81),DUM3(81),DUM4(81)
      DIMENSION PSI(31,50),HNUL(31,1)
      DIMENSION WT(31,50)
      READ (5,10) PE,RE
      READ (5,11) EPST
      READ (5,12) M,N,A
      READ (5,13) KP
      READ (5,15) NLOOPS
      READ (5,15) NSTART
      WRITE (6,51)
   51 FORMAT (1H0,10X,*FORCED CONVECTION AROUND A SOLID SPHERE*//)
      WRITE (6,52)
   52 FORMAT (1H0,10X,*TRIDIAGONALIZATION-ITERATION METHOD*/)
      WRITE (6,53)
   53 FORMAT (1H0,10X,*NEW SEQUENCE WITH CONVERGENCE PROMOTION*/)
      WRITE (6,20) PE,RE
      WRITE (6,22) EPST
      WRITE (6,24) M,N,A
      WRITE (6,54)
   54 FORMAT (1H0,31X,*BIGT*,8X,*RBIGT*,8X,*FAT*,8X,*RFAT*/)
      NM1=N-1
      MP1=M+1

C        READ IN OF VELOCITY PROFILE IN TERMS OF STREAM FUNCTION

      READ (1) ((PSI(I,J),I=1,MP1),J=1,N)

      A2=A*A
      B=3.1416/(FLOAT(M))
      B2=B*B
      DUM1=(1.-A*0.5)/A2
```

```
      DUM2=(1.+A*0.5)/A2
      DUM6=0.5*A2*B2/(A2+B2)
      DUM12=(DUM1+DUM2)*DUM6
      THETA(1)=0.0
      THETA(2)=B
      DO 100 I=2,M
      THETA(I+1)=THETA(I)+B
      ANGLE(I)=THETA(I)*180.0/3.1416
      CO(I)=COS(THETA(I))
      SI(I)=SIN(THETA(I))
       COT(I)=CO(I)/SI(I)
      DUM3(I)=(1.-0.5*B*COT(I))/B2
      DUM4(I)=(1.+0.5*B*COT(I))/B2
  100 DUM34(I)=(DUM3(I)+DUM4(I))*DUM6
      ANGLE(1)=0.0
      ANGLE(MP1)=180.
      SI(1)=0.0
      SI(MP1)=0.0
      CO(1)=1.0
      CO(MP1)=-1.0
      Z(1)=0.0
      DO 110 J=1,N
      Z(J+1)=Z(J)+A
      EZ1(J)=EXP(Z(J))
  110 CONTINUE
      DO 120 I=2,M
      DO 120 J=2,NM1
      DMPSII=PSI(I+1,J)-PSI(I-1,J)
      DMPSIJ=PSI(I,J+1)-PSI(I,J-1)
      PEZSI=PE/(EZ1(J)*SI(I)*A*B*8.)
      PEDMI      =PEZSI*DMPSII
      PEDMJ      =PEZSI*DMPSIJ
      XI=PEDMI*2.*A
      XJ=PEDMJ*2.*B
      XIJ=SQRT(0.5*(XI*XI+XJ*XJ))
      WT(I,J)=3./(1.+XIJ)
      DUMA(I,J)=(DUM2+PEDMI)*DUM6
      DUMB(I,J)=(DUM4(I)-PEDMJ)*DUM6
  120 CONTINUE
      WRITE (6,2010) (EZ1(J),(WT(I,J),I=1,MP1,2),J=1,N)

      IF(NSTART.EQ.1) GO TO 1000

C         INITIAL GUESS OF T(I,J) PROFILE

      DO 200 I=1,MP1
      DO 200 J=2,NM1
      T(I,J)=0.0
  200 CONTINUE

C         SETTING UP OF BOUNDARY CONDITIONS

      DO 400 I=1,MP1
```

```
      T(I,N)=0.0
  400 T(I,1) =1.


      GO TO 1010


C         READ IN OF INTERMEDIATE T(I,J) PROFILE


 1000 CONTINUE
      READ (2) ((T(I,J),I=1,MP1),J=1,N)


 1010 JJ=0
      KK=0
      KKK=0
      EXRA=1.0
      BIGT1=1.0
      FAT1=1.
      RFAT1=1.0
 1100 II=0
      JJ=JJ+1
      KK=KK+1
      KKK=KKK+1
      BIGTA=0.
      FAT=0.
      IBT=JBT=2
      J1=0
      J2=0


      XMN=0.0


  505 CONTINUE
      DO 500 J=2,NM1
      IF(J1.EQ.0) GO TO 501
      J1=0
      GO TO 500
  501 CONTINUE
      J1=1


C         CALL T(I,J) FOR A FIXED J


      CALL TDMS(X,M,J,DUM12)


      IF(J2.EQ.0) GO TO 502
      DO 800 L=2,M
      AT=X(L)-T(L,J)
      IF(ABS(X(L)).LT.0.001) GO TO 801
      ATF=AT/X(L)
      FAT=FAT+ATF*ATF
```

```
      ATA=ABS(ATF)
      IF(ATA.GT.EPST) II=1
      IF(ATA.LT.BIGTA) GO TO 801


      XMN=XMN+1.0


      BIGTA=ATA
      BIGT=ATF
      IBT=L
      JBT=J
  801 CONTINUE
      T(L,J)=T(L,J)+EXRA*WT(L,J)*AT
  800 CONTINUE
      T(1,J)=(4.*T(2,J)-T(3,J))/3.
      T(MP1,J)=(4.*T(M,J)-T(M-1,J))/3.
      GO TO 500
  502 DO 803 L=1,MP1
      T(L,J)=X(L)
  803 CONTINUE
  500 CONTINUE
      IF(J2.EQ.1) GO TO 504
      J1=1
      J2=1
      GO TO 505
  504 CONTINUE


      RBIGT=BIGT/BIGT1
      FAT=(SQRT(FAT))/XMN
      RFAT=FAT/FAT1
      WRITE (6,50) JJ,IBT,JBT,BIGT,RBIGT,FAT,RFAT
   50 FORMAT (1H ,10X,I5,5X,2I3,4E12.3)
      IF(RFAT.GT.1.0) GO TO 3020
      IF(ABS(RFAT1-RFAT).LT.0.0005) GO TO 3001
 3020 CONTINUE
      RFAT1=RFAT
      BIGT1=BIGT
      FAT1=FAT
      EXRA=1.0
 3010 CONTINUE
      IF(KKK.EQ.KP) GO TO 3000
      IF(JJ.EQ.NLOOPS) GO TO 2000
      IF(II.EQ.1) GO TO 1100
      GO TO 3000
 3001 CONTINUE
      EXRA=0.7/(1.-RFAT)
      IF(EXRA.GT.30.) EXRA=30.
      WRITE (6,35) KK
   35 FORMAT (1H0,10X,*KK=*,I10)
      WRITE (6,36) EXRA
   36 FORMAT (1H ,10X,*EXRA=*,F10.6)
      WRITE (6,37) RFAT
   37 FORMAT (1H ,10X,*RFAT=*,F10.6/)
      KK=0
```

```
      GO TO 3010
 3000 CONTINUE


C          CALCULATIONS FOR LOCAL AND AVERAGE NUSSULT NO.

      DO 600 I=1,MP1
  600 HNUL(I,1)=(4.0*T(I,2)-T(I,3)-3.0*T(I,1))/(A*EZ1(1))*(-1.0)
      WRITE (6,33)
      WRITE (6,2050) (HNUL(I,1),I=1,MP1)
      DHNUL=0.0
      DO 610 I=2,M
  610 DHNUL=DHNUL+HNUL(I,1)*SI(I)/2.0
      HNUA=DHNUL*B
      WRITE (6,34) HNUA
      IF(HNUA.GT.500.) GO TO 9999
      KKK=0
      IF(II.NE.1) GO TO 2000
      GO TO 3010


 2000 CONTINUE
      WRITE (7) ((T(I,J),I=1,MP1),J=1,N)
      WRITE (6,23) JJ
      WRITE (6,32)
      WRITE (6,2040) (ANGLE(I),I=1,MP1,2)
      WRITE (6,2010) (EZ1(J),( T (I,J),I=1,MP1,2),J=1,N)
   10 FORMAT (2F10.6)
   11 FORMAT (F10.6)
   12 FORMAT (2I5,F10.6)
   13 FORMAT (I5)
   15 FORMAT ( I5)
   20 FORMAT (1H0,10X,*PE=*,F20.4,5X,*RE=*,F20.4/)
   21 FORMAT (1H0,10X,*WT=*,F10.6/)
   22 FORMAT (1H0,10X,*EPST=*,F10.6/)
   23 FORMAT (1H0,10X,*JJ=*,I10/)
   24 FORMAT (1H0,10X,*M =*,I5,10X,*N =*,I5,10X,*A =*,F10.4/)
   32 FORMAT (1H0,11HTEMPERATURE/)
   33 FORMAT (1H0,17HLOCAL NUSSELT NO./)
   34 FORMAT (1H0,10X,*HNUA(AVERAGE NUSSELT NO.)=*,F15.5/)
 2010 FORMAT (1H ,F7.2,16F8.4)
 2020 FORMAT (1H ,10X,F20.6)
 2030 FORMAT (1H ,6X,8F16.4)
 2040 FORMAT (1H0,7X,16F8.2/)
 2050 FORMAT (1H ,7X,16F8.4)
 9999 STOP
      END
      SUBROUTINE TDMS(X,M,J,DUM12)
C
C          SOLN OF TRIDIAGONAL MATRIX BY GS ELIMINATION AND BW SUBSTN
C
      COMMON T(31,50),DUMA(31,50),DUMB(31,50),DUM34(31)
      DIMENSION X(1),H(61),P(61)
```

```
      H(1)=1.333
      P(1)=-T(3,J)/3.
      DO 700 K=2,M
      C=DUM34(K)-DUMB(K,J)
      D=T(K,J+1)*DUMA(K,J)+T(K,J-1)*(DUM12-DUMA(K,J))
      CH=1.-C*H(K-1)
      H(K)=DUMB(K,J)/CH
      P(K)=(D+C*P(K-1))/CH
  700 CONTINUE
      X(M+1)=(-T(M-1,J)/3.+1.333*P(M))/(1.-1.333*H(M))
      DO 720 K=2,M
      KK=M-(K-2)
      X(KK)=P(KK)+H(KK)*X(KK+1)
  720 CONTINUE
      X(1)=P(1)+H(1)*X(2)
      RETURN
      END
         6400 END OF RECORD

                                CD TOT    0300
```

APPENDIX A.3
****

```
      6400 END OF RECORD
C** SOLUTION OF THE NAVIER-STOKES EQNS AND ENERGY EQN FOR SOLID  SPHERE*******
C*****************************************************************************
C
C*** SEQUENCING WITH CONVERGENCE PROMOTION *******
C
C     PE,GR,RE        =PECLET,GRASHOF AND REYNOLDS NUMBER
C     M,N             =TOTAL NO. OF STEPS IN ANGULAR AND RADIAL DIRECTIONS
C     A,B             =STEP SIZES IN Z AND ANGULAR DIRECTIONS
C     NLOOPS          = MAX. NO. OF ITERATIONS ALLOWED IN ONE RUN
C     KKC             =COUNTER FOR APPLYING CONVERGENCE PROMOTION AND REVISING W
C     NSTART          =CONTROL STATEMENT FOR READING IN INTERMEDIATE
C                      DATA OR CALCULATING INITIAL GUESSES
C                      0-- INITIAL GUESSES
C                      1-- READ IN INTERMEDIATE DATA
C     I1,I2,J1        =SEQUENCEING CONTROL CARDS
C     FIELD FUNCTIONS
C     PSI             =STREAM FUNCTION
C     G               =DUMMY FUNCTION OF VORTICITY
C     T               =TEMPERATURE OR CONCENTRATION
C     RELAXATION FACTORS
C     WS              =FOR PSI
C     WV              =FOR G
C     WT              =FOR T
C
      PROGRAM TST (INPUT,OUTPUT,PUNCHB,TAPE5=INPUT,TAPE6=OUTPUT,TAPE7
     1=PUNCHB,TAPE1,TAPE8)
      DIMENSION Z(62),EZ1(62),EZ2(62),EZ3(62),EZ4(62),EZ5(62),EZ6(62)
      DIMENSION THETA(32),SI(32),CO(32),COT(32),ANGLE(32)
      DIMENSION CS(31),DUMSI(31),DUM3(31),DUM4(31)
      DIMENSION T(31,65),PSI(31,65),G(31,65)
      DIMENSION PEZSI(31,65),GREZ2(65)
      DIMENSION HNUL(32,1),P(32,1),SVORT(32,1)
      DIMENSION VR(100)
      DIMENSION WV(31,60),WT(31,60)
      READ (5,10) PE,GR,RE
      READ (5,12) M,N,A
      READ (5,13) KKC,EXRC
      READ (5,15) NLOOPS
      READ (5,16) NSTART
      WRITE (6,21)
      WRITE (6,20) PE,GR,RE
      WRITE (6,24) M,N,A
      WRITE (6,25) KKC,EXRC
      NM1=N-1
      MP1=M+1
      FMP1=FLOAT(MP1)
      FN=FLOAT(N)
      DMN=3.1416*3.1416*(1./FMP1/FMP1+1./FN/FN)
      WS=1./(1.+SQRT(DMN)/1.4142)
      A2=A*A
      B=3.1416/(FLOAT(M))
      B2=B*B
```

```
      DUM1=(1.-A*0.5)/A2
      DUM2=(1.+A*0.5)/A2
      DUM6=0.5*A2*B2/(A2+B2)
      DUMRE=RE*PE/(A2*B2*64.)
      DREAB=RE/32./A/B
      THETA(1)=0.0
      THETA(2)=B
      DO 100 I=2,M
      THETA(I+1)=THETA(I)+B
      ANGLE(I)=THETA(I)*180.0/3.1416
      CO(I)=COS(THETA(I))
      SI(I)=SIN(THETA(I))
      DUMSI(I)=SI(I)*SI(I)
      COT(I)=CO(I)/SI(I)
      CS(I)=CO(I)*SI(I)
      DUM3(I)=(1.-0.5*B*COT(I))/B2
  100 DUM4(I)=(1.+0.5*B*COT(I))/B2
      ANGLE(1)=0.0
      ANGLE(MP1)=180.
      DUMSI(1)=0.
      DUMSI(MP1)=0.
      SI(1)=0.0
      SI(MP1)=0.0
      CO(1)=1.0
      CO(MP1)=-1.0
      Z(1)=0.0
      DO 110 J=1,N
      Z(J+1)=Z(J)+A
      EZ1(J)=EXP(Z(J))
      EZ2(J)=EZ1(J)*EZ1(J)
      GREZ2(J)=GR*EZ2(J)/(8.0*RE)
      EZ3(J)=EZ2(J)*EZ1(J)
      EZ4(J)=EZ3(J)*EZ1(J)
      EZ5(J)=EZ4(J)*EZ1(J)
  110 EZ6(J)=EZ5(J)*EZ1(J)
      DO 120 I=2,M
      DO 120 J=2,NM1
      PEZSI(I,J)=PE/(EZ1(J)*SI(I)*A*B*8.)
  120 CONTINUE
      IF(NSTART.EQ.1) GO TO 1000
C     INITIAL GUESS OF TEMPERATURE PROFILE
      DO 200 I=1,MP1
      DO 200 J=2,NM1
      T(I,J)=0.0
  200 CONTINUE
C     INITIAL GUESS OF STREAM FUNCTION AND VORTICITY (STOKES FLOW)

      C1=-4.3086
      D1=-2.7935
      C2=-(120.+75.*C1)/29.
      C3=(153.+63.*C1)/29.
      C4=-(47.5+17.*C1)/29.
      D2=-69.*D1/27.
      D3=57.*D1/27.
      D4=-15.*D1/27.
      DO 300 I=2,M
      DO 300 J=1,NM1
```

```
      PSI(I,J)=SI(I)*SI(I)*(0.5*EZ2(J)+C1/EZ1(J)+C2/EZ2(J)+C3/EZ3(J)+C4
     1/EZ4(J)-CO(I)*(D1/EZ1(J)+D2/EZ2(J)+D3/EZ3(J)+D4/EZ4(J)))
      G(I,J)=SI(I)*SI(I)*((4.*C2/EZ4(J)+10.*C3/EZ5(J)+18.*C4/EZ6(J))
     1+CO(I)*(4.*D1/EZ3(J)-6.*D3/EZ5(J)-14.*D4/EZ6(J)))
  300 CONTINUE
      SETTING UP OF BOUNDARY CONDITIONS
C     DO 400 I=1,MP1
      PSI(I,1)=0.0
      G(I,N)=0.0
      T(I,N)=0.0
      T(I,1)=1.0
  400 PSI(I,N)=0.5*EZ2(N)*DUMSI(I)
      DO 410 J=1,N
      PSI(1,J)=0.0
      PSI(MP1,J)=0.0
      G(1,J)=0.0
  410 G(MP1,J)=0.0


      DO 721 I=2,M
      DO 721 J=2,NM1
      AP=2.*A*(PSI(I+1,J)-PSI(I-1,J))
      BP=2.*B*(PSI(I,J+1)-PSI(I,J-1))
      YI=PEZSI(I,J)*AP
      YJ=PEZSI(I,J)*BP
      YIJ=SQRT(0.5*(YI*YI+YJ*YJ))
      WT(I,J)=1./(1.+YIJ)
      XI=DREAB*BP/EZ1(J)/SI(I)
      XJ=DREAB*AP/EZ1(J)/SI(I)
      XIJ=SQRT(0.5*(XI*XI+XJ*XJ))
      WV(I,J)=1./(1.+XIJ)
  721 CONTINUE
      GO TO 1010
 1000 REWIND 8
      READ (8) ((PSI(I,J),I=1,MP1),J=1,N)
      READ (8) (( G (I,J),I=1,MP1),J=1,N)
      READ (8) (( T (I,J),I=1,MP1),J=1,N)
 1010 JJ=0
C---                                                    ---
      CT1=0.0
C ---                                                   ---
      I2=I1=0
       KK=0
       EXRA=1.0
C
 1100 CONTINUE
C ---                                                   ---
      JJ=JJ+1
       KK=KK+1
C ---                                                   ---
       IF(KK.NE.KKC) GO TO 309
       KK=0
       EXRA=EXRC
  309  CONTINUE
C ---                                                   ---
C
```

```
      DO 700 I=2,M
      G(I,1)=(8.0*PSI(I,2)-PSI(I,3))/(2.*A2)
  700 CONTINUE


      DO 710 J=2,NM1
      T(1,J)=(4.0*T(2,J)-T(3,J))/3.0
      T(MP1,J)=(4.0*T(M,J)-T(M-1,J))/3.0
  710 CONTINUE


  310 CONTINUE                                                  ---
C ---
      DO 500 I=2,M
C
      IF(I1.EQ.1) GOTO 312
      I1=J1=1
      GOTO 311
  312 CONTINUE
      I1=J1=0
  311 CONTINUE                                                  ---
C ---
C
      DO 500 J=2,NM1
C
      IF(J1.EQ.0) GOTO 322
      J1=0
      GOTO 321
  322 J1=1
      GOTO 500
  321 CONTINUE                                                  ---
C ---
      DMPSII=PSI(I+1,J)-PSI(I-1,J)
      DMPSIJ=PSI(I,J+1)-PSI(I,J-1)
      PEDMI=PEZSI(I,J)*DMPSII
      DUMA1=DUM2+PEDMI
      DUMA2=DUM1-PEDMI
       PEDMJ=PEZSI(I,J)*DMPSIJ
      DUMB1=DUM4(I)-PEDMJ
      DUMB2=DUM3(I)+PEDMJ
      DUMTI=(T(I+1,J)-T(I-1,J))/B
      DUMTJ=(T(I,J+1)-T(I,J-1))/A
      DUMA=G(I,J+1)/(EZ2(J+1)*DUMSI(I))
      DUMC=G(I,J-1)/(EZ2(J-1)*DUMSI(I))
      IF(I.EQ.2) GO TO 501
      DUMD=G(I-1,J)/(EZ2(J)*DUMSI(I-1))
      GO TO 502
  501 DUMD=G(2,J)/(EZ2(J)*SI(2)*B)
  502 IF(I.EQ.M) GO TO 503
      DUMB=G(I+1,J)/(EZ2(J)*DUMSI(I+1))
      GO TO 504
  503 DUMB=G(M,J)/(EZ2(J)*SI(M)*B)
  504 STRMF=DUM6*(PSI(I,J+1)*DUM1+PSI(I,J-1)*DUM2+PSI(I+1,J)*DUM3(I)
     1+PSI(I-1,J)*DUM4(I)-G(I,J)*EZ2(J))
```

```
      AS=STRMF-PSI(I,J)

     DPSI=DMPSIJ*(DUMB-DUMD)-DMPSII*(DUMA-DUMC)
     VORT=DUM6*(G(I,J+1)*DUM1+G(I,J-1)*DUM2+G(I+1,J)*DUM3(I)+G(I-1,J)*
    1 DUM4(I)-DUMRE*DPSI/PEZSI(I,J)+GREZ2(J)*(CS(I)*DUMTI+DUMSI(I)*
    2DUMTJ))
      AV=VORT-G(I,J)

     TEMP=(T(I,J+1)*DUMA1+T(I,J-1)*DUMA2+T(I+1,J)*DUMB1+T(I-1,J)*DUMB2)
    1*DUM6
      AT=TEMP-T(I,J)

     IF(I2.EQ.1) GOTO 341


C
C
       PSI(I,J)=PSI(I,J)+EXRA*WS*AS
      G(I,J)=G(I,J)+EXRA*WV(I,J)*AV
      T(I,J)=T(I,J)+EXRA*WT(I,J)*AT
      GOTO 500
  341 CONTINUE
      PSI(I,J)=PSI(I,J)+AS
      G(I,J)=G(I,J)+AV
      T(I,J)=T(I,J)+AT
C
  500 CONTINUE                                          ---
C ---
      IF(I2.EQ.0) GOTO 332
      I1=I2=0
      GOTO 331
  332 I1=I2=1
      GOTO 310
  331 CONTINUE                                          ---
C ---
       EXRA=1.0
         IF((KK+1).EQ.KKC) GO TO 3000
 3333    CONTINUE
      IF(JJ.EQ.NLOOPS) GO TO 2000
      GO TO 1100
 3000    CONTINUE
      WRITE (6,66) J
   66 FORMAT (1H0,20X,*J=*,I10/)
      DO 720 I=2,M
      DO 720 J=2,NM1
      AP=2.*A*(PSI(I+1,J)-PSI(I-1,J))
      BP=2.*B*(PSI(I,J+1)-PSI(I,J-1))
      YI=PEZSI(I,J)*AP
      YJ=PEZSI(I,J)*BP
      YIJ=SQRT(0.5*(YI*YI+YJ*YJ))
      WT(I,J)=1./(1.+YIJ)
```

```
      XI=DREAB*BP/EZ1(J)/SI(I)
      XJ=DREAB*AP/EZ1(J)/SI(I)
      XIJ=SQRT(0.5*(XI*XI+XJ*XJ))
      WV(I,J)=1./(1.+XIJ)
  720 CONTINUE
      WRITE (6,2010) (EZ1(J),(WV(I,J),I=1,MP1,2),J=1,N,10)
      WRITE (6,2010) (EZ1(J),(WI(I,J),I=1,MP1,2),J=1,N,10)
C     CALN. FOR FRONTAL STAGNATION PRESS.
      DMGF=0.0
      DO 620 J=2,NM1
  620 DMGF=DMGF+(4.0*G(2,J)/SI(2)-G(3,J)/SI(3))/EZ1(J)
      FSPRES=1.0+(DMGF+0.5*((4.0*G(2,1)/SI(2)-G(3,1)/SI(3))/EZ1(1)
     1+(4.0*G(2,N)/SI(2)-G(3,N)/SI(3))/EZ1(N)))*4.0*A/(RE*B)
C     CALN. FOR SURFACE PRESS. DISTRIBUTION
      P(1,1)=FSPRES
      DO 630 K=2,M
      DUMG=0.0
      DO 631 I=2,K
  631 DUMG=DUMG+(4.0*G(I,2)/EZ1(2)-G(I,3)/EZ1(3)-3.0*G(I,1))
     1/(2.0*A*SI(I))+G(I,1)/SI(I)
  630 P(K,1)=P(1,1)+4.0/RE*B*(DUMG-0.5*((4.0*G(K,2)/EZ1(2)-G(K,3)/EZ1(3)
     1-3.0*G(K,1))/(2.0*A*SI(K))+G(K,1)/SI(K)))
      P(MP1,1)=P(M,1)+4.0/RE*B*(0.5*((4.0*G(M,2)/EZ1(2)-G(M,3)/EZ1(3)
     1-3.0*G(M,1))/(2.0*A*SI(M))+G(M,1)/SI(M)))
C     CALN. FOR FORM DRAG COEFF.
      DUMP=0.0
      DO 640 I=2,M
  640 DUMP=DUMP+P(I,1)*SI(I)*CO(I)*2.0
      CDP=DUMP*B
      WRITE (6,35) CDP
C     CALN. FOR SURFACE VORTICITY
      SVORT(1,1)=0.0
      SVORT(MP1,1)=0.0
      DO 660 I=2,M
  660 SVORT(I,1)=G(I,1)/SI(I)
C     CALN. FOR FRICTION DRAG COEFF.
      DUMPSI=0.0
      DO 650 I=2,M
  650 DUMPSI=DUMPSI+G(I,1)*SI(I)
      CDF=8.0*DUMPSI*B/RE
      WRITE (6,37) CDF
C     CALN. FOR TOTAL DRAG COEFF.
      CTOTAL=CDF+CDP
      IF(ABS(CTOTAL).GT.10000.) GO TO 9999
      WRITE (6,38) CTOTAL
C     CALN. FOR LOCAL NUSSELT NUMBER
      DO 600 I=1,MP1
  600 HNUL(I,1)=(4.0*T(I,2)-T(I,3)-3.0*T(I,1))/(A*EZ1(1))*(-1.0)
      WRITE (6,33)
      WRITE (6,2050) (HNUL(I,1),I=1,MP1)
C     CALN. FOR AVERAGE NUSSELT NO.
      DHNUL=0.0
      DO 610 I=2,M
  610 DHNUL=DHNUL+HNUL(I,1)*SI(I)/2.0
      HNUA=DHNUL*B
      WRITE (6,34)
```

```
      WRITE (6,2020) HNUA
      CTE=ABS((CTOTAL-CT1)/CTOTAL)
      IF(CTE.LT.0.0001) GO TO 2000
      CT1=CTOTAL
      GO TO 3333

 2000 REWIND 8
      WRITE (8) ((PSI(I,J),I=1,MP1),J=1,N)
      WRITE (8) (( G (I,J),I=1,MP1),J=1,N)
      WRITE (8) (( T (I,J),I=1,MP1),J=1,N)
      END FILE 8
      WRITE (7) ((PSI(I,J),I=1,MP1),J=1,N)
      WRITE (7) ((G  (I,J),I=1,MP1),J=1,N)
      WRITE (7) ((T  (I,J),I=1,MP1),J=1,N)
 2100 WRITE (6,22) JJ
      WRITE (6,30)
      WRITE (6,2040) (ANGLE(I),I=1,16)
      WRITE (6,2010) (EZ1(J),(PSI(I,J),I=1,16),J=1,N)
      WRITE (6,2040) (ANGLE(I),I=17,31)
      WRITE (6,2011) (EZ1(J),(PSI(I,J),I=17,31),J=1,N)
      WRITE (6,31)
      WRITE (6,2040) (ANGLE(I),I=1,16)
      WRITE (6,2010) (EZ1(J),( G (I,J),I=1,16),J=1,N)
      WRITE (6,2040) (ANGLE(I),I=17,31)
      WRITE (6,2011) (EZ1(J),( G (I,J),I=17,31),J=1,N)
      WRITE (6,32)
      WRITE (6,2040) (ANGLE(I),I=1,16)
      WRITE (6,2010) (EZ1(J),( T (I,J),I=1,16),J=1,N)
      WRITE (6,2040) (ANGLE(I),I=17,31)
      WRITE (6,2011) (EZ1(J),( T (I,J),I=17,31),J=1,N)
      WRITE (6,2010) (EZ1(J),(WV(I,J),I=1,MP1,2),J=1,N)
      WRITE (6,2010) (EZ1(J),(WT(I,J),I=1,MP1,2),J=1,N)
 2011 FORMAT (1H ,F7.2,15F8.4)
      WRITE (6,36)
      WRITE (6,2030) (P(I,1),I=1,MP1)
      WRITE (6,39)
      WRITE (6,2050) (SVORT(I,1),I=1,MP1)

      WRITE (6,5000) (Z(J),(PSI(I,J),I=1,10),J=1,N)
      WRITE (6,5000) (Z(J),(PSI(I,J),I=11,20),J=1,N)
      WRITE (6,5000) (Z(J),(PSI(I,J),I=21,30),J=1,N)
      WRITE (6,5000) (Z(J),(G(I,J),I=1 ,10),J=1,N)
      WRITE (6,5000) (Z(J),(G(I,J),I=11,20),J=1,N)
      WRITE (6,5000) (Z(J),(G(I,J),I=21,30),J=1,N)
 5000 FORMAT(1H ,F7.2,10E12.3)
      DO 555 J=1,N
      VR(J)=(8.*PSI(M,J)-PSI(M-1,J))/(2.*B2*EZ2(J))
  555 CONTINUE
      WRITE (6,55)
   55 FORMAT (1H0,15HRADIAL VELOCITY/)
      WRITE (6,2070) (EZ1(J),VR(J),J=1,N)
 2070 FORMAT (1H ,20X,F10.4,F20.6)

   10 FORMAT (3F10.6)
   12 FORMAT (2I5,F10.6)
   13 FORMAT (I10,F10.6)
```

```
15 FORMAT (I5)
16 FORMAT (I5)
21 FORMAT (1H0,10X,*NEW SEQUENCE WITH CONVERGENCE PROMOTION*/)
20 FORMAT(1H0,10X,*PE=*,F10.4,5X,*GR=*,F10.4,5X,*RE=*,F10.4/)
22 FORMAT (1H0,10X,*JJ=*,I10/)
23 FORMAT (1H0,10X,*WS=*,F10.4,5X,*WV=*,F10.4,5X,*WT=*,F10.4/)
24 FORMAT (1H0,10X,*M =*,I5,10X,*N =*,I5,10X,*A =*,F10.4/)
25 FORMAT (1H0,10X,*KKC=*,I10,10X,*EXRC=*,F10.4/)
30 FORMAT (1H0,15HSTREAM FUNCTION/)
31 FORMAT (1H0,27HDUMMY FUNCTION OF VORTICITY/)
32 FORMAT (1H0,11HTEMPERATURE/)
33 FORMAT (1H0,17HLOCAL NUSSELT NO./)
34 FORMAT (1H0,19HAVERAGE NUSSELT NO./)
38 FORMAT (1H0,10X,*CTOTAL=*,F17.6/)
37 FORMAT (1H0,10X,*CDF=*,F20.6/)
35 FORMAT (1H0,10X,*CDP=*,F20.6/)
36 FORMAT (1H0,27HSURFACE PRESS. DISTRIBUTION/)
39 FORMAT (1H0,30HSURFACE VORTICITY DISTRIBUTION/)
2010 FORMAT (1H ,F7.2,16F8.4)
2020 FORMAT (1H ,10X,F20.6)
2030 FORMAT (1H ,6X,8F16.6)
2040 FORMAT (1H0,6X,16F8.2/)
2050 FORMAT (1H ,6X,16F8.4)
9999 STOP
     END
        6400 END OF RECORD

                              CD TOT    0421
```

Appendix B. Supplementary Data

APPENDIX B.1
****

SINGLE SPHERE IN AN UNBOUNDED FLUID

SURFACE PRESSURE DISTRIBUTION

ANGLE	RE				
	0.2	0.5	0.75	1.0	2.0
0	33.15	14.36	10.15	7.987	4.738
12	32.41	14.01	9.885	7.771	4.591
24	30.22	12.99	9.123	7.144	4.168
36	26.72	11.36	7.922	6.159	3.513
48	22.11	9.245	6.372	4.898	2.662
60	16.62	6.771	4.582	3.455	1.781
72	10.53	4.089	2.671	1.934	0.858
84	4.156	1.348	0.753	0.431	-0.010
96	-2.222	-1.316	-1.072	-0.975	-0.772
108	-8.321	-3.788	-2.725	-2.222	-1.396
120	-13.89	-5.978	-4.153	-3.273	-1.873
132	-18.73	-7.821	-5.323	-4.112	-2.211
144	-22.66	-9.278	-6.224	-4.742	-2.431
156	-25.26	-10.33	-6.858	-5.175	-2.561
168	-27.33	-10.96	-7.233	-5.426	-2.626
180	-27.93	-11.17	-7.357	-5.507	-2.645

SURFACE VORTICITY DISTRIBUTION

ANGLE	RE				
	0.2	0.5	0.75	1.0	2.0
0	0.0	0.0	0.0	0.0	0.0
12	0.344	0.380	0.406	0.430	0.519
24	0.670	0.736	0.786	0.830	0.966
36	0.962	1.051	1.118	1.177	1.401
48	1.207	1.309	1.385	1.452	1.706
60	1.394	1.498	1.575	1.642	1.899
72	1.517	1.612	1.682	1.742	1.976
84	1.571	1.649	1.705	1.754	1.943
96	1.555	1.612	1.651	1.684	1.816
108	1.472	1.507	1.528	1.545	1.618
120	1.329	1.342	1.348	1.351	1.371
132	1.131	1.136	1.124	1.117	1.099
144	0.889	0.879	0.867	0.856	0.818
156	0.613	0.601	0.589	0.578	0.539
168	0.313	0.306	0.298	0.291	0.267
180	0.0	0.0	0.0	0.0	0.0

SURFACE PRESSURE DISTRIBUTION

ANGLE	RE					
	3.0	5.0	10	20	30	40

0	3.582	2.639	1.890	1.492	1.334	1.257
12	3.457	2.535	1.799	1.396	1.248	1.171
24	3.100	2.237	1.544	1.156	1.030	0.930
36	2.552	1.786	1.164	0.802	0.663	0.582
48	1.873	1.238	0.715	0.399	0.271	0.194
60	1.133	0.657	0.258	0.008	-0.099	-0.166
72	0.400	0.103	-0.150	-0.318	-0.392	-0.441
84	-0.267	-0.375	-0.472	-0.543	-0.578	-0.602
96	-0.826	-0.747	-0.687	-0.661	-0.654	-0.651
108	-1.258	-1.003	-0.799	-0.686	-0.642	-0.616
120	-1.560	-1.151	-0.825	-0.645	-0.575	-0.536
132	-1.748	-1.211	-0.792	-0.570	-0.487	-0.443
144	-1.847	-1.212	-0.727	-0.485	-0.400	-0.358
156	-1.888	-1.184	-0.658	-0.409	-0.328	-0.290
168	-1.899	-1.154	-0.606	-0.356	-0.279	-0.245
180	-1.900	-1.142	-0.586	-0.337	-0.261	-0.228

SURFACE VORTICITY DISTRIBUTION

ANGLE	RE					
	3.0	5.0	10	20	30	40
0	0.0	0.0	0.0	0.0	0.0	0.0
12	0.591	0.719	0.984	1.401	1.734	2.028
24	1.130	1.369	1.862	2.639	3.259	3.805
36	1.580	1.900	2.559	3.594	4.419	5.145
48	1.912	2.274	3.017	4.176	5.096	5.907
60	2.107	2.470	3.210	4.347	5.247	6.030
72	2.165	2.491	3.145	4.129	4.895	5.552
84	2.096	2.354	2.863	3.596	4.149	4.608
96	1.923	2.097	2.429	2.870	3.178	3.414
108	1.676	1.674	1.919	2.084	2.170	2.209
120	1.386	1.399	1.406	1.357	1.283	1.189
132	1.083	1.042	0.948	0.768	0.609	0.455
144	0.785	0.720	0.581	0.354	0.173	0.012
156	0.506	0.443	0.312	0.112	-0.042	-0.178
168	0.247	0.208	0.130	0.012	-0.078	-0.158
180	0.0	0.0	0.0	0.0	0.0	0.0

SURFACE PRESSURE DISTRIBUTION

ANGLE	RE			
	100	200	300	400
0	1.106	1.056	1.038	1.029
6	1.084	1.033	1.014	1.004
12	1.021	0.965	0.943	0.930
18	0.919	0.856	0.829	0.812
24	0.784	0.711	0.680	0.657
30	0.624	0.540	0.503	0.474
36	0.445	0.351	0.308	0.273
42	0.259	0.154	0.107	0.068
48	0.075	-0.040	-0.089	-0.131

54	-0.101	-0.219	-0.268	-0.311
60	-0.256	-0.375	-0.421	-0.460
66	-0.384	-0.450	-0.537	-0.571
72	-0.481	-0.587	-0.612	-0.637
78	-0.545	-0.635	-0.645	-0.657
84	-0.576	-0.645	-0.639	-0.637
90	-0.577	-0.634	-0.601	-0.587
96	-0.554	-0.580	-0.543	-0.520
102	-0.515	-0.523	-0.478	-0.453
108	-0.466	-0.464	-0.418	-0.395
114	-0.414	-0.409	-0.368	-0.351
120	-0.364	-0.363	-0.331	-0.320
126	-0.320	-0.328	-0.304	-0.300
132	-0.282	-0.303	-0.289	-0.292
138	-0.251	-0.286	-0.283	-0.293
144	-0.225	-0.275	-0.282	-0.297
150	-0.203	-0.265	-0.276	-0.295
156	-0.182	-0.250	-0.261	-0.278
162	-0.161	-0.228	-0.232	-0.245
168	-0.145	-0.203	-0.198	-0.202
174	-0.133	-0.183	-0.169	-0.166
180	-0.128	-0.175	-0.158	-0.152

SURFACE VORTICITY DISTRIBUTION

ANGLE	RE 100.	200.	300.	400.
0	0	0	0	0
3	0.819	1.191	1.488	1.771
6	1.630	2.369	2.959	3.521
9	2.427	3.528	4.406	5.242
12	3.207	4.659	5.818	6.920
15	3.962	5.754	7.182	8.541
18	4.687	6.804	8.489	10.09
21	5.377	7.800	9.727	11.56
27	6.630	9.603	11.95	14.19
30	7.183	10.39	12.93	15.34
33	7.683	11.10	13.80	16.36
36	8.123	11.72	14.55	17.24
42	8.816	12.67	15.69	18.57
45	9.063	13.00	16.06	18.98
48	9.241	13.21	16.30	19.24
51	9.347	13.32	16.39	19.32
54	9.383	13.32	16.34	19.22
57	9.347	13.20	16.14	18.95
60	9.242	12.98	15.80	18.51
63	9.067	12.64	15.31	17.88
66	8.827	12.20	14.69	17.09
69	8.524	11.66	13.93	16.17
72	8.163	11.03	13.05	15.02
75	7.749	10.31	12.07	13.78
78	7.289	9.513	10.98	12.42
81	6.790	8.684	9.833	10.98
84	6.240	7.795	8.620	9.482

87	5.708	6.880	7.405	7.966
90	5.143	5.958	6.188	6.475
93	4.574	5.049	5.011	5.050
96	4.010	4.171	3.901	3.733
99	3.461	3.343	2.885	2.557
102	2.934	2.578	1.984	1.547
105	2.435	1.980	1.211	0.717
108	1.972	1.285	0.571	0.065
111	1.549	0.768	0.062	-0.419
114	1.167	0.338	-0.326	-0.756
117	0.839	-0.009	-0.606	-0.973
120	0.534	-0.279	-0.793	-1.089
123	0.281	-0.481	-0.897	-1.113
126	0.067	-0.622	-0.926	-1.041
129	-0.111	-0.711	-0.892	-0.891
132	-0.257	-0.763	-0.829	-0.731
135	-0.377	-0.795	-0.788	-0.661
138	-0.474	-0.830	-0.826	-0.758
141	-0.554	-0.888	-0.977	-1.041
144	-0.619	-0.983	-1.241	-1.489
147	-0.672	-1.116	-1.593	-2.680
153	-0.736	-1.444	-2.381	-3.300
156	-0.744	-1.588	-2.709	-3.807
159	-0.732	-1.681	-2.922	-4.136
162	-0.696	-1.701	-2.982	-4.233
165	-0.635	-1.629	-2.864	-4.070
168	-0.548	-1.459	-2.566	-3.644
171	-0.437	-1.195	-2.098	-2.977
174	-0.305	-0.851	-1.490	-2.112
177	-0.158	-0.446	-0.779	-1.103
180	0	0	0	0

SINGLE CYLINDER IN AN UNBOUNDED FLUID

SURFACE PRESSURE DISTRIBUTION

ANGLE	RE			
	23	40	85	175
0	1.244	1.148	1.076	1.039
12	1.133	1.034	0.949	0.903
24	0.826	0.719	0.602	0.531
36	0.387	0.276	0.123	0.017
48	-0.094	-0.195	-0.367	-0.506
60	-0.527	-0.596	-0.754	-0.905
72	-0.847	-0.860	-0.964	-1.093
84	-1.026	-0.972	-1.004	-1.078
96	-1.077	-0.960	-0.929	-0.957
108	-1.038	-0.880	-0.818	-0.836
120	-0.952	-0.780	-0.725	-0.761
132	-0.856	-0.696	-0.663	-0.724
144	-0.765	-0.631	-0.626	-0.705
156	-0.698	-0.581	-0.601	-0.692
168	-0.636	-0.545	-0.582	-0.683

180	-0.617	-0.531	-0.575	-0.680

SURFACE VORTICITY DISTRIBUTION

ANGLE	RE			
	23	40	85	175
0	0.0	0.0	0.0	0.0
12	1.587	2.191	3.470	5.364
24	2.961	4.073	6.417	9.936
36	3.942	5.372	8.390	13.01
48	4.415	5.926	9.093	14.04
60	4.354	5.697	8.455	12.81
72	3.835	4.804	6.708	9.611
84	3.005	3.511	4.384	5.474
96	2.065	2.150	2.172	1.906
108	1.196	1.007	0.598	-0.095
120	0.514	0.227	-0.222	-0.729
132	0.055	-0.210	-0.505	-0.727
144	-0.197	-0.405	-0.549	-0.628
156	-0.267	-0.422	-0.492	-0.491
168	-0.182	-0.272	-0.306	-0.256
180	0.0	0.0	0.0	0.0

CD TNT 0254

SINGLE SPHERE IN AN UNBOUNDED FLUID

LOCAL NUSSELT NO RE=1.

ANGLE	PR 0.5	0.71	1.0	2.0	3.5	5.0
0	2.368	2.480	2.614	2.973	3.355	2.647
12	2.353	2.464	2.597	2.953	3.333	3.623
24	2.341	2.449	2.579	2.926	3.298	3.582
36	2.323	2.426	2.551	2.884	3.242	3.516
48	2.300	2.396	2.512	2.826	3.166	3.427
60	2.272	2.359	2.465	2.755	3.071	3.316
72	2.240	2.318	2.413	2.673	2.961	3.185
84	2.206	2.273	2.355	2.583	2.838	3.039
96	2.172	2.227	2.295	2.488	2.706	2.879
108	2.138	2.182	2.237	2.391	2.569	2.713
120	2.106	2.139	2.181	2.298	2.433	2.545
132	2.078	2.102	2.131	2.212	2.306	2.284
144	2.056	2.071	2.089	2.138	2.194	2.240
156	2.039	2.048	2.058	2.082	2.107	2.126
168	2.029	2.034	2.039	2.048	2.051	2.052
180	2.027	2.041	2.044	2.047	2.043	2.038

LOCAL NUSSELT NO RE=10.

ANGLE	PR 0.5	0.71	1.0	2.0	3.5	5.0
0	4.197	4.641	5.131	6.317	7.503	8.389
12	4.154	4.594	5.080	6.255	7.430	8.308
24	4.087	4.516	4.988	6.133	7.277	8.132
36	3.979	4.389	4.841	5.936	7.031	7.848
48	3.833	4.218	4.642	5.670	6.698	7.464
72	3.449	3.764	4.113	4.962	5.811	6.443
84	3.226	3.498	3.802	4.543	5.285	5.838
96	2.996	3.221	3.475	4.090	4.727	5.196
108	2.769	2.947	3.149	3.650	4.159	4.541
120	2.559	2.689	2.838	3.215	3.604	3.898
132	2.377	2.462	2.561	2.816	3.086	3.294
144	2.233	2.277	2.333	2.475	2.631	2.756
156	2.129	2.143	2.164	2.213	2.269	2.318
168	2.068	2.063	2.062	2.049	2.034	2.025
180	2.050	2.058	2.050	2.015	1.973	1.943

LOCAL NUSSELT NO RE=30.

ANGLE	PR 0.5	0.71	1.0	2.0	3.5	5.0

0	6.459	7.256	8.134	10.29	12.48	14.16
12	6.393	7.181	8.051	10.17	12.35	14.01
24	6.257	7.023	7.866	9.924	12.02	13.63
36	6.038	6.766	7.568	9.522	11.51	13.03
48	5.739	6.417	7.163	8.977	10.87	12.21
60	5.369	5.984	6.661	8.303	9.959	11.21
72	4.937	5.481	6.077	7.520	8.970	10.06
84	4.462	4.924	5.432	6.657	7.883	8.803
96	3.965	4.341	4.753	5.749	6.723	7.486
108	3.475	3.762	4.078	4.841	5.603	6.172
120	3.025	3.225	3.447	3.984	4.523	4.925
132	2.648	2.771	2.906	3.235	3.567	3.817
144	2.370	2.431	2.498	2.656	2.815	2.933
156	2.194	2.216	2.238	2.283	2.332	2.357
168	2.105	2.108	2.108	2.100	2.104	2.082
180	2.099	2.097	2.093	2.070	2.065	2.031

LOCAL NUSSELT NO RE=57

ANGLE	PR				
	0.5	0.71	1.0	2.0	5.0
0	8.602	9.746	11.02	14.19	20.27
12	8.512	9.644	10.90	14.04	20.02
24	8.308	9.403	10.62	13.64	19.39
36	7.979	9.016	10.16	13.01	18.38
48	7.530	8.488	9.546	12.16	17.04
60	6.969	7.832	8.780	11.11	15.40
72	6.314	7.064	7.886	9.896	13.54
84	5.585	6.211	6.895	8.558	11.53
96	4.818	5.313	5.853	7.158	9.458
108	4.061	4.425	4.820	5.772	7.434
120	3.373	3.611	3.868	4.485	5.556
132	2.817	2.945	3.081	3.396	3.929
144	2.446	2.499	2.550	2.649	2.786
156	2.265	2.292	2.314	2.356	2.534
162	2.230	2.297	2.293	2.350	2.708
168	2.217	2.248	2.282	2.384	2.924
174	2.216	2.252	2.290	2.410	3.095
180	2.234	2.273	2.316	2.458	3.177

LOCAL NUSSELT NO RE=100

ANGLE	PR			
	0.25	0.35	0.5	0.71
0	8.558	9.658	10.97	12.43
12	8.449	9.539	10.84	12.29
24	8.258	9.316	10.58	11.98
36	7.940	8.947	10.15	11.48
48	7.499	8.434	9.549	10.78
60	6.937	7.779	8.783	9.894

72	6.263	6.994	7.863	8.823
84	5.498	6.101	6.816	7.603
96	4.685	5.148	5.695	6.296
108	3.889	4.212	4.590	5.002
120	3.196	3.388	3.608	3.844
126	2.915	3.050	3.202	3.360
132	2.688	2.778	2.873	2.967
138	2.522	2.582	2.638	2.691
144	2.418	2.464	2.506	2.540
150	2.372	2.421	2.479	2.542
156	2.374	2.440	2.523	2.643
168	2.449	2.567	2.728	2.968
180	2.544	2.687	2.886	3.180

LOCAL NUSSELT NO RE=200

ANGLE PR

	0.25	0.35	0.5	0.71
0	11.75	13.33	15.24	17.38
12	11.61	13.18	15.07	17.18
24	11.32	12.85	14.68	16.72
36	10.85	12.29	14.03	15.96
48	10.19	11.52	13.12	14.90
60	9.333	10.53	11.95	13.53
72	8.289	9.309	10.52	11.86
84	7.076	7.891	8.857	9.920
96	5.761	6.352	7.047	7.806
108	4.485	4.853	5.278	5.735
120	3.431	3.608	3.801	3.994
126	3.044	3.154	3.266	3.373
132	2.773	2.849	2.932	3.027
138	2.635	2.724	2.850	3.038
144	2.650	2.808	3.059	3.435
150	2.829	3.113	3.548	4.154
156	3.147	3.585	4.222	5.037
168	3.878	4.588	5.525	6.599
180	4.253	5.062	6.098	7.249

LOCAL NUSSELT NO RE=300

ANGLE PR

	0.25	0.35	0.5	0.71
0	14.25	16.23	18.63	21.34
12	14.08	16.05	18.42	21.10
24	13.72	15.62	17.91	20.50
36	13.11	14.91	17.08	19.51
48	12.27	13.92	15.91	18.13
60	11.17	12.64	14.39	16.35
72	9.812	11.05	12.52	14.16
84	8.210	9.173	10.31	11.57
96	6.457	7.120	7.896	8.741

108	4.784	5.155	5.576	6.020
120	3.595	3.654	3.804	3.945
126	3.104	3.209	3.318	3.450
132	2.888	3.020	3.194	3.470
138	2.898	3.142	3.488	4.019
144	3.219	3.663	4.260	5.067
150	3.866	4.557	5.413	6.459
156	4.700	5.615	6.676	7.912
168	6.176	7.354	8.655	10.16
180	6.778	8.032	9.414	11.03

ASSEMBLAGE OF SPHERES

LOCAL NUSSELT NUMBER RE=100

ANGLE	POROSITY		
	0.417	0.644	0.834
0	23.81	18.37	15.92
12	23.66	18.23	15.79
24	23.20	17.86	15.43
36	22.47	17.24	14.85
48	21.46	16.39	14.05
60	20.21	15.33	13.04
72	18.75	14.07	11.84
84	17.12	12.66	10.49
96	15.36	11.13	9.028
108	13.51	9.564	7.539
120	11.63	8.023	6.124
132	9.731	6.554	4.877
144	7.840	5.155	3.834
156	5.977	3.776	2.936
168	4.194	3.776	2.135
180	3.200	1.565	1.759

SINGLE CYLINDER IN AN UNBOUNDED FLUID

LOCAL NUSSELT NUMBER PR=0.74

ANGLE	RE					
	2	10	23	40	85	175
0	1.351	2.917	4.509	5.883	8.937	12.79
12	1.344	2.895	4.472	5.831	8.849	12.67
24	1.324	2.831	4.362	5.674	8.588	12.31

36	1.292	2.725	4.181	5.415	8.153	11.69
48	1.249	2.582	3.932	5.057	7.549	10.81
60	1.197	2.408	3.622	4.608	6.782	9.647
72	1.137	2.208	3.262	4.083	5.873	8.197
84	1.074	1.990	2.865	3.504	4.864	6.518
96	1.010	1.767	2.452	2.905	3.824	4.770
108	0.947	1.550	2.047	2.326	2.852	3.215
120	0.889	1.353	1.680	1.820	2.096	2.290
132	0.839	1.189	1.387	1.449	1.772	2.496
144	0.798	1.066	1.192	1.256	1.964	3.387
156	0.768	0.985	1.096	1.217	2.442	4.176
168	0.749	0.940	1.062	1.251	2.872	4.586
180	0.744	0.926	1.056	1.272	3.039	4.695

CYLINDER IN A BUNDLE

LOCALL NUSSELT NUMBER RE=100

ANGLE	POROSITY		
	0.399	0.605	0.789
0	17.36	13.64	11.63
12	17.20	13.49	11.51
24	16.90	13.24	11.27
36	16.41	12.82	10.88
48	15.73	12.24	10.32
60	14.89	11.50	9.604
72	13.87	10.61	8.722
84	12.71	9.562	7.681
96	11.43	8.386	6.506
108	10.06	7.120	5.258
120	8.661	5.835	4.038
132	7.276	4.622	2.962
144	5.948	3.559	2.142
156	4.697	2.686	1.760
168	3.678	2.233	1.905
180	3.761	2.236	2.123

CD TNT 0272

APPENDIX B.3
****

SINGLE SPHERE IN AN INFINITE FLUID

LOCAL NUSSELT NUMBER RE=5 PR=0.71

ANGLE	GR 1	5	10	15
0	3.637	3.673	3.716	3.760
12	3.620	3.656	3.700	3.744
24	3.572	3.608	3.652	3.696
36	3.493	3.530	3.574	3.618
48	3.387	3.425	3.469	3.523
60	3.257	3.295	3.339	3.382
72	3.107	3.145	3.188	3.231
84	2.945	2.981	3.022	3.062
96	2.776	2.809	2.847	2.884
108	2.609	2.636	2.668	2.670
120	2.452	2.470	2.495	2.519
132	2.311	2.320	2.335	2.351
144	2.195	2.193	2.198	2.204
156	2.109	2.097	2.092	2.089
168	2.055	2.037	2.025	2.016
180	2.036	2.016	2.002	1.991

SURFACE PRESSURE DISTRIBUTION RE=5 PR=0.71

ANGLE	GR 1	5	10	15
0	2.656	2.704	2.760	2.818
12	2.549	2.590	2.635	2.683
24	2.244	2.262	2.278	2.296
36	1.783	1.762	1.731	1.700
48	1.221	1.149	0.056	0.961
60	0.624	0.491	0.323	0.151
72	0.054	-0.148	-0.399	-0.656
84	-0.440	-0.715	-1.053	-1.397
96	-0.828	-1.175	-1.599	-2.031
108	-1.098	-1.514	-2.019	-2.532
120	-1.259	-1.737	-2.315	-2.900
132	-1.331	-1.861	-2.501	-3.148
144	-1.343	-1.915	-2.604	-3.298
156	-1.323	-1.925	-2.650	-3.380
168	-1.298	-1.920	-2.666	-3.416
180	-1.288	-1.915	-2.669	-3.426

SURFACE VORTICITY DISTRIBUTION RE=5 PR=0.71

ANGLE	GR

	1	5	10	15
0	0.	0.	0.	0.
12	0.731	0.769	0.815	0.862
24	1.391	1.468	1.559	1.652
36	1.932	2.046	2.179	2.315
48	2.313	2.461	2.633	2.808
60	2.514	2.693	2.899	3.108
72	2.537	2.740	2.973	3.207
84	2.402	2.621	2.872	3.122
96	2.145	2.370	2.628	2.883
108	1.810	2.031	2.283	2.531
120	1.442	1.647	1.881	2.110
132	1.079	1.258	1.463	1.661
144	0.750	0.893	1.057	1.215
156	0.464	0.564	0.679	0.789
168	0.219	0.271	0.330	0.367
180	0.	0.	0.	0.

LOCAL NUSSELT NUMBER RE=5 PR=0.71

ANGLE	GR			
	-1	-5	-10	-15
0	0.618	3.573	3.504	3.415
12	3.602	3.556	3.487	3.398
24	3.553	3.507	3.437	3.348
36	3.474	3.428	3.357	3.267
48	3.367	3.321	3.250	3.160
60	3.237	3.190	3.120	3.031
72	3.088	3.042	2.973	2.887
84	2.926	2.883	2.818	2.738
96	2.760	2.719	2.662	2.592
108	2.595	2.561	2.514	2.458
120	2.441	2.415	2.382	2.345
132	2.305	2.290	2.273	2.257
144	2.193	2.189	2.189	2.194
156	2.111	2.116	2.130	2.154
168	2.061	2.072	2.097	2.132
180	2.044	2.058	2.086	2.126

SURFACE PRESSURE DISTRIBUTION RE=5 PR=0.71

ANGLE	GR			
	-1	-5	-10	-15
0	2.632	2.574	2.487	2.378
12	2.529	2.480	2.405	2.308
24	2.236	2.213	2.717	2.113
36	1.793	1.811	1.824	1.826
48	1.257	1.329	1.414	1.496

60	0.691	0.828	0.999	1.174
72	0.155	0.364	0.629	0.907
84	-0.303	-0.019	0.344	0.726
96	-0.655	-0.297	0.163	0.648
108	-0.891	-0.423	0.088	0.669
120	-1.020	-0.529	0.104	0.773
132	-1.065	-0.518	0.186	0.931
144	-1.053	-0.462	0.301	1.110
156	-1.016	-0.392	0.416	1.274
168	-0.987	-0.337	0.499	1.388
180	-0.967	-0.315	0.530	1.429

SURFACE VORTICITY DISTRIBUTION RE=5 PR=0.71

ANGLE	GR			
	1	-5	-10	-15
0	0.	0.	0.	0.
12	0.712	0.668	0.606	0.533
24	1.354	1.268	1.146	1.002
36	1.877	1.750	1.571	1.362
48	2.241	2.077	1.847	1.578
60	2.427	2.232	1.958	1.639
72	2.438	2.217	1.910	1.554
84	2.294	2.057	1.730	1.351
96	2.033	1.799	1.456	1.072
108	1.699	1.462	1.136	0.763
120	1.338	1.117	0.815	0.470
132	0.988	0.795	0.531	0.230
144	0.676	0.520	0.308	0.066
156	0.412	0.303	0.154	-0.016
168	0.192	0.136	0.059	-0.029
180	0.	0.	0.	0.

LOCAL NUSSELT NUMBER RE=10 PR=0.71

ANGLE	GR				
	5	10	25	50	100
0	2.628	4.640	4.679	4.740	4.842
12	4.601	4.614	4.654	4.714	4.877
24	4.524	4.536	4.577	4.639	4.744
36	4.397	4.411	4.453	4.518	4.625
48	4.226	4.240	4.286	4.352	4.463
60	4.016	4.031	4.078	4.148	4.263
72	3.774	3.789	3.839	3.910	4.028
84	3.508	3.524	3.575	3.647	3.766
86	3.231	3.247	3.296	3.367	3.482
108	2.955	2.970	3.015	3.080	3.187
120	2.695	2.707	2.744	2.798	2.888
132	2.464	2.472	2.497	2.534	2.599
144	2.276	2.278	2.287	2.304	2.335

15	2.137	2.135	2.127	2.122	2.119
168	2.053	2.047	2.027	2.006	1.976
180	2.025	2.017	1.993	1.966	1.925

SURFACE PRESSURE DISTRIBUTION RE=10 PR=0.71

ANGLE	GR				
	5	10	25	50	100
0	1.899	1.904	1.922	1.948	1.992
12	1.806	1.809	1.820	1.836	1.861
24	1.544	1.541	1.533	1.519	1.487
36	1.152	1.139	1.102	1.039	0.914
48	0.688	0.663	0.585	0.457	0.209
60	0.215	0.174	0.047	-0.158	-0.555
72	-0.210	-0.269	-0.450	-0.742	-1.306
84	-0.549	-0.626	-0.864	-1.245	-1.983
96	-0.780	-0.876	-1.168	-1.638	-2.547
108	-0.907	-1.019	-1.363	-1.914	-2.982
120	-0.946	-1.074	-1.461	-2.083	-3.291
132	-0.924	-1.064	-1.487	-2.168	-3.491
144	-0.869	-1.019	-1.471	-2.197	-3.608
156	-0.807	-0.965	-1.437	-2.196	-3.669
168	-0.760	-0.923	-1.407	-2.187	-3.695
180	-0.743	-0.907	-1.395	-2.187	-3.702

SURFACE VORTICITY DISTRIBUTION RE=10 PR=0.71

ANGLE	GR				
	5	10	25	50	100
0	0.	0.	0.	0.	0.
12	1.002	1.015	1.056	1.121	1.237
24	1.898	1.924	2.006	2.134	2.365
36	2.610	2.649	2.772	2.963	3.307
48	3.080	3.132	3.294	3.545	3.996
60	3.281	3.345	3.544	3.848	4.396
72	3.222	3.295	3.525	3.874	4.503
84	2.942	3.023	3.274	3.655	4.342
96	2.508	2.593	2.853	3.248	3.962
108	1.995	2.079	2.336	2.725	3.429
120	1.476	1.556	1.795	2.157	2.815
132	1.010	1.081	1.289	1.606	2.180
144	0.631	0.689	0.856	1.110	1.569
156	0.349	0.389	0.507	0.686	1.006
168	0.149	0.171	0.232	0.324	0.488
180	0.	0.	0.	0.	0.

LOCAL NUSSELT NUMBER RE=10 PR=0.71

ANGLE	GR

	-5	-10	-25	-50
0	4.598	4.582	4.525	4.410
12	4.572	4.555	4.498	4.382
24	4.493	4.476	4.418	4.299
36	4.366	4.348	4.288	4.165
48	4.193	4.175	4.113	3.984
60	3.982	3.962	3.898	3.764
72	3.738	3.718	3.651	3.513
84	3.472	3.452	3.385	3.246
96	3.195	3.176	3.111	2.978
108	3.923	2.905	2.847	2.731
120	2.668	2.654	2.609	2.522
132	2.447	2.438	2.410	2.364
144	2.270	2.267	2.260	2.261
156	2.142	2.146	2.159	2.205
168	2.067	2.074	2.103	2.180
180	2.042	2.051	2.085	2.173

SURFACE PRESSURE DISTRIBUTION RE=10 PR=0.71

	-5	-10	-25	-50
ANGLE		GR		
0	1.886	1.879	1.854	1.804
12	1.797	1.792	1.774	1.737
24	1.547	1.549	1.552	1.552
36	1.176	1.188	1.226	1.286
48	0.740	0.766	0.848	0.988
60	0.300	0.343	0.479	0.711
72	-0.088	-0.027	0.164	0.499
84	-0.389	-0.308	-0.058	0.378
96	-0.584	-0.485	-0.179	0.357
108	-0.677	-0.561	-0.205	0.414
120	-0.687	-0.556	-0.156	0.537
132	-0.640	-0.497	-0.061	0.697
144	-0.565	-0.412	0.053	0.865
156	-0.488	-0.328	0.161	1.015
168	-0.432	-0.267	0.237	1.119
180	-0.411	-0.244	0.264	1.157

SURFACE VORTICITY DISTRIBUTION RE=10 PR=0.71

	-5	-10	-25	-50
ANGLE		GR		
0.	0.	0.	0.	0.
12	0.972	0.957	0.905	0.806
24	1.839	1.808	1.705	1.510
36	2.523	2.476	2.324	2.035
48	2.966	2.905	2.707	2.331
60	3.143	3.069	2.831	2.380
72	3.063	2.979	2.710	2.199

84	2.769	2.678	2.389	1.841
96	2.329	2.235	1.939	1.381
108	1.818	1.726	1.438	0.895
120	1.311	1.226	0.958	0.454
132	0.865	0.799	0.555	0.113
144	0.513	0.452	0.262	-0.097
156	0.265	0.222	0.087	-0.169
168	0.105	0.083	0.012	-0.121
180	0.	0.	0.	0.

LOCAL NUSSELT NUMBER RE=20

ANGLE	GR					
	10	25	50	99	179	293
0	6.083	6.097	6.116	6.135	6.193	6.281
12	6.042	6.056	6.075	6.096	6.153	6.242
24	5.920	5.935	5.955	5.978	6.037	6.128
36	5.723	5.739	5.760	5.787	5.847	5.943
48	5.455	5.472	5.495	5.527	5.591	5.692
60	5.123	5.142	5.168	5.206	5.273	5.380
72	4.738	4.759	4.787	4.832	4.903	5.016
84	4.315	4.338	4.367	4.418	4.494	4.611
96	3.871	3.895	3.926	3.982	4.061	4.178
108	3.429	3.453	3.484	3.541	3.619	3.732
120	3.016	3.037	3.065	3.118	3.189	3.290
132	2.656	2.673	2.694	2.735	2.789	2.868
144	2.375	2.383	2.392	2.412	2.440	2.486
156	2.180	2.178	2.174	2.169	2.164	2.172
168	2.068	2.058	2.043	2.176	1.985	1.961
180	2.033	2.020	2.001	1.966	1.923	1.886

SURFACE PRESSURE DISTRIBUTION RE=20

ANGLE	GR					
	10	25	50	99	179	293
0	1.483	1.485	1.486	1.489	1.489	1.511
12	1.396	1.396	1.397	1.395	1.396	1.399
24	1.153	1.149	1.143	1.130	1.110	1.080
36	0.797	0.785	0.768	0.737	0.693	0.600
48	0.386	0.365	0.333	0.277	0.178	0.024
60	-0.013	-0.046	-0.096	-0.185	-0.338	-0.576
72	-0.346	-0.394	-0.463	-0.590	-0.802	-1.133
84	-0.581	-0.642	-0.732	-0.890	-1.174	-1.599
96	-0.707	-0.781	-0.891	-1.099	-1.433	-1.948
108	-0.738	-0.824	-0.951	-1.196	-1.586	-2.179
120	-0.702	-0.797	-0.939	-1.216	-1.653	-2.310
132	-0.630	-0.732	-0.886	-1.187	-1.663	-2.369
144	-0.547	-0.654	-0.817	-1.138	-1.644	-2.385
156	-0.473	-0.584	-0.754	-1.088	-1.616	-2.381
168	-0.421	-0.535	-0.710	-1.053	-1.595	-2.374

180	-0.402	-0.518	-0.694	-1.040	-1.587	-2.370

SURFACE VORTICITY DISTRIBUTION RE=20

ANGLE	GR 10	25	50	99	179	293
0	0.0	0.0	0.0	0.0	0.0	0.0
12	1.407	1.421	1.441	1.468	1.530	1.626
24	2.652	2.680	2.721	2.777	2.899	3.091
36	3.615	3.659	3.720	3.809	3.990	4.277
48	4.207	4.266	4.348	4.475	4.712	5.091
60	4.389	4.463	4.564	4.733	5.022	5.485
72	4.180	4.266	4.385	4.595	4.929	5.461
84	3.655	3.750	3.883	4.127	4.497	5.074
96	2.932	3.031	3.170	3.437	3.827	4.419
108	2.144	2.241	2.379	2.651	3.043	3.615
120	1.411	1.501	1.630	1.888	2.260	2.780
132	0.814	0.892	1.006	1.235	1.565	2.006
144	0.390	0.453	0.546	0.734	1.004	1.348
156	0.137	0.182	0.250	0.384	0.578	0.815
168	0.026	0.050	0.085	0.157	0.259	0.381
180	0.0	0.0	0.0	0.0	0.0	0.0

LOCAL NUSSELT NUMBER RE=20

ANGLE	GR -10	-25	-50	-100	-200
0	6.065	6.050	6.024	5.956	5.779
12	6.023	6.007	5.981	5.913	5.733
24	5.900	5.884	5.857	5.786	5.599
36	5.701	5.684	5.655	5.580	5.382
48	5.575	5.413	5.381	5.301	5.086
60	5.272	5.077	5.043	4.956	4.722
72	4.909	4.688	4.651	4.558	4.302
84	4.500	4.261	4.221	4.122	3.848
96	3.838	3.815	3.774	3.672	3.391
108	3.398	3.375	3.334	3.236	2.971
120	2.988	2.968	2.933	2.848	2.642
132	2.637	2.623	2.598	2.542	2.443
144	2.367	2.361	2.312	2.336	2.377
156	2.184	2.187	2.196	2.224	2.402
168	2.082	2.094	2.116	2.178	2.454
180	2.050	2.095	2.093	2.167	2.478

SURFACE PRESSURE DISTRIBUTION RE=20

ANGLE	GR -10	-25	-50	-100	-200

0	1.480	1.478	1.474	1.463	1.434
12	1.395	1.394	1.393	1.388	1.373
24	1.158	1.162	1.168	1.181	1.206
36	0.811	0.823	0.842	0.883	0.972
48	0.415	0.436	0.472	0.551	0.725
60	0.032	0.065	0.121	0.244	0.517
72	-0.285	-0.238	-0.161	0.011	0.388
84	-0.501	-0.441	-0.342	-0.134	0.354
96	-0.610	-0.539	-0.419	-0.158	0.407
108	-0.627	-0.545	-0.408	-0.112	0.522
120	-0.580	-0.490	-0.339	-0.015	0.670
132	-0.499	-0.402	-0.240	0.105	0.828
144	-0.409	-0.308	-0.137	0.226	0.983
156	-0.330	-0.224	-0.046	0.331	1.119
168	-0.275	-0.166	0.016	0.434	1.216
180	-0.255	-0.146	0.039	0.431	1.251

SURFACE PRESSURE DISTRIBUTION RE=20

ANGLE	GR				
	-10	-25	-50	-100	-200
0	0.0	0.0	0.0	0.0	0.0
12	1.389	1.374	1.349	1.287	1.137
24	2.614	2.584	2.534	2.410	2.111
36	3.558	3.512	3.436	3.252	2.803
48	4.129	4.069	3.968	3.725	3.132
60	4.292	4.218	4.093	3.797	3.074
72	4.065	3.980	3.836	3.497	2.675
84	3.528	3.436	3.279	2.914	2.037
96	2.801	2.706	2.545	2.174	1.297
108	2.017	1.926	1.769	1.416	0.588
120	1.296	1.212	1.069	0.746	0.505
132	0.726	0.634	0.517	0.239	-0.401
144	0.311	0.252	0.149	-0.078	-0.602
156	0.081	0.039	-0.036	-0.201	-0.582
168	-0.004	-0.027	-0.067	-0.155	-0.359
180	0.0	0.0	0.0	0.0	0.0

LOCAL NUSSELT NUMBER RE=30 PR=0.71

ANGLE	GR				
	25	50	100	200	300
0	7.247	7.257	7.278	7.317	7.350
12	7.193	7.203	7.224	7.264	7.298
24	7.035	7.046	7.068	7.110	7.146
36	6.780	6.791	6.815	6.860	6.899
48	6.432	6.445	6.471	6.521	6.564
60	6.001	6.016	6.045	6.100	6.148
72	5.499	5.516	5.548	5.609	5.663

84	4.945	4.964	4.999	5.066	5.126
96	4.363	4.383	4.421	4.493	4.558
108	3.784	3.805	3.844	3.918	3.984
120	3.246	3.266	3.302	3.372	3.434
132	2.786	2.802	2.831	2.886	2.937
144	2.436	2.445	2.459	2.489	2.518
156	2.209	2.207	2.202	2.199	2.198
168	2.089	2.079	2.057	2.025	1.998
180	2.053	2.040	2.011	1.967	1.930

SURFACE PRESSURE DISTRIBUTION RE=30 PR=0.71

ANGLE	GR 25	50	100	200	300
0	1.335	1.335	1.337	1.340	1.343
6	1.313	1.313	1.314	1.316	1.318
12	1.248	1.248	1.247	1.246	1.245
18	1.144	1.142	1.139	1.134	1.128
24	1.006	1.002	0.996	0.983	0.977
30	0.840	0.834	0.823	0.802	0.781
36	0.654	0.645	0.629	0.597	0.566
42	0.456	0.445	0.422	0.378	0.335
48	0.255	0.240	0.211	0.152	0.097
54	0.059	0.041	0.003	-0.069	-0.139
60	-0.123	-0.146	-0.191	-0.281	-0.367
66	-0.286	-0.313	-0.367	-0.474	-0.577
72	-0.425	-0.457	-0.520	-0.645	-0.765
78	-0.537	-0.574	-0.646	-0.788	-0.926
84	-0.621	-0.662	-0.743	-0.903	-1.058
90	-0.676	-0.721	-0.811	-0.988	-1.161
96	-0.705	-0.755	-0.852	-1.046	-1.235
102	-0.712	-0.765	-0.871	-1.079	-1.238
108	-0.700	-0.755	-0.869	-1.091	-1.310
114	-0.674	-0.734	-0.852	-1.087	-1.318
120	-0.639	-0.701	-0.825	-1.070	-1.312
126	-0.598	-0.663	-0.791	-1.045	-1.296
132	-0.554	-0.621	-0.753	-1.015	-1.275
138	-0.511	-0.580	-0.715	-0.984	-1.251
144	-0.470	-0.540	-0.689	-0.953	-1.226
150	-0.432	-0.504	-0.645	-0.925	-1.203
156	-0.400	-0.472	-0.616	-0.900	-1.183
162	-0.373	-0.446	-0.592	-0.880	-1.166
168	-0.352	-0.427	-0.574	-0.865	-1.154
174	-0.339	-0.415	-0.563	-0.856	-1.146
180	-0.335	-0.410	-0.559	-0.853	-1.144

SURFACE VORTICITY DISTRIBUTION RE=30 PR=0.71

ANGLE	GR 25	50	100	200	300

0	0.	0.	0.	0.	0.
6	0.891	0.896	0.907	0.928	0.947
12	1.746	1.757	1.779	1.821	1.859
18	2.551	2.567	2.600	2.662	2.720
24	3.283	3.305	3.349	3.434	3.510
30	3.924	3.951	4.006	4.113	4.210
36	4.456	4.489	4.556	4.685	4.802
42	4.868	4.907	4.985	5.137	5.274
48	5.149	5.194	5.284	5.458	5.617
54	5.296	5.347	5.448	5.645	5.825
60	5.310	5.368	5.480	5.698	5.899
66	5.198	5.261	5.383	5.622	5.843
72	4.969	5.037	5.169	5.427	5.666
78	4.640	4.713	4.853	5.127	5.383
84	4.221	4.308	4.454	4.741	5.010
90	3.764	3.843	3.994	4.289	4.569
96	3.262	3.343	3.496	3.796	4.081
102	2.751	2.831	2.984	3.283	3.570
108	2.250	2.329	2.480	2.773	3.056
114	1.780	1.856	2.002	2.285	2.560
120	1.354	1.427	1.565	1.834	2.097
126	0.982	1.050	1.180	1.432	1.678
132	0.669	0.732	0.853	1.085	1.312
138	0.416	0.473	0.583	0.794	1.000
144	0.222	0.273	0.372	0.559	0.742
150	0.082	0.127	0.213	0.376	0.535
156	-0.006	0.031	0.104	0.240	0.371
162	-0.050	-0.021	0.036	0.142	0.244
168	-0.058	-0.037	0.002	0.075	0.146
174	-0.038	-0.027	-0.007	0.030	0.066
180	0.	0.	0.	0.	0.

LOCAL NUSSELT NUMBER RE=30 PR=0.71

ANGLE	GR				
	-25	-50	-100	-200	-300
0	7.224	7.212	7.190	7.129	7.063
12	7.169	7.157	7.134	7.073	7.006
24	7.010	6.997	6.973	6.910	6.839
36	6.753	6.739	6.713	6.644	6.568
48	6.403	6.387	6.358	6.283	6.198
60	5.968	5.951	5.917	5.834	5.739
72	5.462	5.443	5.405	5.312	5.205
84	4.904	4.883	4.839	4.738	4.618
96	4.319	4.296	4.249	4.140	4.011
108	3.739	3.716	3.667	3.556	3.425
120	3.204	3.182	3.136	3.036	2.921
132	2.754	2.737	2.703	2.633	2.564
144	2.422	2.415	2.402	2.383	2.389
156	2.216	2.221	2.235	2.277	2.365
168	2.115	2.130	2.167	2.257	2.408
180	2.086	2.105	2.151	2.260	2.433

SURFACE PRESSURE DISTRIBUTION RE=30 PR=0.71

ANGLE	GR				
	-25	-50	-100	-200	-300
0	1.333	1.332	1.330	1.325	1.320
6	1.317	1.311	1.309	1.306	1.301
12	1.248	1.248	1.249	1.248	1.248
18	1.147	1.148	1.151	1.157	1.163
24	1.012	1.016	1.022	1.036	1.050
30	0.851	0.857	0.868	0.892	0.917
36	0.671	0.679	0.696	0.733	0.771
42	0.479	0.941	0.515	0.566	0.619
48	0.286	0.302	0.332	0.399	0.470
54	0.098	0.118	0.157	0.242	0.331
60	-0.075	-0.051	-0.003	0.099	0.208
66	-0.229	-0.200	-0.143	-0.021	-0.107
72	-0.359	-0.326	-0.259	-0.117	-0.032
78	-0.461	-0.423	-0.347	-0.185	-0.015
84	-0.535	-0.493	-0.407	-0.227	-0.037
90	-0.582	-0.535	-0.440	-0.242	-0.033
96	-0.603	-0.552	-0.449	-0.234	-0.009
102	-0.602	-0.547	-0.436	-0.207	0.031
108	-0.584	-0.525	-0.408	-0.166	0.084
114	-0.552	-0.491	-0.367	-0.115	0.146
120	-0.512	-0.448	-0.320	-0.058	0.211
126	-0.467	-0.401	-0.269	0.000	0.276
132	-0.420	-0.352	-0.216	0.059	0.341
138	-0.373	-0.304	-0.164	0.116	0.403
144	-0.330	-0.259	-0.116	0.169	0.462
150	-0.290	-0.218	-0.072	0.219	0.517
156	-0.254	-0.181	-0.033	0.263	0.567
162	-0.225	-0.151	-0.001	0.300	0.609
168	-0.203	-0.128	0.023	0.329	0.642
174	-0.189	-0.114	0.039	0.347	0.663
180	-0.185	-0.109	0.044	0.353	0.670

SURFACE VORTICITY DISTRIBUTION RE=30 PR=0.71

ANGLE	GR				
	-25	-50	-100	-200	-300
0	0.	0.	0.	0.	0.
6	0.879	0.873	0.862	0.833	0.813
12	1.723	1.710	1.687	1.631	1.570
18	2.515	2.497	2.462	2.377	2.285
24	3.235	3.211	3.164	3.050	2.927
30	3.864	3.833	3.773	3.630	3.475
36	4.383	4.346	4.274	4.102	3.914
42	4.282	4.738	4.652	4.451	4.231
48	5.050	5.000	4.901	4.671	4.418
54	5.185	5.128	5.016	4.757	4.472

60	5.187	5.124	4.998	4.713	4.398
66	5.062	4.994	4.856	4.546	4.202
72	4.823	4.749	4.600	4.268	3.901
78	4.486	4.407	4.248	3.899	3.512
84	4.070	3.988	3.821	3.460	3.060
90	3.598	3.514	3.342	2.975	2.568
96	3.095	3.011	2.837	2.469	2.064
102	2.585	2.501	2.328	1.967	1.570
108	2.089	2.008	1.838	1.489	1.108
114	1.626	1.548	1.385	1.052	0.691
120	1.209	1.135	0.980	0.668	0.331
126	0.847	0.778	0.633	0.343	0.030
132	0.548	0.481	0.347	0.080	-0.208
138	0.303	0.245	0.123	-0.121	-0.386
144	0.120	0.068	-0.041	-0.263	-0.503
150	-0.006	-0.051	-0.149	-0.345	-0.558
156	-0.080	-0.119	-0.202	-0.368	-0.551
162	-0.109	-0.140	-0.205	-0.337	-0.483
168	-0.099	-0.120	-0.166	-0.258	-0.360
174	-0.059	-0.070	-0.094	-0.142	-0.195
180	0.	0.	0.	0.	0.

CD TNT 0641

APPENDIX B.4
****

SINGLE SPHERE IN AN UNBOUNDED FLUID

SURFACE PRESSURE DISTRIBUTIONS PR=1.0 RE=0.01

ANGLE	GR			
	0.5E-3	0.1E-2	0.5E-2	1E -2
0	1298	1799	3957	5524
12	1270	1760	3870	5400
24	1188	1646	3613	5035
36	1056	1461	3197	4443
48	878.7	1214	2639	3651
60	664.7	915.4	1965	2692
72	423.2	578.1	1203	1605
84	164.6	216.7	3843	439.0
96	-99.81	-153.1	-4542	-757.4
108	-358.5	-515.1	-0.276	-1932
120	-600.3	-853.6	-2046	-3032
132	-814.6	-1154	-2730	-4010
144	-991.9	-1402	-3297	-4821
156	-1125	-1588	-3721	-5429
168	-1207	-1703	-3985	-5806
180	-1235	-1743	-4074	-5934

SURFACE VORTICITY DISTRIBUTIONS PR=1.0 RE=0.01

ANGLE	GR			
	0.5E-3	0.1E-2	0.5E-2	1E-2
0	0	0	0	0
12	0.676	0.943	2.114	2.991
24	1.319	1.839	4.126	5.838
36	1.903	2.655	5.959	8.435
48	2.404	3.355	7.537	10.67
60	2.801	3.909	8.790	12.45
72	3.075	4.294	9.665	13.70
84	3.216	4.493	10.12	14.36
96	3.217	4.495	10.14	14.39
108	3.078	4.302	9.715	13.80
120	2.804	3.921	8.864	12.60
132	2.408	3.369	7.621	10.84
144	1.907	3.668	6.040	8.593
156	1.322	1.849	4.189	5.962
168	0.677	0.948	2.149	3.059
180	0	0	0	0

SURFACE PRESSURE DISTRIBUTIONS PR=1.0 RE=0.01

ANGLE	GR

	-0.5E-3	-0.1E-2	-0.5E-2	-1E-2
0	-413.3	-1418	-3857	-5328
12	-404.1	-1387	-3768	-5199
24	-376.7	-1295	-3505	-4821
36	-332.4	-1146	-3081	-4210
48	-273.2	-947.9	-2515	-3395
60	-201.6	-708.1	-1833	-2413
72	-120.7	-437.7	-1065	-1307
84	-34.08	-148.7	-245.5	-128.4
96	54.66	146.3	590.1	1073
108	141.5	434.5	1405	2244
120	222.7	703.3	2164	3334
132	294.7	941.2	2836	4297
144	354.4	1138	3389	5092
156	399.1	1285	3803	5685
168	426.1	1376	4059	6052
180	436.1	1407	4146	6177

SURFACE VORTICITY DISTRIBUTIONS PR=1.0 RE=0.01

ANGLE GR

	-0.5E-3	-0.1E-2	-0.5E-2	-1E-2
0	0	0	0	0
12	-0.225	-0.758	-2.145	-3.076
24	-0.439	-1.477	-4.182	-5.996
36	-0.634	-2.131	-6.029	-8.642
48	-0.801	-2.690	-7.606	-10.90
60	-0.933	-3.131	-8.844	-12.67
72	-1.025	-3.434	-9.692	-13.87
84	-1.072	-3.587	-10.11	-14.47
96	-1.073	-3.584	-10.09	-14.44
108	-1.027	-3.425	-9.636	-13.77
120	-0.936	-3.117	-8.782	-12.52
132	-0.804	-2.674	-7.511	-10.73
144	-0.636	-2.116	-5.938	-8.477
156	-0.441	-1.465	-4.111	-5.867
168	-0.226	-0.751	-2.106	-3.005
180	0	0	0	0

SURFACE PRESSURE DISTRIBUTION PR=1.0 RE=0.1

ANGLE GR

	0.0005	0.001	0.05	0.1
0	65.06	66.45	137.8	180.0
12	63.65	65.00	134.5	175.5
24	59.47	60.73	124.8	163.4
36	52.76	53.87	109.3	141.1
48	43.85	44.76	88.43	112.6
60	33.17	33.83	63.25	78.14

72	21.23	21.61	34.85	39.13
84	8.578	8.662	4.455	-2.736
96	-4.269	-4.431	-26.59	-45.65
108	-16.38	-17.10	-56.96	-87.74
120	-28.01	-28.81	-85.31	-127.2
132	-38.03	-39.09	-110.4	-162.2
144	-46.26	-47.52	-131.2	-19.12
156	-52.37	-53.79	-146.7	-212.9
168	-56.14	-57.65	-156.3	-226.4
180	-57.41	-58.96	-159.6	-231.0

SURFACE VORTICITY DISTRIBUTIONS PR=1.0 RE=0.1

ANGLE	GR			
	0.0005	0.001	0.05	0.1
0	0	0	0	0
12	0.336	0.344	0.768	1.034
24	0.655	0.670	1.500	2.020
36	0.943	0.965	2.165	2.920
49	1.187	1.215	2.737	3.697
60	1.377	1.409	3.191	4.319
72	1.505	1.540	3.508	4.756
84	1.566	1.603	3.672	4.990
96	1.558	1.595	3.677	5.008
108	1.483	1.518	3.522	4.807
120	1.344	1.377	3.212	4.394
132	1.149	1.177	2.761	3.784
144	0.907	0.929	2.188	3.003
156	0.627	0.642	1.517	2.085
168	0.321	0.329	0.778	1.070
180	0	0	0	0

SURFACE PRESSURE DISTRIBUTIONS PR=1.0 RE=0.1

ANGLE	GR		
	-0.005	-0.01	-0.05
0	51.74	35.83	-115.9
12	50.64	35.11	-112.7
24	47.34	33.02	-103.4
36	42.29	29.67	-88.38
48	35.48	25.26	-68.35
60	27.35	20.04	-44.23
72	18.29	14.28	-17.13
84	8.748	8.266	11.76
96	-0.851	2.288	41.14
108	-10.09	-3.396	69.75
120	-18.58	-8.559	96.75
132	-25.99	-13.02	119.8
144	-32.04	-16.62	139.1
156	-36.52	-19.26	153.6
168	-39.28	-20.88	162.5

180	-40.21	-21.42	165.5

SURFACE VORTICITY DISTRIBUTIONS PR=1.0 , RE=0.1

ANGLE	GR		
	-0.005	-0.01	-0.05
0	0	0	0
12	0.259	0.170	-0.744
24	0.505	0.33	-1.449
36	0.726	0.473	-2.086
48	0.912	0.593	-2.628
60	1.056	0.683	-3.051
72	1.151	0.741	-3.336
84	1.195	0.764	-3.474
96	1.185	0.754	-3.460
108	1.125	0.711	-3.296
120	1.017	0.640	-2.991
132	0.868	0.543	-2.560
144	0.683	0.426	-2.021
156	0.471	0.293	-1.397
168	0.241	0.149	-0.715
180	0	0	0

LOCAL NUSSELT NUMBERS PR=1.0 RE=1.0

ANGLE	GR			
	0.05	0.1	0.5	1.0
0	2.608	2.615	2.663	2.713
12	2.603	2.609	2.657	2.707
24	2.585	2.591	2.639	2.688
36	2.556	2.563	2.609	2.656
48	2.518	2.524	2.568	2.614
60	2.471	2.476	2.518	2.561
72	2.417	2.422	2.400	2.500
84	2.359	2.363	2.397	2.432
96	2.299	2.302	2.330	2.360
108	2.238	2.241	2.263	2.287
120	2.182	2.184	2.199	2.215
132	2.131	2.131	2.140	2.149
144	2.088	2.088	2.090	2.093
156	2.056	2.055	2.052	2.050
168	2.036	2.034	2.028	2.022
180	2.029	2.027	2.020	2.013

SURFACE PRESSURE DISTRIBUTIONS PR=1.0 RE=1.0

ANGLE	GR			
	0.05	0.1	0.5	1.0

0	8.084	8.183	8.880	9.615
12	7.863	7.957	8.620	9.315
24	7.222	7.302	7.862	8.040
36	6.217	6.274	6.666	7.056
48	4.927	4.953	5.120	5.256
60	3.450	.3439	3.333	3.161
72	1.890	1.836	1.421	0.897
84	0.344	0.244	-0.505	-1.407
96	-1.105	-1.251	-2.346	-3.637
108	-2.395	-2.587	-4.021	-5.698
120	-3.486	-3.722	-5.476	-7.515
132	-4.361	-4.636	-6.676	-9.039
144	-5.021	-5.329	-7.607	-10.24
156	-5.476	-5.809	-8.266	-11.10
168	-5.742	-6.089	-8.658	-11.62
180	-5.828	-6.181	-8.788	-11.79

SURFACE VORTICITY DISTRIBUTION PR=1.0 RE=1.0

ANGLE	GR			
	0.05	0.1	0.5	1.0
0	0	0	0	0
12	0.438	0.446	0.507	0.573
24	0.845	0.862	0.980	1.110
36	1.199	1.223	1.396	1.585
48	1.481	1.512	1.733	1.975
60	1.676	1.713	1.974	2.261
72	1.780	1.821	2.114	2.435
84	1.794	1.838	2.149	2.492
96	1.725	1.770	2.087	2.437
108	1.585	1.628	1.938	2.280
120	1.388	1.428	1.715	2.033
132	1.149	1.184	1.435	1.713
144	0.881	0.910	1.111	1.333
156	0.596	0.464	0.756	0.913
168	0.301	0.156	0.383	0.464
180	0	0	0	0

LOCAL NUSSELT NUMBERS PR=1.0 RE=1.0

ANGLE	GR			
	-0.05	-0.1	-0.5	-1.0
0	2.596	2.588	2.517	2.360
12	2.590	2.582	2.511	2.356
24	2.572	2.565	2.495	2.343
36	2.544	2.537	2.470	2.324
48	2.507	2.499	2.436	2.300
60	2.461	2.453	2.395	2.269
72	2.408	2.401	2.349	2.238

84	2.351	2.345	2.300	2.206
96	2.293	2.287	2.250	2.175
108	2.235	2.230	2.202	2.148
120	2.180	2.176	2.158	2.125
132	2.131	2.128	2.120	2.106
144	2.090	2.088	2.088	2.092
156	2.060	2.058	2.065	2.082
168	2.040	2.039	2.051	2.076
180	2.034	2.033	2.046	2.075

SURFACE PRESSURF DISTRIBUTIONS PR=1.0 RE=1.0

ANGLE	GR			
	-0.05	-0.1	-0.5	-1.0
0	7.883	7.777	6.788	4.737
12	7.671	7.570	6.624	4.649
24	7.058	6.971	6.157	4.401
36	6.097	6.033	5.417	4.028
48	4.866	4.833	4.491	2.584
60	3.461	3.467	3.455	3.129
72	1.983	2.032	2.394	2.722
84	0.525	0.621	1.385	2.411
96	-0.833	-0.689	0.488	2.226
108	-2.034	-1.841	-0.258	2.175
120	-3.041	-2.803	-0.839	2.244
132	-3.842	-3.563	-1.259	2.401
144	-4.440	-4.127	-1.541	2.598
156	-4.848	-4.510	-1.711	2.786
168	-5.084	-4.730	-1.798	2.921
180	-5.161	-4.801	-1.825	2.969

SURFACE VORTICITY DISTRIBUTION PR=1.0 RE=1.0

ANGLE	GR			
	-0.05	-0.1	-0.5	-1.0
0	0	0	0	0
12	0.421	0.413	0.333	0.181
24	0.812	0.795	0.639	0.342
36	1.152	1.126	0.900	0.468
48	1.420	1.387	1.099	0.557
60	1.604	1.566	1.226	0.580
72	1.700	1.657	1.279	0.570
84	1.709	1.663	1.262	0.516
96	1.638	1.591	1.185	0.433
108	1.500	1.454	1.060	0.337
120	1.310	1.267	0.903	0.240
132	1.081	1.044	0.728	0.155
144	0.827	0.797	0.544	0.089
156	0.558	0.537	0.361	0.044
168	0.281	0.270	0.179	0.017

180 0 0 0 0

CD TNT 0343

APPENDIX B.5
****

SINGLE SPHERE IN AN UNBOUNDED FLUID OF PR=0

SURFACE PRESSURE DISTRIBUTION RE=0.01

ANGLE	GR			
	0.5E-5	1.0E-5	2.0E-5	3.0E-5
0	650.0	671.6	703.9	797.5
12	636.3	657.5	688.7	780.4
24	596.1	615.7	643.9	729.8
36	531.3	548.4	571.7	648.2
48	444.6	458.4	475.1	539.2
60	340.0	349.7	358.5	407.6
72	222.1	227.3	227.1	259.2
84	95.94	96.32	86.48	100.6
96	-32.83	-37.40	-57.07	-61.46
108	-158.6	-168.0	-197.3	-219.8
120	-276.0	-289.9	-323.2	-367.5
132	-379.9	-397.9	-444.1	-498.2
144	-465.9	-487.1	-539.9	-606.4
156	-530.1	-553.8	-611.6	-687.2
168	-569.8	-595.1	-655.9	-737.2
180	-583.3	-609.1	-670.9	-754.2

SURFACE VORTICITY DISTRIBUTION RE=0.01

ANGLE	GR			
	0.5E-5	1.0E-5	2.0E-5	3.0E-5
0	0.0	0.0	0.0	0.0
12	0.333	0.345	0.365	0.414
24	0.649	0.672	0.712	0.808
36	0.936	0.970	1.026	1.165
48	1.182	1.225	1.296	1.471
60	1.376	1.426	1.509	1.713
72	1.610	1.564	1.656	1.880
84	1.578	1.635	1.731	1.964
96	1.577	1.634	1.730	1.960
108	1.508	1.562	1.654	1.877
120	1.373	1.422	1.506	1.709
132	1.178	1.221	1.292	1.467
144	0.932	0.966	1.023	1.161
156	0.646	0.669	0.708	0.804
168	0.331	0.343	0.363	0.412
180	0.0	0.0	0.0	0.0

SURFACE PRESSURE DISTRIBUTION RE=0.01

ANGLE	GR			
	-0.5E-5	-1.0E-5	-2.0E-5	-3.0E-5
0	607.2	582.3	537.3	446.0
12	594.5	570.1	526.0	436.6
24	557.2	534.1	492.7	409.0
36	496.8	476.0	439.1	364.4
48	416.3	398.3	367.4	304.9
60	319.1	304.6	280.8	233.0
72	209.4	199.8	183.2	151.9
84	92.24	86.01	78.90	65.31
96	-27.44	-29.33	-27.61	-23.16
108	-144.4	-142.0	-131.7	-109.6
120	-253.5	-247.2	-228.8	-190.2
132	-350.0	-340.2	-314.7	-261.6
144	-429.9	-417.2	-385.8	-320.6
156	-489.6	-474.7	-438.9	-364.7
168	-526.5	-510.3	-471.8	-392.0
180	-539.0	-522.4	-482.9	-401.3

SURFACE VORTICITY DISTRIBUTION RF=0.01

ANGLE	GR			
	-0.5E-5	-1.0E-5	-2.0E-5	-3.0E-5
0	0.0	0.0	0.0	0.0
12	0.310	0.298	0.275	0.228
24	0.605	0.581	0.535	0.444
36	0.872	0.837	0.772	0.641
48	1.101	1.058	0.975	0.809
60	1.281	1.231	1.135	0.942
72	1.406	1.351	1.246	1.033
84	1.470	1.412	1.302	1.079
96	1.467	1.411	1.301	1.079
108	1.404	1.349	1.244	1.031
120	1.278	1.228	1.132	0.939
132	1.097	1.054	0.972	0.806
144	0.868	0.834	0.769	0.637
156	0.612	0.578	0.533	0.442
168	0.308	0.296	0.273	0.226
180	0.0	0.0	0.0	0.0

SURFACE PRESSURE DISTRIBUTION RE=0.05

ANGLE	GR				
	0.0	0.125E-3	0.25E-3	0.5E-3	0.75E-3
0	124.7	134.4	141.4	154.8	175.1
12	122.0	131.5	138.3	151.5	171.3
24	114.1	123.1	129.4	141.7	160.2

36	101.4	108.5	115.1	125.9	142.2
48	84.54	91.33	95.90	104.9	118.4
60	64.19	69.50	72.87	79.59	89.68
72	41.34	44.99	47.02	51.20	57.49
84	17.02	18.91	19.49	20.98	23.24
96	-7.714	-7.604	-8.471	-9.719	-11.53
108	-31.76	-33.38	-35.66	-39.56	-45.31
120	-54.11	-57.31	-60.92	-67.08	-76.67
132	-73.81	-78.43	-83.18	-91.70	-104.3
144	-90.04	-95.82	-101.5	-111.8	-127.0
156	-102.1	-108.8	-115.2	-126.8	-143.9
168	-109.6	-116.8	-123.6	-136.1	-154.4
180	-112.2	-119.5	-126.5	-139.2	-157.9

SURFACE VORTICITY DISTRIBUTION RE=0.05

ANGLE	GR				
	0.0	0.125E-3	0.25E-3	0.5E-3	0.75E-3
0	0.0	0.0	0.0	0.0	0.0
12	0.321	0.346	0.365	0.401	0.454
24	0.625	0.674	0.711	0.781	0.885
36	0.901	0.971	1.024	1.125	1.276
48	1.136	1.225	1.291	1.419	1.608
60	1.321	1.424	1.501	1.649	1.868
72	1.447	1.559	1.643	1.805	2.046
84	1.509	1.626	1.714	1.882	2.132
96	1.505	1.621	1.709	1.877	2.126
108	1.436	1.546	1.630	1.791	2.027
120	1.305	1.405	1.481	1.627	1.842
132	1.118	1.204	1.269	1.394	1.577
144	0.883	0.951	1.003	1.101	1.246
156	0.611	0.658	0.694	0.762	0.862
168	0.313	0.337	0.355	0.390	0.442
180	0.0	0.0	0.0	0.0	0.0

SURFACE PRESSURE DISTRIBUTION RE=0.05

ANGLE	GR			
	-.125E-3	-.25E-3	-.5E-3	-.75E-3
0	119.4	111.7	95.58	66.53
12	116.8	109.3	93.56	65.16
24	109.4	102.3	87.62	61.10
36	97.32	91.07	78.06	54.56
48	81.27	76.08	65.30	45.86
60	61.69	58.05	49.96	35.39
72	40.28	37.81	32.75	23.65
84	17.19	16.25	14.41	11.15
96	-6.262	-5.655	-4.213	-1.551
108	-29.07	-26.96	-22.33	-13.89
120	-50.26	-46.75	-39.15	-25.35

132	-68.80	-64.19	-53.98	-35.44
144	-84.33	-78.57	-66.20	-43.76
156	-95.80	-89.28	-75.31	-49.95
168	-102.9	-95.90	-80.93	-53.78
180	-105.3	-98.14	-82.84	-55.07

SURFACE VORTICITY DISTRIBUTION RE=0.05

ANGLE	GR			
	-.125E-3	-.25E-3	-.5E-3	-.75E-3
0	0.0	0.0	0.0	0.0
12	0.306	0.286	0.243	0.166
24	0.596	0.556	0.473	0.324
36	0.859	0.802	0.682	0.467
48	1.083	1.011	0.859	0.588
60	1.259	1.175	0.999	0.684
72	0.378	1.286	1.094	0.748
84	1.437	1.342	1.140	0.780
96	1.433	1.338	1.137	0.776
108	1.367	1.276	1.085	0.741
120	1.242	1.159	0.986	0.673
132	1.064	0.994	0.844	0.577
144	0.841	0.785	0.667	0.456
156	0.582	0.543	0.462	0.315
168	0.298	0.278	0.236	0.161
180	0.0	0.0	0.0	0.0

SURFACE PRESSURE DISTRIBUTION RE=0.1

ANGLE	GR				
	0.0	0.5E-3	1.0E-3	2.0E-3	3.0E-3
0	64.50	68.39	72.02	79.14	85.88
12	63.10	66.89	70.44	77.39	83.96
24	58.98	62.51	65.80	72.24	78.34
36	52.36	55.46	58.34	63.97	69.30
48	43.56	46.10	48.43	52.99	57.31
60	33.02	34.88	36.57	39.85	42.95
72	21.25	22.35	23.31	25.16	26.92
84	8.777	9.079	9.273	9.622	9.964
96	-3.825	-4.328	-4.905	-6.071	-7.151
108	-16.01	-17.29	-18.61	-21.23	-23.68
120	-27.26	-29.26	-31.26	-35.23	-38.93
132	-37.13	-39.76	-42.36	-47.49	-52.28
144	-45.23	-48.37	-51.45	-57.55	-63.23
156	-51.24	-54.76	-58.21	-65.01	-71.35
168	-54.95	-58.70	-62.37	-69.60	-76.35
180	-56.20	-60.03	-63.77	-71.16	-78.04

SURFACE VORTICITY DISTRIBUTION RE=0.1

ANGLE	GR				
	0.0	0.5E-3	1.0E-3	2.0E-3	3.0E-3
0	0.0	0.0	0.0	0.0	0.0
12	0.333	0.354	0.374	0.414	0.452
24	0.648	0.689	0.729	0.806	0.879
36	0.933	0.992	1.049	1.160	1.265
48	1.174	1.249	1.320	1.460	1.592
60	1.362	1.449	1.531	1.693	1.846
72	1.488	1.583	1.673	1.849	2.017
84	1.547	1.646	1.740	1.923	2.097
96	1.539	1.638	1.731	1.913	2.085
108	1.465	1.558	1.646	1.819	1.983
120	1.328	1.412	1.492	1.649	1.797
132	1.135	1.207	1.276	1.409	1.536
144	0.895	0.952	1.006	1.112	1.211
156	0.619	0.658	0.695	0.768	0.837
168	0.317	0.337	0.356	0.393	0.428
180	0.0	0.0	0.0	0.0	0.0

SURFACE PRESSURE DISTRIBUTION RE=0.1

ANGLE	GR				
	-0.5E-4	-0.5E-3	-1.0E-3	-2.0E-3	-3.0E-3
0	64.04	61.08	56.27	47.53	31.90
12	62.64	59.76	55.06	46.52	31.25
24	58.55	55.88	51.49	43.55	29.33
36	51.96	49.64	45.77	38.77	26.26
48	43.21	41.35	38.17	32.43	22.18
60	32.72	31.42	29.06	24.84	17.29
72	21.00	20.32	18.89	16.35	11.84
84	8.594	8.570	8.136	7.369	6.073
96	-3.947	-3.307	-2.788	-1.711	0.253
108	-16.07	-14.79	-13.32	-10.49	-5.368
120	-27.28	-25.39	-23.06	-18.60	-10.55
132	-37.10	-34.70	-31.59	-25.71	-15.09
144	-45.16	-42.33	-38.59	-31.54	-18.82
156	-51.14	-47.99	-43.79	-35.87	-21.58
168	-54.83	-51.48	-47.00	-38.54	-23.28
180	-56.08	-52.66	-48.08	-39.44	-23.85

SURFACE VORTICITY DISTRIBUTION RE=0.1

ANGLE	GR				
	-0.5E-4	-0.5E-3	-1.0E-3	-2.0E-3	-3.0E-3
0	0.0	0.0	0.0	0.0	0.0
12	0.331	0.314	0.287	0.240	0.156
24	0.444	0.611	0.560	0.467	0.303

36	0.926	0.979	0.836	0.672	0.436
48	1.166	1.136	1.015	0.846	0.548
60	1.353	1.283	1.176	0.981	0.636
72	1.478	1.402	1.285	1.072	0.694
84	1.537	1.458	1.337	1.115	0.721
96	1.530	1.453	1.330	1.108	0.716
108	1.455	1.380	1.266	1.054	0.681
120	1.319	1.251	1.147	0.956	0.617
132	1.128	1.069	0.981	0.817	0.527
144	0.889	0.843	0.774	0.644	0.415
156	0.615	0.583	0.535	0.445	0.287
168	0.315	0.298	0.274	0.228	0.147
180	0.0	0.0	0.0	0.0	0.0

CD TNT 0297

9382-1